Universidade do Minho
Escola de Ciências

Filipa Diana da Silva Mendes

Novel tools and data for the detection and assessment of ecological risks of fungicides

august 2024

UMinho | 2024 Filipa Diana da Silva Mendes
Novel tools and data for the detection and assessment of ecological risks of fungicides

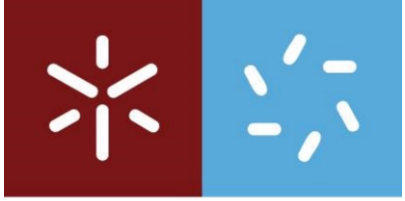

Universidade do Minho
Escola de Ciências

Filipa Diana da Silva Mendes

Novel tools and data for the detection and assessment of ecological risks of fungicides

Doctoral Thesis in Biology
Doctoral Program in Molecular and Environmental Biology Specialization in Molecular Biotechnology

Work supervised by
Doctor Susana Alexandra Rodrigues Chaves
Professor Doctor Bruno Branco Castro
Professor Doctor Maria João Marques Ferreira Sousa Moreira

august 2024

COPYRIGHT AND TERMS OF USE OF THE WORK BY THIRD PARTIES

This is an academic work that can be used by third parties as long as they respect internationally accepted rules and good practices, with regard to copyright and related rights. Thus, the work may be used under the terms of the license indicated below. If the user needs permission to use the work under conditions not provided for in the licensing, should contact the author through the RepositóriUM of the University of Minho.



Atribuição-NãoComercial-SemDerivações

CC BY-NC-ND

https://creativecommons.org/licenses/by-nc-nd/4.0/

Acknowledgements

Chega assim ao fim a mais longa das caminhadas. E ao longo desta pude contar com o companheirismo, a amizade, o carinho e a força de muitas pessoas, sem as quais eu não teria conseguido.

Aos meus orientadores, doutora Susana Chaves, professora Maria João Sousa e professor Bruno Castro, agradeço a partilha de conhecimento, os conselhos e a paciência durantes todos estes anos. Obrigado pelas palavras de incentivo nos momentos mais difíceis, pela confiança que sempre depositaram em mim, e por me terem feito crescer enquanto investigadora e pessoa. Um obrigado especial à minha orientadora doutora Susana Chaves que acompanha o meu percurso enquanto investigadora desde o início, e já lá vão 6 anos. Obrigado pelas oportunidades e pelos ensinamentos ao longo estes anos, levo-os para a vida. I want to express my gratitude to Professor Maya Schuldiner and Professor Anne Devin, as well as their teams, for their warm welcome and support during my stay. It was a challenge, but with your help I have grown personally and professionally. A todos os meus colegas da Micro I, com quem me fui cruzando ao longo destes 6 anos, em especial aos amigos que levo para a vida, à Joana, à Cátia, ao António, à Vitória, à Marta, à Leslie e à Bruna, e aos meus vizinhos da frente (Micro II), ao Gusto, à Inês, à Patrícia, à Ticiana e à Carolina, obrigado pela ajuda, pelo convívio e pela alegria constante, é bom saber que posso sempre contar com vocês. Um obrigado também a todas as pessoas do DB/CBMA, em especial ao Sr. Luís, à Dona Manuela e à Inês, pelo apoio técnico e por toda a ajuda ao longo destes anos.

Aos meus amigos, a minha maior força, obrigado por existirem. Aos meus fiéis companheiros de mestrado e de doutoramento, Joana, Gusto, Anabela e Clau; ao "Gang Machado" Joana, Cátia, António, Taxti, TT, Nuno, Matias, Rita, Beli e Carlinha; às minhas reformadas sem tempo Ju, Sofia, Diana, Raquel e Catarina, obrigado pela bonita história que estamos a contar. Às minhas Choquinhas, Joana e Catarina, obrigado por partilharem as minhas alegrias e as minhas tristezas como se fossem vossas, que bom que os nossos caminhos se cruzaram. A todos, obrigado pelos sorrisos, pelos abraços, mas acima de tudo, obrigado pela amizade.

Por último agradeço a toda a minha família, pelo apoio e incentivo ao longo destes anos. Sou muito mais feliz com vocês. Aos meus pais, os grandes impulsionadores desta caminhada e sem os quais eu não seria ninguém, OBRIGADO. Não houve um único momento que tenham questionado a minha escolha e sempre que as incertezas chegaram, e elas chegaram, eu soube que vocês estavam comigo. Para a minha Avó que me ensinou que a força está no querer.

A todos vocês por me inspiram a ser cada dia melhor e por me terem acompanhado nesta longa caminhada, obrigado. É a vocês que dedico este trabalho.

Este trabalho foi financiado pela Fundação para a Ciência e Tecnologia através da bolsa SFRH/BD/147574/2019; por fundos nacionais (Fundação para a Ciência e a Tecnologia) e pelo Fundo Europeu de Desenvolvimento Regional (programas COMPETE2020 e PT2020) através do projeto de investigação FunG-Eye (PTDC/CTA-AMB/29505/2017).

Statement of Integrity

I hereby declare having conducted this academic work with integrity. I confirm that I have not used plagiarism or any form of undue use of information or falsification of results along the process leading to its elaboration.

I further declare that I have fully acknowledged the Code of Ethical Conduct of the University of Minho.

Abstract

Novel tools and data for the detection and assessment of ecological risk of fungicides

Food production is highly dependent on pesticides, which pose significant risks to ecosystems and human health. Despite their ubiquitous use, the mode of action of many agrochemicals is poorly characterized and their routine monitoring is complex and expensive. Among pesticides, fungicides are of particular concern, as their ecological effects have been overlooked compared to insecticides and herbicides. In the present thesis, we aimed to address these challenges by using the yeast *Saccharomyces cerevisiae* as a eukaryotic model to study two agrochemical fungicides, using complementary approaches. First, we used the yeast *S. cerevisiae* to dissect mechanisms underlying the toxic effects of cymoxanil (CYM), which is a widespread used synthetic fungicide whose mode of action remains poorly characterized. We found that CYM inhibits cytochrome *c* oxidase (C*c*O) during oxidative phosphorylation. CYM acts by blocking the interaction of cytochrome *c* (cyt *c*) with C*c*O, hampering electron transfer and inhibiting C*c*O catalytic activity. Additionally, under conditions repressing respiration, CYM induces genome-wide changes, specifically in membrane transporter systems. These changes are linked to perturbations of lipid-raft organization and to the inhibition of Pma1p, resulting in a reduction in plasma membrane potential and in intracellular acidification. Second, we developed a biosensor for environmental monitoring of tebuconazole (TEB), a commonly used fungicide with a well-known mode of action in the synthesis of sterols. Yeast cells were engineered with a reporter gene downstream of specific promoters that are expressed after exposure to TEB. We found that this easy-to-use biosensor consistently detects TEB and does not respond to realistic environmental concentrations of other tested azoles, suggesting its specificity. Therefore, we propose the use of this new method to analyze samples from aquatic environments prone to TEB contamination, and as a complementary tool to conventional methods. Altogether, this thesis reveals new cellular and molecular events triggered by CYM and contributes to improve fungicide monitoring programs. It also highlights the benefits of using yeast as a simple and valuable organism to evaluate the effects of fungicides on both target and non-target organisms.

Keywords: Environmental monitoring tools, Fungicides, Mode of action, Yeast-based biosensor

Resumo

Novas ferramentas e dados para a deteção e avaliação do risco ecológico dos fungicidas

A produção alimentar é altamente dependente dos pesticidas, que representam riscos significativos para os ecossistemas e para a saúde humana. Apesar da sua utilização omnipresente, o modo de ação de muitos agroquímicos está mal caracterizado e a sua monitorização de rotina é complexa e dispendiosa. Entre os pesticidas, os fungicidas são particularmente preocupantes, uma vez que os seus efeitos ecológicos têm sido negligenciados em comparação com os inseticidas e herbicidas. Na presente tese, o nosso objetivo foi responder a estes desafios utilizando a levedura *Saccharomyces cerevisiae* como modelo eucariótico para estudar dois fungicidas agroquímicos, utilizando abordagens complementares. Em primeiro lugar, utilizámos a levedura *S. cerevisiae* para dissecar os mecanismos subjacentes aos efeitos tóxicos do cimoxanil (CYM), que é um fungicida sintético de uso generalizado cujo modo de ação permanece mal caracterizado. Descobrimos que o CYM inibe a citocromo *c* oxidase (C*c*O) durante a fosforilação oxidativa. O CYM atua bloqueando a interação do citocromo *c* (cyt *c*) com a C*c*O, dificultando a transferência de eletrões e inibindo a atividade catalítica da C*c*O. Além disso, em condições de repressão da respiração, o CYM induz alterações em todo o genoma, e especificamente nos sistemas de transportadores de membrana. Estas alterações estão ligadas a perturbações da organização da estrutura lipídica da membrana plasmática e à inibição da Pma1p, resultando numa redução do potencial da membrana e na acidificação intracelular. Em segundo lugar, desenvolvemos um biossensor para a monitorização ambiental do tebuconazol (TEB), um fungicida vulgarmente utilizado com um modo de ação bem conhecido na inibição da síntese de esteróis. As células de levedura foram modificadas com um gene repórter a jusante de promotores específicos que são expressos após a exposição ao TEB. Verificámos que este biossensor de fácil utilização deteta consistentemente o TEB e não responde a concentrações ambientais realistas de outros azóis testados, o que sugere a sua especificidade. Assim, propomos a utilização deste novo método, para analisar amostras de ambientes aquáticos em risco de contaminação por TEB, e como ferramenta complementar aos métodos convencionais. No seu conjunto, esta tese revela novos eventos celulares e moleculares desencadeados pelo CYM e contribui para melhorar os programas de monitorização de fungicidas. Destaca também os benefícios da utilização da levedura como um organismo simples e valioso para avaliar os efeitos dos fungicidas em organismos alvo e não alvo.

Palavras-chave: Ferramentas de monitorização ambiental, Fungicidas, Modo de ação, Biossensor à base de Levedura

Table of contents

Acknowledgements iii

Statement of Integrity iv

Abstract v

Resumo vi

Outputs xi

List of Abbreviations and Acronyms xiii

List of Figures xvii

List of Tables xix

CHAPTER 1 - General Introduction 20

1.1. Pesticides as an environmental problem 22

1.1.1. Impact of pesticides on aquatic environments 24

1.1.2. Monitorization of pesticides to mitigate risks 26

1.2. Biosensors as a tool to screen pesticides in water 28

1.2.1. Enzyme-based biosensors 34

1.2.2. Antibody-based biosensors 36

1.2.3. Aptamer-based biosensors 37

1.2.4. Whole cell-based biosensors 39

1.3. Understanding pesticide toxicity mechanisms 41

1.3.1. The yeast *S. cerevisiae* as a tool to unveil toxicity mechanisms 41

1.3.2. *S. cerevisiae*-based toxicogenomics studies of pesticides 44

1.4. References 48

CHAPTER 2 - Rationale and Aims 65

2.1. Rationale 66

2.2. Aims 69

2.3. References 72

CHAPTER 3 - Unveiling the Mechanisms Underlying Cymoxanil Cytotoxicity in *S. cerevisiae* Yeast Cells 75

Background 77

3.1. Unveiling the impact of cymoxanil in yeast cells respiration 79

3.1.1. Materials and Methods 79

3.1.1.1. Yeast strain, culture medium, growth conditions and treatment 79

3.1.1.2. Mitochondria preparation 79

3.1.1.3. Oxygen consumption assays 79

3.1.1.4. Determination of mitochondrial complex III (Ubiquinol: Cytochrome *c* Oxidoreductase) activity 80

3.1.1.5. Docking studies 81

3.1.1.6. Statistical analysis 83

3.1.2. Results 83

3.1.2.1. Cymoxanil impairs respiration of whole cells 83

3.1.2.2. Cymoxanil compromises the mitochondrial electron transport chain 85

3.1.2.3. Model for cymoxanil inhibition of cytochrome *c* oxidase activity 87

3.1.3. Discussion 92

3.1.4. References 95

3.1.5. Supplementary Material 99

3.2. Molecular bases of the antifungal activity of cymoxanil 101

3.2.1. Materials and Methods 101

3.2.1.1. Yeast strains 101

3.2.1.2. Growth conditions and treatments 101

3.2.1.3. Cell growth and survival 101

3.2.1.4. Assessment of plasma membrane integrity 102

3.1.1.5. Transcriptomic analysis 102

RNA extraction 102

RNAseq analysis 102
qRT-PCR 102
3.2.1.6. High-throughput fluorescence microscopic screen 103
3.2.1.7. Gene ontology (GO) term analysis 103
3.2.1.8. Evaluation of autophagy 104
3.2.1.9. Evaluation of lipid raft distribution 104
3.2.1.10. Analysis of efflux pumps 105
3.2.1.11. Proton movements assays 105
3.2.1.12. Evaluation of intracellular ATP concentration 105
3.2.1.13. Analysis of vacuolar pH variations 106
3.2.1.14. Assessment of membrane potential 106
3.2.1.15. Flow cytometry 106
3.2.1.16. Statistical analysis 106
3.2.2. Results 107
3.2.2.1. Cymoxanil inhibits growth and decreases cell viability independently of an active respiratory chain 107
3.2.2.2. Transcriptome alterations induced by cymoxanil 108
3.2.2.3. Proteome-wide alterations induced by cymoxanil 109
3.2.2.4. Cymoxanil does not induce autophagy in yeast cells 111
3.2.2.5. Cymoxanil induces intracellular accumulation of ergosterol, perturbing lipid rafts of yeast cells without affecting ergosterol biosynthesis 111
3.2.2.6. Cymoxanil does not affect efflux pumps but inhibits Pma1p activity and leads to plasma membrane depolarization of yeast cells 112
3.2.3. Discussion 116
3.3.4. References 119
3.2.5. Supplementary Material 122

CHAPTER 4 - Development and Application of a Yeast-Based Biosensor for Environmental Monitoring of Tebuconazole in Water Samples 145

4.1. Background 147

4.2. Materials and methods 148

4.2.1. Yeast strains and plasmids 148

4.2.2. Growth conditions and treatments 149

4.2.5 Evaluation of lipid raft distribution by filipin staining 150

4.2.6. qRT-PCR 150

4.2.7. Evaluation of biosensor performance in environmental water samples 151

4.2.8. Bioluminescence measurements 151

4.2.9. Statistical analysis 151

4.3. Results 152

4.3.1. TEB induces transcription of *ERG* genes at concentrations that do not affect growth, viability, and ergosterol distribution 152

4.3.2. A novel biosensor design based on yNLuc expression from *ERG* promoters 155

4.4. Discussion 158

4.5. References 162

4.6. Supplementary Material 166

4.6.1. Supplementary References 168

CHAPTER 5 - Final Considerations and Future perspectives 169

5.1. Final considerations and future perspectives 170

5.2. In short 176

5.3. References 177

5.4. Supplementary Material 180

Outputs

Peer-reviewed publications

- Filipa Mendes, Eduarda Miranda, Leslie Amaral, Carla Carvalho, Bruno B. Castro, Maria João Sousa, Susana R. Chaves. (2024) Novel yeast-based biosensor for environmental monitoring of tebuconazole. *Applied Microbiology and Biotechnology*. 108:1-12. doi.org/10.1007/s00253-023-12944-z

- Filipa Mendes, Cátia Santos-Pereira, Tatiana F. Vieira, Mélanie Martins Pinto, Bruno B. Castro, Sérgio F. Sousa, Maria João Sousa, Anne Devin, Susana R. Chaves. The widely used cymoxanil fungicide impairs respiration in *Saccharomyces cerevisiae* via cytochrome *c* oxidase inhibition. (*Under revision at FEBS Letters)*

- Filipa Mendes, Hadar Meyer, Leslie Amaral, Bruno B. Castro, Maya Schuldiner, Maria João Sousa, Susana R. Chaves. The antifungal activity of cymoxanil is associated with proton pump inhibition and disruption of plasma membrane potential. *DOI: doi.org/10.1101/2024.03.01.583004 (pre-print)*

- Filipa Mendes, Beatriz Machado, Bruno B. Castro, Maria João Sousa, Susana R. Chaves. The power of biosensors for environmental monitoring of pesticides in water. (*manuscript in preparation*)

Oral Presentations

- Filipa Mendes, Eduarda Miranda, Leslie Amaral, Bruno B. Castro, Maria João Sousa, Susana R. Chaves. (2023) "Yeast a novel tool for the detection and assessment of ecological risks of fungicides". I Symposium PhD Bio, 8th February, Braga, Portugal
- Filipa Mendes, Eduarda Miranda, Leslie Amaral, Bruno B. Castro, Maria João Sousa, Susana R. Chaves. (2021) "Bio-deteção de fungicidas azólicos". At the workshop "Uma abordagem funcional para compreender a interação entre a poluição por fungicidas e os processos do ecossistema mediados por fungos", promoted by FunG-Eye project, 6th December, Braga, Portugal

- Leslie Amaral, Filipa Mendes, Eduarda Miranda, Bruno B. Castro, Maria João Sousa, Susana R. Chaves. (2021) "Bio-Detection of fungicides: An alternative to traditional methods" At the webinar "Bio-Deteção e Efeitos ecológicos de fungicidas em sistemas aquáticos: modelos biológicos e resultados do projeto FunG-Eye", promoted by FunG-Eye project, 31st March, Braga, Portugal

Poster Presentations

- Filipa Mendes, Cátia Santos-Pereira, Tatiana F. Vieira, Mélanie Martins Pinto, Bruno B. Castro, Sérgio F. Sousa, Maria João Sousa, Anne Devin, Susana R. Chaves. (2024) "The cymoxanil fungicide impairs *Saccharomyces cerevisiae* respiration via complex IV inhibition". I CBMA Open Day & II PhD|Bio Symposium, 2nd February, Braga, Portugal.
- Filipa Mendes, Tatiana F. Vieira, Cátia Santos-Pereira, Mélanie Martins Pinto, Bruno B. Castro, Sérgio F. Sousa, Maria João Sousa, Anne Devin, Susana R. Chaves. (2023) "Cymoxanil inhibits respiration through inhibition of mitochondrial complex IV". 31st International Conference on Yeast Genetics and Molecular Biology, 20th-25th August, Florence, Italy.
- Filipa Mendes, Eduarda Miranda, Leslie Amaral, Bruno B. Castro, Maria João Sousa, Susana R. Chaves. (2022) "A yeast-based biosensor to monitor tebuconazole in environmental samples". The Biochemistry Global Summit, 9th-14th July, Lisbon, Portugal.
- Filipa Mendes, Eduarda Miranda, Leslie Amaral, Bruno B. Castro, Maria João Sousa, Susana R. Chaves. (2021) "Novel yeast-based biosensor for environmental monitoring". 15th International Congress on Yeasts meets the 30th International Conference on Yeast Genetics and Molecular Biology, 23rd-27th August, Vienna, Austria.
- Tiago Cardoso, Filipa Mendes, António Rego, Maria João Sousa, Susana R. Chaves (2021) "Exploring the mechanism of action of cymoxanil". Microbiotec'21, 23rd-26th November, Lisbon, Portugal.

Awards

- Early career investigator fellowship from Federation of European Microbiological Societies (FEMS) to the 31st International Conference on Yeast Genetics and Molecular Biology (ICYGMB31) held in Florence, Italy from 20 to 25th August 2023

List of Abbreviations and Acronyms

4-MU	4-methyllumbeliferone
4-MUS	4-methyllumbeliferone sulfate
a.u.	Arbitrary Units
ABC	ATP-binding cassette
AChE	Acetylcholinesterase
ADP	Adenosine diphosphate
ANOVA	Analysis Of Variance
ATP	Adenosine Triphosphate
B	Bud
Botrytis cinerea	*B. cinerea*
C	Cytosol
c.f.u.	Colony Forming Units
CCCP	Carbonyl cyanide *m*-chlorophenylhydrazone
C*c*O	Cytochrome *c* oxidase/complex IV
CDCF	5-(and-6)-carboxy-2',7'-dichlorofluorescein
CDCFDA	5-(and-6)-carboxy-2′,7′-dichlorofluorescein diacetate
CHO	Choline oxidase
ChpA	Chlorpyrifos responsive promoter
ChpR	Chlorpyrifos-responsive transcription regulator
CLO	Clotrimazole
Complex III	Ubiquinol: Cytochrome *c* Oxidoreductase
CP	Cell Periphery
cryo-EM	Cryo-Electron Microscopy
CYM	Cymoxanil
Cyt *c*	Cytochrome *c*
DAmP	Decreased Abundance by mRNA Perturbation

$DiBAC_4(3)$	Bis-(1,3-dibutylbarbituric acid) trimethine oxonol
DMSO	Dimethyl Sulfoxide
DW	Dry weight
EC	Electrical conductivity
ER	Endoplasmic reticulum
E. coli	*Escherichia coli*
EU	European Union
FAO	Food and Agriculture Organization of the United Nations
FGE	Formylglycine-generating enzyme
fGly	Formylglycine
FLU	Fluconazole
FRAC	Fungicide Resistance Action Committee
Gal	Galactose
GFP	Green Fluorescent Protein
Glu	Glucose
GO	Gene ontology
IUPAC	International Union of Pure and Applied Chemistry
JO_2	Respiratory flux
K_{oc}	Adsorption coefficient
LoD	Limit of Detection
M	Mitochondria
Min	Minute
MYC	Myclobutanil
N	Nucleus
ND	Not detected
NP	Nuclear Periphery
OD	Optical Density

OPs	Organophosphorus pesticides
P	Punctate
P. infestans	*Phytophthora infestans*
PBS	Phosphate buffered saline
PBST	PBS-Tween
PCP	Punctate Cell Periphery
PCR	Polymerase chain reaction
Pgk1p	Phosphoglycerate kinase 1
PI	Propidium iodide
Pma1p	Plasma Membrane ATPase 1
PQ-15 aptamer	Paraquat-aptamer
pr	Promoter
PVDF	Polyvinylidene Difluoride
qRT-PCR	quantitative Real-Time PCR
RT	Room temperature
S. cerevisiae	*Saccharomyces cerevisiae*
S.D.	Standard deviation
SC	Synthetic Complete
SD	Synthetic Defined
SDS-PAGE	Sodium Dodecyl Sulphate-polyacrylamide gel electrophoresis
SELEX	Systematic Evolution of Ligands by Exponential Enrichment
SGD	*Saccharomyces* Genome Database
TDS	Total Dissolved Solids
TEB	Tebuconazole
TET	Triethyltin bromide
TMB	3,3′,5,5′ -tetramethylbenzidine
TMPD	*N,N,N′,N′*-tetramethyl-p-phenylenediamine

V	Vacuole
V-ATPase	Vacuolar-ATPase
VM	Vacuole Membrane
YEPD	Yeast Extract-Peptone-Dextrose
yNLuc	Yeast NanoLuciferase

List of Figures

Figure 1.1. Schematic representation of pesticide classification.. 23

Figure 1.2. Global pesticide use. 24

Figure 1.3. General structure of a biosensor. 29

Figure 1.4. Schematic representation of enzyme-based biosensors. 35

Figure 1.5. Schematic representation of aptasensor examples. 38

Figure 1.6. Schematic representation of the whole cell-based biosensor for environmental water monitoring of the chlorpyrifos insecticide.. 40

Figure 1.7. Examples of yeast collections and fitness-based assays available for functional toxicogenomics in *S. cerevisiae*.. 43

Figure 1.8. Application of yeast-based omics technologies to obtain toxicological mechanistic insights for environmental contaminants.. 45

Figure 2.1. Examples of fungicides according to the FRAC list code.. 67

Figure 3.1.1. Schematic representation of the electron transport chain in *S. cerevisiae* isolated mitochondria and strategies used to determine the effect of CYM on mitochondrial complexes III and IV.. 81

Figure 3.1.2. Structure of the C*c*O - cyt *c* complex used in this work. 82

Figure 3.1.3. Effect of CYM on the respiratory flux (JO_2) of yeast cells, along time.. 84

Figure 3.1.4. Effect of CYM on the JO_2 of yeast cells in the presence of an inhibitor or an uncoupler.. 85

Figure 3.1.5. Effect of CYM on the oxygen consumption rate of isolated yeast mitochondria.. 86

Figure 3.1.6. Effect of CYM on the activity of mitochondrial complex III and complex IV. 87

Figure 3.1.7. Correlation between the PLP score and the Non-H atoms of each molecule studied. ... 90

Figure 3.1.8. PLP docking poses for CYM, N-acetylcyanoglycine, ethylparabanic acid, demethoxylated cymoxanil and ADDA-5 on chain B (subunit II) of bovine C*c*O (structure PDB: 5IY5, blue) or yeast C*c*O (structure PDB: 8DH6, purple). 91

Figure S3.1.i. PLP Docking poses of CYM, its metabolites and ADDA-5 on chain A of C*c*O. 100

Figure 3.2.1. Influence of the carbon source on CYM effects on growth and viability of *S. cerevisiae* BY4741 cells. 108

Figure 3.2.2. Transcriptomic analysis of CYM effect in *S. cerevisiae* BY4741 cells. 109

Figure 3.2.3. Effects of CYM on protein localization.. 110
Figure 3.2.4. Effect of CYM on autophagy in yeast cells. 111
Figure 3.2.5. Effect of CYM on the distribution of ergosterol-rich lipid rafts. 112
Figure 3.2.6. Effect of CYM on efflux pumps and Pma1p activity.. 113
Figure 3.2.7. Effect of CYM on intracellular levels of ATP, vacuolar pH and membrane potential of BY4741 cells.. 115
Figure 4.1. Effect of high concentrations of TEB on growth, cell survival, plasma membrane integrity and lipid rafts distribution of *S. cerevisiae* BY4741 cells.. 153
Figure 4.2. Effect of low TEB concentrations on genes involved in ergosterol biosynthetic pathway of *S. cerevisiae*.. 154
Figure 4.3. Response of biosensor after exposure to TEB. 155
Figure 4.4. Biosensor sensitivity and selectivity to TEB. 156
Figure 4.5. Proof-of-concept of biosensor functionality. 157
Figure 4.6. Schematic representation of the novel reporter strain for TEB detection in environmental water samples. 161
Figure S5.i. Representative images of the chemogenomic study using two distinct and complementary collections. 181
Figure S5.ii. Response of BY471 + *ERG25*pr and AD1-9 + *ERG25*pr strains to TEB. 189

List of Tables

Table 1.1. Examples of biosensors for environmental water monitoring of different classes of pesticides. 31

Table 3.1.1. Docking results between bovine C*c*O (structure PDB: 5IY5) or yeast C*c*O (structure PDB: 8DH6) and the tested compound using the GOLD software. 89

Table S3.1.i. Docking results between chain A of C*c*O and the tested compound using the GOLD software. 99

Table S3.2.i. Genes whose expression decreases after exposure to CYM. 122

Table S3.2.ii. Genes whose expression increases after exposure to CYM. 125

Table S3.2.iii. List of proteins that changed their localization after treatment with CYM, when compared with nontreated cells. 130

Table 4.1. List of *S. cerevisiae* strains and plasmids used in this chapter. 148

Table 4.2. LoD and concentration of fungicides (carbendazim, copper, dimetomorph, metalaxyl and TEB) detected at environmental water samples analyzed by analytical methods. 158

Table S4.i. Mutator phenotype of *mlh1*Δ cells exposed to TEB. 166

Table S4.ii. Environmental water sample locations and characteristics. 167

Table S5.i. List of genes whose overexpression confers resistance to CYM. 182

Table S5. ii. List of genes whose overexpression confers sensitivity to CYM. 183

Table S5.iii. List of essential genes whose decreased abundance by mRNA perturbation confers resistance to CYM. 186

Table S5.iv. List of essential genes whose decreased abundance by mRNA perturbation confers sensitivity to CYM 187

CHAPTER 1 - General Introduction

This chapter is adapted from the following publication:

Filipa Mendes, Beatriz Machado, Bruno B. Castro, Maria João Sousa, Susana R. Chaves **The power of biosensors for environmental monitoring of pesticides in water.** *Manuscript in preparation*

1.1. Pesticides as an environmental problem

The world population has changed dramatically over the last few centuries. According to the United Nations, the world population increased from 2.5 billion in 1950 to 7.9 billion in 2021, representing over a threefold increase in half a century. The most recent projections suggest that the global population will reach approximately 8.5 billion in 2030 and 9.7 billion in 2050 (1). To sustain the ever-growing population, it was necessary to increase the production of essential commodities, particularly food. As a result, there has been a concomitant increase in the use of agrochemicals, particularly chemical fertilizers and pesticides (2).

A pesticide is a substance or a biological agent, or a mixture, that is intentionally released into the environment to prevent and control disease. On average, and at a global scale, between 10 to 28 % of crop production is lost to pests (3), and thus using pesticides for pest mitigation has become a widespread practice around the world, mainly due to their ability to increase crop yields and maintain food security. These substances are mainly used in agricultural (food production) or in public health protection programs (to prevent illnesses, such as malaria, dengue fever, and schistosomiasis), but also to improve and maintain non-agricultural areas like public urban green areas and sports fields (4,5).

Pesticides can be classified by their origin, composition or the target organism (functional classification) (**Figure 1.1**). According to their origin, pesticides can be broadly divided into natural or synthetic pesticides. Natural pesticides, also called biopesticides, are naturally occurring substances or agents that are obtained from animals, plants, and microorganisms. Due to their mild effects on the environment compared to their synthetic counterparts, use of biopesticides has been encouraged in recent years (6), namely within more sustainable practices such as integrated crop/pest management and organic farming (7,8). These naturally-derived compounds have emerged as eco-friendly alternative solutions to prevent and manage plant diseases and insect pests (9–11). However, these alternatives are extremely susceptible to climatic conditions, have a slow action and mild toxicity to the pathogens, explaining their lower effectiveness and the continued preference for non-natural pesticides (12,13). Synthetic pesticides, also known as chemical pesticides, are man-made chemicals, developed through chemical reactions. Pesticides of this type are widely used worldwide due to their efficient targeting of pests (14,15). According to their composition pesticides can be classified into inorganic and organic pesticides. Inorganic pesticides tend to be simpler and more soluble in water and normally include inorganic salts such as salts containing copper, ferrous sulfate, or sulfur. Organic pesticides can be synthetic or natural (16,17). Synthetic organic pesticides are more complex and less soluble in water than inorganic pesticides and can be categorized further according to the functional groups present,

leading to countless chemical families and subfamilies (18). According to their target organisms, pesticides can be classified into insecticides, herbicides, fungicides, bactericides, rodenticides, nematicides, and algicides (19). Indeed, this is the classification most frequently used when referring to pesticides.

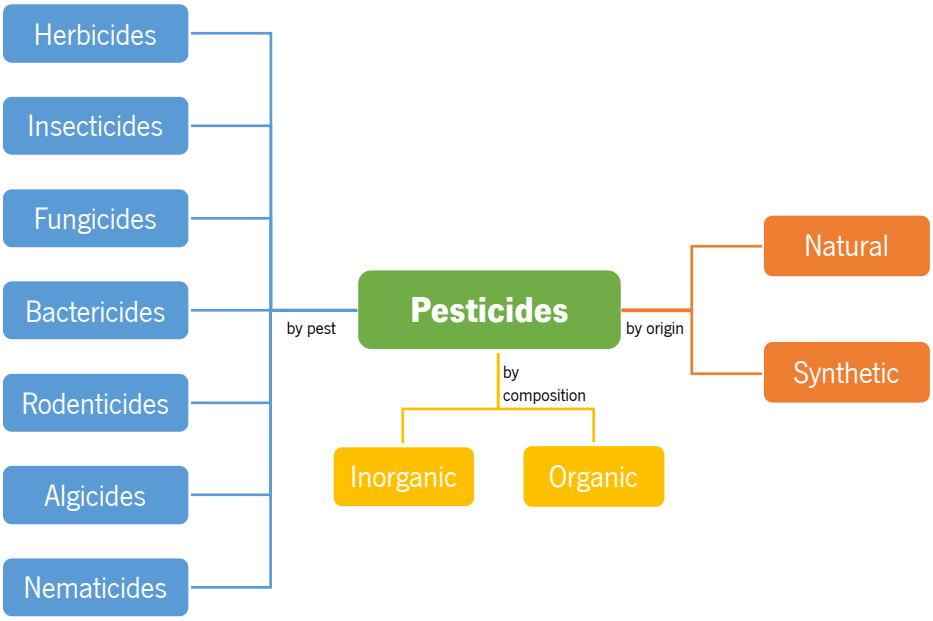

Figure 1.1. Schematic representation of pesticide classification. Pesticides are classified according to the target organism ("pest"), by their origin or by their chemical composition.

According to the Food and Agriculture Organization of the United Nations (FAO), primary crop production (cereals, sugar, vegetables and oil crops) grew 54 % between 2000 and 2021 (20), associated with an increase in the use of pesticides (**Figure 1.2**). Furthermore, there are concerns that the ongoing climate change will affect numerous crop-related processes (increased disease risk and pathogen resistance, augmented pesticide loss and inefficiency), leading to more frequent pesticide applications (21).

The latest data revealed that 3.54 million tonnes of pesticides were used in agriculture in 2021, which represents a 4 % increase relative to 2020. Herbicides were the dominant pesticide class (52 %), followed by fungicides and bactericides (25 %) and insecticides (22 %) (**Figure 1.2**); approximately 1 % consisted of other pesticides (rodenticides, plant growth regulators). Pesticide sales are heterogeneous across continents, with South America emerging as the largest contributor (29 %), followed by Asia (25 %), North America (22 %) and Europe (18 %). Moreover, the relative proportion of sales of each type of pesticide contrasts across continents. In North America, South America and Oceania, herbicides are

predominant and represent 60 to 70 % of total pesticide sales. In Europe, Africa and Asia, fungicides represent the highest percentages of sales [41 %, 34 % and 30 %, respectively (22)].

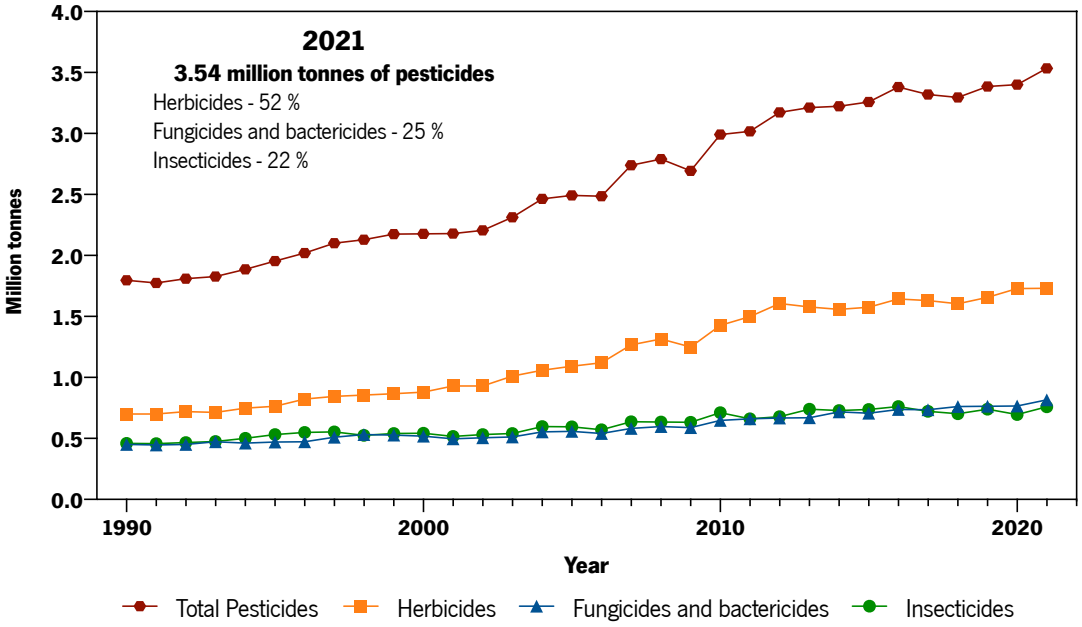

Figure 1.2. Global pesticide use. Worldwide agricultural consumption of total pesticides and by category (herbicides, fungicides and bactericides and insecticides) from 1990 to 2021, in million tonnes, and percentage data from 2021. Data retrieved from https://www.fao.org/faostat/en/#data/RP (assessed on 14 Nov 2023).

In summary, the use of pesticides has constituted the main strategy to minimize crop losses and maximize yields of intensive agriculture, essential to meet the escalating demands of food and resources of a growing global population. However, such a strong reliance on the application of pesticides is far from environmentally sustainable, and thus public concerns about their detrimental effects on ecosystems and human health have increased.

1.1.1. Impact of pesticides on aquatic environments

Pesticides enter the environment when they are applied to a target crop or disposed of, posing risks to non-target biota. Once released, the environmental fate of these chemicals can be affected by many factors, such as the properties of the soil (hydraulic loading, organic matter content, particle size distribution), but also the intrinsic properties of the pesticide, namely half-life, water solubility, adsorption coefficient and volatility (23,24). Pesticides can also move from target sites to other areas through leaching, adsorption, spray drift, volatilization, and runoff, thereby migrating across soil, air, and

groundwater (25,26). Indeed, it is estimated that approximately 0.1 % of applied pesticides reach the target site, while the main portion is lost via spray drift, run-off, and accumulation in off-target sites (27). Apart from being highly inefficient, pesticide application ultimately leads to accumulation of pesticide residues in the atmosphere, soil, water and biota. Aquatic ecosystems are the main sink for these residues via runoff, leaching and erosion processes; at the same time, aquatic life is particularly vulnerable to their effects (28–30). The vulnerability of aquatic ecosystems to pesticide pollution is clearly recognized in the Directive 2009/128/EC of the European Parliament and of the Council of 21 October 2009, which establishes a framework for Community action to achieve the sustainable use of pesticides (31).

In the aquatic ecosystems, the different types of pesticides (namely, insecticides, herbicides and fungicides) may induce deleterious effects at various levels. For instance, insecticides can cause genotoxic effects and alter fish swimming behavior (32–34). Using zebrafish as a model organism to study the toxicity of environmental contaminants in larval and embryo development (35), various studies reported that insecticides increase teratogenic effects and early stage mortality (32,33,36). Insecticides also significantly affect locomotion of invertebrates organisms, leading to a loss of movements and ultimately impairing their survival (33,34,36). Studies on the effect of insecticides on phytoplankton and aquatic microorganisms are limited, since they are considered less susceptible to these chemicals than other aquatic organisms, but inhibition of growth has been reported for some species (32,37,38). Herbicides have also been shown to be dangerous to aquatic life. For example, they can affect fish liver function by inducing enzymatic and metabolic changes, or cause alterations in fish swimming behavior, as well as teratogenic and genotoxic effects (39–42). Amphibians seem to be particularly susceptible to herbicides, since these substances can impact their development, growth, and movement, and exert genotoxic effects, ultimately affecting survival (41,43). These chemical compounds can also inhibit growth of aquatic microorganisms and algae, and in the former case, effects on carbon uptake and photosynthesis have also been reported (38,41–43). Additionally, these chemicals can interfere with the normal function of the reproductive system of aquatic organisms (44–46). Fungicides have been described to affect development and reproduction and induce oxidative stress and genotoxicity in fish (47–49), as well as growth, carbon uptake and photosynthesis in algae (38,50). Additionally, growth inhibition, biomass decrease, metabolic stress, and inhibition of sterol biosynthesis have been reported as negative effects of fungicides in aquatic microorganisms, particularly in non-target aquatic fungi (51). Overall, it has been demonstrated that pesticides have a negative impact on non-target aquatic organisms, ultimately affecting biodiversity (52,53).

Most of the studies mentioned investigated the impact of single pesticides and are often biased in terms of the tested substances or biological models. As aquatic environments can have a mixture of chemical compounds, aquatic organisms are often exposed to mixtures rather than just a single chemical. This is a research gap that needs to be addressed (33,41,48). Another important mismatch is the fact that research agendas on the ecological effects of pesticides do not align with sales or usage trends (22). Also, there is a clear bias in the specialized literature towards insecticides and herbicides in aquatic environments, as both surpass studies on the impacts of fungicide. Furthermore, most of the studies focus on the effects on vertebrates (particularly fish), invertebrates and primary producers, and the effect of pesticides on other aquatic organisms such as microorganisms is often overlooked. Indeed, this problem has already been recognized by several authors (22,51,54) that identify freshwater fungi as particularly susceptible to fungicides, for example.

In conclusion, the current risk assessment framework for pesticides in aquatic environments requires a more comprehensive characterization of their mechanisms of action on both target and non-target organisms. Moreover, the impact of pesticides on more ecologically relevant species needs to be addressed. Monitoring pesticides is also a valuable tool to preserve ecosystem health, safeguarding biodiversity, ensuring water quality, and mitigating potential human health risks associated with contaminated water sources. Continuous monitoring enables timely interventions when levels surpass acceptable limits and long-term monitoring provides crucial data to identify trends in pesticide contamination, recognize emerging concerns, and evaluate the efficacy of management practices and regulatory measures.

1.1.2. Monitorization of pesticides to mitigate risks

Water contamination by pesticides has become widespread, and pesticide residues are frequently detected in surface waters (55–59). Although aquifers are less vulnerable to pesticide contamination, pesticide residues have also been detected in groundwater (60–62). A study that compiled data on worldwide pesticide occurrence in surface waters reported concentrations between 7 ng L^{-1} to 121 μg L^{-1} in rivers and lakes. In wastewaters, concentrations ranged from 23 ng L^{-1} to 3.2 μg L^{-1}, similar to levels observed in groundwater (20 ng L^{-1} to 1.1 μg L^{-1}) but lower than those in drinking water (141 ng L^{-1} to 14.6 μg L^{-1}) (63). A review about the detection of pesticides in worldwide surface waters identified a total of 15 insecticides, 14 herbicides and 10 fungicides. Among these, the most frequently identified were the herbicides atrazine and metolachlor, the insecticides dimethoate and chlorpyrifos, and the

fungicides tebuconazole and carbendazim (29). In European surface waters, a comprehensive meta-analysis showed higher median concentrations for fungicides (0.96 μg L^{-1}) compared to herbicides (0.063 μg L^{-1}) and insecticides (0.034 μg L^{-1}) (64).

Despite the widespread presence of pesticides, legislation for pesticide limits in water is still very scarce, and some countries do not establish maximum residue levels for pesticides in surface waters or groundwaters. In the European Union, the Drinking Water Directive 98/83/EC sets a maximum concentration of 0.1 μg L^{-1} for each individual pesticide and their degradation products and 0.5 μg L^{-1} for the sum of all pesticides present in a sample (65). Furthermore, the Water Framework Directive [Directive 2000/60/EC of the European Parliament and of the Council of 23 October 2000, establishing a framework for Community action in the field of water policy (66)] and its follow-up [Directive 2008/105/EC of the European Parliament and of the Council of 16 December 2008 on environmental quality standards in the field of water policy (67)], set limits for some individual substances (priority substances and other specific pollutants). Moreover, the new European Union Directive 2020/2184 for the quality of water intended for human consumption recommends a risk-based approach for pesticide monitorization, specifically emphasizing the identification of pesticides likely to be present in a given environment (68).

Analyzing pesticide residues in aquatic samples faces the challenges of identification and quantification of hundreds of compounds with distinct physicochemical properties. Given that pesticide concentration in water is commonly low, at levels of μg L^{-1} or ng L^{-1}, employing ultra-sensitive analytical methods is essential. Thus, analytical methods based on advanced separation and detection techniques such as gas chromatography or liquid chromatography along with mass spectrometry are the conventional and most frequently used tools for identification and quantification of pesticides in aquatic environments (69). Analysis of environmental water samples with these techniques requires a previous concentration step to increase the amount of analyte and method sensitivity. Additionally, more complex water samples (e.g., wastewaters, aquaculture waters) require a clean-up step to eliminate interferences. Therefore, sample preparation is the most limiting step of the entire analytical process (70). Various sample preparation methods have been used for analysis of organic pollutants in water samples such as liquid-liquid extraction or solid-phase extraction. However, these techniques require the use of toxic organic compounds, and thus solventless methods, such as solid-phase microextraction, or liquid-phase microextraction, among others, have been pursued (69–71).

The analytical method used depends on whether the goal is detection (screening method), quantification (determinative method), or confirmation of the presence (confirmatory method) of a

potential compound (70). It is also based on characteristics of the compounds analyzed. Therefore, gas chromatography-mass spectrometry has been primarily used as the main analytical technique for multi-residue analysis of non-polar and volatile pesticides like organochlorines. In contrast, products with more polar structures and low volatility, mainly herbicides, fungicides and some insecticides, have been analyzed using liquid chromatography coupled to tandem mass spectrometry as the preferred analytical method (69,70,72). Although these methods are reliable and extremely sensitive, offering low detection limits (ng L^{-1}), they present several drawbacks. They are time-consuming, expensive, and most do not align with green chemistry practices due to the requirement for sample preparation involving solvents. Additionally, the need for highly trained technicians and complex procedures prevents implementation in low-tech local laboratories (72–74). Thus, newer and more suitable methodologies, with the ability to monitor the increasing number of relevant analytes as quickly and cheaply as possible, are being developed (75). This would allow detection of these pollutants resourcing to fast, cost-effective and disposable systems to be used in extensive monitoring programs. In this context, biosensors have demonstrated a great potential and thus appear as an alternative or a complementary tool for detection and quantification of environmental contaminants.

1.2. Biosensors as a tool to screen pesticides in water

A biosensor, according to the International Union of Pure and Applied Chemistry (IUPAC), is a self-contained integrated device capable of measuring chemical and biological reactions and providing quantitative or semi-quantitative information (76). Biosensors operate on the principle of specific biological-recognition and contain three main features: a bio-recognizing element, a transducer, and a signal processing system (**Figure 1.3**). The bio-recognition element interacts with the sample target analyte, generating a biochemical signal that is subsequently converted into a quantifiable signal by the transducer element; then, the processing system translates it into a readable format. The generated signal is therefore related to the concentration of the analyte in the reaction (75,77). Generally, biosensors are classified according to (i) the transduction method used for detection or (ii) the biological receptor used as a recognition element. According to the former, biosensors can be classified as optical, electrochemical, piezoelectric, or calorimetric. Most biosensors reported in the literature are electrochemical or optical. According to the bio-recognition element, biosensors can be classified as enzymatic, immunosensors, aptasensors or whole cell-based (78–80).

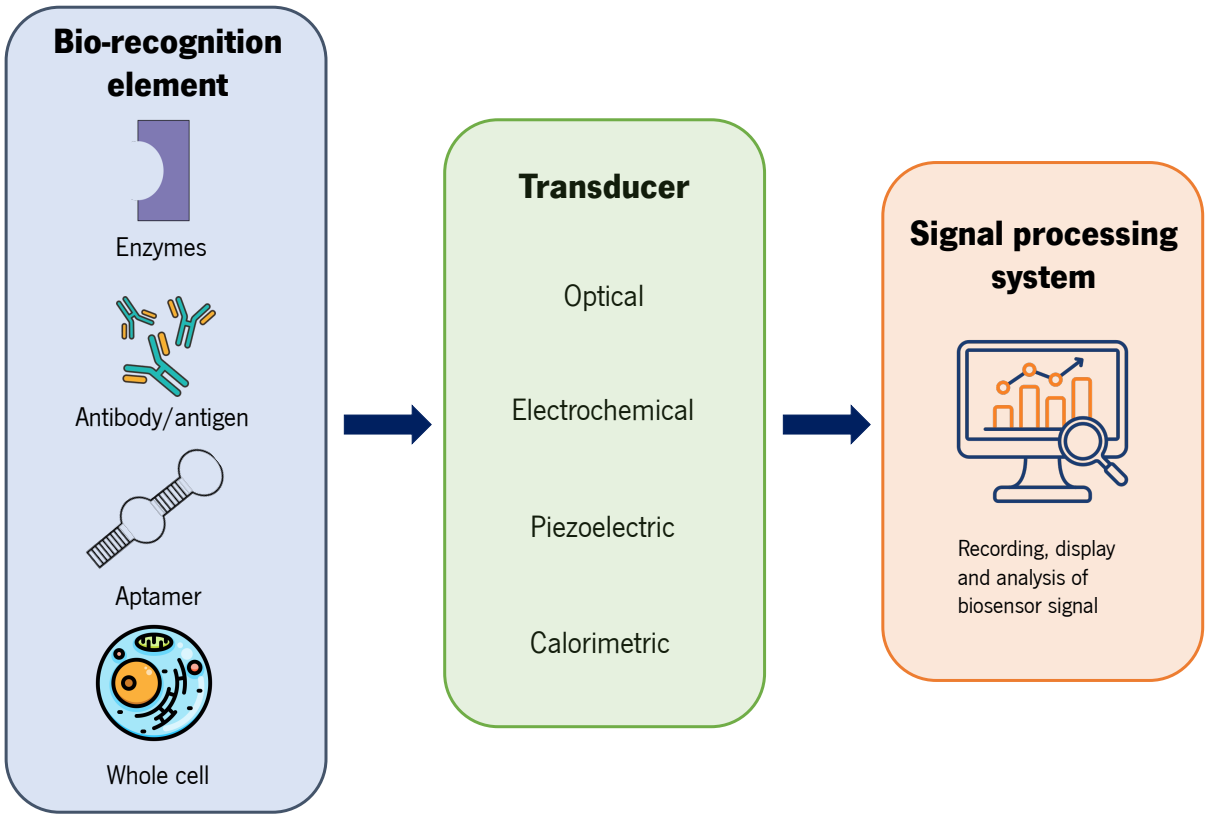

Figure 1.3. General structure of a biosensor. Target analyte is recognized by the biological recognition element, leading to an alteration that is detected and converted into a measurable signal by the transducer.

Over the years, biosensors have been employed in different fields such as food quality monitoring, pathogen and drug discovery, disease detection and environmental monitoring [reviewed in (81–84)]. Due to their advantages over classical methods, a plethora of biosensors have been developed for environmental monitoring of a variety of pollutants such as pesticides (**Table 1.1**), phenols, metals, and endocrine-disrupting chemical compounds. Biosensors are simple in operation and less labor-intensive than chemical methods, enabling minimal sample preparation when measuring pollutants in complex matrices. Moreover, they offer the possibility of portability, miniaturization, on-site detection, and are faster and more cost-effective than conventional methods. Biosensors can also be more sensitive than chemical methods (80,85). In recent years, the incorporation of nanotechnology and nanomaterials into biosensors have revolutionized and accelerated their development. The use of nanotechnology and nanomaterials enhances selectivity, sensitivity, and performance, making analysis more efficient, easy, fast, and economical, with improved accuracy and robustness (86). Diverse nanomaterials such as metal nanoparticles (e.g., silver and gold nanoparticles), graphene and graphene-based nanocomposites, carbon nanotubes, quantum dots and magnetic nanoparticles among others, are often used in biosensors as sensing elements (87,88).

The next sections provide an overview of the use of enzymatic, immunosensors, aptasensors and whole cell-based biosensors for environmental water monitoring of different classes of pesticides (**Table 1.1**).

Table 1.1. Examples of biosensors for environmental water monitoring of different classes of pesticides. For each example the pesticide class (insecticide, herbicide or fungicide), pesticide name, the biosensor type (enzymatic, Immunosensor, aptasensor or whole cell), transducer, sample matrix used to test biosensor applicability and limit of detection (LoD) are indicated.

Pesticide		Biosensor Type	Transducer	Sample Matrix	LoD	Reference
Insecticide	**Acetamiprid**	Aptasensor	Optical	Wastewater and tap water	0.3 nM	(89)
	Carbofuran	Enzymatic (enzyme: AChE[1])	Electrochemical	Seawater	1E-12 g L^{-1}	(90)
	Chlorpyrifos	Enzymatic (enzyme: Tyrosinase)	Electrochemical	Tap and river water	3 nM	(91)
		Aptasensor	Optical	River water	0.2 µM	(92)
		Whole cell (*Escherichia coli* cells expressing a chpR vector and a vector containing the chpA promoter fused with formylglycine-generating enzyme (FGE)–sulfatase system)	Optical	Sea water and wastewater treatment plants	5 nM	(93)
	Diazon	Aptasensor	Electrochemical	River water	11 fmol L^{-1}	(94)
	Imidacloprid	Immunosensor	Electrochemical	Tap water	22 pmol L^{-1}	(95)
		Aptasensor	Electrochemical	Wastewater	0.19 ng mL^{-1}	(96)
	Isocarbophos	Aptasensor	Optical	Tap water	0.81 nM	(97)
	Malathion	Aptasensor	Optical	River and tap water	0.465 nM	(98)
	Paraoxon (parathion metabolite)	Enzymatic (enzyme: AChE)	Electrochemical	Tap water	0.5 nM	(99)
		Enzymatic (enzyme: BChE)	Electrochemical	Tap water	0.212 µM	(100)
		Enzymatic (AChE and CHO[2])	Optical	Irrigation water	4.7 ppb	(101)

Insecticide	**Paraoxon (parathion metabolite)**	Whole cell (Organophosphorus hydrolase expression onto the periplasmic space of *Escherichia coli*)	Optical	Tap water	5 μM	(102)
		Whole cell (Organophosphorus hydrolase expression on the cell surface space of *Moraxella* sp.)	Electrochemical	Lake water	0.1 μM	(103)
	Paraoxon-methyl	Whole cell (*Chlorella vulgaris*)	Electrochemical	-	-	(104)
	Parathion	Enzymatic (enzyme: AChE)	Optical	Tap and seawater	0.7 ppm	(105)
	Thiamethoxam	Aptasensor	Optical	Lake water	1.23 nM	(106)
	Carbofuran Chlorpyrifos	Enzymatic (enzyme: AChE)	Electrochemical	Tap and lake water	5E-13 M (carbofuran) 5E-14 M (chlorpyrifos)	(107)
	Demeton Dichlorvos	Enzymatic (enzyme: AChE and CHO)	Optical	Lake water	0.32 μg L^{-1} (demeton) 8.1E-3 μg L^{-1} (dichlorvos)	(108)
	Fipronil Fipronil-desulfinyl Fipronil-sulfide Fipronil-sulfone	Immunosensor	Optical	River water	2.04 mg L^{-1} (fipronil) 2.98 mg L^{-1} (fipronil-desulfinyl) 3.05 mg L^{-1} (fipronil-sulfide) 3.69 mg L^{-1} (fipronil-sulfone)	(109)
	Malathion Trichlorfon	Enzymatic (enzyme: AChE)	Electrochemical	Tap water	0.032 μg L^{-1} (malathion) 0.001μg L^{-1} (trichlorfon)	(110)
	Carbaryl Diazinon Malathion Phorate	Enzymatic (enzyme: AChE)	Optical	River water	0.1 μg L^{-1} (carbaryl) 0.1 μg L^{-1} (diazinon) 0.3 μg L^{-1} (malathion) 1 μg L^{-1} (phorate)	(111)
	Carbaryl Carbofuran Carbosulfan Isoprocarb Propoxur	Immunosensor	Optical	Surface water samples	2.5 ng mL^{-1} (carbaryl) 0.1 ng mL^{-1} (carbofuran) 4.2 ng mL^{-1} (carbosulfan) 0.1 ng mL^{-1} (isoprocarb) 0.02 ng mL^{-1} (propoxur)	(112)

Herbicide	**Ametryn**	Aptasensor	Optical	Wastewater and sewage treatment plant	0.15 μg L^{-1}	(113)
	Atrazine	Immunosensor	Electrochemical	Drinking water	0.011 ng mL^{-1}	(114)
		Aptasensor	Electrochemical	River water	0.1 pM	(115)
	Chlortoluron	Immunosensor	Electrochemical	Groundwater	22.4 ng L^{-1}	(116)
	Dicamba	Immunosensor	Optical	Surface water samples	0.24 ng mL^{-1}	(117)
	Diuron	Whole cell (*Chlamydomonas reinhardtii*)	Electrochemical	-	0.2 mM	(118)
	Glyphosate	Enzymatic (enzyme: urease)	Electrochemical	Tap water	0.5 ppm	(119)
		Immunosensor	Optical	Bottled and tap water	10 pg mL^{-1}	(120)
	Paraquat	Aptasensor	Optical	Tap water	16.5 μg·L-1	(121)
	Triazine	Whole cell (*Arthrospira platensis*)	Electrochemical	Effluent and wastewater treatment plant samples	1.00E-13 μM	(122)
Fungicide	**Carbendazim**	Aptasensor	Electrochemical	River and tap water	0.2 fmol L^{-1}	(123)

1 AChE – Acetylcholinesterase
2 CHO – Choline Oxidase

1.2.1. Enzyme-based biosensors

Enzymatic biosensors were the first class of biosensors to be developed. In 1962, Clark and Lyons developed the first 'true' biosensor for glucose detection, by incorporating the enzyme glucose oxidase into a Clark oxygen electrode (124). Since then, enzyme-based biosensors have been the most used and well-studied type of biosensors (125). In enzyme-based biosensors, the analyte serves as the substrate for the enzymatic reaction and detection occurs through its outcome (126).

Among the distinct groups of enzymes, the cholinesterase group, particularly acetylcholinesterase (AChE), is the most widely used in pesticide biosensing. This enzyme exhibits sensitivity to a broad spectrum of chemical compounds, including organophosphate and carbamate pesticides. Hence, AChE is a pivotal component in biosensing assays targeting these compounds (79,127). Yang et al. (99) developed an enzyme-based biosensor for the amperometric detection of the paraoxon, metabolite of the organophosphorus insecticide parathion. In this study, AChE was encapsulated into in a silica matrix immobilized onto a glassy carbon electrode modified with gold nanoparticles, polypyrrole, and reduced graphene oxide sheets. The developed biosensor was tested in solutions with the substrate (acetylthiocholine chloride), both with and without paraoxon. In samples without paraoxon, acetylthiocholine chloride is hydrolyzed by AChE into thiocholine, resulting in a higher electrocatalytic activity due to its oxidation. In contrast, the enzymatic reaction is inhibited in the presence of paraoxon, leading to a reduced electrocatalytic activity (**Figure 1.4A**). Biosensor activity was further tested in tap water samples spiked with paraoxon, yielding a detection limit of 0.5 nM. Along with AChE, butyrylcholinesterase, aldehyde dehydrogenases, phosphatases and tyrosinases are also inhibited by organophosphate and carbamate pesticides and, thus, are also used in enzyme-based biosensors to monitor these chemical compounds (80,128).

Generally, only one enzyme is used, but the combined effect of several enzymes can yield better results in some cases, broadening the spectrum of detected analytes. A recent work developed a biosensor composed by two enzymes, AChE and choline oxidase (CHO), and gold nanorods. In the presence of AChE and CHO, the substrate acetylcholine is catalyzed to generates H_2O_2, leading to the etching of gold nanorods. In the presence of organophosphorus pesticides, the activity of AChE is inhibited, preventing generation of H_2O_2 and the etching of gold nanorods. Etching of the gold nanorods leads to distinct colors that are recorded with an UV spectrophotometer (**Figure 1.4B**). Biosensor applicability was tested in lake water samples spiked with dichlorvos and demeton, and detection limits of 8.1×10^{-3} μg L^{-1} and 0.32 μg L^{-1}, for dichlorvos and demeton, respectively, were observed (108). More

examples of enzyme-based biosensors, specific for environmental water monitorization of pesticides, are summarized in **Table 1.1**, highlighted in orange.

Enzyme-based biosensors are rapid, user-friendly, and easily automatized, facilitating scalability. Moreover, they are very sensitive, allowing for detection of analytes even at low concentrations. This can be explained by the high catalytic activity and wide availability of enzymes for a variety of functions and substrates (129–131). However, enzyme production is highly costly, and enzymes have limited stability as they are susceptible to degradation or denaturation, which affects biosensor performance and longevity. Additionally, enzymatic activity can be influenced by the presence of various compounds, pH, temperature, and other environmental conditions, affecting biosensor selectivity, accuracy, and reliability (130,132).

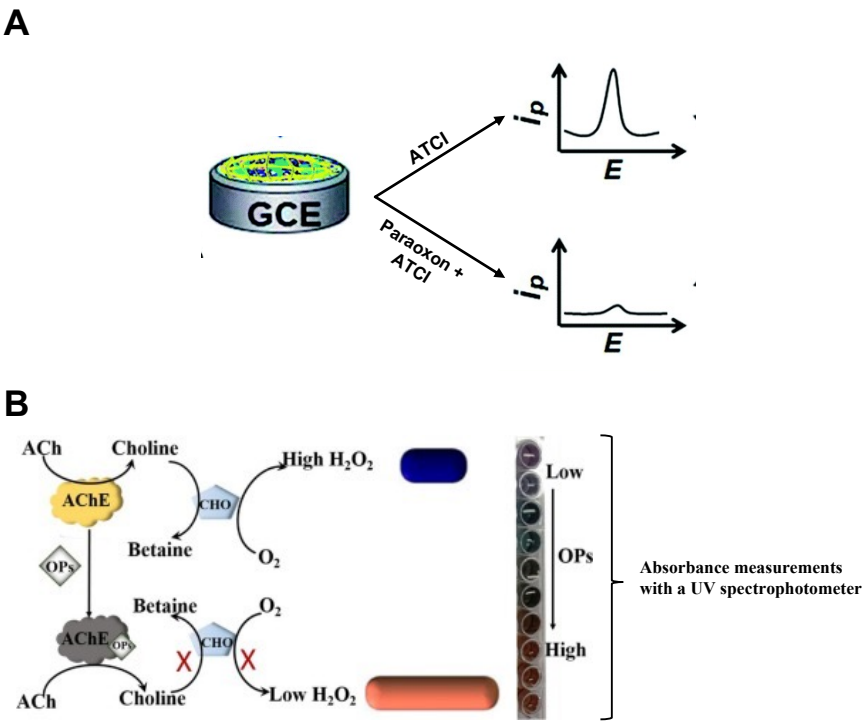

Figure 1.4. Schematic representation of enzyme-based biosensors. A) Application of the enzymatic biosensor for the electrochemical detection of paraoxon, based on AChE inhibition and thiocholine electrocatalytic activity, adapted from (99). **(B)** Organophosphorus pesticides (OPs) detection, based on the inhibition of AChE enzyme and etching of gold nanorods, adapted from (108).

1.2.2. Antibody-based biosensors

Antibody-based biosensors, also called immunosensors, depend on a reaction between an antigen and an antibody, thus the bio-recognition element is the antigen-antibody complex. The formation of this complex generates a read-out signal further detected by a transducer (81,133). By definition, an antigen is a molecule that elicits an immune response and is capable of combining with the specific antibody. The first step in developing an immunosensor is the production and isolation of antibodies to the desired analyte. Then, it needs to be integrated into an assay system that generates a visible reaction (134–136).

Immunosensors are generally classified into label-free and labeled sensors. Label-free immunosensors measure the physical changes as a result of the antigen-antibody complex formation. The binding event can lead to alterations in mass, refractive index, conductivity, or other characteristics which are then detected and transduced into measurable signals by the sensor system. In contrast, labeled immunosensors use signal-producing labels (such as enzymes, fluorescent dyes or electroactive compounds) attached to the target analyte or the bioreceptor so that the activity of the marker is linked to the amount of analyte, allowing for a more sensitive and versatile detection (81,135).

Immunosensors provide an easy, rapid, and high-throughput method for pesticide detection with greater accuracy, specificity, and sensitivity than traditional methods. However, the production of antibodies is laborious, highly costly, and challenging, and alterations of temperature or pH can affect immunosensor performance (133). Moreover, antibody cross-reactivity with similar analytes is commonly observed, potentially leading to false positive results. The need to develop specialized reagents for each compound is also a weakness of immunosensors. Therefore, development of broad-specificity antibodies can be the solution. In this case and based on a similar structure of a group of molecules, an antibody with broad cross-reactivity, capable of detecting multiple analytes, is produced. Antibodies with this broad detection spectrum are an attractive approach for multi-residue monitoring (136). For instance, Li and co-workers (109) developed a broad-specificity antibody for detection of the pesticide fipronil and three major metabolites (fipronil-sulfone, fipronil-sulfide and fipronil-desulfinyl). Then, using an antibody-based immunoassay, namely the enzyme-linked immunosorbent assay, authors were able to detect fipronil and its metabolites in river water with a detection limit varying from 2.04 $\mu g\ L^{-1}$ to 3.69 $\mu g\ L^{-1}$, depending on the metabolite. More examples of immunosensors for environmental water monitorization of pesticides are presented in **Table 1.1**, highlighted in red.

1.2.3. Aptamer-based biosensors

Aptamer-based biosensors, also known as aptasensors, use aptamers as bio-recognition elements. An aptamer is an artificial and short (10-100 nucleotides in length) single-stranded DNA or RNA sequence that displays a specific tertiary structure through folding. They are obtained by an *in vitro* screening called Systematic Evolution of Ligands by Exponential Enrichment (SELEX), and are therefore often named "chemical antibodies" (137). The SELEX methodology involves three main steps: (i) incubation of the target analyte with a library; (ii) selection of aptamer–target complexes from unbound oligonucleotides; and (iii) amplification of the bound sequences. Briefly, a random library of single-stranded nucleic acids (DNA or RNA) is incubated with the target analytes. After incubation, unbound variants are eliminated, and the target-bound oligonucleotides are amplified through PCR and used in the following rounds of SELEX. After several rounds (8–15), sequences with a higher affinity for the target analyte become dominant in the library. Finally, the sequences are analyzed, and the highest prevalence sequence is identified as the potential aptamer (138–140).

Aptamers interact with their target molecules similarly to how an antigen interacts with an antibody. However, aptasensors have several advantages compared to biosensors using natural receptors such as antibodies or enzymes. Aptamers have a unique tertiary structure such as hairpins, internal loops, pseudoknots, T-shaped structures, and G-quadruplexes, allowing them to bind to any given target, ranging from small molecules to large proteins and even cells, thus making it possible to develop a wide range of aptamer-based biosensors. Unlike the preparation of antibodies, which require biological systems to be generated, aptamers can be easily produced via chemical synthesis, which offers a higher specificity and affinity with the target and eliminates the use of animals. Such production decreases batch-to-batch variations, and reduces the cost and time needed for production. Furthermore, aptamers are more structurally and functionally stable over a wide range of pH and temperatures (137,141,142). Similar to immunosensors, aptasensors can also be functionalized with enzymes or fluorescent probes, and are thus further categorized as label-free or labeled aptasensors (143).

In the past few years, considerable time and effort have been dedicated to aptamer screening and aptasensor development. Thus, research in this field has significantly expanded, culminating in the development of aptasensors for pesticide monitoring. Several aptamers have already been developed to selectively recognize various types of pesticides, such as organochlorines, organophosphates, neonicotinoids, and others [reviewed in (144)]. For example, Zeng et al. (121) developed an aptamer-based biosensor for detection of the herbicide paraquat, based on the oxidation of 3,3′ ,5,5′ -tetramethylbenzidine (TMB) by Ag^{+}. When the paraquat-aptamer (PQ-15 aptamer) is in the presence of

Ag^{+}, the electron transfer from the aptamer-Ag^{+} complex to dissolved oxygen increases, enhancing the release of superoxide anion radicals (O_2) and facilitating the oxidation of TMB, resulting in a dark blue solution. On the other hand, in the presence of paraquat, the PQ-15 aptamer preferentially binds to paraquat to form a more stable complex. This decreases the catalytic activity of Ag^{+}, leading to less TMB oxidase and a light blue or colorless solution. The absorbance of solutions is recorded with a UV/VIS spectrophotometer (**Figure 1.5A**). The authors tested the aptasensor selectivity for other pesticides, but it was specific for paraquat, with a detection limit of 16.5 µg L^{-1}. The color shift based on gold nanoparticles aggregation is widely used in aptasensors (92,113,145). Briefly, in the absence of the target molecules, aptamers and a destabilizing agent, such as NaCl, prevents aggregation of gold nanoparticles and the solution remains red. In contrast, in the presence of the analyte, aptamers dissociate from gold nanoparticles to bind to their specific target, leading to gold nanoparticle aggregation and color change, even in the presence of a destabilizing agent. The absorbance of solutions is measured with a UV/VIS spectrophotometer (92). **Figure 1.5B** provides a schematic representation of this mechanism, used for detection of chlorpyrifos. More examples of aptasensors for environmental water monitorization of pesticides are displayed in **Table 1.1**, highlighted in green.

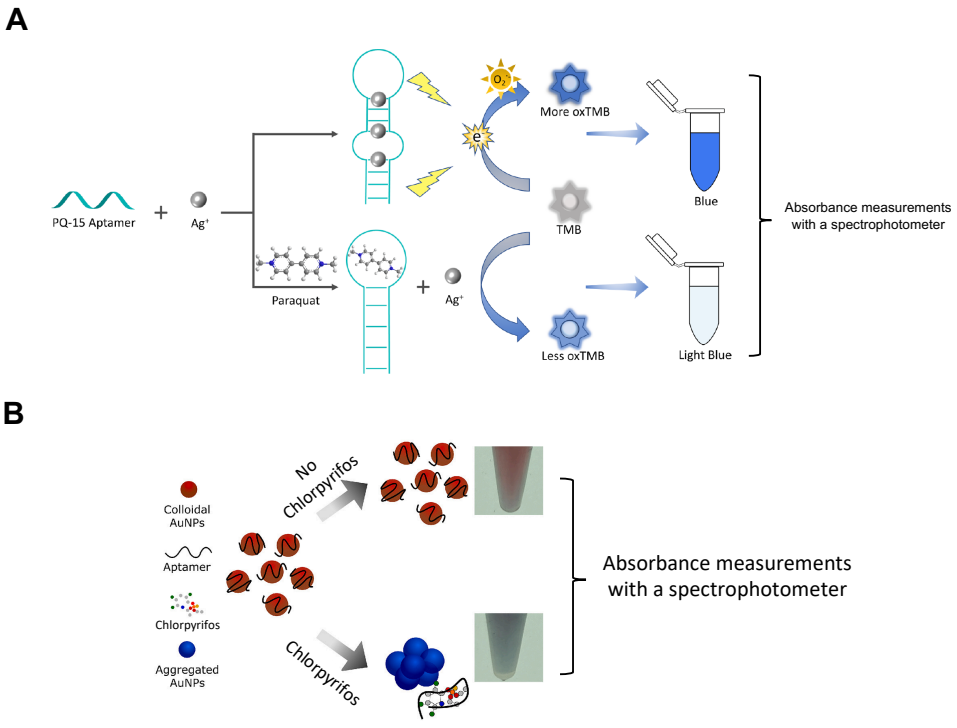

Figure 1.5. Schematic representation of aptasensor examples. A) Application of the aptamer-based biosensor for detection of the herbicide paraquat, based on the oxidation of TMB, by Ag+. Adapted from (121). **(B)** Aptasensor for chlorpyrifos detection in water samples, based on color shift gold nanoparticles aggregation, adapted from (92).

1.2.4. Whole cell-based biosensors

Instead of using isolated molecules, such as enzymes, antibodies, or aptamers, living cells can also be used as biorecognition elements, denominated as whole cell-based biosensors. Different types of cells, from bacteria, yeast and other fungi to higher eukaryotes like fish, rats, and human cells, have been used in biosensor development. Algae and microbial cells, namely bacteria, yeast and other fungi, are predominantly used in biosensors for environmental monitoring and to assess toxicity of environmental contaminants. In contrast, higher eukaryotic cell lines play significant roles in exploring fundamental cellular processes and comprehending disease development (146).

Whole cell-based biosensors can operate in two ways: by employing the inherent ability of a particular microorganism to respond to specific substances or by incorporating specially engineered genetic constructs into the organism to detect bioavailable analytes (146,147). Biosensors using the natural sensing abilities of cells offer advantages in detecting a variety of compounds. However, they are more vulnerable to interference from other species. Hence, engineered biosensors can be used as an alternative (147). For example, Kim and colleagues (102) developed an engineered biosensor for detection of paraoxon. They used recombinant *E. coli* cells expressing the organophosphorus hydrolase enzyme at the periplasmic space. In the presence of paraoxon, the enzyme catalyzes its hydrolysis into *p*-nitrophenol and diethylphosphoric acid, then absorbance of *p*-nitrophenol is measured, which is directly correlated with paraoxon concentration.

Reporter gene expression under the control of a specific promoter is another powerful readout used in microbial engineered biosensors. Upon exposure to the target, the promoter is activated, inducing or increasing the expression of the reporter gene. Then, this biological response is converted into a detectable signal via a transducer (78,148,149). The typical reporter genes used in microbial biosensors are firefly luciferase, calreticulin, β-galactosidase, Green Fluorescent Protein (GFP), and bacterial luciferase (150,151). However, other reporter genes can also be used. For instance, Chouichit et al. (93), developed a whole cell reporter system for detection of chlorpyrifos. First, they identified the *Sinorhizobium meliloti* chpA promoter as highly induced by chlorpyrifos and dependent on the chlorpyrifos-responsive transcription regulator (ChpR) (152). Then, they engineered *E. coli* cells with a chpR expression vector and a plasmid encoding the chlorpyrifos responsive promoter (chpA) fused with formylglycine-generating enzyme (FGE)–sulfatase system. Therefore, when cells are exposed to chlorpyrifos, ChpR activates the expression of the FGE–sulfatase system via the chpA promoter. Then, the FGE modifies a serine residue of the sulfatase, resulting in the formation of the activated sulfatase [formylglycine (fGly)], which cleaves the 4-methyllumbeliferone sulfate (4-MUS) to produce the

fluorescent product 4-methyllumbeliferone (4-MU) (**Figure 1.6**) (153). The authors were able to detect chlorpyrifos in spiked sea water and wastewater treatment plant samples, with a detection limit of 5 nM, with the same system but using a plasmid that overexpressed ChpR (93). More examples of whole cell-based biosensors, specific for environmental water monitorization of pesticides, are summarized in **Table 1.1**, highlighted in light blue.

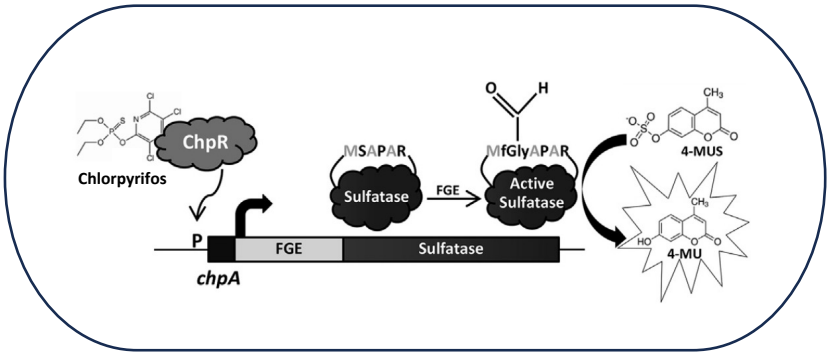

Figure 1.6. Schematic representation of the whole cell-based biosensor for environmental water monitoring of the chlorpyrifos insecticide. Adapted from (153).

Whole cell systems may provide a reliable alternative to molecular biosensors, since they are relatively easy to develop and are able to metabolize a wide range of chemical compounds, since the necessary cofactors are already present intracellularly. Thus, there is no need to isolate subcellular components like enzymes or proteins. Moreover, microbial biosensors can be massively produced through simple culturing steps, and have a higher stability over a wide range of environmental changes, including alterations in temperature and pH, and can be modified through simple genetic engineering methods (149,154,155). Additionally, this type of biosensors can not only detect specific analytes but also offer additional information that molecule-based biosensors cannot provide, such as information related to the pharmacology, cell physiology alterations and toxicology of the sample (149). Nevertheless, preserving cell activity and viability under adverse environmental conditions can limit the use of whole cell-based biosensors. Moreover, when using genetically engineered biosensors, a prolonged response is often required for expression of the reporter gene, representing a significant limitation for biosensors aiming for real-time detection (146,156).

Along with the microbial biosensors that use bacteria as biorecognition elements, the yeast-based systems, especially those using *Saccharomyces cerevisiae*, can also be a promising alternative (157,158). The yeast *S. cerevisiae* is a particularly interesting model for biosensing strategies due to its resistance to harsh conditions, suitability for fast high-throughput functional genomics to identify specific

traits, and amenability to genetic manipulation (159,160). Indeed, biosensors based on this fungal model have already been used to detect endocrine disruptive substances (161–163). Nonetheless, despite its potential and the invaluable add-on to the available analytical toolbox, yeast-based biosensing is still underexplored. Expanding the range of compounds detected by yeast-based biosensors could lead to a comprehensive and more efficient environmental monitoring, allowing for much needed streamlined monitoring of environmental contaminants.

1.3. Understanding pesticide toxicity mechanisms

As mentioned in previous sections, a significant portion of agrochemicals lack sufficient toxicological data. Current toxicity testing methods are based on extensive animal testing, which is time-consuming, expensive and inadequate to meet the challenge of current requirements for toxicity assessment of a high volume of compounds (164). Therefore, it is crucial to develop novel and more efficient approaches. The use of biological models with well-known and conserved cellular and molecular processes is highly advantageous to study pesticide toxicity and seek mechanistic explanations. Depending on the study model, exposure effects of pesticides can be extrapolated to microbial, plant and animal targets, covering risks to both environmental and human health.

Recent advances in post-genomic techniques have greatly enhanced classical toxicological studies, enabling a shift towards mechanism-centered analyses at the genome-wide level. In this context, toxicogenomics has emerged as a novel transdisciplinary field that integrates the traditional toxicological studies with genome-wide approaches, known as omics (164,165). Toxicogenomic studies collect, analyze, and interpret data on changes in gene expression, protein activity and functional alterations in response to environmental stressors, drugs, and other toxicants. By employing high-throughput molecular profiling techniques and computational tools to handle the vast amount of resulting data, toxicogenomics moves from studying a few genes of interest under a given condition to investigate changes across whole genomes (genomics), transcriptomes (transcriptomics), proteomes (proteomics), and metabolomes (metabolomics) (164,166,167). Phenomics, also termed functional genomics, aims to uncover gene function by identifying the phenotypes associated with gene mutants under different conditions (165). Together, these subfields contribute to the understanding of biological systems and their responses to environmental stressors and other toxicants.

1.3.1. The yeast *S. cerevisiae* as a tool to unveil toxicity mechanisms

Toxicogenomic studies typically rely on the use of model organisms selected for their genetic tractability, short generation time, and well-characterized biology, which allow researchers to efficiently study complex biological processes and mechanisms of toxicity. Several model organisms can be used in toxicogenomic studies, including the mouse *Mus musculus*, the zebrafish *Danio rerio*, the plant *Arabidopsis thaliana*, the arthropods *Drosophila melanogaster* and *Daphnia magna*, the nematode *Caenorhabditis elegans*, and the budding yeast *S. cerevisiae*. Each organism offers unique advantages and capabilities for studying different aspects of toxicology (168).

The budding yeast *S. cerevisiae* is a well-established eukaryotic model organism that has been one of the most used in toxicogenomic studies. There are several key features that make yeast such a powerful model system: (1) it is a unicellular, nonpathogenic microorganism with rapid and inexpensive growth; (2) genome-wide analyses are easily implemented due to the vast array of experimental tools and protocols available; (3) it exhibits a strikingly high level of functional conservation with lower and higher eukaryotes, including humans; and (4) has public databases, namely the *Saccharomyces* Genome Database (SGD), which offer integrated biological information for the budding yeast *S. cerevisiae* and analysis tools to explore these data, enabling the discovery of functional relationships between sequence and gene products in fungi and higher organisms (169–172).

A major breakthrough in studies on the mechanism of action and toxicity of chemical compounds was the development of high-throughput screening assays using yeast strain collections, also named libraries, that were constructed systematically, in which each gene is modified in a similar manner to enable genome-wide studies (173). These collections have been used extensively in functional toxicogenomic screens, to uncover the biological function of genes and proteins involved in the response of an organism to an adverse external event, establishing a direct link between genes and toxicants (164,174). Usually, this type of studies can be performed using:

(i) a homozygous or knockout deletion collection, where non-essential genes are individually knocked out, leading to a complete loss of function. This allows the identification of biological functions that are affected by a given stress or reveals crucial genes for conferring stress resistance (**Figure 1.7A**) (165,174);

(ii) a heterozygous deletion collection, with partial loss of gene function. This allows the identification of molecular targets, since decreasing the gene dosage increases its susceptibility (**Figure 1.7A**) (165,174);

(iii) a multicopy or overexpression collection, which allows the identification of genes that, when overexpressed, can confer resistance to toxicants (**Figure 1.7A**) (165,174).

Since the growth rate of yeast cells can be easily measured, it is often used as an indicator of cellular fitness within yeast mutant collections. Evaluating the fitness of strains following exposure to toxicants can be performed individually in non-competitive assays (**Figure 1.7B**). Alternatively, mutant collections can be "barcoded," enabling the analysis of individual strain fitness in competitive assays conducted in pooled cultures, with fitness assessed by determining the abundance of the different mutant strains using the "barcode" (**Figure 1.7C**) (165,175).

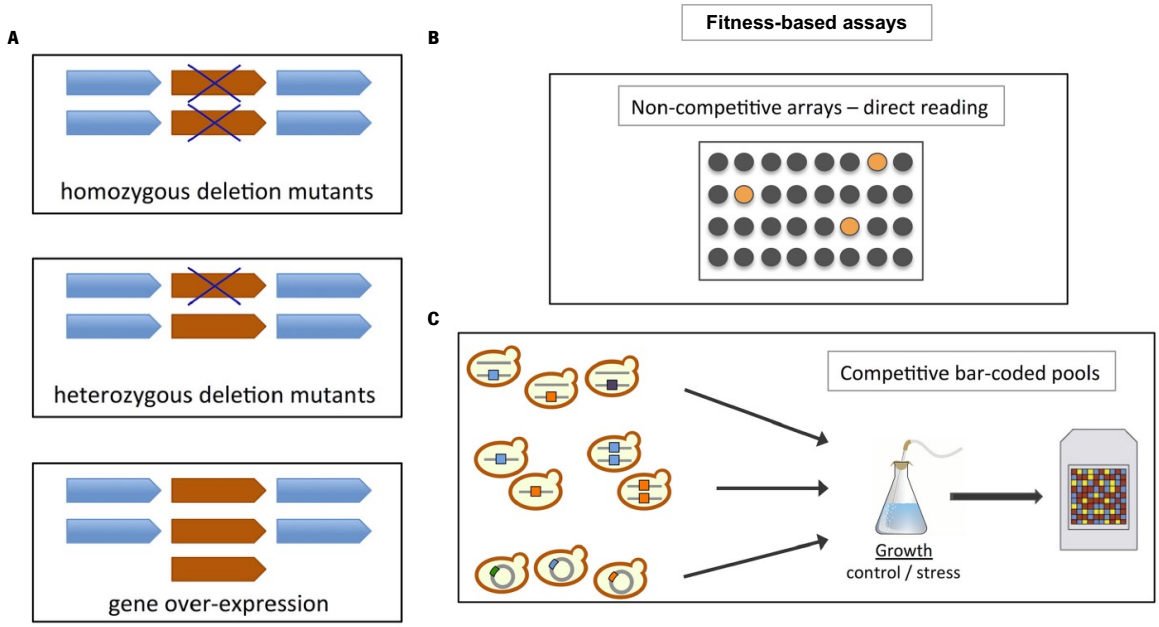

Figure 1.7. Examples of yeast collections and fitness-based assays available for functional toxicogenomics in *S. cerevisiae*. Yeast collections **(A)** and fitness-based assays: **(B)** non-competitive arrays, the toxicant is added to a solid medium plate or to liquid medium added to a well plate, each mutant is placed separately and the individual growth of each strain is monitored; or in competitive barcoded pools **(C)**, gene deletion mutants are pooled together and subject to drug treatment and the fitness profiling of pooled strains is assessed by "barcode". Adapted from (165).

In addition to the yeast collections mentioned above, advances in genetic manipulation and high-throughput mutagenesis strategies have enabled the construction of multiple genome-wide collections of genetically modified strains. For instance, Yofe and co-workers developed a new methodology for the construction of tagged yeast libraries (176). In these libraries every gene is tagged with the sequence encoding a fluorescence protein, such as GFP, enabling the characterization of the different proteins by

assessing their abundance or cellular localization under different growth conditions or after exposure to toxicants (177,178). Nevertheless, these high-throughput screening assays require automated microscopy and sophisticated robotic setups and therefore are used less commonly.

1.3.2. *S. cerevisiae*-based toxicogenomics studies of pesticides

The yeast *S. cerevisiae* has been used in several functional toxicological screens to study a wide range of toxicants, such as metals, pesticides, pharmaceuticals, and other environmental pollutants [reviewed in (170,174)]. As referred above, application of yeast-based omics technologies can be a valuable tool to unveil mechanisms of action of these bioactive molecules, contributing to the identification of target and off-target effects across organisms, including potential links to human diseases, and clarification of resistance mechanisms in target organisms (**Figure 1.8**). In particular, chemogenomics identify genetic alterations that confer sensitivity or resistance to bioactive compounds, establishing functional relationships between specific genes and chemical compounds and thus providing a deeper understanding of the cellular pathways affected, including unintended off-target effects (179–182). As the collection of chemical-genetic profiles grows, researchers can leverage this data to categorize compounds based on their profile similarity; those with a similar profile likely share a common mode of action (182). However, despite the plethora of data from these studies, they are under-utilized in environmental risk assessment. Nonetheless, there are some examples of yeast-based omics technologies providing critical insight into pesticide toxicology.

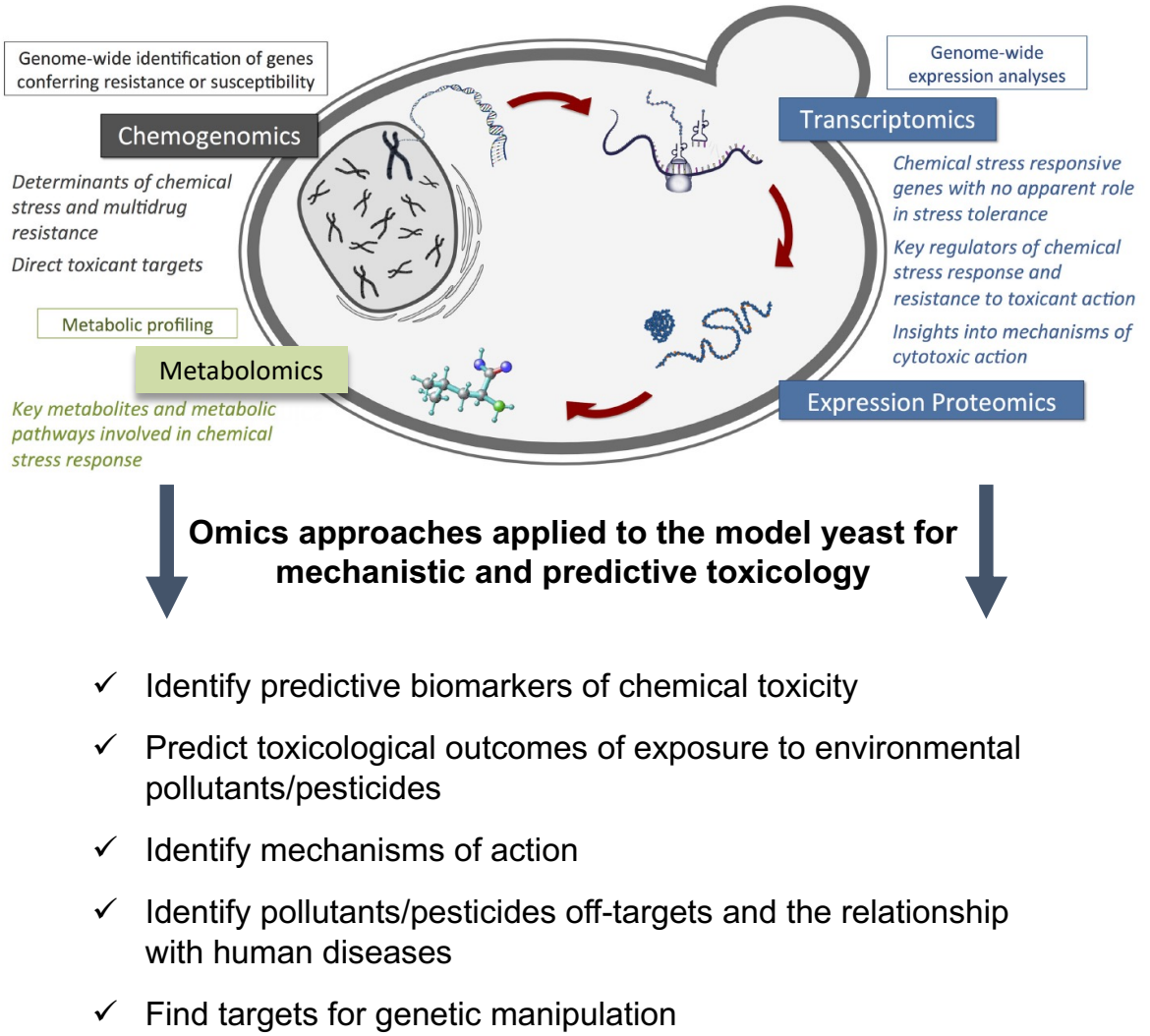

Figure 1.8. Application of yeast-based omics technologies to obtain toxicological mechanistic insights for environmental contaminants. Adapted from (165).

One of such examples is the screen of the yeast disruptome to identified genes responsible for yeast tolerance to the agricultural fungicide mancozeb. Several of the genes identified as crucial for resistance to this fungicide have close orthologs in the phytopathogenic fungus *Botrytis cinerea*, providing insight into the resistance mechanisms of phytopathogenic fungi to this agricultural fungicide (183). The same group also used proteomic analysis to further assess the effects of mancozeb, showing that it significantly affects proteins associated with the antioxidant response, carbohydrate and energy metabolism, and protein synthesis and degradation. Notably, 70 % of the proteins with altered levels possess human orthologs, suggesting a potential conservation of mancozeb toxicity mechanisms in humans (184). Other studies also shed light on mechanisms underlying human toxicity associated with pesticide exposure. The yeast deletion collection and competitive barcoded pools were used to study the

effects of the insecticides dieldrin (185) and toxaphene (186). Several of the yeast genes identified in these studies have conserved functions, which can help elucidate the toxicity mechanism of these insecticides in humans. Yeast mutants defective in amino acid signaling or nitrogen uptake were sensitive to dieldrin, then found to affect leucine availability, leading to amino acid and nitrogen starvation (185). Toxaphene had a significant impact on transcription elongation, but with a mechanism of action distinct from other transcription elongation inhibitors, therefore likely affecting a cellular process closely associated with this pathway (186). Other studies highlighted the effect of pesticides in conserved metabolic pathways across various ecotoxicological species, including humans. Transcriptional profiling of *S. cerevisiae* revealed significant changes in gene expression induced by the herbicide alachlor (187) or the fungicide pyrimethanil (188). Alachlor altered expression of genes involved in metabolism of nitrogen and sulfur, carbohydrates, energy, lipid/fatty acids, as well as vitamins and cofactors. Six of the genes with altered transcript levels had conserved functions in essential metabolic pathways and physiological processes such as the TCA cycle, carbohydrate metabolism and amino acid metabolism, across seven ecotoxicological species including *Mus musculus*, *Drosophila melanogaster*, *Danio rerio*, *Xenopus tropicalis*, *Caenorhabditis elegans*, *Arabidopsis thaliana*, and humans (187). Pyrimethanil significantly affected transcription of genes related with biosynthesis of the amino acid arginine but also with production of volatile acidity during yeast fermentation. Considering its widespread use in vineyards, this result suggested that pyrimethanil may affect the organoleptic properties and quality of the final wine (188). Assessment of the impact of pyrimethanil and two other fungicides (cyprodinil, fludioxonil) on the production of aroma-related metabolites by inoculating commercial *S. cerevisiae*, *S. cerevisiae* (syn *bayanus*), or S*. cerevisiae* (syn. *uvarum*) strains in sterile must (189) identified distinct metabolite profiles depending on both the fungicide and the yeast strain used. The combination of cyprodinil and *S. cerevisiae* (syn. *bayanus*) resulted in production of wine with the lowest quality, but this strain was highly affected by all fungicides, with increased levels of ethyl acetate and isoamyl acetate, associated with negative aromas that decrease wine quality. Given the crucial role of wine aroma in its commercial success, these findings highlight the potential negative impact of chemical compounds, specifically fungicides, in the quality of the final product (189). Further examples of yeast-based omics approaches to the study of pesticide-induced effects in *S. cerevisiae* were reviewed elsewhere (170).

As mentioned above, using the yeast *S. cerevisiae* as model organism offers countless advantages. However, this model organism also displays limitations. Its simplicity and unicellular nature, while often an advantage, presents a challenge when extrapolating findings to multicellular organisms.

Moreover, yeast cannot fully represent the complex responses of whole organisms, particularly regarding organ or tissue toxicity (170,175). Many compounds interact with specific mechanisms in their target organism that may not exist in yeasts, which can limit the ability of the yeast model to accurately predict responses in target organisms (165). Consequently, relying exclusively on yeast findings may not be adequate. In this sense, to ensure a more relevant ecological risk assessment framework, it is crucial to integrate yeast studies with research conducted on more complex models or target organisms. Nonetheless, omics technologies applied to yeast provide a unique cell model for a comprehensive toxicological assessment of pesticides. These powerful approaches allow investigation of toxicity at different levels, from genes to metabolites, offering a deeper understanding of mechanisms underlying environmental pollutant toxicity.

1.4. References

1. United Nations Department of Economic and Social Affairs, Population Division. World Population Prospects 2022: Summary of Results. 2022. UN DESA/POP/2022/TR/NO. 3.
2. Bommarco R, Kleijn D, Potts SG. Ecological intensification: Harnessing ecosystem services for food security. Trends Ecol Evol. 2013;28:230–8.
3. Savary S, Willocquet L, Pethybridge SJ, Esker P, McRoberts N, Nelson A. The global burden of pathogens and pests on major food crops. Nat Ecol Evol. 2019;3:430–9.
4. Nishant N, Upadhyay R. Interventions in handling of pesticides in agriculture : a review. J Agric Environ Sci. 2016;5:113–33.
5. Sarwar M. The dangers of pesticides associated with public health and preventing of the risks. Int J Bioinforma Biomed Eng. 2015;1:130–6.
6. Ayilara MS, Adeleke BS, Akinola SA, Fayose CA, Adeyemi UT, Gbadegesin LA, et al. Biopesticides as a promising alternative to synthetic pesticides: A case for microbial pesticides, phytopesticides, and nanobiopesticides. Front Microbiol. 2023;14:1–16.
7. Hezakiel HE, Thampi M, Rebello S, Sheikhmoideen JM. Biopesticides: a green approach towards agricultural pests. Appl Biochem Biotechnol. 2023;41:1-30.
8. Fenibo EO, Ijoma GN, Matambo T. Biopesticides in Sustainable Agriculture: A Critical Sustainable Development Driver Governed by Green Chemistry Principles. Front Sustain Food Syst. 2021;5:1–6.
9. Benelli G, Pavela R, Drenaggi E, Desneux N, Maggi F. Phytol, (E)-nerolidol and spathulenol from Stevia rebaudiana leaf essential oil as effective and eco-friendly botanical insecticides against Metopolophium dirhodum. Ind Crops Prod. 2020;155:1-8.
10. Wang N, Shao X, Wei Y, Jiang S, Xu F, Wang H. Quantitative proteomics reveals that tea tree oil effects *Botrytis cinerea* mitochondria function. Pestic Biochem Physiol. 2020;164:156–64.
11. Cui K, He L, Zhao Y, Mu W, Lin J, Liu F. Comparative analysis of *Botrytis cinerea* in response to the microbial secondary metabolite benzothiazole using iTRAQ-based quantitative proteomics. Phytopathology. 2021;111:1313–26.
12. Deguine JP, Aubertot JN, Flor RJ, Lescourret F, Wyckhuys KAG, Ratnadass A. Integrated pest management: good intentions, hard realities. A review. Agron Sustain Dev. 2021;41:1–35.
13. Khursheed A, Rather MA, Jain V, Wani AR, Rasool S, Nazir R, et al. Plant based natural products as potential ecofriendly and safer biopesticides: a comprehensive overview of their advantages over conventional pesticides, limitations and regulatory aspects. Microb Pathog. 2022;173:1-26.

14. Sharma A, Shukla A, Attri K, Kumar M, Kumar P, Suttee A, et al. Global trends in pesticides: a looming threat and viable alternatives. Ecotoxicol Environ Saf. 2020;201:1–15.
15. Abubakar Y, Tijjani H, Egbuna C, Adetunji CO, Kala S, Kryeziu TL, et al. Pesticides, history, and classification. In: Egbuna C, Sawicka B, editors. Natural Remedies for Pest, Disease and Weed Control. Academic Press; 2020. p. 29–42.
16. Pathak VM, Verma VK, Rawat BS, Kaur B, Babu N, Sharma A, et al. Current status of pesticide effects on environment, human health and it's eco-friendly management as bioremediation: A comprehensive review. Front Microbiol. 2022;13:1–29.
17. Parra-Arroyo L, González-González RB, Castillo-Zacarías C, Melchor Martínez EM, Sosa-Hernández JE, Bilal M, et al. Highly hazardous pesticides and related pollutants: Toxicological, regulatory, and analytical aspects. Sci Total Environ. 2022;807:1–16.
18. Kim KH, Kabir E, Jahan SA. Exposure to pesticides and the associated human health effects. Sci Total Environ. 2017;575:525–35.
19. Mahmood I, Ruqia SI, Shazadi K, Gul A, Khalid HR. Effects of pesticides on environment. In: Hakeem KR, Akhtar MS, Abdullah SNA, editors. Plant, Soil and Microbes. Switzerland: Springer International Publishing; 2016. p. 253–69.
20. FAO. Agricultural production statistics 2000–2021. FAOSTAT analytical briefs, 2022. No. 60. Rome.
21. Delcour I, Spanoghe P, Uyttendaele M. Literature review: Impact of climate change on pesticide use. Food Res Int. 2015;68:7–15.
22. Pimentão AR, Cuco AP, Pascoal C, Cássio F, Castro BB. Current trends and mismatches on fungicide use and assessment of the ecological effects in freshwater ecosystems. Environ Pollut. 2024;347:1–12.
23. Kerle EA, Jenkins JJ, Vogue PA. Understanding pesticide persistence and mobility for groundwater and surface water protection. Oregon State Univ. 2007;1–8.
24. Gavrilescu M. Fate of pesticides in the environment and its bioremediation. Eng Life Sci. 2005;5:497–526.
25. de Araújo MC, de Assis CRD, de Queiroz Cavalcanti de Sá RA, da Silva JG, de Veras BO, Silva KCC, et al. Impacts of Agricultural Toxicity on Non-Target Organisms in Aquatic Ecosystem. In: Nuro A, editor. Emerging Contaminants. IntechOpen; 2020.
26. Dad K, Zhao F, Hassan R, Javed K, Nawaz H, Saleem MU, et al. Pesticides uses, impacts on environment and their possible remediation strategies - a review. Pakistan J Agric Res.

2022;35:274–84.

27. Parween T, Jan S, Mahmooduzzafar S, Fatma T, Siddiqui ZH. Selective effect of pesticides on plant - a review. Crit Rev Food Sci Nutr. 2016;56:160–79.
28. Stehle S, Schulz R. Agricultural insecticides threaten surface waters at the global scale. Proc Natl Acad Sci U S A. 2015;112:5750–5.
29. de Souza RM, Seibert D, Quesada HB, de Jesus Bassetti F, Fagundes-Klen MR, Bergamasco R. Occurrence, impacts and general aspects of pesticides in surface water: A review. Process Saf Environ Prot. 2020;135:22–37.
30. Rumschlag SL, Mahon MB, Hoverman JT, Raffel TR, Carrick HJ, Hudson PJ, et al. Consistent effects of pesticides on community structure and ecosystem function in freshwater systems. Nat Commun. 2020;11:1–9.
31. Directive 2009/128/EC of the European Parliament and of the Council of 21 October 2009 establishing a framework for Community action to achieve the sustainable use of pesticides. Off J Eur Union L. 2009;309:71-86.
32. Devillers J. Fate and ecotoxicological effects of pyriproxyfen in aquatic ecosystems. Environ Sci Pollut Res. 2020;27:16052–68.
33. Rezende-Teixeira P, Dusi RG, Jimenez PC, Espindola LS, Costa-Lotufo L V. What can we learn from commercial insecticides? Efficacy, toxicity, environmental impacts, and future developments. Environ Pollut. 2022;300:1–20.
34. Sánchez-Bayo F, Goka K, Hayasaka D. Contamination of the aquatic environment with neonicotinoids and its implication for ecosystems. Front Environ Sci. 2016;4:1–14.
35. Li H, Liu Y, Chen Q, Jin L, Peng R. Research progress of Zebrafish model in aquatic ecotoxicology. Water. 2023;15:1–21.
36. Malhotra N, Chen KHC, Huang JC, Lai HT, Uapipatanakul B, Roldan MJM, et al. Physiological effects of neonicotinoid insecticides on non-target aquatic animals—an updated review. Int J Mol Sci. 2021;22:1–35.
37. Le VG, Nguyen MK, Nguyen HL, Thai VA, Le VR, Vu QM, et al. Ecotoxicological response of algae to contaminants in aquatic environments: a review. Environ Chem Lett. 2024;
38. Staley ZR, Harwood VJ, Rohr JR. A synthesis of the effects of pesticides on microbial persistence in aquatic ecosystems. Crit Rev Toxicol. 2015;45:813–36.
39. Li H, Jiao Y, Li L, Jiao X. Research progress and trend of effects of organophosphorus pesticides on aquatic organisms in the past decade. Comp Biochem Physiol Part - C. 2023;271:1–10.

40. Mohanty SS, Jena HM. A systemic assessment of the environmental impacts and remediation strategies for chloroacetanilide herbicides. J Water Process Eng. 2019;31:1–12.
41. de Albuquerque FP, de Oliveira JL, Moschini-Carlos V, Fraceto LF. An overview of the potential impacts of atrazine in aquatic environments: Perspectives for tailored solutions based on nanotechnology. Sci Total Environ. 2020;700:1–9.
42. Donaher SE, Van den Hurk P. Ecotoxicology of the herbicide paraquat: effects on wildlife and knowledge gaps. Ecotoxicology. 2023;32:1187–99.
43. Annett R, Habibi HR, Hontela A. Impact of glyphosate and glyphosate-based herbicides on the freshwater environment. J Appl Toxicol. 2014;34:458–79.
44. Yang C, Lim W, Song G. Reproductive toxicity due to herbicide exposure in freshwater organisms. Comp Biochem Physiol Part C. 2021;248:1–12.
45. Islam F, Wang J, Farooq MA, Khan MSS, Xu L, Zhu J, et al. Potential impact of the herbicide 2,4-dichlorophenoxyacetic acid on human and ecosystems. Environ Int. 2018;111:332–51.
46. Lares BA, Vignatti AM, Echaniz SA, Gutiérrez MF. Effects of glyphosate on cladocera: A synthetic review. Aquat Toxicol. 2022;249:1–13.
47. Wang X, Li X, Wang Y, Qin Y, Yan B, Martyniuk CJ. A comprehensive review of strobilurin fungicide toxicity in aquatic species: Emphasis on mode of action from the zebrafish model. Environ Pollut. 2021;275:1–12.
48. Bhagat J, Singh N, Nishimura N, Shimada Y. A comprehensive review on environmental toxicity of azole compounds to fish. Chemosphere. 2021;262:2–16.
49. Zhou T, Guo T, Wang Y, Wang A, Zhang M. Carbendazim: Ecological risks, toxicities, degradation pathways and potential risks to human health. Chemosphere. 2023;314:1–14.
50. Solé S, Merkoçi A, Alegret S. Determination of toxic substances based on enzyme inhibition. Part I. Electrochemical biosensors for the determination of pesticides using batch procedures. Crit Rev Anal Chem. 2003;33:89–126.
51. Ittner LD, Junghans M, Werner I. Aquatic fungi: a disregarded trophic level in ecological risk assessment of organic fungicides. Front Environ Sci. 2018;6:1–18.
52. Malaj E, Von Der Ohe PC, Grote M, Kühne R, Mondy CP, Usseglio-Polatera P, et al. Organic chemicals jeopardize the health of freshwater ecosystems on the continental scale. Proc Natl Acad Sci USA. 2014;111:9549–54.
53. Brühl CA, Zaller JG. Biodiversity Decline as a Consequence of an Inappropriate Environmental Risk Assessment of Pesticides. Front Environ Sci. 2019;7:1–4.

54. Zubrod JP, Bundschuh M, Arts G, Brühl CA, Imfeld G, Knäbel A, et al. Fungicides: An Overlooked Pesticide Class? Environ Sci Technol. 2019;53:3347–65.
55. Laicher D, Benkendorff K, White S, Conrad S, Woodrow RL, Butcherine P, et al. Pesticide occurrence in an agriculturally intensive and ecologically important coastal aquatic system in Australia. Mar Pollut Bull. 2022;180:1–11.
56. Chow R, Curchod L, Davies E, Veludo AF, Oltramare C, Dalvie MA, et al. Seasonal drivers and risks of aquatic pesticide pollution in drought and post-drought conditions in three Mediterranean watersheds. Sci Total Environ. 2023;858:1–12.
57. Monticelli Barizon RR, Kummrow F, Fernandes de Albuquerque A, Assalin MR, Rosa MA, Cassoli de Souza Dutra DR, et al. Surface water contamination from pesticide mixtures and risks to aquatic life in a high-input agricultural region of Brazil. Chemosphere. 2022;308:1–10.
58. Kruć-Fijałkowska R, Dragon K, Drożdżyński D, Górski J. Seasonal variation of pesticides in surface water and drinking water wells in the annual cycle in western Poland, and potential health risk assessment. Sci Rep. 2022;12:1–12.
59. Lundqvist J, von Brömssen C, Rosenmai AK, Ohlsson Å, Le Godec T, Jonsson O, et al. Assessment of pesticides in surface water samples from Swedish agricultural areas by integrated bioanalysis and chemical analysis. Environ Sci Eur. 2019;31:1–13.
60. Chaza C, Sopheak N, Mariam H, David D, Baghdad O, Moomen B. Assessment of pesticide contamination in Akkar groundwater, northern Lebanon. Environ Sci Pollut Res. 2018;25:14302–12.
61. Bexfield LM, Belitz K, Lindsey BD, Toccalino PL, Nowell LH. Pesticides and pesticide degradates in groundwater used for public supply across the United States: occurrence and human-health context. Environ Sci Technol. 2021;55:362–72.
62. Gonçalves CM, Da Silva JCGE, Alpendurada MF. Evaluation of the pesticide contamination of groundwater sampled over two years from a vulnerable zone in Portugal. J Agric Food Chem. 2007;55:6227–35.
63. Mojiri A, Zhou JL, Robinson B, Ohashi A, Ozaki N, Kindaichi T, et al. Pesticides in aquatic environments and their removal by adsorption methods. Chemosphere. 2020; 253:1-24.
64. Stehle S, Schulz R. Pesticide authorization in the EU—environment unprotected? Environ Sci Pollut Res. 2015;22:19632–47.
65. Directive 98/83/EC of the Council of the European Union of 2 November October 1998 on the quality of water intended for human consumption. Off J Eur Union L. 1998;330:32-54.

66. Directive 2000/60/EC of the European Parliament and of the Council of 23 October 2000 establishing a framework for Community action in the field of water policy. Off J Eur Union L. 2000;327:1-73.
67. Directive 2008/105/EC of the European Parliament and of the Council of 16 December 20008 on environmental quality standards in the field of water policy. Off J Eur Union L. 2008;348:84-97.
68. Directive 2020/2184 of the European Parliament and of the Council of 16 December 2020 on the quality of water intended for human consumption (recast). Off J Eur Union L. 2020;435:1-62.
69. Vasiljević T, Dujaković N, Radišić M, Grujić S, Laušević M, Dimkić M. Methods for monitoring of pesticide residues in water: Current status and recent trends. Water Sci Technol. 2012;66:965–75.
70. Campanale C, Massarelli C, Losacco D, Bisaccia D, Triozzi M, Uricchio VF. The monitoring of pesticides in water matrices and the analytical criticalities: a review. TrAC - Trends Anal Chem. 2021;144:2–16.
71. Samsidar A, Siddiquee S, Shaarani SM. A review of extraction, analytical and advanced methods for determination of pesticides in environment and foodstuffs. Trends Food Sci Technol. 2018;71:188–201.
72. Bhadekar R, Pote S, Tale V, Nirichan B. Developments in analytical methods for detection of pesticides in environmental samples. Am J Anal Chem. 2011;2:1–15.
73. Daverey A, Dutta K, Sarkar A. An overview of analytical methodologies for environmental monitoring. In: Brar KS, Hedged K, Pachapur VL, editors. Tools, Techniques and Protocols for Monitoring Environmental Contaminants. Elsevier Inc.; 2019. p. 3–17.
74. Rani L, Thapa K, Kanojia N, Sharma N, Singh S, Grewal AS, et al. An extensive review on the consequences of chemical pesticides on human health and environment. J Clean Prod. 2021;283:2–33.
75. Rodriguez-Mozaz S, Lopez De Alda MJ, Barceló D. Biosensors as useful tools for environmental analysis and monitoring. Anal Bioanal Chem. 2006;386:1025–41.
76. Thévenot DR, Toth K, Durst RA, Wilson GS. Electrochemical biosensors: recommended definitions and classification. Biosens Bioelectron. 2001;16:121–31.
77. Upadhyay LSB, Verma N. Role of biosensors in environmental monitoring. In: Sukla L, Pradhan N, Panda S, Mishra B, editors. Environmental Microbial Biotechnology, Soil Biology, vol 45. Springer, Cham; 2015. p. 77–90.

78. Justino CIL, Freitas AC, Pereira R, Duarte AC, Rocha Santos TAP. Recent developments in recognition elements for chemical sensors and biosensors. TrAC - Trends Anal Chem. 2015;68:2–17.
79. Sassolas A, Prieto-Simón B, Marty J-L. Biosensors for pesticide detection: new trends. Am J Anal Chem. 2012;3:210–32.
80. Verma N, Bhardwaj A. Biosensor technology for pesticides—a review. Appl Biochem Biotechnol. 2015;175:3093–119.
81. Gavrilaş S, Ursachi C Ştefan, Perţa-Crişan S, Munteanu FD. Recent trends in biosensors for environmental quality monitoring. Sensors. 2022;22:2–19.
82. Huang CW, Lin C, Nguyen MK, Hussain A, Bui XT, Ngo HH. A review of biosensor for environmental monitoring: principle, application, and corresponding achievement of sustainable development goals. In: Brar SK, Hegde K, Pachapur VL, editors. Bioengineered. Taylor & Francis; 2023. p. 58–80.
83. Lozano MG, García YP, Gonzalez JAS, Bañuelos CVO, Escareño MPL, Balagurusamy N. Biosensors for food quality and safety monitoring: fundamentals and applications. In: Kuddus M, editor. Enzymes in Food Biotechnology. Academic Press; 2019. p. 691–709.
84. Haleem A, Javaid M, Singh RP, Suman R, Rab S. Biosensors applications in medical field: a brief review. Sensors Int. 2021;2:1–10.
85. Salouti M, Derakhshan FK. Biosensors and nanobiosensors in environmental applications. In: Ghorbanpour M, Bhargava P, Varma A, Choudhary D, editors. Biogenic Nano-Particles and their Use in Agro-ecosystems. Singapore: Springer; 2020. p. 515–90.
86. Berkal MA, Nardin C. Pesticide biosensors: trends and progresses. Anal Bioanal Chem. 2023;415:5899–924.
87. Hassani S, Momtaz S, Vakhshiteh F, Maghsoudi AS, Ganjali MR, Norouzi P, et al. Biosensors and their applications in detection of organophosphorus pesticides in the environment. Arch Toxicol. 2017;91:109–30.
88. Mirres AC de M, Silva BEP de M da, Tessaro L, Galvan D, Andrade JC de, Aquino A, et al. Recent advances in nanomaterial-based biosensors for pesticide detection in foods. Biosensors. 2022;12:1–33.
89. Saberi Z, Rezaei B, Ensafi AA. Fluorometric label-free aptasensor for detection of the pesticide acetamiprid by using cationic carbon dots prepared with cetrimonium bromide. Microchim Acta. 2019;186:1-7.

90. Li Z, Qu S, Cui L, Zhang S. Detection of carbofuran pesticide in seawater by using an enzyme biosensor. J Coast Res. 2017;SI:1–5.

91. Mayorga-Martinez CC, Pino F, Kurbanoglu S, Rivas L, Ozkan SA, Merkoçi A. Iridium oxide nanoparticle induced dual catalytic/inhibition based detection of phenol and pesticide compounds. J Mater Chem B. 2014;2:2233–9.

92. Macagno J, Gerlero GS, Satuf ML, Berli CLA. Field-deployable aptasensor with automated analysis of stain patterns for the detection of chlorpyrifos in water. Talanta. 2023;252:1–10.

93. Chouichit P, Whangsuk W, Sallabhan R, Mongkolsuk S, Loprasert S. A highly sensitive biosensor with a single-copy evolved sensing cassette for chlorpyrifos pesticide detection. Microbiology. 2020;166:1019–24.

94. Khosropour H, Rezaei B, Rezaei P, Ensafi AA. Ultrasensitive voltammetric and impedimetric aptasensor for diazinon pesticide detection by VS2 quantum dots-graphene nanoplatelets/carboxylated multiwalled carbon nanotubes as a new group nanocomposite for signal enrichment. Anal Chim Acta. 2020;1111:92–102.

95. Pérez-Fernández B, Mercader J V., Abad-Fuentes A, Checa-Orrego BI, Costa-García A, Escosura-Muñiz A de la. Direct competitive immunosensor for Imidacloprid pesticide detection on gold nanoparticle-modified electrodes. Talanta. 2020;209:1–8.

96. Bor G, Man E, Ugurlu O, Ceylan AE, Balaban S, Durmus C, et al. *in vitro* selection of aptamer for imidacloprid recognition as model analyte and construction of a water analysis platform. Electroanalysis. 2020;32:1922–9.

97. Wang Y, Zhu F, Yin L, Qu G, Ma DL, Leung CH, et al. Ratiometric fluorescent detection of pesticide based on split aptamer and magnetic separation. Sensors Actuators B Chem. 2022;367:1–8.

98. Nguyen DK, Jang CH. A cationic surfactant-decorated liquid crystal-based aptasensor for label-free detection of malathion pesticides in environmental samples. Biosensors. 2021;11:1–11.

99. Yang Y, Asiri AM, Du D, Lin Y. Acetylcholinesterase biosensor based on a gold nanoparticle-polypyrrole-reduced graphene oxide nanocomposite modified electrode for the amperometric detection of organophosphorus pesticides. Analyst. 2014;139:3055–60.

100. Turan J, Kesik M, Soylemez S, Goker S, Coskun S, Unalan HE, et al. An effective surface design

based on a conjugated polymer and silver nanowires for the detection of paraoxon in tap water and milk. Sensors Actuators, B Chem. 2016;228:278–86.

101. Guo L, Li Z, Chen H, Wu Y, Chen L, Song Z, et al. Colorimetric biosensor for the assay of paraoxon in environmental water samples based on the iodine-starch color reaction. Anal Chim Acta. 2017;967:59–63.

102. Kim CS, Choi BH, Seo JH, Lim G, Cha HJ. Mussel adhesive protein-based whole cell array biosensor for detection of organophosphorus compounds. Biosens Bioelectron. 2013;41:199–204.

103. Mulchandani P, Chen W, Mulchandani A. Microbial biosensor for direct determination of nitrophenyl-substituted organophosphate nerve agents using genetically engineered *Moraxella* sp. Anal Chim Acta. 2006;568:217–21.

104. Chouteau C, Dzyadevych S, Durrieu C, Chovelon JM. A bi-enzymatic whole cell conductometric biosensor for heavy metal ions and pesticides detection in water samples. Biosens Bioelectron. 2005;21:273–81.

105. Wu S, Li D, Wang J, Zhao Y, Dong S, Wang X. Gold nanoparticles dissolution based colorimetric method for highly sensitive detection of organophosphate pesticides. Sensors Actuators, B Chem. 2017;238:427–33.

106. Luo Y, Jin Z, Wang J, Ding P, Pei R. The isolation of a DNA aptamer to develop a fluorescent aptasensor for the thiamethoxam pesticide. Analyst. 2021;146:1986–95.

107. Yang L, Wang G, Liu Y, Wang M. Development of a biosensor based on immobilization of acetylcholinesterase on NiO nanoparticles–carboxylic graphene–nafion modified electrode for detection of pesticides. Talanta. 2013;113:135–41.

108. Liu Y, Lv B, Liu A, Liang G, Yin L, Pu Y, et al. Multicolor sensor for organophosphorus pesticides determination based on the bi-enzyme catalytic etching of gold nanorods. Sensors Actuators, B Chem. 2018;265:675–81.

109. Li P, Bai Y, Jiang H, Zhang Y, Li Y, Duan C, et al. Broad-specificity antibody profiled by hapten prediction and its application in immunoassay for fipronil and major metabolites. J Hazard Mater. 2023;441:1–12.

110. Zhang P, Sun T, Rong S, Zeng D, Yu H, Zhang Z, et al. A sensitive amperometric AChE-biosensor

for organophosphate pesticides detection based on conjugated polymer and Ag-rGO-NH_2 nanocomposite. Bioelectrochemistry. 2019;127:163–70.

111. Liu D, Chen W, Wei J, Li X, Wang Z, Jiang X. A highly sensitive, dual-readout assay based on gold nanoparticles for organophosphorus and carbamate pesticides. Anal Chem. 2012;84:4185–91.

112. Zou R, Guo Y, Chen Y, Zhao Y, Zhao L, Zhu G, et al. Computer-aided profiling of a unique broad-specific antibody and its application to an ultrasensitive fluoroimmunoassay for five N-methyl carbamate pesticides. J Hazard Mater. 2022;426:1–11.

113. Qu Y, Qian H, Mi Y, He J, Gao H, Lu R, et al. Rapid determination of the pesticide ametryn based on a colorimetric aptasensor of gold nanoparticles. Anal Methods. 2020;12:1919–25.

114. Zumpano R, Manghisi M, Polli F, D'Agostino C, Ietto F, Favero G, et al. Label-free magnetic nanoparticles-based electrochemical immunosensor for atrazine detection. Anal Bioanal Chem. 2022;414:2055–64.

115. Fan L, Zhang C, Yan W, Guo Y, Shuang S, Dong C, et al. Design of a facile and label-free electrochemical aptasensor for detection of atrazine. Talanta. 2019;201:156–64.

116. Surribas A, Barthelmebs L, Noguer T. Monoclonal antibody-based immunosensor for the electrochemical detection of chlortoluron herbicide in groundwaters. Biosensors. 2021;11:1–13.

117. López-Puertollano D, Agulló C, Mercader J V., Abad-Somovilla A, Abad-Fuentes A. Design of a novel hapten and development of a sensitive monoclonal immunoassay for dicamba analysis in environmental water samples. Sci Total Environ. 2022;848:1–9.

118. Tsopela A, Lale A, Vanhove E, Reynes O, Séguy I, Temple-Boyer P, et al. Integrated electrochemical biosensor based on algal metabolism for water toxicity analysis. Biosens Bioelectron. 2014;61:290–7.

119. Vaghela C, Kulkarni M, Haram S, Aiyer R, Karve M. A novel inhibition based biosensor using urease nanoconjugate entrapped biocomposite membrane for potentiometric glyphosate detection. Int J Biol Macromol. 2018;108:32–40.

120. Stavra E, Petrou PS, Koukouvinos G, Economou A, Goustouridis D, Misiakos K, et al. Fast, sensitive and selective determination of herbicide glyphosate in water samples with a White Light Reflectance Spectroscopy immunosensor. Talanta. 2020;214:1–8.

121. Zeng H, Yang H, Tang Y, Niu X, Wu Y. Aptamer-enhanced the Ag(I) ion-3,3′,5,5′-tetramethylbenzdine catalytic system as a novel colorimetric biosensor for ultrasensitive and selective detection of paraquat. Spectrochim Acta - Part A Mol Biomol Spectrosc. 2022;280:1–10.

122. Tekaya N, Saiapina O, Ouada H Ben, Lagarde F, Namour P, Ouada H Ben, et al. Bi-Enzymatic conductometric biosensor for detection of heavy metal ions and pesticides in water samples based on enzymatic inhibition in *Arthrospira platensis*. J Environ Prot. 2014;5:441–53.

123. Khosropour H, Maeboonruan N, Sriprachuabwong C, Tuantranont A, Laiwattanapaisal W. A new double signal on electrochemical aptasensor based on gold nanoparticles/graphene nanoribbons/MOF-808 as enhancing nanocomposite for ultrasensitive and selective detection of carbendazim. OpenNano. 2022;8:1–14.

124. Clark LC, Lyons C. Electrode systems for continuous monitoring in cardiovascular surgery. Ann N Y Acad Sci. 1962;102:29–45.

125. Kucherenko IS, Soldatkin OO, Kucherenko DY, Soldatkina O V., Dzyadevych S V. Advances in nanomaterial application in enzyme-based electrochemical biosensors: a review. Nanoscale Adv. 2019;1:4560–77.

126. Chadha U, Bhardwaj P, Agarwal R, Rawat P, Agarwal R, Gupta I, et al. Recent progress and growth in biosensors technology: A critical review. J Ind Eng Chem. 2022;109:21–51.

127. Štěpánková Š, Vorčáková K. Cholinesterase-based biosensors. J Enzyme Inhib Med Chem. 2016;31:180–93.

128. Trojanowicz M. Determination of pesticides using electrochemical enzymatic biosensors. Electroanalysis. 2002;14:1311–28.

129. Hara TO, Singh B. Electrochemical biosensors for detection of pesticides and heavy metal toxicants in water: recent trends and progress. ACS Environ Sci Technol Water. 2021;1:462–78.

130. Alvarado-Ramírez L, Rostro-Alanis M, Rodríguez-Rodríguez J, Sosa-Hernández JE, Melchor-Martínez EM, Iqbal HMN, et al. Enzyme (single and multiple) and nanozyme biosensors: Recent developments and their novel applications in the water-food-health nexus. Biosensors. 2021;11:1–23.

131. Rebollar-Pérez G, Campos-Terán J, Ornelas-Soto N, Méndez-Albores A, Torres E. Biosensors

based on oxidative enzymes for detection of environmental pollutants. Biocatalysis. 2015;1:118–29.

132. Luque de Castro MD, Herrera MC. Enzyme inhibition-based biosensors and biosensing systems: questionable analytical devices. Biosens Bioelectron. 2003;18:279–94.

133. Jain R, Miri S, Pachapur VL, Brar SK. Advances in antibody-based biosensors in environmental monitoring. In: Brar SK, Hegde K, Pachapur VL, editors. Tools, Techniques and Protocols for Monitoring Environmental Contaminants. Elsevier Inc.; 2019. p. 285–305.

134. Hartzler RG. Immunoassays for Pesticide Detection. In: Proceedings of the Integrated Crop Management Conference. 1990. p. 78–82.

135. Fang L, Liao X, Jia B, Shi L, Kang L, Zhou L, et al. Recent progress in immunosensors for pesticides. Biosens Bioelectron. 2020;164:1–17.

136. Reynoso EC, Torres E, Bettazzi F, Palchetti I. Trends and perspectives in immunosensors for determination of currently-used pesticides: the case of glyphosate, organophosphates, and neonicotinoids. Biosensors. 2019;9:1–20.

137. Toh SY, Citartan M, Gopinath SCB, Tang TH. Aptamers as a replacement for antibodies in enzyme-linked immunosorbent assay. Biosens Bioelectron. 2015;64:392–403.

138. Wilson DS, Szostak JW. In vitro selection of functional nucleic acids. Annu Rev Phys Chem. 1999;69:611–47.

139. Ellington AD, Szostak JW. *In vitro* selection of RNA molecules that bind specific ligandas. Nature. 1990;346:818–22.

140. Tuerk C, Gold L. Systematic evolution of ligands by exponential enrichment: RNA ligands to bacteriophage T4 DNA polymerase. Science. 1990;249:505–10.

141. Xie M, Zhao F, Zhang Y, Xiong Y, Han S. Recent advances in aptamer-based optical and electrochemical biosensors for detection of pesticides and veterinary drugs. Food Control. 2022;131:1–17.

142. Song S, Wang L, Li J, Fan C, Zhao J. Aptamer-based biosensors. TrAC - Trends Anal Chem. 2008;27:108–17.

143. Liu M, Khan A, Wang Z, Liu Y, Yang G, Deng Y, et al. Aptasensors for pesticide detection. Biosens Bioelectron. 2019;130:174–84.

144. Qin N, Liu J, Li F, Liu J. Recent advances in aptasensors for rapid pesticide residues detection. Crit Rev Anal Chem. 2023;1–22.

145. Bai W, Zhu C, Liu J, Yan M, Yang S, Chen A. Gold nanoparticle-based colorimetric aptasensor for rapid detection of six organophosphorous pesticides. Environ Toxicol Chem. 2015;34:2244–9.

146. Gupta N, Renugopalakrishnan V, Liepmann D, Paulmurugan R, Malhotra BD. Cell-based biosensors: Recent trends, challenges and future perspectives. Biosens Bioelectron. 2019;141:1–23.

147. Moraskie M, Or H, Connor GO, Dikici E, Zingg J, Deo S, et al. Microbial whole-cell biosensors: Current applications, challenges, and future perspectives. Biosens Bioelectron. 2021;191:1–18.

148. Saini R, Hegde K, Brar SK, Verma M. Advances in whole cell-based biosensors in environmental monitoring. In: Brar SK, Hegde K, Pachapur VL, editors. Tools, Techniques and Protocols for Monitoring Environmental Contaminants. Elsevier Inc.; 2019. p. 263–84.

149. Gui Q, Lawson T, Shan S, Yan L, Liu Y. The application of whole cell-based biosensors for use in environmental analysis and in medical diagnostics. Sensors. 2017;17:1–17.

150. Gu MB, Mitchell RJ, Kim BC. Whole-cell-based biosensors for environmental biomonitoring and application. Adv Biochem Eng Biotechnol. 2004;87:269–305.

151. Aynalem B, Muleta D. Microbial biosensors as pesticide detector: an overview. J Sensors. 2021;2021:1–9.

152. Whangsuk W, Dubbs JM, Sallabhan R, Somsongkul K, Mongkolsuk S, Loprasert S. ChpR is a chlorpyrifos-responsive transcription regulator in *Sinorhizobium meliloti.* J Mol Microbiol Biotechnol. 2010;18:141–7.

153. Whangsuk W, Thiengmag S, Dubbs J, Mongkolsuk S, Loprasert S. Specific detection of the pesticide chlorpyrifos by a sensitive genetic-based whole cell biosensor. Anal Biochem. 2016;493:11–3.

154. Park M, Tsai SL, Chen W. Microbial biosensors: engineered microorganisms as the sensing machinery. Sensors. 2013;13:5777–95.

155. Plekhanova Y V., Reshetilov AN. Microbial biosensors for the determination of pesticides. J Anal Chem. 2019;74:1159–73.

156. Bilal M, Iqbal HMN. Microbial-derived biosensors for monitoring environmental contaminants:

Recent advances and future outlook. Process Saf Environ Prot. 2019;124:8–17.

157. Adeniran A, Sherer M, Tyo KEJ. Yeast-based biosensors: Design and applications. FEMS Yeast Res. 2015;15:1–15.

158. Chamas A, Pham HTM, Baronian K, Kunze G. Biosensors based on yeast/fungal cells. In: Biotechnology of Yeasts and Filamentous Fungi. 2017. p. 1–412.

159. Khurana V, Lindquist S. Modelling neurodegeneration in *Saccharomyces cerevisiae*: Why cook with baker's yeast? Nat Rev Neurosci. 2010;11:436–49.

160. Schofield DA, Westwater C, Barth JL, DiNovo AA. Development of a yeast biosensor-biocatalyst for the detection and biodegradation of the organophosphate paraoxon. Appl Microbiol Biotechnol. 2007;76:1383–94.

161. Lobsiger N, Venetz JE, Gregorini M, Christen M, Christen B, Stark WJ. YestroSens, a field-portable *S. cerevisiae* biosensor device for the detection of endocrine-disrupting chemicals: Reliability and stability. Biosens Bioelectron. 2019;146:1–7.

162. Sanseverino J, Gupta RK, Layton AC, Patterson SS, Ripp SA, Saidak L, et al. Use of *Saccharomyces cerevisiae* BLYES expressing bacterial bioluminescence for rapid, sensitive detection of estrogenic compounds. Appl Environ Microbiol. 2005;71:4455–60.

163. Cevenini L, Lopreside A, Calabretta MM, D'Elia M, Simoni P, Michelini E, et al. A novel bioluminescent NanoLuc yeast-estrogen screen biosensor (nanoYES) with a compact wireless camera for effect-based detection of endocrine-disrupting chemicals. Anal Bioanal Chem. 2018;410:1237–46.

164. North M, Vulpe CD. Functional toxicogenomics: Mechanism-centered toxicology. Int J Mol Sci. 2010;11:4796–813.

165. dos Santos SC, Teixeira MC, Cabrito TR, Sá-Correia I. Yeast toxicogenomics: genome-wide responses to chemical stresses with impact in environmental health, pharmacology, and biotechnology. Front Genet. 2012;3:1–17.

166. Martins C, Dreij K, Costa PM. The state-of-the art of environmental toxicogenomics: Challenges and perspectives of "omics" approaches directed to toxicant mixtures. Int J Environ Res Public Health. 2019;16:1–16.

167. Vailati-Riboni M, Palombo V, Loor JJ. What are omics sciences. In: Ametaj B, editor.

Periparturient Diseases of Dairy Cows. Springer, Cham; 2017. p. 1–7.

168. Piña B, Raldúa D, Barata C, Portugal J, Navarro-Martín L, Martínez R, et al. Functional Data Analysis: Omics for Environmental Risk Assessment. In: Jaumot J, Bedia C, Romà T, editors. Comprehensive Analytical Chemistry. Elsevier; 2018. p. 583–611.

169. dos Santos SC, Teixeira MC, Cabrito TR, Sá-Correia I. Yeast toxicogenomics: Genome-wide responses to chemical stresses with impact in environmental health, pharmacology, and biotechnology. Front Genet. 2012;3:1–17.

170. Braconi D, Bernardini G, Santucci A. *Saccharomyces cerevisiae* as a model in ecotoxicological studies: a post-genomics perspective. J Proteomics. 2016;137:19–34.

171. Suter B, Auerbach D, Stagljar I. Yeast-based functional genomics and proteomics technologies: the first 15 years and beyond. Biotechniques. 2006;40:625–44.

172. Botstein D, Fink GR. Yeast: An experimental organism for 21st century biology. Genetics. 2011;189:695–704.

173. Giaever G, Nislow C. The yeast deletion collection: a decade of functional genomics. Genetics. 2014;197:451–65.

174. Gaytán BD, Vulpe CD. Functional toxicology: tools to advance the future of toxicity testing. Front Genet. 2014;5:1–10.

175. dos Santos SC, Sá-Correia I. Yeast toxicogenomics: Lessons from a eukaryotic cell model and cell factory. Curr Opin Biotechnol. 2015;33:183–91.

176. Yofe I, Weill U, Chuartzman S, Zalckvar E, Schütze C, Wiedemann N, et al. One library to make them all: streamlining yeast library creation by a SWAp-Tag (SWAT) strategy. Nat Methods. 2016;13:371–8.

177. Cohen Y, Schuldiner M. Adcanced methods for high-throughput microscopy screening of genetically modified yeast libraries. In: Cagney G, Emili A, editors. Network Biology Methods in Molecular Biology. Humana Press; 2011. p. 127–59.

178. Chuartzman SG, Schuldiner M. Database for high throughput screening hits (dHITS): a simple tool to retrieve gene specific phenotypes from systematic screens done in yeast. Yeast. 2018;35(7):1–7.

179. Parsons AB, Brost RL, Ding H, Li Z, Zhang C, Sheikh B, et al. Integration of chemical-genetic and

genetic interaction data links bioactive compounds to cellular target pathways. Nat Biotechnol. 2004;22:62–9.

180. Simpkins SW, Nelson J, Deshpande R, Li SC, Piotrowski JS, Wilson EH, et al. Predicting bioprocess targets of chemical compounds through integration of chemical-genetic and genetic interactions. Vol. 14, PLoS Computational Biology. 2018. 1–31 p.

181. Baryshnikova A. Systematic Functional Annotation and Visualization of Biological Networks. Cell Syst. 2016;2:412–21.

182. Hoepfner D, Helliwell SB, Sadlish H, Schuierer S, Filipuzzi I, Brachat S, et al. High-resolution chemical dissection of a model eukaryote reveals targets, pathways and gene functions. Microbiol Res. 2014;169:107–20.

183. Dias PJ, Teixeira MC, Telo JP, Sá-Correia I. Insights into the mechanisms of toxicity and tolerance to the agricultural fungicide mancozeb in yeast, as suggested by a chemogenomic approach. Omi A J Integr Biol. 2010;14:211–27.

184. Santos PM, Simões T, Sá-Correia I. Insights into yeast adaptive response to the agricultural fungicide mancozeb: A toxicoproteomics approach. Proteomics. 2009;9:657–70.

185. Gaytán BD, Loguinov A V., Lantz SR, Lerot JM, Denslow ND, Vulpe CD. Functional profiling discovers the dieldrin organochlorinated pesticide affects leucine availability in yeast. Toxicol Sci. 2013;132:347–58.

186. Gaytán BD, Loguinov A V., Peñate X, Lerot JM, Chávez S, Denslow ND, et al. A genome-wide screen identifies yeast genes required for tolerance to technical toxaphene, an organochlorinated pesticide mixture. PLoS One. 2013;8:1–12.

187. Gil FN, Gonçalves AC, Jacinto MJ, Becker JD, Viegas CA. Transcriptional profiling in *Saccharomyces cerevisiae* relevant for predicting alachlor mechanisms of toxicity. Environ Toxicol Chem. 2011;30:2506–18.

188. Gil FN, Becker JD, Viegas CA. Potential mechanisms underlying response to effects of the fungicide pyrimethanil from gene expression profiling in *Saccharomyces cerevisiae*. J Agric Food Chem. 2014;62:5237–47.

189. García MA, Oliva J, Barba A, Cámara MÁ, Pardo F, Díaz-Plaza EM. Effect of fungicide residues on the aromatic composition of white wine inoculated with three *Saccharomyces cerevisiae*

strains. J Agric Food Chem. 2004;52:1241–7.

CHAPTER 2 - Rationale and Aims

2.1. Rationale

It has been recognized that environmentally relevant concentrations of fungicides pose a significant threat to aquatic communities, namely to non-target organisms such as cyanobacteria (1), invertebrates (2,3), amphibians (4), and fish (5,6). Microbial communities are particularly susceptible to fungicides, especially non-target aquatic fungi (7–9). Indeed, the current risk assessment framework for fungicides may not be sufficiently protective for non-target fungi and the services where they intervene (10). Furthermore, according to our perspective and that of other authors, the environmental fate and effects of fungicides have received less attention compared to other types of pesticides (11–13). Thus, to contribute to the risk assessment process as part of a weight-of-evidence approach, it is important to understand fungicide toxicity profiles, mode of action, environmental occurrence, and off-target effects.

The term fungicide conventionally refers to a substance that controls fungi and fungi-like (e.g., oomycetes) pathogens. Fungicides are very diverse, both in terms of chemical nature and mode of action (**Figure 2.1**). They can be natural or synthetic, and control diseases by either preventing cell growth and reproduction (fungistatic), or by eliminating existing infections (fungicidal) (14,15), from both fungi and oomycetes (16,17). The latter are important agents of plant disease, especially genera *Phytophthora*, *Plasmopara*, and *Pythium*, causing mildews and blights in various important crops and tree species (18,19). For a long time, oomycetes, also known as water molds, were placed in the Fungi kingdom due to their filamentous growth, nutrition by absorption and reproduction via spores. Nevertheless, several features distinguish oomycetes from fungi, including cell wall composition, which is mainly formed by β-glucans and hydroxyproline in oomycetes, whereas chitin is the main component of the fungal cell wall (20,21). It is now clear that oomycete pathogens are unrelated to true fungi, and are instead more closely related to diatoms and brown algae. Given the devastating effects of the diseases they cause on crops, ornamental plants and trees, they are major contributors to the use of fungicides and represent a recurrent threat for global food security (18,19).

Fungicides can be classified according to their biological action (protectant or eradicant), or their chemical nature (inorganic or organic); however, the most common classification is based on the biological mode of action (14). The Fungicide Resistance Action Committee (FRAC) categorizes fungicides based on their mode of action to accommodate cross-resistance patterns. Their focus is to assess the risk of resistance development and offer guidelines for farmers, researchers, and industry professionals, ensuring the efficiency of these essential agricultural tools (22). The FRAC list classifies fungicides on the basis of the processes they target in pathogenic fungi and oomycetes. For that purpose, a code with different letters is used to distinguish fungicide groups: Group A targets nucleic

acid metabolism; group B targets cytoskeleton and motor proteins; group C affects respiration; group D targets amino acid and protein synthesis; group E affects signal transduction; group F targets lipid synthesis or transport/membrane integrity or function; group G targets sterol biosynthesis in membranes; group H affects cell wall biosynthesis; and group I affects cell wall melanin synthesis; host plant defense inducers belong to group P; group U comprises molecules with an unknown mode of action and unknown resistance risk; chemicals with multi-site activity are placed in group M[1]. Examples of fungicides present in each group and their target site code are displayed in **Figure 2.1**. Recently, a new category termed 'Biologicals with multiple modes of action' (BM) was introduced and includes agents of biological origin that exhibit multiple mechanisms of action (group and examples not included in **Figure 2.1**)[1].

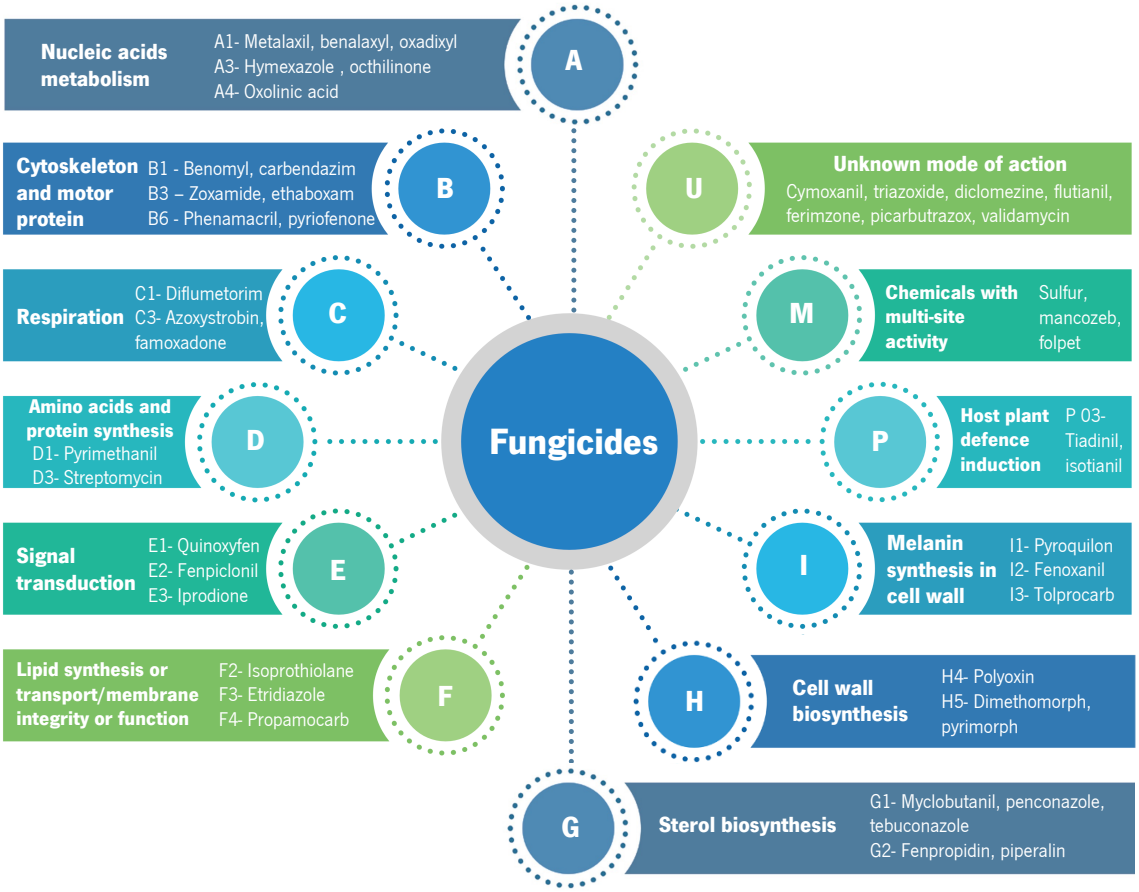

Figure 2.1. Examples of fungicides according to the FRAC list code. The biochemical mode of action in the plant pathogens (group A to I and group P, M and U), the target site code and a few examples of the fungicides displayed in the different groups.

[1] https://www.frac.info/ (assessed 3 Jan 2024)

Despite current efforts towards a more sustainable use of pesticides, fungicide use is predicted to increase as a result of increased fungal resistance, invasive species, and climate change (12). In 2021, 816 384 tonnes of fungicides and bactericides were used worldwide in agriculture, representing 25 % of the global pesticide use and the second most used class of agricultural pesticides (FAO 2021)[2]. The European Union is one of the dominant markets for fungicides, where they attain a share of 44 % of total pesticides (data from 2021 (13)). Sales of inorganic fungicides comprised 59.7 %, while organic counterparts consisted of 40.2 %, of which 10.6 % were (dithio)carbamates and 7 % from imidazole and triazole families (Eurostat 2021)[3]. Fungicide use is highly heterogeneous, varying across continents, but also regionally; in the EU, regional asymmetries are striking, in terms of the amount (in kg per hectare of arable land) and type (chemical families) of fungicides. Pimentão et al. (13) reviewed the heterogenous landscape of fungicide application in the EU. In the Portuguese case, pesticide sales are clearly dominated by fungicides (52 %) (Eurostat 2021)[3]. Among the most important crops in Portugal, especially in the north of the country, viniculture stands out due to its strongly dependence on fungicide applications to prevent a vast array of diseases caused by fungi and fungus-like organisms, such as oomycetes (23). Indeed, grapes are highly susceptible to diseases since they can be transferred from grapes into the winery, affecting wine production and quality (24). Consequently, fungicides are preventively and repeatedly used, resulting in their frequent occurrence in aquatic ecosystems.

Over the years, regulatory agencies have enforced the protection of surface and groundwaters, along with other aquatic environments vulnerable to pesticide contamination. The European Union implemented regulations like the Water Framework Directive [Directive 2000/60/EC of the European Parliament (25)], as well as its follow-up Directive 2008/105/EC of the European Parliament (26) and, more recently, Directive 2020/2184, recommending a targeted approach to pesticide monitoring, emphasizing the identification of pesticides most likely to be present in a given environment (27). Monitoring studies have consistently found fungicide residues in surface water and groundwater (28–30), with instances when fungicide concentrations exceed those of other pesticides (31). Locally, efforts to implement the Water Framework Directive, in collaboration with the Regional Coordination and Development Commissions, identified specific fungicides to monitor to assess the quality of drinking water in Portugal; many of these are commonly applied to prevent diseases in vineyards.

Despite regulatory actions (see above) and intense research on the subject (see Pimentão et al., 2024), we identify two major challenges in fungicide research: (i) there is still reduced information on the impact of fungicides on non-target microbes, with many antifungal substances having an unknown

[2] https://www.fao.org/faostat/en/#data/RP (assessed on 3 Jan 2024)

[3] https://ec.europa.eu/eurostat/statistics-explained/index.php?title=Agri-environmental_indicator_-_consumption_of_pesticides (assessed on 3 Jan 2024)

mode of action; and (ii) fungicide detection in environmental samples is costly and monitoring programs are often logistically impractical. To contribute to address these challenges, relevant tools and models are required for a cost-effective analysis of potential risk/toxicity of environmental samples and elucidation of the biological targets of poorly characterized fungicides. The yeast *S. cerevisiae* presents a versatile and well-established model system for comprehensively advancing our knowledge and tackling challenges associated with fungicide research.

Our group previously conducted a study on the effects of several fungicides on the growth and viability of the model system *S. cerevisiae*. The selected fungicides were chosen on the basis of their relevance in the context of disease management in vineyards, and included ergosterol biosynthesis inhibitors (tebuconazole and myclobutanil, FRAC group C), a respiration (quinone-outside) inhibitor (azoxystrobin FRAC group C), an RNA synthesis inhibitor (metalaxyl, FRAC group A) and an active ingredient with unknown mode of action (cymoxanil, FRAC group U). The results showed that azoxystrobin and metalaxyl had no effect on the growth or viability of yeast cells, while tebuconazole and myclobutanil inhibited growth in a concentration-dependent manner. In contrast, cymoxanil, despite its unknown mode of action, not only inhibited growth but also led to loss of cell viability. This indicates that in *S. cerevisiae,* tebuconazole and myclobutanil exhibited a fungistatic effect, while cymoxanil displayed fungicidal activity (32).

2.2. Aims

Considering the current state of art, we set out to use the yeast *S. cerevisiae* as a model organism to further explore the effects of two fungicides: (i) cymoxanil (CYM), a cyanoacetamide-oxime fungicide, for which the mechanism of action is not fully known, and (ii) tebuconazole (TEB), a triazole fungicide that belongs to the group of sterol biosynthesis inhibitors[4]. The main research aims of this thesis were:

- To elucidate phenotypic responses elicited by both fungicides in yeast cells. For that purpose, analysis of the functional effects in cell growth and cell viability and flow cytometry analyses of *S. cerevisiae* cells exposed to the fungicides were performed;

[4] https://www.frac.info/ (assessed on 6 Jan 2024)

- To uncover molecular targets underlying cytotoxicity of CYM. For that purpose, different and complementary genome-wide screens, transcriptomics, proteome localization, and functional genomics were performed;

- To develop a yeast-based biosensor to detect TEB, using synthetic biology techniques. The yeast-based biosensor developed was validated and tested under laboratory conditions, assessing its sensitivity, detection limit, and specificity towards a selected subset of fungicides family. Moreover, the developed biosensor was tested in aquatic samples.

Having previously presented the general background and state of the art of this thesis (**Chapter 1**), the present section (**Chapter 2**) showcases its rationale, goals and general outline. The main results of the adopted approach are structured in the following two chapters, which comprise the core of this thesis:

- **Chapter 3** comprises work performed with the fungicide CYM, and is divided in two sections. In **section 3.1**, we used the yeast *S. cerevisiae* to investigate the effect of CYM on respiration and mitochondrial respiratory complexes. Through biochemical studies and molecular docking algorithms, we demonstrate that, in yeast cells, CYM acts on respiration by blocking the interaction of cytochrome *c* (cyt *c*) with cytochrome *c* oxidase (C*c*O), inhibiting C*c*O catalytic activity. In **section 3.2**, we used the yeast *S. cerevisiae* to assess CYM phenotypic and transcriptomic responses. By examining cell growth, cell viability, transcriptomics, proteome localization, and functional genomics responses, we identified genome-wide alterations that provide insights into the mode of action of CYM. Our findings suggest that the antifungal activity of CYM can be associated with proton pump inhibition and disruption of plasma membrane potential. Overall, the findings in both sections contribute to clarify the mechanism of action of CYM, which was previously unknown.

- **Chapter 4** includes the work performed with the fungicide TEB. The yeast *S. cerevisiae* was used to assess TEB phenotypic responses in cell growth and cell viability as well as effects on plasma membrane lipid rafts and effects on *ERG* gene expression. Based on transcriptional responses elicited by TEB, a novel yeast-based biosensor to monitor this fungicide in aquatic ecosystems was developed. The findings in this study highlight the potential of this new method

as a complementary tool to analytical methods, namely in scenarios requiring screening of numerous samples.

At the end of the thesis (**Chapter 5**), we present and discuss the overall conclusions and future directions based on the open questions left by the present work.

2.3. References

1. Ortiz-Cañavate BK, Wolinska J, Agha R. Fungicides at environmentally relevant concentrations can promote the proliferation of toxic bloom-forming cyanobacteria by inhibiting natural fungal parasite epidemics. Chemosphere. 2019;229:18–21.
2. Cuco AP, Abrantes N, Gonçalves F, Wolinska J, Castro BB. Interplay between fungicides and parasites: Tebuconazole, but not copper, suppresses infection in a *Daphnia-Metschnikowia* experimental model. PLoS One. 2017;12:1–16.
3. Machado C, Cuco AP, Cássio F, Wolinska J, Castro BB. Antiparasitic potential of agrochemical fungicides on a non-target aquatic model (*Daphnia* × *Metschnikowia* host-parasite system). Sci Total Environ. 2022;833:1–9.
4. Hanlon SM, Lynch KJ, Kerby JL, Parris MJ. The effects of a fungicide and chytrid fungus on anuran larvae in aquatic mesocosms. Environ Sci Pollut Res. 2015;22:12929–40.
5. Bhagat J, Singh N, Nishimura N, Shimada Y. A comprehensive review on environmental toxicity of azole compounds to fish. Chemosphere. 2021;262:2–16.
6. Zhou T, Guo T, Wang Y, Wang A, Zhang M. Carbendazim: Ecological risks, toxicities, degradation pathways and potential risks to human health. Chemosphere. 2023;314:1–14.
7. Pimentão AR, Pascoal C, Castro BB, Cássio F. Fungistatic effect of agrochemical and pharmaceutical fungicides on non-target aquatic decomposers does not translate into decreased fungi- or invertebrate-mediated decomposition. Sci Total Environ. 2020;712:135676.
8. Zubrod JP, Bundschuh M, Feckler A, Englert D, Schulz R. Ecotoxicological impact of the fungicide tebuconazole on an aquatic decomposer-detritivore system. Environ Toxicol Chem. 2011;30:2718–24.
9. Baudy P, Zubrod JP, Konschak M, Röder N, Nguyen TH, Schreiner VC, et al. Environmentally relevant fungicide levels modify fungal community composition and interactions but not functioning. Environ Pollut. 2021;285:1–11.
10. Zubrod JP, Englert D, Feckler A, Koksharova N, Konschak M, Bundschuh R, et al. Does the current fungicide risk assessment provide sufficient protection for key drivers in aquatic ecosystem functioning? Environ Sci Technol. 2015;49:1173–81.
11. Ittner LD, Junghans M, Werner I. Aquatic fungi: a disregarded trophic level in ecological risk assessment of organic fungicides. Front Environ Sci. 2018;6:1–18.
12. Zubrod JP, Bundschuh M, Arts G, Brühl CA, Imfeld G, Knäbel A, et al. Fungicides: An Overlooked Pesticide Class? Environ Sci Technol. 2019;53:3347–65.

13. Pimentão AR, Cuco AP, Pascoal C, Cássio F, Castro BB. Current trends and mismatches on fungicide use and assessment of the ecological effects in freshwater ecosystems. Environ Pollut. 2024;347:1–12.
14. Rouabhi R. Introduction and Toxicology of Fungicides. In: Carisse O, editor. Fungicides. IntechOpen; 2010. p. 363–82.
15. Oliver RP, Hewitt HG. Plant pathology and plant pathogens. In: Oliver RP, Hewitt HG, editors. Fungicides in Crop Protection. CABI Publishing; 2014. p. 11–20.
16. Lamberth C, Rendine S, Sulzer-Mosse S. Agrochemical disease control: The story so far. In: Maienfisch P, Mangelinckx S, editors. Recent Highlights in the Discovery and Optimization of Crop Protection Products. Academic Press; 2021. p. 65–85.
17. Gisi U, Sierotzki H. Oomycete fungicides: phenylamides, quinone outside inhbitors, and carboxylic acid amides. In: Ishii H, Hollomon D, editors. Fungicide Resistance in Plant Pathogens. Tokyo: Springer; 2015. p. 145–74.
18. Derevnina L, Petre B, Kellner R, Dagdas YF, Sarowar MN, Giannakopoulou A, et al. Emerging oomycete threats to plants and animals. Philos Trans R Soc B Biol Sci. 2016;371:1–9.
19. Kamoun S, Furzer O, Jones JDG, Judelson HS, Ali GS, Dalio RJD, et al. The top 10 oomycete pathogens in molecular plant pathology. Mol Plant Pathol. 2015;16:413–34.
20. Richards TA, Dacks JB, Jenkinson JM, Thornton CR, Talbot NJ. Evolution of filamentous plant pathogens: gene exchange across Eukaryotic Kingdoms. Curr Biol. 2006;16:1857–64.
21. Latijnhouwers M, De Wit PJGM, Govers F. Oomycetes and fungi: Similar weaponry to attack plants. Trends Microbiol. 2003;11:462–9.
22. Kuck KH, Leadbeater A, Gisi U. FRAC Mode of Action Classification and Resistance Risk of Fungicides. In: Jeschke P, Witschel M, Krämer W, Schirmer U, editors. Modern Crop Protection Compounds. Wiley-VCH Verlag GmbH & Co. KGaA; 2008. p. 415–32.
23. Bereswill R, Golla B, Streloke M, Schulz R. Entry and toxicity of organic pesticides and copper in vineyard streams: Erosion rills jeopardise the efficiency of riparian buffer strips. Agric Ecosyst Environ. 2012;146:81–92.
24. Pinto C, Pinho D, Sousa S, Pinheiro M, Egas C, Gomes AC. Unravelling the diversity of grapevine microbiome. PLoS One. 2014;9:1–12.
25. Directive 2000/60/EC of the European Parliament and of the Council of 23 October 2000 establishing a framework for Community action in the field of water policy. Off J Eur Union L. 2000;327:1-73.

26. Directive 2008/105/EC of the European Parliament and of the Council of 16 December 20008 on environmental quality standards in the field of water policy. Off J Eur Union L. 2008;348:84-97
27. Directive 2020/2184 of the European Parliament and of the Council of 16 December 2020 on the quality of water intended for human consumption (recast). Off J Eur Union L. 2020;435:1-62.
28. Reilly TJ, Smalling KL, Orlando JL, Kuivila KM. Occurrence of boscalid and other selected fungicides in surface water and groundwater in three targeted use areas in the United States. Chemosphere. 2012;89:228–34.
29. Stehle S, Schulz R. Agricultural insecticides threaten surface waters at the global scale. Proc Natl Acad Sci U S A. 2015;112:5750–5.
30. Wightwick AM, Bui AD, Zhang P, Rose G, Allinson M, Myers JH, et al. Environmental fate of fungicides in surface waters of a horticultural-production catchment in Southeastern Australia. Arch Environ Contam Toxicol. 2012;62:380–90.
31. Stehle S, Schulz R. Pesticide authorization in the EU—environment unprotected? Environ Sci Pollut Res. 2015;22:19632–47.
32. Carvalho C. Novel yeast biosensors for environmental monitoring. University of Minho; 2018. (Master thesis).

CHAPTER 3 - Unveiling the Mechanisms Underlying Cymoxanil Cytotoxicity in *S. cerevisiae* Yeast Cells

This chapter is adapted from the following publications:

Filipa Mendes, Cátia Santos-Pereira, Tatiana F. Vieira, Mélanie Martins Pinto, Bruno B. Castro, Sérgio F. Sousa, Maria João Sousa, Anne Devin, Susana R. Chaves **The widely used cymoxanil fungicide impairs respiration in *Saccharomyces cerevisiae* via cytochrome *c* oxidase inhibition.**
Under revision at FEBS Letters

Filipa Mendes, Hadar Meyer, Leslie Amaral, Bruno B. Castro, Maya Schuldiner, Maria João Sousa, Susana R. Chaves **The antifungal activity of cymoxanil is associated with proton pump inhibition and disruption of plasma membrane potential.**
DOI: doi.org/10.1101/2024.03.01.583004 (pre-print)

Background

CYM [(1E)-2-(ethylcarbamoylamino)-N-methoxy-2-oxoethanimidoyl cyanide] is a synthetic acetamide compound used as a curative and preventive fungicide. It is normally applied as a foliar spray, and is thus designated as a foliar fungicide (1). It was first introduced in 1977, and has since been considered an important tool to protect grape and vegetable crops from oomycete pathogens of the Peronosporales order (2). In practical applications, CYM effectively combats downy mildew diseases caused by *Plasmopara viticola* in grapevine cultures and late blight diseases triggered by *Phytophthora infestans* in tomato and potato crops (3,4). Due to its weak persistence (half-life of a few days, depending on the conditions) and mobile nature (adsorption coefficient, K_{oc} 39–238), CYM displays a relatively short period of activity when used alone (5). As a result, it is often combined with other fungicides, such as mancozeb and copper, which are known for their multisite mode of action and longer protective effects, to enhance overall efficacy (6). While the biochemical mode of action of many fungicides is well characterized, in some cases knowledge is lacking. Indeed, many fungicides are commercially available despite an unknown biochemical mode of action, since fungicide registration often relies solely on fulfilling toxicological and environmental requirements (7). CYM is one of these, since its precise mode of action remains unknown.

According to some authors, CYM acts as a pro-fungicide and undergoes biotransformation by fungi into one (or several) fungitoxic metabolite(s). Studies in *B. cinerea* demonstrated that CYM is rapidly metabolized (half-life $\leq$ 2 h) by a highly sensitive strain, resulting in the formation of three main metabolites, N-acetylcyanoglycine, ethylparabanic acid and demethoxylated cymoxanil. Among these, N-acetylcyanoglycine was fungitoxic against this sensitive strain, suggesting it plays an important role in the toxicity of CYM (8–10). Mechanistically, in the case of *P. infestans*, CYM has been reported to inhibit mycelial growth and is highly effective against germ tube formation by sporangia. CYM was also shown to inhibit DNA and RNA synthesis, assessed by measuring [methyl-^{3}H] thymidine and [^{3}H] uridine incorporation, respectively, with DNA synthesis more sensitive to CYM than RNA synthesis. Nonetheless, no effect on RNA polymerase activity was observed, indicating that these alterations are secondary effects. Furthermore, CYM had no effect on mycelial respiration even at concentrations up to 100 mg mL^{-1} (11). In contrast, a study reported that addition of CYM to the culture medium inhibited cell growth and biomass production and decreased respiratory rates of an *S. cerevisiae* strain (12). Additionally, CYM inhibited ATP synthesis in a commercial *S. cerevisiae* strain (2), whereas a slight effect of CYM on the respiration of *Botrytis cinerea* was reported (13). Beyond its primary targets (oomycetes and fungi),

CYM can also affect the growth of non-target organisms, such as the bacterium *Rhodopirellula rubra* and the microalgae *Raphidocelis subcapitata* (1).

Despite the interest from several laboratories in studying CYM cytological effects and biochemical mode of action, available data so far has not yielded conclusive results, leaving its mechanism of action still unclarified. Even though the toxicological profile poorly characterized, the European Commission has renewed the authorization to use CYM and products containing CYM until 2026. This highlights the need to uncover the mode of action of CYM and gain comprehensive understanding of its effects on various organisms. Further in-depth investigations are crucial to underscore the importance of careful consideration when using this fungicide.

Taking in consideration the contrasting reports regarding the effect of CYM on respiration and its uncharacterized mode of action. In this chapter we sought to:

(i) investigate the role of CYM on respiration of *S. cerevisiae* cells (section 3.1-unveiling the impact of cymoxanil in yeast cells respiration);

(ii) explore the well-characterized *S. cerevisiae* model system to further dissect mechanisms underlying the toxicological effects of CYM, using omics-based approaches (section 3.2-molecular bases of the antifungal activity of cymoxanil).

3.1. Unveiling the impact of cymoxanil in yeast cells respiration

3.1.1. Materials and Methods

3.1.1.1. Yeast strain, culture medium, growth conditions and treatment

The yeast *S. cerevisiae* BY4742 (*Mat a; his3Δ1; leu2Δ0; lys2Δ0; ura3Δ0*) was used throughout this study. Cells were grown aerobically at 28 °C in the following medium: 0.175 % yeast nitrogen base without amino acids and without ammonium sulphate, 0.2 % casein hydrolysate, 0.5 % $(NH_4)_2SO4$, 0.1 % KH_2PO_4, 2 % lactate (w/v), pH 5.5, 20 mg L^{-1} L-tryptophan, 40 mg L^{-1} adenine hydrochloride, and 20 mg L^{-1} uracil. When applicable, cells were exposed, in the culture medium, to 50 μg mL^{-1} CYM from Sigma-Aldrich and/or the equivalent volume of DMSO as a negative control (lower than 0.5 %). Cell growth was measured indirectly as optical density at 600 nm in a Safas spectrophotometer (Monaco).

3.1.1.2. Mitochondria preparation

For mitochondria preparation, yeast cells grew in YPL medium (1 % yeast extract, 0.1 % potassium phosphate, 0.12 % ammonium sulphate, supplemented with 2 % lactate as carbon source, pH 5.5) without any treatment and were harvested in stationary phase for mitochondria preparation. Yeast mitochondria were isolated from spheroplasts as described elsewhere (14) and suspended in buffer A (0.6 M mannitol, 2 mM EGTA, and 10 mM Tris-Maleate, pH 6.8). Protein Concentration was performed using the biuret method (15) using bovine serum albumin to build the standard curve.

3.1.1.3. Oxygen consumption assays

Oxygen consumption was measured in a 1 mL thermostatically controlled chamber, at 28 °C, equipped with a Clark electrode connected to a recorder. Respiratory rates were determined from the slope of a plot of O_2 concentration *versus* time. Respiration assays in whole cells were performed in the growth medium and, when indicated, CYM, triethyltin bromide (TET), a lipophilic inhibitor of mitochondrial ATP synthase that mimics ADP depletion (16,17), or carbonyl cyanide *m*-chlorophenylhydrazone (CCCP), a well-known uncoupling agent that increases oxygen consumption rates by dissipating the electrochemical proton gradient across the inner mitochondrial membrane, allowing the electron transport chain to function at maximum speed (18,19), were added to the chamber.

For assays with purified mitochondria, 0.2 mg of protein mL^{-1} were suspended in buffer A and ethanol (100 mM) was used as respiratory substrate. For assays performed under phosphorylating

conditions (state 3, or ADP-stimulated respiration), when protons drive into the mitochondrial matrix from outside the inner membrane and ADP is consumed by phosphorylating systems, thus with oxygen consumption associated with ATP synthesis, ADP was added at the concentration indicated in the figure legends. For assays performed under non-phosphorylating conditions (state 4), when no ATP is produced and oxygen consumption is maintained at low rates (20), ADP was not added. When used, the uncoupler CCCP was used at the concentration indicated in the figure legends. For C*c*O-mediated respiration, mitochondria (0.2 mg of protein mL^{-1}) were suspended in buffer A and incubated in the presence of antimycin A (2.5 μg/mg of protein), 2.5 mM ascorbate, 100 μM *N,N,N',N'*-tetramethyl-*p*-phenylenediamine (TMPD), and 100 mM ethanol as the respiratory substrate, as described elsewhere (21). Schematic representation of the electron transport chain and strategy used to determine C*c*O activity is displayed in **Figure 3.1.1**. All the experiments using isolated mitochondria were performed after 6 min of incubation with CYM for accurate inhibition.

3.1.1.4. Determination of mitochondrial complex III (Ubiquinol: Cytochrome *c* Oxidoreductase) activity

Mitochondrial complex III activity was determined as described previously (21). Briefly, mitochondria (0.2 mg of protein mL^{-1}) were incubated in buffer A in the presence of 1 mM KCN, 1 mM ferricyanide, and 100 mM ethanol as the respiratory substrate. Ferricyanide has been used as an artificial electron acceptor, thus, under these circumstances, the ferricyanide reduction rate serves as an indicator of complex III activity (22,23). Absorbance changes were followed at 436 nm in a Safas spectrophotometer (Monaco). The rate of ferricyanide reduction was calculated from the slope of absorbance change as a function of time. A molar extinction coefficient of 0.21 mM^{-1} cm^{-1} was used. The strategy used to determine complex III activity is systematized in **Figure 3.1.1**.

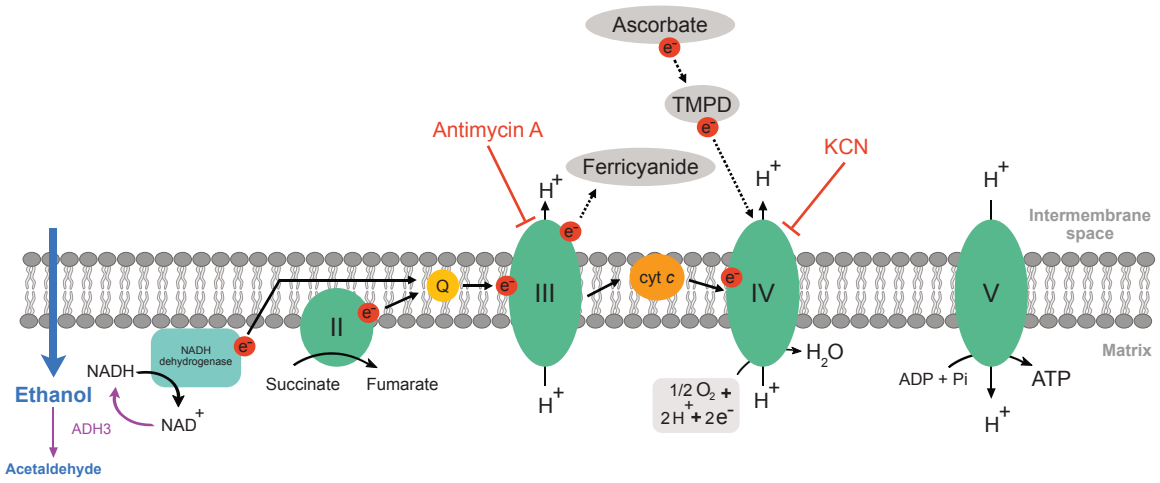

Figure 3.1.1. Schematic representation of the electron transport chain in *S. cerevisiae* isolated mitochondria and strategies used to determine the effect of CYM on mitochondrial complexes III and IV. All experiments were performed in the presence or absence of CYM using ethanol as substrate, thanks to the presence of mitochondrial alcohol dehydrogenase (ADH3) that catalyzes the conversion of ethanol to acetaldehyde and NADH inside the matrix (24). The activity of complex III was based on the reduction rate of ferricyanide, an electron acceptor (22,23). For that purpose, isolated mitochondria were incubated in respiration buffer A containing ethanol, ferricyanide and KCN [inhibitor of complex IV (25)]. After monitorization of the reduction of ferricyanide, antimycin A [inhibitor of complex III (26)] was added to the reaction to ensure that the activity herein measured was indeed mediated by complex III. The activity of complex IV was based on oxygen consumption. For that purpose, isolated mitochondria were incubated in respiration buffer A with ethanol, antimycin A and ascorbate, which is the electron donor of TMPD, which in turn donates electrons to C*c*O (complex IV) (27,28). After monitorization of the oxygen consumption, KCN was added to the reaction to ensure that the activity measured in this experiment was indeed mediated by complex IV.

3.1.1.5. Docking studies

To predict the binding affinity and possible modes of action of four compounds (CYM, ethylparabanic acid, N-acetylcyanoglycine and demethoxylated cymoxanil) towards C*c*O, a detailed protein-ligand docking study was performed using the GOLD software (with its four scoring functions: PLP, ChemScore, ASP and GoldScore). All the docking runs were performed in triplicate for increased sampling. The structures of the four compounds were prepared using Datawarrior (29) and Open babel (30).

Based on a deep literature search, two different hypotheses were tested to explore how CYM could potentially inhibit C*c*O: (i) docking between the heme a_3 and the copper ion Cu_B at the known binding position of KCN, blocking the electron transfer mechanism. We used a cyanide ion as reference

for docking coordinates and applied a 6 Å docking radius to thoroughly explore this region; (ii) docking at the interfacial region that C*c*O forms with cyt *c*, potentially interfering with their interaction. For this approach, the residues of chain B of C*c*O (subunit II) described by Shimada and coworkers (31) as important for protein-protein interaction with cyt *c* were used for the definition of the binding site (Ser117, Asp139, Tyr121, Asp119, Tyr105). The docking radius was 15 Å and the number of runs was set to 500, ensuring in this way that all possible configurations were considered. An additional compound, ADDA-5, (1-[2-(1-adamantyl)-ethoxy]-3-(3,4-dihydro-2(1H)-isoquinolinyl)-2-propanol hydrochloride), which was described as a C*c*O inhibitor with an IC_{50} of 21.42 µM (32), was used as a reference for the second hypothesis.

The X-ray structures selected for the preparation of the docking models were: structure 3X2Q, which contains a cyanide ion between with group heme a_3 and Cu_B (25) (hypothesis 1); structure 5IY5, which represents the bovine X-ray structure of the C*c*O-cyt *c* complex at 2.0 Å resolution (31) (hypothesis 2); and structure 8DH6, which is the Cryo-EM structure of CcO of *S. cerevisiae* at 2.94 Å (to confirm hypothesis 2). The three structures were aligned to ensure consistency in the docking coordinates. The chains primarily evaluated in this work are highlighted in **Figure 3.1.2**.

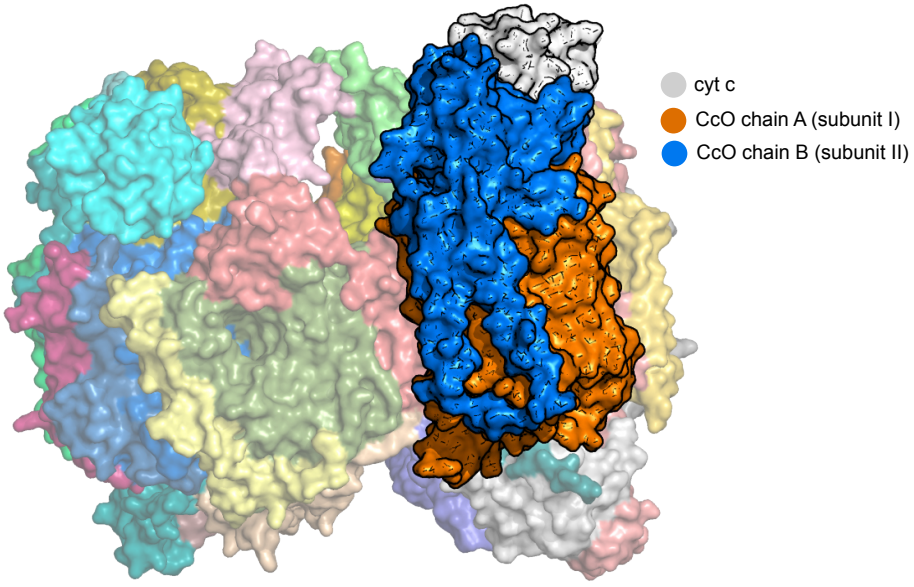

Figure 3.1.2. Structure of the C*c*O - cyt *c* complex used in this work. The bovine structure (PDB: 5IY5) is shown in surface representation with all chains in a different color. The two chains evaluated for docking (in orange and blue), as well as cyt *c* (in gray) are highlighted.

3.1.1.6. Statistical analysis

The statistical analysis of the results was performed using GraphPad Prism software (version 8.4.0). In all assays, data are expressed as the mean and standard deviation (S.D.) of at least three independent experiments. A one- or two-way analysis of variance (ANOVA) was used to test the effect of CYM on respiration of isolated mitochondria or whole-cells, respectively. A Dunnett test was used to assess differences relatively to BY, state 4, state 3, state 4 + 2 μM CCCP, complex III, or complex IV. A significance level of 0.05 was employed in all analyses.

3.1.2. Results

3.1.2.1. Cymoxanil impairs respiration of whole cells

To investigate the role of CYM on respiration in whole cells, the *S. cerevisiae* BY4742 strain was first cultured in a respiratory substrate (lactate) with or without the addition of 50 μg mL^{-1} CYM, and assessed the respiratory flux hourly for 8 h. We found that CYM significantly inhibited the respiratory rate, reducing it by approximately 50 % after 3-4 h of treatment in comparison with nontreated cells (BY) (**Figure 3.1.3**). Thereafter, the percentage of inhibition remained similar until 8 h of exposure to the fungicide. Adding CYM to untreated cells directly in the electrode chamber led to a less pronounced respiration inhibition, regardless of the growth phase, although this inhibition was not statistically significant (**Figure 3.1.3**).

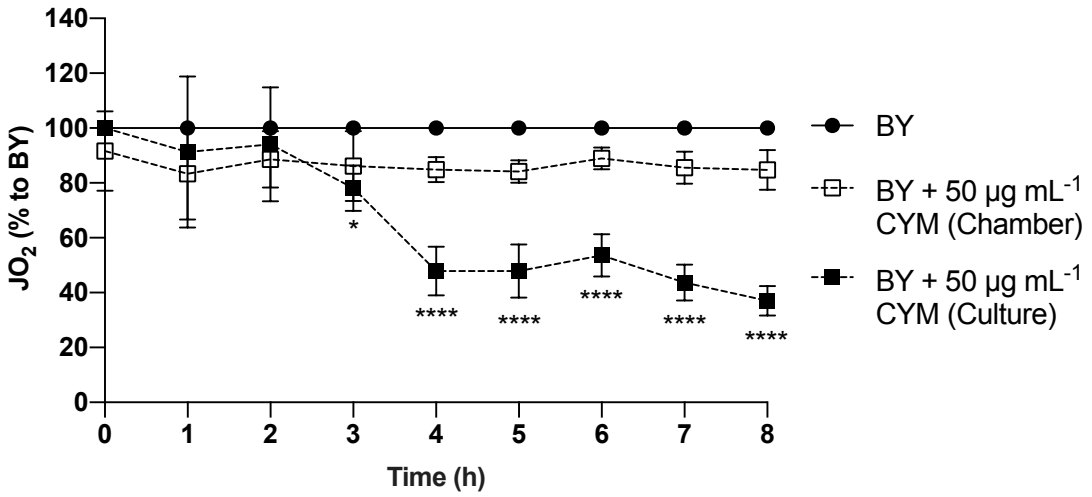

Figure 3.1.3. Effect of CYM on the respiratory flux (JO_2) of yeast cells, along time. The rate of oxygen consumption of BY4742 cells was monitored as described in "Materials and Methods". At each time point, oxygen consumption was evaluated in nontreated cells (●), cells with 50 µg mL^{-1} of CYM added in the chamber (□), and cells with 50 µg mL^{-1} of CYM added to the culture at time 0 (■). The data are displayed as the percentage of inhibition in relation to BY (100 %) and represent mean values ± S.D. of at least three independent experiments. Asterisks (*, $P \leq 0.05$; ****, $P \leq 0.0001$) depict significant differences relative to BY.

Next, we assessed the effect of the mitochondrial ATP synthase inhibitor TET, and found it decreased respiratory rates by approximately 50 % in untreated BY4742 cells. TET also similarly decreased respiratory rates of cells grown in the presence of CYM for up to 4 h, but respiratory rates decreased further in cells exposed to the fungicide for longer times (**Figure 3.1.4A**). As such, we observed that, after CYM inhibition of respiratory rates was apparent (from 4 h on), it could still be inhibited further by inhibition of ATP synthase.

We also addressed the effect of CCCP and found, as expected, that addition of this uncoupler nontreated cells increased the respiratory flux by almost 50 % (**Figure 3.1.4B**). However, addition of CCCP to CYM-treated cells resulted in two different phenotypes. In the first 3 h of exposure to CYM, CCCP increased the respiration rate to the maximal capacity of the mitochondrial electron transport system. However, after that, CCCP progressively lost the ability to increase respiration, indicating that incubation with CYM for at least 3 h decreases the maximum respiration capacity of cells (**Figure 3.1.4B**).

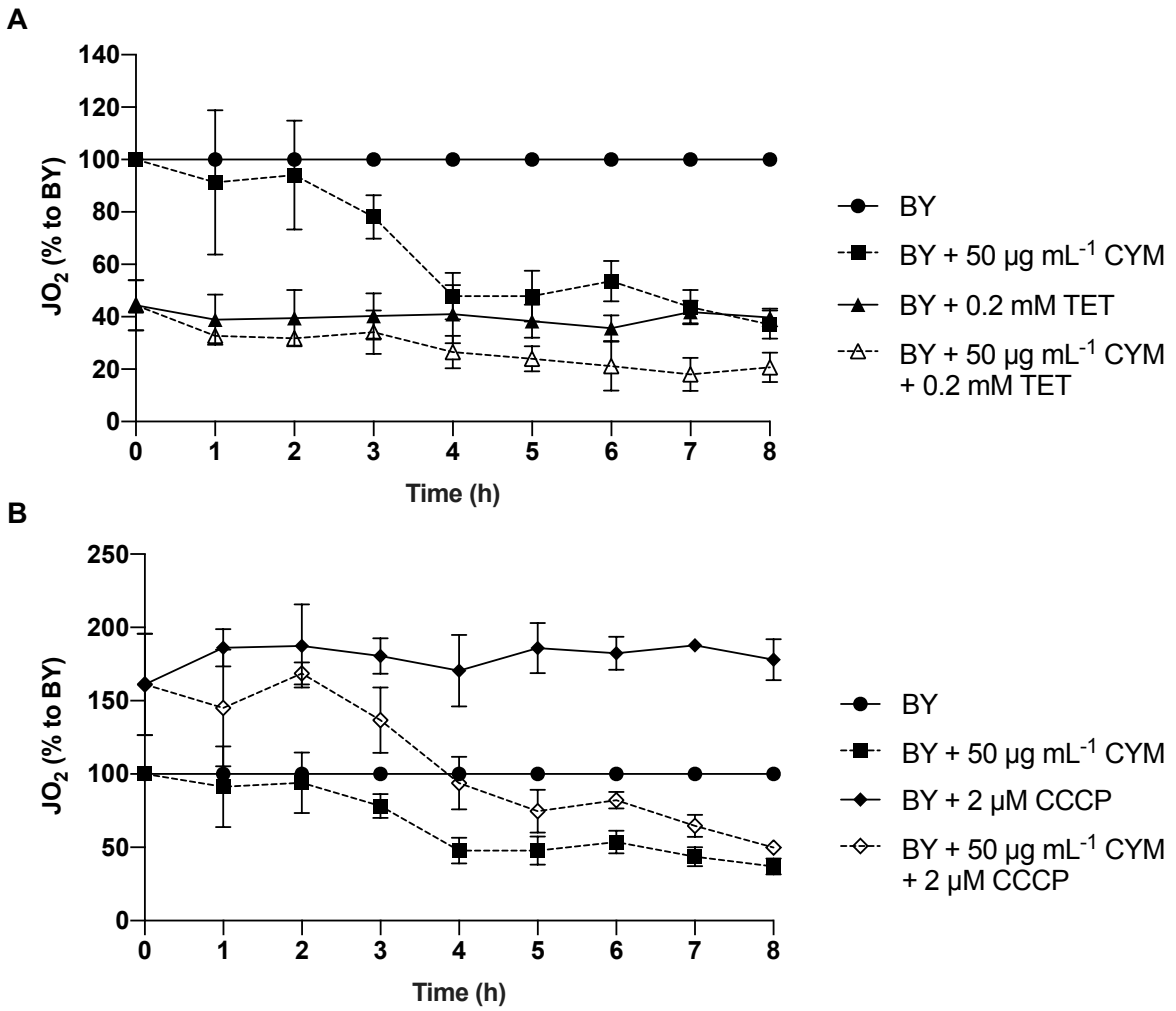

Figure 3.1.4. Effect of CYM on the JO_2 of yeast cells in the presence of an inhibitor or an uncoupler. The rate of oxygen consumption was assessed as described in "Materials and Methods", with the addition of CYM to the culture, with 0.2 mM TET **(A)** or 2 µM CCCP **(B)** in the chamber. The data are displayed as the percentage of inhibition in relation to BY (100 %) and represent mean values ± S.D. of at least three independent experiments.

3.1.2.2. Cymoxanil compromises the mitochondrial electron transport chain

We next tested the effect of CYM on BY4742 isolated mitochondria. Unlike the delayed inhibition observed in whole cells, direct addition of CYM to isolated mitochondria immediately inhibited respiration (**Figure 3.1.5**). This inhibition was dependent on the concentration of CYM and independent of the respiratory state, as similar results were obtained under non-phosphorylating conditions (state 4, blue bars) and phosphorylating conditions (state 3, orange bars). Moreover, similarly to whole cells, we observed a concentration-dependent inhibition of maximal respiration by CYM (state 4 + CCCP, green bars).

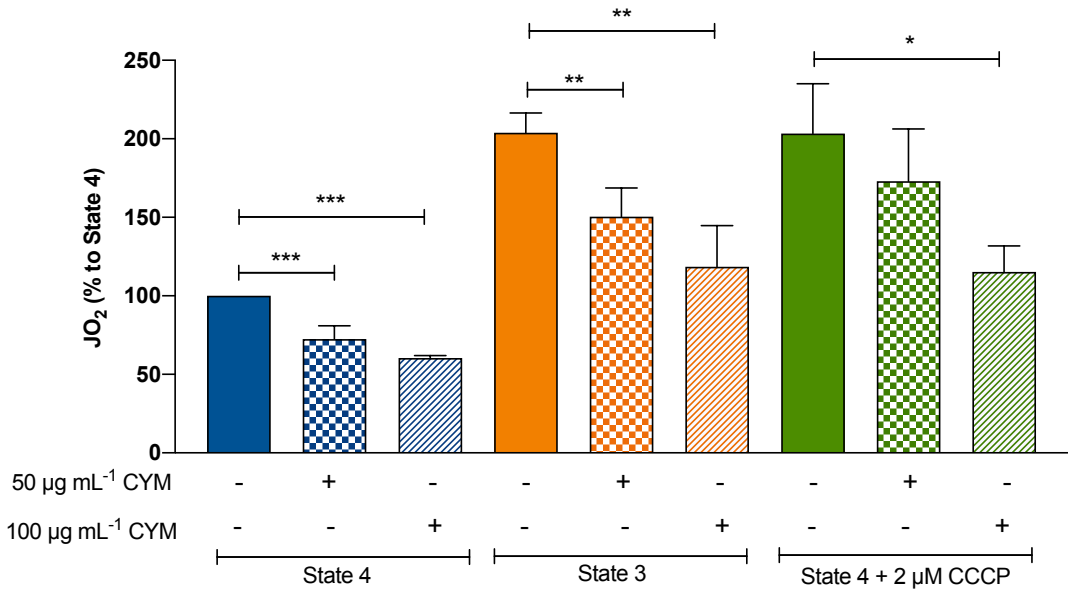

Figure 3.1.5. Effect of CYM on the oxygen consumption rate of isolated yeast mitochondria. Mitochondria (0.2 mg of protein mL^{-1}) were suspended in buffer A and oxygen consumption was monitored under non-phosphorylating conditions (state 4) and phosphorylating conditions (state 3), upon addition of 1 mM ADP. The rate of oxygen consumption was also measured when state 4 was induced and 2 µM CCCP was added. All assays were performed using 100 mM ethanol as the respiratory substrate and conducted in the absence or presence of 50 and 100 µg mL^{-1} CYM. Results are expressed as a percentage of inhibition in relation to state 4, without CYM (100 %), and represent mean values ± S.D. of at least three independent experiments. Asterisks (*, $P \leq 0.05$; **, $P \leq 0.01$; ***, $P \leq 0.001$) depict significant differences relative to state 4, state 3 or state 4 + 2 µM CCCP.

Since we found that CYM inhibits the electron transport chain, likely independently of ATP synthase, we further assessed the effect of CYM on the activity of individual complexes. We found that complex III activity was not altered significantly, even at the higher concentration tested (**Figure 3.1.6A**). We verified that the activity measured was indeed mediated by complex III, as it was sensitive to antimycin A, inhibitor of complex III [data not shown, (26)]. On the other hand, activity of complex IV (C*c*O) was strongly inhibited by both concentrations tested (**Figure 3.1.6B**). Moreover, the CYM effects shown in **Figure 3.1.6B** were sensitive to KCN, inhibitor of C*c*O activity [data not shown, (25)], as evidence that the oxygen consumption assessed in this assay was indeed mediated by C*c*O.

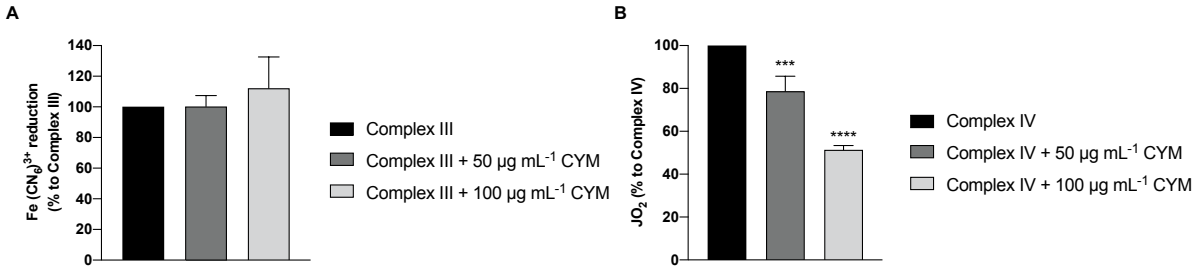

Figure 3.1.6. Effect of CYM on the activity of mitochondrial complex III and complex IV. (A) For determination of complex III activity, mitochondria (0.2 mg of protein mL^{-1}) were incubated in respiration buffer A containing 1 mM KCN, 2 mM ferricyanide and 100 mM ethanol. The reduction of ferricyanide was monitored spectrophotometrically at 436 nm, in the absence or presence of 50 or 100 µg mL^{-1} CYM. **(B)** For determination of complex IV (C*c*O) activity, mitochondria (0.2 mg of protein mL^{-1}) were incubated in respiration buffer A with 100 mM ethanol, 2.5 µg of antimycin A/mg of protein, 2.5 mM ascorbate, and 100 µM TMPD. Oxygen consumption was monitored in the absence or presence of 50 or 100 µg mL^{-1} CYM. Results are expressed as a percentage of inhibition in relation to complex III or complex IV (100 %) and represent mean values ± S.D. of at least three independent experiments. Asterisks (***, $P \leq 0.001$; ****, $P \leq 0.0001$) depict significant differences relative to complex IV.

3.1.2.3. Model for cymoxanil inhibition of cytochrome *c* oxidase activity

Since we found that CYM directly inhibits mitochondrial C*c*O, we sought to predict a possible mechanism by which it inhibits this complex by using computational tools. Since the respiratory rate in whole cells was significantly impaired by CYM only after 4 h incubation, and when directly added to isolated mitochondria the inhibition was less pronounced, we hypothesized that the effect of CYM on respiration of whole cells might also be linked to its metabolization and the potential action of generated metabolites. We therefore analyzed possible hypotheses of C*c*O inhibition by CYM or its metabolites: (i) docking between the heme a_3 and the copper ion Cu_B at the known binding position of KCN, blocking the electron transfer mechanism; (ii) docking at the interfacial region that C*c*O forms with cyt *c*, potentially interfering with their interaction, and using ADDA-5 as a reference.

When testing the first hypothesis, we observed that the selected docking site (heme a_3-Cu_B center) was strongly unfavorable, with strong steric tension, due to the very limited accessible space. Possible docking poses were obtained, but they were 5-6 Å away from this center, positioned at the surface of the protein, where the molecule interacted with the propionate groups of heme a and heme a_3. As shown in supplementary material **table S3.1.i**, these values were very low, suggesting the existence of extreme steric clashes, particularly for the molecules with higher molecular weights, with demethoxylated cymoxanil and ADDA-5 exhibiting negative scores. Supplementary material **figure S3.1.i** depicts the docked position of each tested compound, and consistent results were observed in docking runs performed with other scoring functions such as ASP, Chemscore and GoldScore (data not shown).

Further analysis of the C*c*O structure and comparison with other X-ray structures of C*c*O confirmed that there is insufficient space for molecules with more than two or three atoms to bind between the copper ion and heme a_3.

The second hypothesis explored the possibility of these molecules inhibiting C*c*O activity by interfering with electron transfer between cyt *c* and C*c*O. During testing, we observed interesting and highly consistent results across different evaluation methods. Indeed, the tendency in terms of docking scores remained the same across all scoring functions tested for this hypothesis. The variation in scores is attributed to the distinct aspects of protein-ligand interactions that each scoring functions considers (**Table 3.1.1** – Bovine C*c*O).

Table 3.1.1. Docking results between bovine C*c*O (structure PDB: 5IY5) or yeast C*c*O (structure PDB: 8DH6) and the tested compound using the GOLD software. Results of the different GOLD scoring functions (PLP, ChemScore, ASP and GoldScore) for the docking between C*c*O and CYM, or its potential metabolites ethylparabanic acid, N-acetylcyanoglycine, demethoxylated cymoxanil and ADDA-5. The latter was used as a reference compound.

GOLD scoring function	Compound	Bovine C*c*O	Yeast C*c*O
PLP	Ethylparabanic acid	19.15 ± 0.01	19.15 ± 0.00
	N-acetylcyanoglycine	24.70 ± 0.01	21.16 ± 1.05
	CYM	31.38 ± 0.25	26.66 ± 0.12
	Demethoxylated cymoxanil	25.06 ± 0.01	27.35 ± 0.22
	ADDA-5	50.64 ± 0.50	43.38 ± 0.91
ChemScore	Ethylparabanic acid	14.33 ± 0.02	12.48 ± 0.63
	N-acetylcyanoglycine	12.43 ± 0.02	11.72 ± 0.02
	CYM	14.55 ± 0.12	13.29 ± 0.18
	Demethoxylated cymoxanil	11.83 ± 0.20	12.20 ± 0.06
	ADDA-5	23.91 ± 0.33	22.59 ± 1.38
ASP	Ethylparabanic acid	13.48 ± 0.09	13.34 ± 0.25
	N-acetylcyanoglycine	11.78 ± 0.23	11.89 ± 0.03
	CYM	16.40 ± 0.27	13.61 ± 0.45
	Demethoxylated cymoxanil	15.74 ± 0.20	17.17 ± 0.44
	ADDA-5	25.05 ± 0.81	26.88 ± 0.90
GoldScore	Ethylparabanic acid	19.69 ± 0.02	20.67 ± 0.02
	N-acetylcyanoglycine	28.77 ± 0.56	29.98 ± 0.04
	CYM	29.25 ± 0.07	35.52 ± 0.56
	Demethoxylated cymoxanil	24.73 ± 0.16	28.81 ± 0.35
	ADDA-5	40.15 ± 0.79	32.83 ± 0.35

Based on the analysis of the absolute GOLD/PLP scores (**Figure 3.1.7**), ethylparabanic acid exhibited the lowest binding affinity, while the reference compound ADDA-5 displayed the highest affinity, primarily attributed to its much larger size and molecular weight (**Figure 3.1.7**). Among the test compounds, CYM presented the highest score. This consistent trend was observed across all scoring functions (**Table 3.1.1** – Bovine C*c*O).

To address the potential overestimation of ligands with higher molecular weight during docking, especially when comparing molecules with very different scales like the tested compounds and ADDA-5, we normalized the scoring values by the number of heavy atoms (**Figure 3.1.7**). N-acetylcyanoglycine

and ethylparabanic acid exhibited higher normalized scores, but CYM stood out with a much higher normalized score than ADDA-5. Overall, CYM displayed both high absolute and normalized scores.

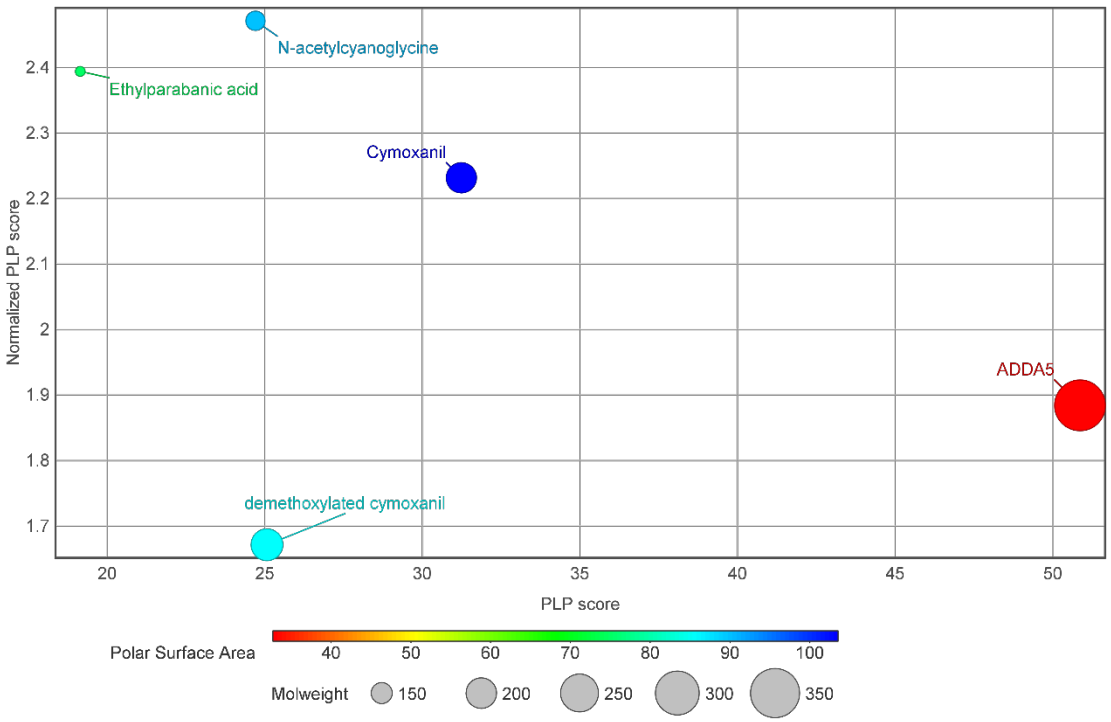

Figure 3.1.7. Correlation between the PLP score and the Non-H atoms of each molecule studied. The x-axis corresponds to the PLP score, while the y-axis depicts the PLP score normalized to the number of heavy atoms. The size of each marker reflects the molecular weight, and the color corresponds to the polar surface area of each compound.

Figure 3.1.8 (upper panel) displays the docking poses of all the tested compounds (using the PLP scoring function) with the contacting residues of subunit II of C*c*O (Ser117, Asp139, Tyr121, Asp119, Tyr105) highlighted in red. The figure also displays the typical binding region of cyt *c*. The presence of these residues suggests the possibility of an allosteric site, indicating that the tested compounds may inhibit the protein-protein interactions between cyt *c* and C*c*O, hampering electron transfer.

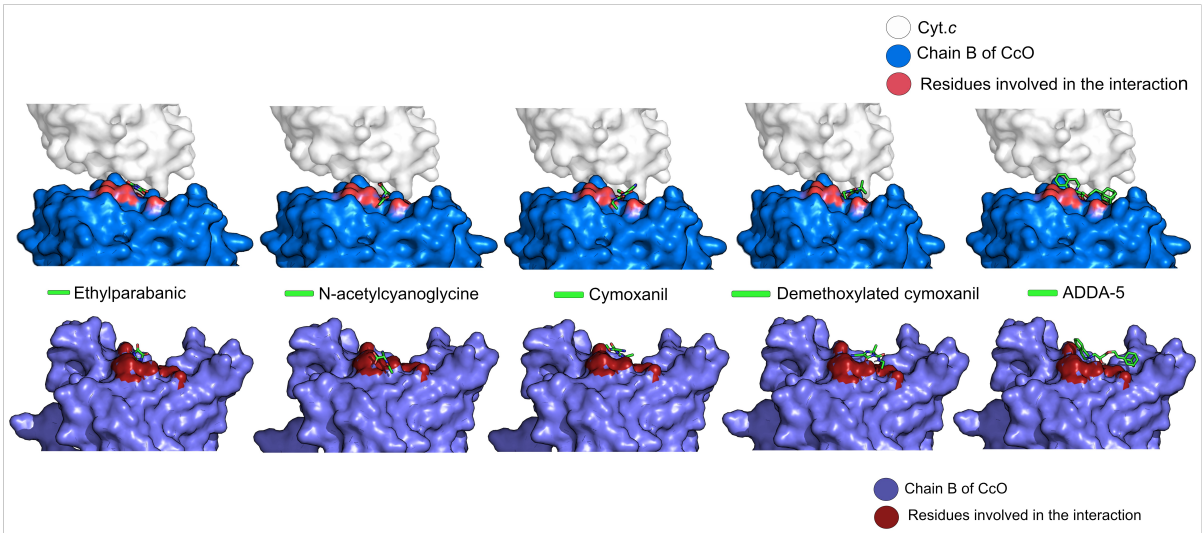

Figure 3.1.8. PLP docking poses for CYM, N-acetylcyanoglycine, ethylparabanic acid, demethoxylated cymoxanil and ADDA-5 on chain B (subunit II) of bovine C*c*O (structure PDB: 5IY5, blue) or yeast C*c*O (structure PDB: 8DH6, purple). Surface representation of normal binding mode of cyt *c* (white) in the absence of the inhibitor molecules and of chain B of C*c*O from bovine (blue) or yeast (purple) origin. The important residues for the interaction between cyt *c* and chain B are highlighted in red (bovine) and dark red (yeast). The tested compounds are shown in sticks, with carbon atoms represented in green, oxygen atoms in red and nitrogen atoms in blue.

A bovine X-ray structure of the C*c*O-*c*yt c complex was used since it is one of the crystallographic structures with higher resolution (31). However, to investigate the possibility of these molecules interfering with electron transfer between C*c*O and cyt *c* in yeast, docking was also performed with the C*c*O Cryo-EM structure of *S. cerevisiae* (PDB: 8DH6, lower resolution). The docking scores on the yeast structure exhibit a similar trend as the docking scores of the bovine structure 5IY4 (**Table 3.1.1**). Among the test compounds, CYM and ADDA-5 presented the highest score, indicating a higher affinity.

Figure 3.1.8 (lower panel) shows the docked poses of all the compounds studied (using the PLP scoring function) with the residues of subunit II of C*c*O important for interaction highlighted in dark red (Tyr125, Glu142, Glu144, Tyr146, Asp164). There is a difference in the docking poses when compared to the bovine X-ray structure, as expected, due to the difference in the type and position of some of the amino acid residues present (**Figure 3.1.8**). Nevertheless, the results suggest that protein-protein interaction of C*c*O with cyt *c* can be effectively blocked in yeast by these compounds.

3.1.3. Discussion

In this study, we investigated the effects of CYM on oxygen consumption using a well characterized *S. cerevisiae* laboratory strain, further proposing a mechanism of action. Using whole cells, we found that inhibition of respiration by CYM was not immediate, and was mainly apparent after 4 h. Furthermore, TET decreased respiratory rates both in untreated and treated cells. However, CCCP progressively lost the ability to increase respiration in CYM-treated cells, suggesting that the proton electrochemical gradient across the membrane and the electron flow to oxygen are progressively decreased. CCCP prevents ATP synthesis by transporting protons across the mitochondrial inner membrane, interfering with the proton gradient, thus oxygen consumption of yeast cells in the presence of CCCP is independent of ATP synthase (33). Taking into account the inability of CCCP to increase respiration of CYM-treated cells after 4 h and the fact that TET still has an effect on CYM-treated cells even after 4 h, we hypothesized that CYM acts on the mitochondrial electron transport chain. This hypothesis was supported by our findings that CYM immediately inhibited respiration of isolated mitochondria in a concentration-dependent manner under both non-phosphorylating and phosphorylating conditions, indicating that CYM inhibition is independent of the respiratory state. Altogether, these results strongly indicate that CYM directly or indirectly inhibits the electron transport chain, independently of ATP synthase.

Mitochondria of the yeast *S. cerevisiae* do not possess complex I (NADH:ubiquinone oxidoreductase) but have internal and external NADH dehydrogenases that transfer electrons to the quinone pool, thus the respiratory chain comprises three complexes: succinate dehydrogenase (complex II), complex III and C*c*O (complex IV) (34,35). Since our results indicate that CYM does not inhibit ATP synthase, we assessed its impact on the activity of complexes III and IV. While complex III activity was not affected, CYM directly inhibited complex IV (C*c*O). As such, we sought to predict a possible mechanism using computational tools.

C*c*O is a heme/copper-containing protein with multiple subunits that plays a pivotal role in electron transfer and oxygen reduction. It receives electrons from cyt *c* and transfers them to O_2, reducing it to water. This electron transfer and O_2 reduction releases free energy, which is coupled to proton pumping across the membrane (36). While C*c*O is composed of multiple subunits, subunits I and II and their redox centers are the most important for its functioning. Subunit II contains the Cu_A center, which has two copper ions and acts as the initial electron acceptor from cyt *c*. It then transfers electrons to the heme a center, which in turn transmits them to the heme a_3-Cu_B center, where oxygen reduction occurs. Both heme centers are located in subunit I (25,37). Many C*c*O inhibitors hinder its

catalytic activity by targeting the heme a_3-Cu_B center, including compounds like KCN (25), sodium azide (38), and nitric oxide (39). Conversely, ADDA-5 was described as a non-competitive C*c*O inhibitor with respect to cyt *c* (32). We therefore used computational methods to explore how CYM or three potential CYM-derived metabolites (N-acetylcyanoglycine, ethylparabanic acid and demethoxylated cymoxanil) could potentially inhibit C*c*O. Two putative mechanisms were explored: (i) docking occurs between the heme a_3 and the copper ion Cu_B, blocking the electron transfer mechanism (hypothesis 1); (ii) docking occurs at the interfacial region that C*c*O forms with cyt *c*, interfering with the interaction between C*c*o and cyt *c* (hypothesis 2). Values for hypothesis 1 were much lower than the typical values normally obtained in docking of reasonable inhibitors with GOLD/PLP (40). Indeed, in the context of GOLD scoring functions, the score values are dimensionless, and a higher score is indicative of a good docking result. Furthermore, analysis of the C*c*O structure confirmed that there is insufficient space for molecules with more than two or three atoms to bind between the copper ion and heme a_3, supported by the work of Yano and coworkers (25), who provided electron density maps of C*c*O bound to cyanide. Taking all these facts into account, we could confidently rule out hypothesis 1 as a plausible binding mechanism for the interaction of CYM or its metabolites with C*c*O. In contrast, highly consistent results were observed for hypothesis 2, and we therefore propose a mechanism where CYM (and its metabolites) can block the interaction of cyt *c* with C*c*O, hampering electron transfer and inhibiting C*c*O catalytic activity, by interacting with five key residues of subunit II of C*c*O: Ser117, Asp139, Tyr121, Asp119, Tyr105 (bovine x-ray structure) and Tyr125, Glu142, Glu144, Tyr146 and Asp164 (yeast cryo-EM structure). Among the tested compounds, CYM exhibited a higher affinity to C*c*O than its metabolites, suggesting that CYM metabolization is not required for its inhibitory effect towards C*c*O, and suggesting that the delayed inhibitory effect observed in whole cells more likely results from intracellular accumulation of CYM to levels sufficient to cause the inhibition. We also identified, for the first time, the potential binding site of ADDA-5, since there was previous experimental evidence that it inhibits C*c*O, but no mechanism had been proposed. Our data also suggest that CYM is a promising scaffold molecule for the development of compounds designed to disrupt the C*c*O/cyt *c* interaction.

The here suggested mechanism may also be true for the target organisms of CYM commercial formulations [oomycete pathogens causers of mildews, rots, blights and other crop diseases (41)], since mitochondrial complexes and the mitochondrial respiration process are for the most part conserved (42). Fungicides that inhibit mitochondrial respiration at complex III are highly effective against oomycetes and play an important role in downy mildew management programs (43,44). The groups of mitochondrial complex III inhibitors that display fungicidal activity against these pathogens are quinone

outside inhibitors (e.g., azoxystrobin, famoxadone and fenamidone) and quinone inside inhibitors (e.g., cyazofamid, amisulbrom). Both target the mitochondrial cytochrome *b* protein by binding at either the outer quinol-oxidizing pocket (Qo site) or the inner quinone-reducing pocket (Qi site). In both cases, the electron transfer process is blocked, leading to the inhibition of mitochondrial respiration (45–47). Indeed, the quinone inside inhibitors used in agriculture are highly specific against oomycete pathogens (48,49). Furthermore, it has previously been demonstrated that *P. infestans* mitochondria exhibit sensitivity to cyanide, a known inhibitor of C*c*O activity in yeast cells (50). This indicates that are similar mechanisms between yeasts and oomycetes, suggesting that the anti-oomycete activity displayed by CYM can occur through inhibition of mitochondrial respiration by blocking the C*c*O/cyt *c* interaction, as demonstrated in this work for yeast cells. Yeast mitochondrial complexes and the mitochondrial respiration process are extremely similar to those found in higher eukaryotic organisms, including humans. Thus, this work also provides cues of the potential harmful effects of CYM in non-target organisms.

Altogether, these insights contribute to a better understanding of the mechanism of action of CYM. Further research on the specific molecular interactions between CYM and C*c*O will shed light on the basis of its inhibitory activity, aiding in the development of new antifungal agents targeting mitochondrial function.

3.1.4. References

1. Marinho M da C, Diogo BS, Lage OM, Antunes SC. Ecotoxicological evaluation of fungicides used in viticulture in non-target organisms. Environ Sci Pollut Res. 2020;27:43958–69.
2. Estève K, Poupot C, Dabert P, Mietton-Peuchot M, Milisic V. A *Saccharomyces cerevisiae*-based bioassay for assessing pesticide toxicity. J Ind Microbiol Biotechnol. 2009;36:1529–34.
3. Fidente P, Di Giovanni C, Seccia S, Morrica P. Determination of cymoxanil in drinking water and soil using high-performance liquid chromatography. Biomed Chromatogr. 2005;19:766–70.
4. Rekanović E, Potočnik I, Milijašević-Marčić S, Stepanović M, Todorović B, Mihajlović M. Toxicity of metalaxyl, azoxystrobin, dimethomorph, cymoxanil, zoxamide and mancozeb to *Phytophthora infestans* isolates from Serbia. J Environ Sci Heal - Part B Pestic Food Contam Agric Wastes. 2012;47:403–9.
5. Kim S, Chen J, Cheng T, Gindulyte A, He J, He S, et al. PubChem 2023 update. Nucleic Acids Res. 2023;51:D1373–80.
6. Toffolatti SL, Venturini G, Campia P, Cirio L, Bellotto D, Vercesi A. Sensitivity to cymoxanil in Italian populations of *Plasmopara viticola* oospores. Pest Manag Sci. 2015;71:1182–8.
7. Hillebrand S, Zundel JL. Fungicides with Unknown Mode of Action. In: Jeschke P, Witschel M, Krämer W, Schirmer U, editors. Modern Crop Protection Compounds. Wiley-VCH Verlag GmbH & Co. KGaA; 2019. p. 911–32.
8. Tellier F, Fritz R, Leroux P, Carlin-Sinclair A, Cherton JC. Metabolism of cymoxanil and analogs in strains of the fungus *Botrytis cinerea* using high-performance liquid chromatography and ion-pair high-performance thin-layer chromatography. J Chromatogr B Anal Technol Biomed Life Sci. 2002;769:35–46.
9. Tellier F, Fritz R, Kerhoas L, Ducrot PH, Einhorn J, Carlin-Sinclair A, et al. Characterization of metabolites of fungicidal cymoxanil in a sensitive strain of *Botrytis cinerea*. J Agric Food Chem. 2008;56:8050–7.
10. Tellier F, Fritz R, Kerhoas L, Ducrot PH, Carlin-Sinclair A, Einhorn J, et al. Metabolism of fungicidal cyanooximes, cymoxanil and analogues in various strains of *Botrytis cinerea*. Pest Manag Sci. 2009;65:129–36.
11. Ziogas BN, Davidse LC. Studies on the mechanism of action of cymoxanil in *Phytophthora infestans*. Pestic Biochem Physiol. 1987;29:89–96.
12. Ribeiro IC, Veríssimo I, Moniz L, Cardoso H, Sousa MJ, Soares AMVM, et al. Yeasts as a model for assessing the toxicity of the fungicides penconazol, cymoxanil and dichlofluanid.

Chemosphere. 2000;41:1637–42.

13. Tellier F, Carlin-Sinclair A, Fritz R, Cherton JC, Leroux P. Activity and metabolism of cyano-oxime derivatives in various strains of *Botrytis cinerea*. Pestic Biochem Physiol. 2004;78:151–60.
14. Guérin B, Labbe P, Somlo M. Preparation of Yeast Mitochondria (*Saccharomyces Cerevisiae*) with Good P/O and Respiratory Control Ratios. Methods Enzymol. 1979;55:149–59.
15. Gornall AG, Bardawill CJ, David MM. Determination of serum proteins by means of the biuret reaction. J Biol Chem. 1949;177:751–66.
16. Cain K, Griffiths DE. Localization of the site of action of trialkyltin in yeast mitochondria. Biochem J. 1977;162:575–80.
17. Aguilaniu H, Gustafsson L, Rigoulet M, Nyström T. Protein oxidation in G0 cells of *Saccharomyces cerevisiae* depends on the sstate rather than rate of respiration and is enhanced in *pos9* but not *yap1* Mutants. J Biol Chem. 2001;276:35396–404.
18. Zhang YQ, Shen X, Xiao XL, Liu MY, Li SL, Yan J, et al. Mitochondrial uncoupler carbonyl cyanide m-chlorophenylhydrazone induces vasorelaxation without involving K_{ATP}channel activation in smooth muscle cells of arteries. Br J Pharmacol. 2016;173:3145–58.
19. Ruas JS, Siqueira-Santos ES, Amigo I, Rodrigues-Silva E, Kowaltowski AJ, Castilho RF. Underestimation of the maximal capacity of the mitochondrial electron transport system in oligomycin-treated cells. PLoS One. 2016;11:1–20.
20. de Vries S, Marres CAM. The mitochondrial respiratory chain of yeast. Structure and biosynthesis and the role in cellular metabolism. BBA Rev Bioenerg. 1987;895:205–39.
21. Díaz-Ruiz R, Avéret N, Araiza D, Pinson B, Uribe-Carvajal S, Devin A, et al. Mitochondrial oxidative phosphorylation is regulated by fructose 1,6-bisphosphate: a possible role in crabtree effect induction? J Biol Chem. 2008;283:26948–55.
22. Klingenberg M. The Ferricyanide Method for Elucidating the Sidedness of Membrane-Bound Dehydrogenases. Methods Enzymol. 1979;56:229–33.
23. Mourier A, Devin A, Rigoulet M. Active proton leak in mitochondria: A new way to regulate substrate oxidation. Biochim Biophys Acta - Bioenerg. 2010;1797:255–61.
24. Manon S. Dependence of yeast mitochondrial unselective channel activity on the respiratory chain. Biochim Biophys Acta - Bioenerg. 1999;1410:85–90.
25. Yano N, Muramoto K, Mochizuki M, Shinzawa-Itoh K, Yamashita E, Yoshikawa S, et al. X-ray structure of cyanide-bound bovine heart cytochrome *c* oxidase in the fully oxidized state at 2.0 Å resolution. Acta Crystallogr Sect F Struct Biol Commun. 2015;71:726–30.

26. Roberts H, Smith SC, Marzuki S, Linnane AW. Evidence that cytochrome *b* is the antimycin-binding component of the yeast mitochondrial cytochrome *bc1* complex. Arch Biochem Biophys. 1980;200:387–95.
27. Packer L, Mustafa MG. Pathways of electron flow established by tetramethylphenylenediamine in mitochondria and ascites tumor cells. Biochim Biophys Acta. 1966;113:1–12.
28. Wilson DF, Harrison DK, Vinogradov A. Mitochondrial cytochrome *c* oxidase and control of energy metabolism: Measurements in suspensions of isolated mitochondria. J Appl Physiol. 2014;117:1424–30.
29. López-López E, Naveja JJ, Medina-Franco JL. DataWarrior: an evaluation of the open-source drug discovery tool. Expert Opin Drug Discov. 2019;14:335–41.
30. O'Boyle NM, Banck M, James CA, Morley C, Vandermeersch T, Hutchison GR. Open Babel: An Open chemical toolbox. J Cheminform. 2011;3:1–14.
31. Shimada S, Shinzawa-Itoh K, Baba J, Aoe S, Shimada A, Yamashita E, et al. Complex structure of cytochrome *c* –cytochrome *c* oxidase reveals a novel protein–protein interaction mode . EMBO J. 2017;36:291–300.
32. Oliva CR, Markert T, Ross LJ, White EL, Rasmussen L, Zhang W, et al. Identification of small molecule inhibitors of human cytochrome *c* oxidase that target chemoresistant glioma cells. J Biol Chem. 2016;291:24188–99.
33. Yoboue ED, Augier E, Galinier A, Blancard C, Pinson B, Casteilla L, et al. cAMP-induced mitochondrial compartment biogenesis: role of glutathione redox state. J Biol Chem. 2012;287:14569–78.
34. Matus-Ortega MG, Cárdenas-Monroy CA, Flores-Herrera O, Mendoza-Hernández G, Miranda M, González-Pedrajo B, et al. New complexes containing the internal alternative NADH dehydrogenase (Ndi1) in mitochondria of *Saccharomyces cerevisiae*. Yeast. 2008;2:191–8.
35. Overkamp KM, Bakker BM, Kötter P, Van Tuijl A, De Vries S, Van Dijken JP, et al. *In vivo* analysis of the mechanisms for oxidation of cytosolic NADH by *Saccharomyces cerevisiae* mitochondria. J Bacteriol. 2000;182:2823–30.
36. Brzezinski P, Moe A, Adelroth P. Structure and mechanism of respiratory III-IV supercomplexes in bioenergetic membranes. Chem Rev. 2021;121:9644–73.
37. Kadenbach B. Complex IV – The regulatory center of mitochondrial oxidative phosphorylation. Mitochondrion. 2021;58:296–302.
38. Bowler MW, Montgomery MG, Leslie AGW, Walker JE. How azide inhibits ATP hydrolysis by the F-

ATPases. PNAS. 2006;103:8646–9.

39. Sarti P, Giuffré A, Forte E, Mastronicola D, Barone MC, Brunori M. Nitric oxide and cytochrome *c* oxidase: mechanisms of inhibition and NO degradation. Biochem Biophys Res Commun. 2000;274:183–7.
40. Li Y, Liu Z, Li J, Han L, Liu J, Zhao Z, et al. Comparative assessment of scoring functions on an updated benchmark: 1. compilation of the test set. J Chem Inf Model. 2014;54:1700–16.
41. Kamoun S, Furzer O, Jones JDG, Judelson HS, Ali GS, Dalio RJD, et al. The Top 10 oomycete pathogens in molecular plant pathology. Mol Plant Pathol. 2015;16:413–34.
42. Sierotzki H. Respiration Inhibitors: Complex III. In: Ishii H, Hollomon DW, editors. Fungicide Resistance in Plant Pathogens. Springer, Tokyo; 2015. p. 119–43.
43. Gisi U, Sierotzki H. Oomycete fungicides: phenylamides, quinone outside inhbitors, and carboxylic acid amides. In: Ishii H, Hollomon D, editors. Fungicide Resistance in Plant Pathogens. Tokyo: Springer; 2015. p. 145–74.
44. Lamberth C, Rendine S, Sulzer-Mosse S. Agrochemical disease control: The story so far. In: Maienfisch P, Mangelinckx S, editors. Recent Highlights in the Discovery and Optimization of Crop Protection Products. Academic Press; 2021. p. 65–85.
45. Becker W, Von Jagow G, Anke T, Steglich W. Oudemansin, strobilurin A, strobilurin B and myxothiazol: new inhibitors of the *bc1* segment of the respiratory chain with a E-β-methoxyacrylate system as common structural elemen. FEBS Lett. 1981;132:329–33.
46. Von Jagow G, Link TA. Use of specific inhibitors on the mitochondrial *bc1* complex. Methods Enzymol. 1986;126:1–832.
47. Bartlett DW, Clough JM, Godwin JR, Hall AA, Hamer M, Parr-Dobrzanski B. The strobilurin fungicides. Pest Manag Sci. 2002;58:649–62.
48. Cherrad S, Gillet B, Dellinger J, Bellaton L, Roux P, Hernandez C, et al. New insights from short and long reads sequencing to explore cytochrome *b* variants in *Plasmopara viticola* populations collected from vineyards and related to resistance to complex III inhibitors. PLoS One. 2023;18:1–20.
49. Leroux P, Gredt M, Leroch M, Walker AS. Exploring mechanisms of resistance to respiratory inhibitors in field strains of *Botrytis cinerea*, the causal agent of gray mold. Appl Environ Microbiol. 2010;76:6615–30.
50. Scheepens PC, Fehrmann H. Metabolic anomalies as a possible cause of biotrophy: abbreviated electron transport in *Phytophthora infestans*. Physiol Plant Pathol. 1977;11:71–8.

3.1.5. Supplementary Material

Table S3.1.i.

Figure S3.1.i.

Table S3.1.i. Docking results between chain A of C*c*O and the tested compound using the GOLD software. Results of the GOLD scoring function (PLP) for the docking between C*c*O and CYM, or its potential metabolites ethylparabanic acid, N-acetylcyanoglycine, demethoxylated cymoxanil and ADDA-5. The latter was used as a reference compound.

COMPOUND	SCORING FUNCTION
	PLP
Ethylparabanic acid	19.95 ± 0.01
N-acetylcyanoglycine	15.27 ± 0.02
CYM	12.07 ± 0.27
Demethoxylated cymoxanil	-14.03 ± 0.03
ADDA-5	-17.28 ± 0.62

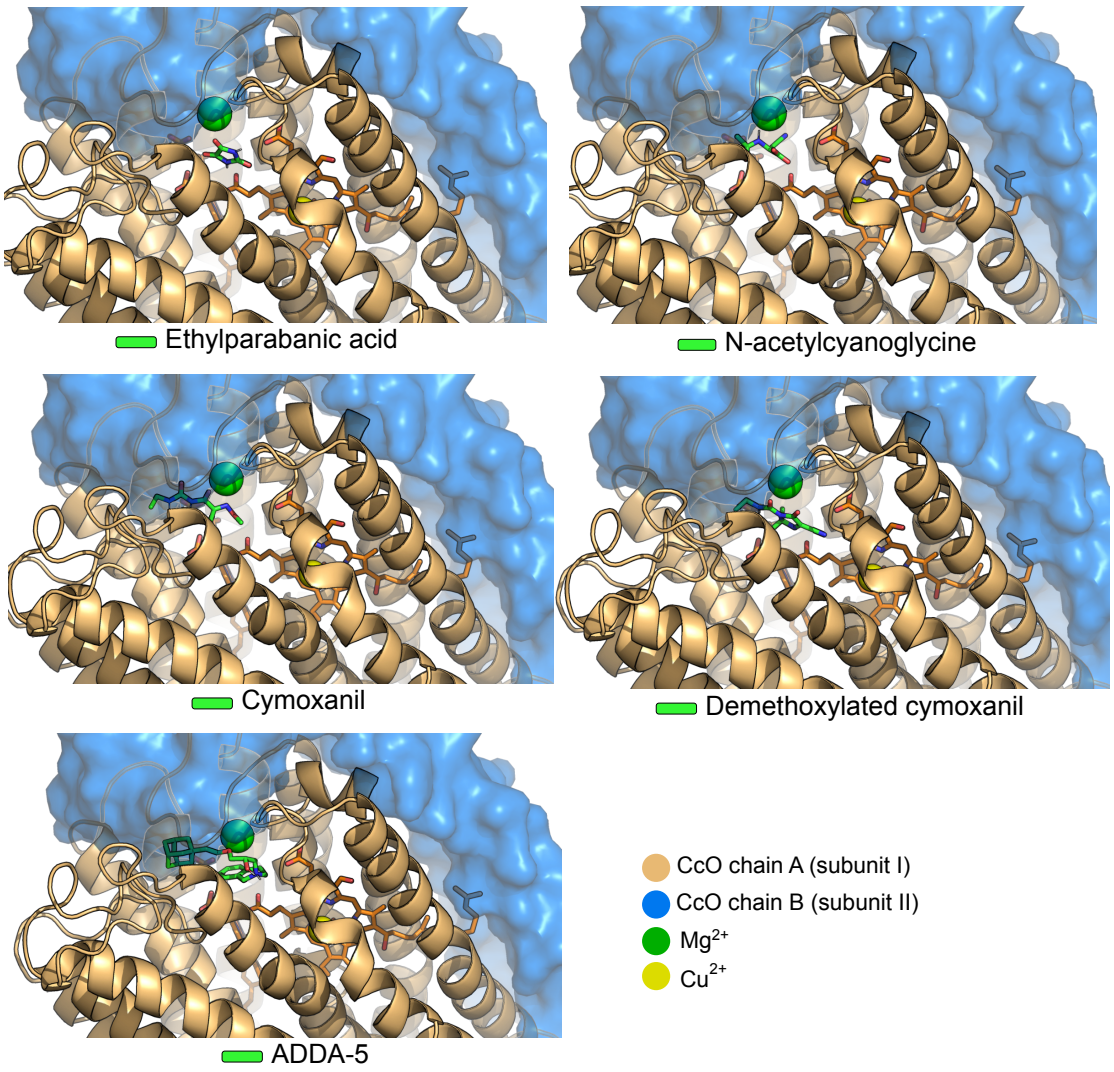

Figure S3.1.i. PLP Docking poses of CYM, its metabolites and ADDA-5 on chain A of C*c*O. Chain A is represented as new cartoon in beige, chain B (subunit II) is in surface representation in blue. Heme a_3 is shown as sticks in orange. The ions Mg^{2+} and Cu^{2+} are depicted as green and yellow spheres, respectively. The tested compounds are shown in sticks, with carbon atoms represented in green, oxygen atoms in red and nitrogen atoms in blue.

3.2. Molecular bases of the antifungal activity of cymoxanil

3.2.1. Materials and Methods

3.2.1.1. Yeast strains

The yeast *S. cerevisiae* BY4741 (MAT a *his3Δ1; leu2Δ0; met15Δ0; ura3Δ0*) was used throughout this study as the wild-type strain. The *end3Δ* mutant in the same background was obtained from the Euroscarf collection. BY4741 cells were transformed with the pRS416 GFP-Atg8 plasmid (1) using the LiAc/SS Carrier DNA/PEG method (2).

3.2.1.2. Growth conditions and treatments

BY4741 and *end3Δ* were cultured in Synthetic Complete medium [SC; 0.5 % (w/v) ammonium sulfate; 0.17 % (w/v) yeast nitrogen base without amino acids and without ammonium sulphate; 0.14 % (w/v) drop-out mixture lacking leucine, histidine, tryptophan, and uracil; 0.04 % (w/v) leucine; 0.008 % (w/v) tryptophan; 0.008 % (w/v) histidine, and 0.008 % (w/v) uracil] with 2 % of glucose (Glu) or galactose (Gal) as the carbon source. The BY4741 strain expressing pRS416 GFP-Atg8 was grown in SC medium with glucose, but lacking uracil. All yeast strains were grown at 30 °C in an orbital shaker at 200 rpm, with a ratio of flask volume/medium of 5:1.

For all assays, cells were grown overnight, then diluted in fresh medium to $OD_{640\ nm}$ = 0.1 and treated with CYM (25 or 50 μg mL^{-1}, as indicated in the figure legends) from Sigma-Aldrich and/or the equivalent volume of DMSO as a negative control (lower than 0.5 %) for up 8 h. Samples were taken at specific time points for subsequent analyses. Additionally, samples of wild-type strain BY4741, grown in glucose and treated for 8 h, were collected for transcriptomic analysis, evaluation of lipid raft distribution, quantitative Real-Time PCR (qRT-PCR), analysis of efflux pumps, and assessment of proton movements, intracellular ATP concentration, vacuolar pH variations and plasma membrane potential. The evaluation of lipid raft distribution was also assessed at the *end3Δ* mutant. BY4741 strain harboring pRS416 GFP-Atg8 was used to assess autophagy.

3.2.1.3. Cell growth and survival

Cell growth was assessed by measuring the $OD_{640\ nm}$ of yeast cells at time point 0, 4 and 8 h in the absence or presence of CYM. Cell survival was evaluated by counting of colony forming units (c.f.u.). Briefly, five serial dilutions of the cultures were performed, and 40 μL of 10^{-4} or 10^{-5} dilutions (according to each condition) were plated onto yeast extract-peptone-dextrose plates [YEPD; 1 % (w/v) yeast extract; 2 % (w/v) peptone; 2 % (w/v) glucose and 2 % (w/v) agar] and incubated for 48 h at 30 °C. The

percentage of cell survival was calculated from the number of c.f.u. of each condition in relation to time zero and the control without any treatment.

3.2.1.4. Assessment of plasma membrane integrity

To assess loss of plasma membrane integrity, cells were stained with the cell-impermeant dye propidium iodide (PI, Sigma-Aldrich). At each timepoint, 500 µl of cells at $OD_{640\ nm}$ = 0.1 were harvested and resuspended in phosphate buffered saline (PBS) 1× (PBS 10×; 137 mM NaCl, 2.7 mM KCl, 10 mM Na_2HPO4, 1.8 mM $KH2PO_4$, pH 7). PI was added to the yeast cell suspension to a final concentration of 2 µg mL^{-1} and incubated for 10 min at room temperature (RT). Cells with red fluorescence (PI positive cells) were considered to have lost their plasma membrane integrity.

3.1.1.5. Transcriptomic analysis

RNA extraction

Total RNA was extracted from cells using TRIzol/chloroform and RNA Clean & Concentrator-5 Kit (Zymo Research) according to manufacturer's instructions. Briefly, the upper aqueous phase from TRIzol/chloroform extraction was transferred to a new tube, and RNA was purified with the RNA Clean & Concentrator-5 Kit. The extracted RNA was used for RNA-sequencing (RNAseq) analysis and for qRT-PCR.

RNAseq analysis

RNAseq analysis was performed by the Genomics Facility at the Gulbenkian Institute of Science, as a paid service. Samples were processed with the RNA Lexogen QuantSeq 3' mRNA-Seq V2 Library Prep Kit FWD with UDI 12 nt. The differential expression gene analysis between CYM-treated cells and nontreated cells was performed with the package DESeq2. The threshold for up-regulated genes as log2 fold change > 2 and adjusted p value < 0.05 and for down-regulated genes as log2 fold change < -2 and adjusted p value < 0.05, the genes satisfying these criteria were identified as differentially expressed genes.

qRT-PCR

cDNA was synthesized by reverse transcription from 500 ng of total RNA according to manufacturer's instructions (iScript™ cDNA Synthesis Kit, Bio-Rad Laboratories). Real-time PCR reactions using primers hybridizing with *ERG25* or *ACT1* transcripts were performed in an CFX96™ Real-

Time System C100™ Thermal Cycler (Bio-Rad Laboratories) using the KAPA SYBR® FAST qPCR Master Mix (2×) Kit (Sigma-Aldrich) according to manufacturer's instructions. PCR controls with no template were also performed for each primer pair. Two biological replicates were performed, and each sample was measured in duplicate. Quantification was performed using the $2^{-\Delta\Delta C_t}$ method (3) and expression of *ERG25* was normalized to A*CT1*.

3.2.1.6. High-throughput fluorescence microscopic screen

A high-throughput fluorescence microscopy screen was performed using a collection of 5 330 strains containing an N-terminal SWAT cassette harboring the *NOP1* constitutive promotor and GFP upstream of each gene start codon (N′ NOP1pr-GFP library) (4,5). The strains were grown in Synthetic Defined medium [SD; 0.67 % (w/v) yeast nitrogen base without amino acids and 2 % (w/v) glucose]. Cells were moved from agar plates into liquid 384-well polystyrene growth plates using the ROTOR HDA (Singer Instruments). Liquid cultures were grown overnight in 50 µl of SD medium in a shaking incubator (LiCONiC Instruments) at 30 °C. Afterwards, 5 µl of overnight culture was back-diluted into 95 µl of SD medium with 25 µg mL^{-1} of CYM and/or the equivalent volume of DMSO as a negative control (lower than 0.5 %), using a Tecan freedom EVO liquid handler (Tecan) connected to the incubator. Plates were then transferred back to the incubator and grown for 8 h at 30 °C. The liquid handler was then used to transfer strains into glass-bottom 384-well microscope plates (Brooks Bioscience) coated with Concanavalin A (Sigma-Aldrich) to allow cell adhesion. Wells were washed twice in SD medium to remove floating cells and obtain a cell monolayer. Plates were then transferred into an automated microscopy system using a KiNEDx robotic arm (Peak Robotics).

Imaging was performed with an automated Olympus SpinSR system using a Hamamatsu flash Orca 4.0 camera and a CSUW1-T2SSR SD Yokogawa spinning disk unit with a 50 µm pinhole disk. Images were acquired using a 60× air lens NA 0.9 (Olympus), laser excitation 488 nm, intensity 50 % and exposure time 500 ms, with CSU dichroic mirror D405/488/561 and emission filter set B525/50. Images were manually inspected using ImageJ software (version 1.53).

3.2.1.7. Gene ontology (GO) term analysis

GO term enrichment analysis was performed using the SGD GO Term Finder. The background set for each analysis (RNAseq and microscopy) was defined as all the genes for which data was available. A p value < 0.05 was considered statistically significant.

3.2.1.8. Evaluation of autophagy

Autophagy was assessed by western blot analysis of GFP-Atg8 cleavage. Atg8p is incorporated into the autophagosome and later degraded in the vacuolar lumen (6); however, GFP is resistant to degradation in the vacuole and thus free GFP detected by western blot in cells expressing GFP-Atg8 is indicative of autophagy (1). At each timepoint, 1 mL of BY4741 cells harboring pRS416 GFP-Atg8 cells at an $OD_{640\ nm}$ = 1 were harvested by centrifugation at 5000 ×g for 3 min and washed once with distilled water. For preparation of whole cell extracts, cells were then resuspended in 500 μL of water containing 50 μL lysis buffer [3.5 % (v/v) β- mercaptoethanol in 2 M NaOH] and incubated for 15 min on ice. Next, 50 μL of 3 M trichloroacetic acid were added and tubes incubated for 40 min on ice to precipitate the proteins. Extracts were centrifuged at 12000 ×g for 10 min at 4 °C, washed with 100 μL of acetone and centrifuged again at 12000 ×g for 5 min at 4 °C. Finally, protein extracts were resuspended in Laemmli buffer [2 % (v/v) β- mercaptoethanol, 0.1 M Tris pH 8.8, 20 % (v/v) glycerol, 0.02 % (v/v) bromophenol blue]. Samples were heated at 70 °C for 15 min and stored at -20 °C, or were used immediately for western blot.

Samples were separated electrophoretically on a 12.5 % sodium dodecyl sulphate-polyacrylamide gel (SDS-PAGE) and transferred to Polyvinylidene Difluoride (PVDF, GE Healthcare) membranes at 60 mA per membrane for 90 min in a semi-dry transfer unit (TE77X Hoefer). To avoid non-specific interactions, membranes were blocked in 5 % non-fat milk in PBS-Tween 0.1 % (v/v) solution (1× PBST) with agitation at RT for 1 h. Afterwards, membranes were incubated overnight at 4 °C with anti-GFP (1:3000, Sigma-Aldrich) and anti-yeast phosphoglycerate kinase 1 (Pgk1p) mouse monoclonal primary antibodies (1:5000, Molecular Probes). Pgk1p was used as the loading control. The following day, membranes were incubated with the Peroxidase-AffiniPure goat anti-mouse IgG secondary antibody (1:5000, Jackson ImmunoResearch). Chemiluminescence detection was performed using an ECL detection system (Millipore-Merck) in a G:BOX Chemi XX9 system (Syngene).

3.2.1.9. Evaluation of lipid raft distribution

The distribution of lipid rafts was inferred by fluorescence microscopy (Leica Microsystems DM-5000B epifluorescence microscope) using filipin staining (Filipin III from *Streptomyces filipinensis*, Sigma-Aldrich) as previously described (7,8). Filipin is a naturally fluorescent antibiotic dye that binds to ergosterol and thus is used to detect regions with high sterol content in the plasma membrane of fungal species (9). Briefly, cells were collected at an $OD_{640\ nm}$ = 0.5 and concentrated 20× in sterile water. Immediately before visualization, cells were incubated for 1 min in the dark with 0.1 g L^{-1} filipin from a

stock solution of 5 g L^{-1} (w/v) in methanol. Cells were then mounted on slides with the anti-fading agent Vectashield (Vector Laboratories) to overcome the instability of this dye, and then visualized in an epifluorescence microscope.

3.2.1.10. Analysis of efflux pumps

To assess presence of efflux pumps cells were stained with the cell-permeant dye calcein AM (Molecular probes), as previously described (10). Briefly, cells were harvested (500 µl at $OD_{640\ nm}$ = 0.1), resuspended in 1× PBS and incubated with 100 µM of verapamil, a known inhibitor of fungal efflux pumps (11–13), for 90 min at RT. Then, 10 µM of calcein AM, a cell-permeant and non-fluorescent dye that is cleaved by intracellular esterases into green-fluorescent calcein (14,15), but can be extruded by efflux pumps (16), was added to both verapamil-treated and untreated cells. After 30 min of incubation at RT, cells were analyzed by flow cytometry. Data are presented as the ratio of between the median green fluorescence intensity of verapamil-treated and untreated cells (+ verapamil/ - verapamil).

3.2.1.11. Proton movements assays

Cells were harvested (3 mL of cells at $OD_{640\ nm}$ = 20), washed and resuspended in distilled water. Proton movements were measured at RT by recording the pH of cell suspensions with a standard pH meter (PHM 82; Radiometer) connected to a potentiometer recorder (BBC-GOERZ METRAWATT, SE460). The pH electrode was immersed in 4.5 mL water and 0.5 mL of yeast suspensions with magnetic stirring. For measurement of proton efflux, the initial pH was adjusted to 5.5 and a baseline was established. Afterwards, 20 mM of glucose was added to trigger H^+ efflux, leading to an acidification of the extracellular environment (17). The rate of acidification, calibrated with 0.1 mM NaOH, was taken as a measure of proton extrusion activity. A sample was taken from each condition to estimate the dry weight (DW) after incubation at 80 °C for two days. Data is presented as Protons min^{-1} mg^{-1} DW.

3.2.1.12. Evaluation of intracellular ATP concentration

Intracellular ATP was quantified using the BacTiter-Glo™ Microbial Cell Viability kit as recommended. Cells were transferred to a 96-well opaque plate, mixed with an equal volume of BacTiter-Glo reagent and incubated for 15 min in the dark. The emitted luminescence was recorded in a Varioskan flash multimode reader (1000 ms integration time). Data are shown in arbitrary units (a.u.) as fold change expressed in relation to untreated cells (control, considered as 1).

3.2.1.13. Analysis of vacuolar pH variations

Vacuolar pH alterations were detected using the 5-(and-6)-carboxy-2′,7′-dichlorofluorescein diacetate (CDCFDA, Invitrogen) probe. CDCFDA, a non-fluorescent cell permeant dye, is cleaved by intracellular esterases and yields the fluorescent and pH-sensitive 5-(and-6)-carboxy-2',7'-dichlorofluorescein (CDCF). At higher pH values, CDCF accumulates in the yeast vacuole, and cells exhibit higher fluorescence intensity (18,19). Cells were harvested by centrifugation (0.5 mL $OD_{640\ nm}$ = 0.1), washed once with sterile water and resuspended in CF buffer [50 mM glycine, 10 mM NaCl, 5 mM KCl, 1 mM MgCl2, 40 mMTris, 100 mM MES pH 4.5 supplemented with 2 % (w/v) glucose] (8,18). The cell suspension was then incubated with 1.6 μM CDCFDA for 20 min at 30 °C with 200 rpm orbital agitation. Afterwards, cells were washed and resuspended in CF buffer without glucose for further analysis in the flow cytometer. Flow cytometry data are presented as the median of the green fluorescence intensity in relation to the autofluorescence of each sample and untreated cells.

3.2.1.14. Assessment of membrane potential

Plasma membrane potential was monitored using Bis-(1,3-dibutylbarbituric acid) trimethine oxonol [$DiBAC_4(3)$, Molecular Probes]. Normally, this dye is excluded by polarized cells, but accumulates inside depolarized cells. Therefore, increased fluorescence is indicative of loss of plasma membrane potential (20). Cells were harvested by centrifugation (0.5 mL $OD_{640\ nm}$ = 0.1) and resuspended in 1× PBS. $DiBAC_4(3)$ and PI were added to the yeast cell suspension to a final concentration of 1 μg mL^{-1} and 2 μg mL^{-1}, respectively, and samples incubated for 10 min at RT and analyzed by flow cytometry. Data are presented as percentage of cells with green fluorescence [$DiBAC_4(3)$ positive cells] and without red fluorescence (PI negative cells), corresponding to depolarized but non-permeabilized cells.

3.2.1.15. Flow cytometry

Flow cytometry analysis was performed with CytoFLEX (Beckman Coulter Inc.) with 488 nm emission. Filter set included a 525/40 nm bandpass filter for “green” fluorescence FITC channel and a 585/42 nm bandpass filter for “red” fluorescence PE channel. For each sample, 10 000 events were evaluated. Data were analyzed using CytExpert software.

3.2.1.16. Statistical analysis

The statistical analysis of the results was performed using GraphPad Prism software (version 8.4.0). In all assays, data are expressed as the mean and S.D. A one-way ANOVA was used to test the

effect of CYM and a Dunnett test was used to assess differences relatively to control. A significance level of 0.05 was employed in all analyses.

3.2.2. Results

3.2.2.1. Cymoxanil inhibits growth and decreases cell viability independently of an active respiratory chain

To ascertain if the cytotoxic effect of CYM in *S. cerevisiae* is due to its previously described effect in inhibiting respiration, we directly compared how it affects growth and viability of cells in medium containing glucose or galactose as the carbon source, where respiration is repressed or not, respectively. As seen in **Figure 3.2.1A**, CYM inhibited growth of yeast cells independently of the carbon source but a significant viability decrease was observed after 4 h of treatment in glucose (**Figure 3.2.1B**, blue bars), but only after 8 h of treatment in medium containing galactose (**Figure 3.2.1B**, orange bars). Cells exposed to CYM in glucose-containing medium also lost plasma membrane integrity earlier, as staining with PI was already visible after 4 h, and the percentage of cells with a compromised plasma membrane after 8 h was much higher in glucose- than galactose-grown cells (**Figure 3.2.1C**). Taken together, our data indicates that cells are more sensitive to CYM in medium containing glucose, and we therefore pursued further characterization of the effects of CYM in this medium.

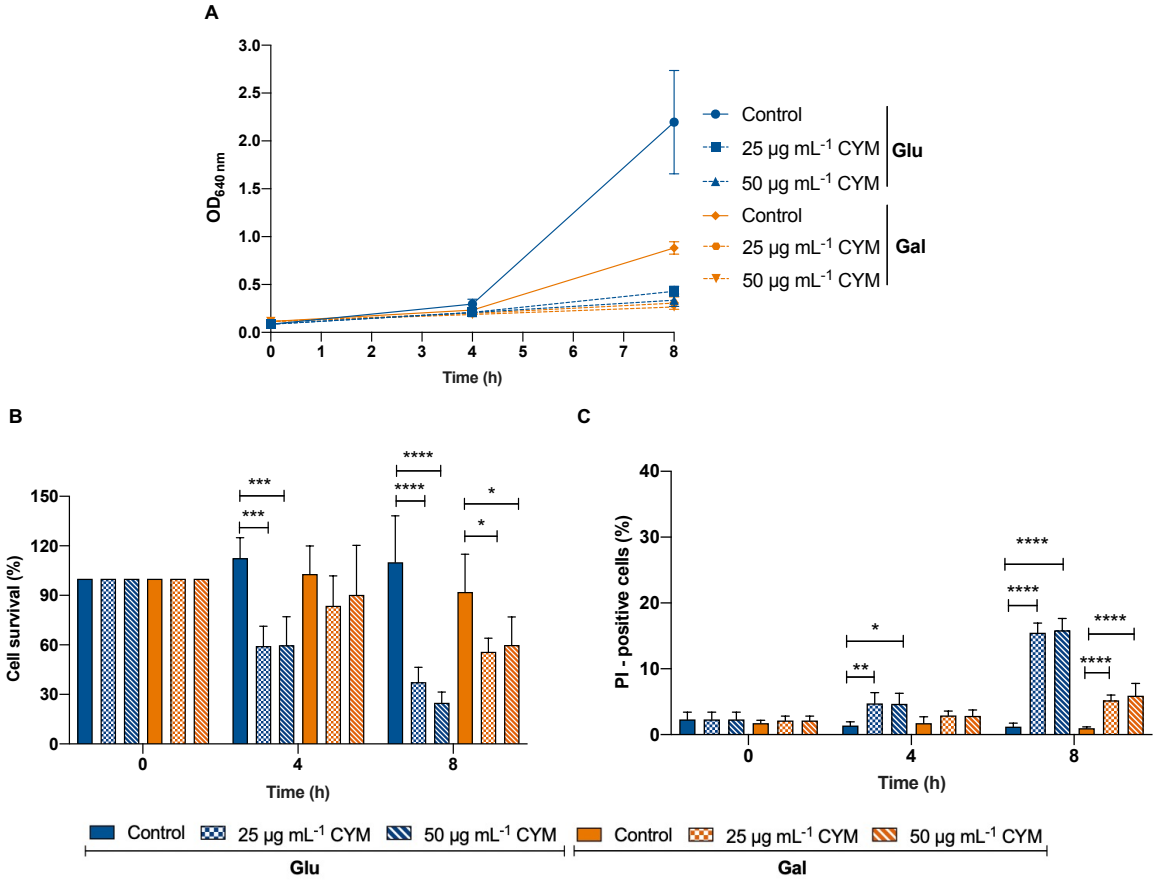

Figure 3.2.1. Influence of the carbon source on CYM effects on growth and viability of *S. cerevisiae* BY4741 cells. Cells were grown overnight in SC medium containing 2 % Glu or 2 % Gal then were diluted to an $OD_{640\ nm}$ = 0.1, transferred to fresh medium and treated with 25 or 50 µg mL^{-1} CYM and/or the equivalent volume of DMSO (control). **(A)** $OD_{640\ nm}$ were registered at time point 0, 4 and 8 h of treatment. **(B)** Cell survival of CYM-treated cells was determined by standard dilution plate counts and expressed as a percentage of c.f.u. on YEPD plates in relation to time 0. **(C)** Plasma membrane integrity was determined by PI staining of cells treated with 0, 25 and 50 µg mL^{-1} CYM at time point 0, 4, 8 h of treatment in SC medium containing Glu or Gal. The data displayed are the mean ± S.D. of three independent experiments. Asterisks (* ≤ 0.05; **, P ≤ 0.01; ***, P ≤ 0.001; ****, P ≤ 0.0001) depict significant differences relative to the control at each time point.

3.2.2.2. Transcriptome alterations induced by cymoxanil

To uncover the global cellular effects of CYM on yeast cells, we used two non-biased approaches: RNAseq to determine how this fungicide affects the RNA level of yeast genes and a high-throughput microscopic screen to assess its effects on protein localization.

Transcriptomic analysis performed in cells incubated in the presence of 25 µg mL^{-1} CYM, for 8 h, indicated that a total of 70 genes were differentially expressed, when compared with cells incubated with the CYM vehicle, DMSO, for the same time. From these, 50 were up-regulated, whereas 20 were down-regulated considering a threshold of log2 fold change > 2 and adjusted p value < 0.05 and log2

fold change < -2 and adjusted *p* value < 0.05, respectively (**Figure 3.2.2A** and supplementary material **Table S3.2.i and S3.2.ii**). The top 10 up-regulated genes and top 10 down-regulated genes are shown in **figure 3.2.2B**. GO enrichment showed that sulfur metabolism, oxoacid metabolism and organic acid metabolism were the biological functions highly up-regulated with CYM (**Figure 3.2.2C**), whereas one-carbon, glycine, small molecule, and serine family amino acid metabolism were those most enriched in the dataset of down-regulated genes (**Figure 3.2.2D**). In both data sets, cell periphery was most enriched cellular component (**Figure 3.2.2C** and **3.2.2D**).

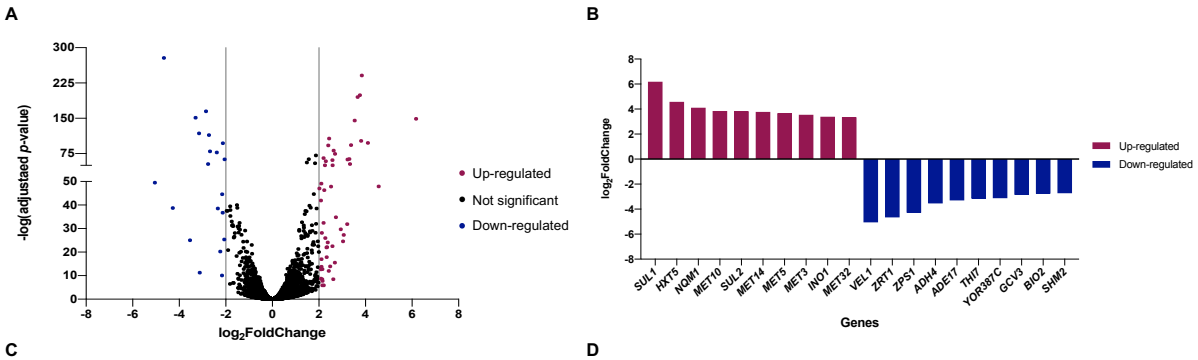

C

GO term enrichment of up-regulated genes

Biological process GO term	***p* value**
Sulfur amino acid metabolic process	2.78E-14
Sulfur compound metabolic process	2.30E-12
Oxoacid metabolic process	4.00E-08
Organic acid metabolic process	4.19E-08
Sulfate assimilation	1.76E-07
Cellular component GO term	***p* value**
Cell periphery	2.25E-03
Sulfite reductase complex (NADPH)	2.28E-03
Plasma membrane	2.84E-03

D

GO term enrichment of down-regulated genes

Biological process GO term	***p* value**
One-carbon metabolic process	1.73E-07
Glycine metabolic process	4.18E-05
Small molecule metabolic process	2.14E-03
Glycine catabolic process	2.50E-03
Serine family amino acid metabolic process	4.09E-03
Cellular component GO term	***p* value**
Cell periphery	1.03E-05
Glycine cleavage complex	5.70E-04
Cell wall	3.78E-03
Fungal-type cell wall	3.78E-03
External encapsulating structure	4.47E-03

Figure 3.2.2. Transcriptomic analysis of CYM effect in *S. cerevisiae* BY4741 cells. Cells were treated for 8 h in the presence of 25 µg mL^{-1} of CYM and/or the equivalent volume of DMSO (control), and RNA was purified for RNAseq analysis. **(A)** Volcano plot of the differentially expressed genes. The x-axis represents log2Fold change and the y-axis represents -log10(adjusted *p*-value). The purple points represent up-regulated genes, and blue points represent down-regulated genes. Genes not significantly altered are shown in black. The threshold for differential expression was set as log2 fold change > 2 and log2 fold change < -2, and adjusted *p* value < 0.05. **(B)** The top 10 up-regulated genes (purple) and the top 10 down-regulated genes (blue). The top 5 of GO term enrichment analysis of the 50 up-regulated genes **(C)** and the 20 down-regulated genes **(D)**.

3.2.2.3. Proteome-wide alterations induced by cymoxanil

To look at the effect of CYM on the proteome we imaged a collection of yeast strains each expressing one yeast protein tagged with a GFP at its N terminus under control of a constitutive *NOP1*

promoter. The advantage of this collection is that the control of a constitutive promoter allows us to focus on post transcriptional events.

Proteome alterations were assessed in cells incubated in the presence of 25 μg mL^{-1} CYM, for 8 h, and proteins were considered to display altered localization (partially or totally) when compared with cells incubated with the CYM vehicle, DMSO, for the same time (examples in **Figure 3.2.3A**). We found that, of a total of 1659 proteins analyzed, 126 changed their localization (supplementary material **Table S3.2.iii**).

A

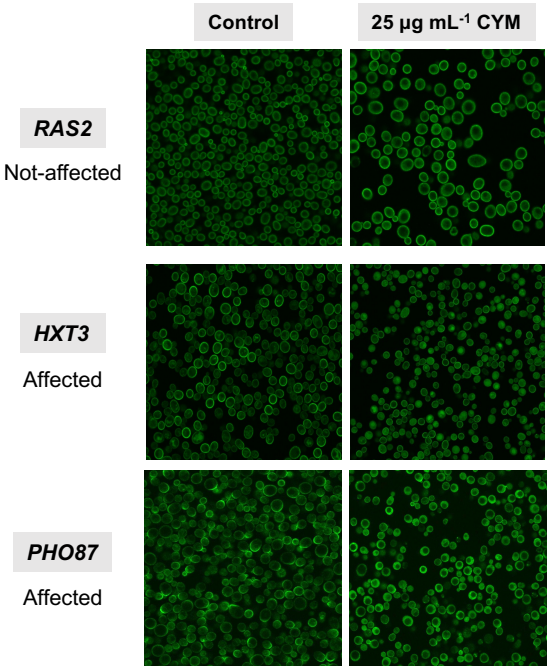

B

GO term enrichment of affected proteins

Biological process GO term	***p* value**
Establishment of localization	8.89E-06
Transport	2.25E-06
Localization	4.86E-05
Transmembrane transport	4.90E-05
Organic substance transport	3.14E-05
Cellular component GO term	***p* value**
Cell periphery	7.91E-19
Endoplasmic reticulum	2.55E-13
Plasma membrane	4.10E-11
Membrane	1.44E-09
Endomembrane system	4.71E-06

Figure 3.2.3. Effects of CYM on protein localization. Yeast strains in the collection (N′ *NOP1*pr-GFP library) were grown overnight in SD liquid medium, back-diluted 1:20 into 95 μl of fresh medium with 25 μg mL^{-1} of CYM and/or the equivalent volume of DMSO as a negative control, and grown for 8 h at 30 °C before image acquisition and manual assessment of the localization of the GFP tagged protein. Proteins for which data was obtained were divided into two groups: proteins that do not change their localization, proteins demonstrating altered localization. **(A)** Representative images from the two groups. **(B)** The top 5 of GO term enrichment analysis of proteins affected by CYM.

GO enrichment analysis showed that proteins involved in biological processes related to establishment of localization, transport, and transmembrane transport were overrepresented in the dataset of proteins whose localization was altered by exposure to CYM (**Figure 3.2.3B**). Furthermore, the cellular components with higher representation were cell periphery, with many proteins accumulating in the vacuole, and the endoplasmic reticulum, with several protein displaying additional diffuse localization (**Figure 3.2.3B** and supplementary material **Table S3.2.iii**).

3.2.2.4. Cymoxanil does not induce autophagy in yeast cells

Results from the two screens seemed to suggest that CYM may induce a response similar to starvation, with increased catabolism and accumulation of several membrane proteins in the vacuole. We thus investigated if these observations could be a result of autophagy induction. However, as seen in **Figure 3.2.4**, CYM did not lead to an increase in GFP-Atg8 delivery to the vacuole and consequent cleavage to free GFP, one of the most commonly used markers to ascertain autophagy in yeast.

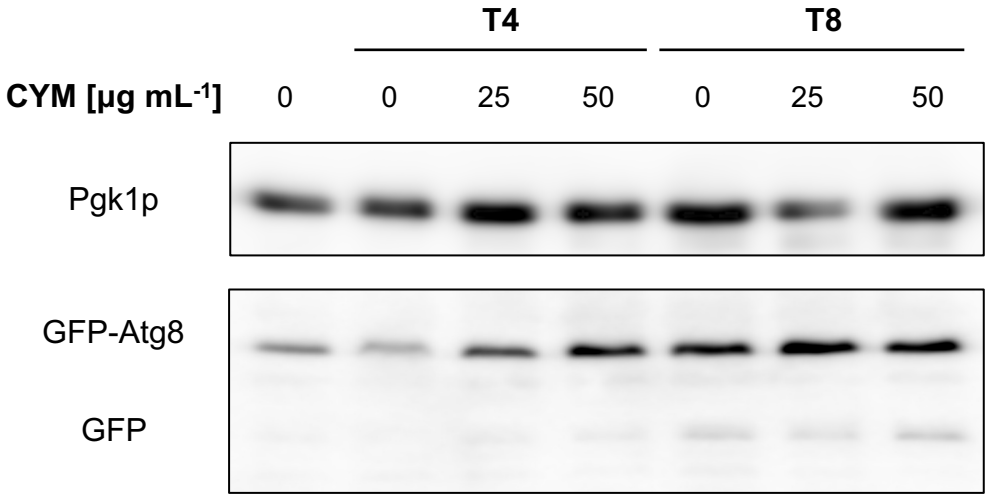

Figure 3.2.4. Effect of CYM on autophagy in yeast cells. BY4741 cells harboring pRS416 GFP-ATG8 were treated for 8 h in the or presence of 25 or 50 µg mL^{-1} of CYM and/or the equivalent volume of DMSO (0). Samples were collected before (time 0) and after 4 and 8 h of treatment. Autophagy was monitored by western-blot analysis of GFP-Atg8 cleavage. Pgk1p was used as the loading control.

3.2.2.5. Cymoxanil induces intracellular accumulation of ergosterol, perturbing lipid rafts of yeast cells without affecting ergosterol biosynthesis

Results from both screens also indicated that CYM affects transporter proteins, which may be a direct effect or a result of alterations in the plasma membrane. We therefore assessed if CYM affects the distribution of lipid rafts, domains enriched in ergosterol and sphingolipids, with the fluorescent sterol marker filipin. In untreated cells, a normal punctate pattern of filipin staining in the plasma membrane was observed (arrows), while intracellular spots (arrowheads) were evident in CYM-treated cells (**Figure 3.2.5A**). This phenotype was also observed in the *end3*Δ mutant, which is defective in the internalization step of endocytosis (**Figure 3.2.5A**). These CYM-induced alterations were not a result of ergosterol depletion, which would result in up-regulation of *ERG* genes, which we did not

observe by transcriptomic analysis of CYM-treated cells (supplementary material **Table S3.2.ii**). We further confirmed there was no up-regulation of *ERG25* by qRT-PCR (**Figure 3.2.5B**).

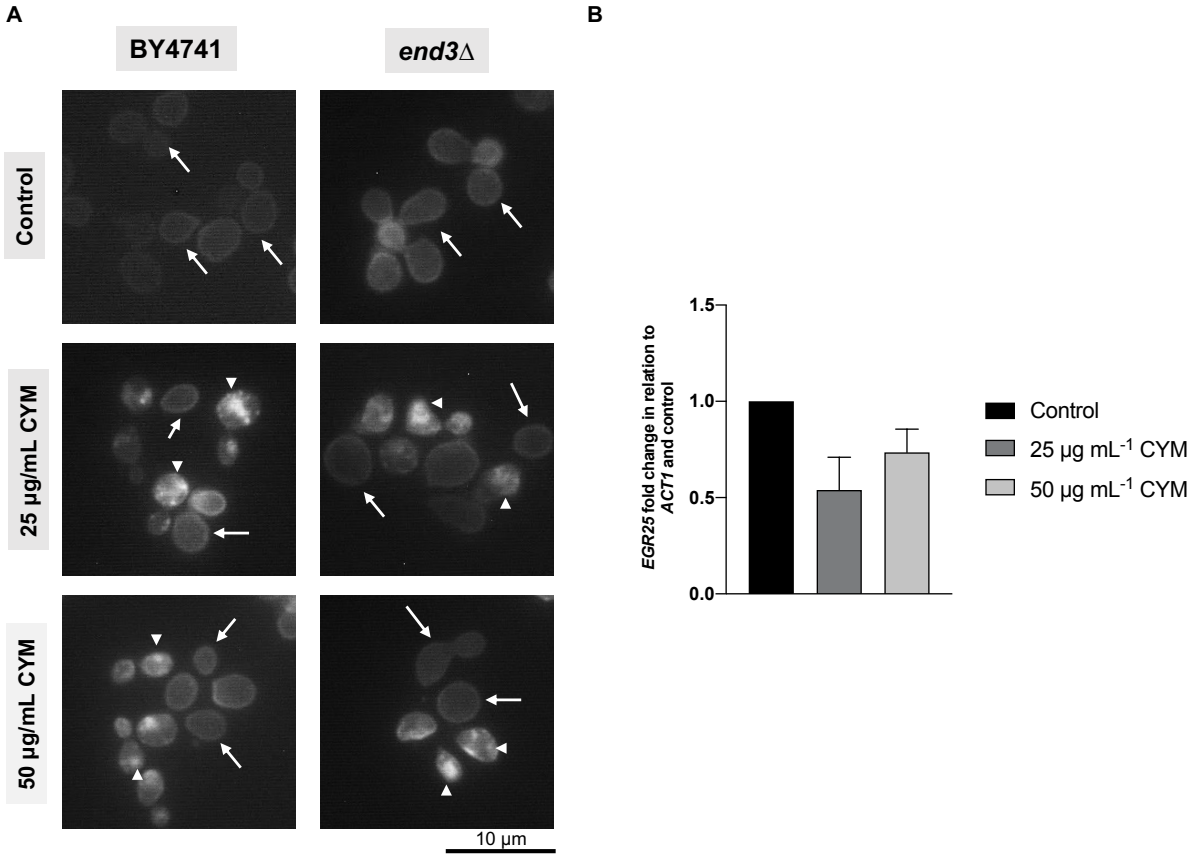

Figure 3.2.5. Effect of CYM on the distribution of ergosterol-rich lipid rafts. (A) BY4741 wild type and *end3*Δ cells were treated for 8 h in the presence of 25 or 50 µg mL^{-1} of CYM and/or the equivalent volume of DMSO (control). Then, cells were collected and stained in the dark with 0.1 µg L^{-1} filipin, immediately before visualization under the microscope. Representative fluorescence images of each condition are shown. Due to fast photobleaching of filipin, fluorescence intensity is not associated with ergosterol levels and only localization can be inferred. Head arrows: intracellular filipin staining. Arrows: plasma membrane filipin staining. **(B)** Wild type cells were treated for 8 h in absence (control) or presence of 25 or 50 µg mL^{-1} CYM and *ERG25* expression levels were analyzed by qRT-PCR using *ACT1* as normalizer. The expression values are represented as the fold change relative to the nontreated cells (control) and correspond to the mean ± S.D. of two independent experiments.

3.2.2.6. Cymoxanil does not affect efflux pumps but inhibits Pma1p activity and leads to plasma membrane depolarization of yeast cells

As alterations in lipid rafts can influence the activity of proteins that are normally localized in these domains, we next assessed whether CYM can affect efflux pumps. For that purpose, cells were exposed to CYM and then stained with calcein AM in the absence or presence of the efflux pump

inhibitor verapamil. If CYM caused an inhibition or decrease of efflux pumps in the membrane, it would be expected that the ratio between the fluorescence intensity of cells that were treated with verapamil or left untreated would be different in CYM-treated cells in comparison with the control. However, this ratio of fluorescence intensity (+ verapamil/ - verapamil) was similar in CYM-treated cells and nontreated cells, indicating that CYM does not affect efflux pumps in yeast cells (**Figure 3.2.6A**).

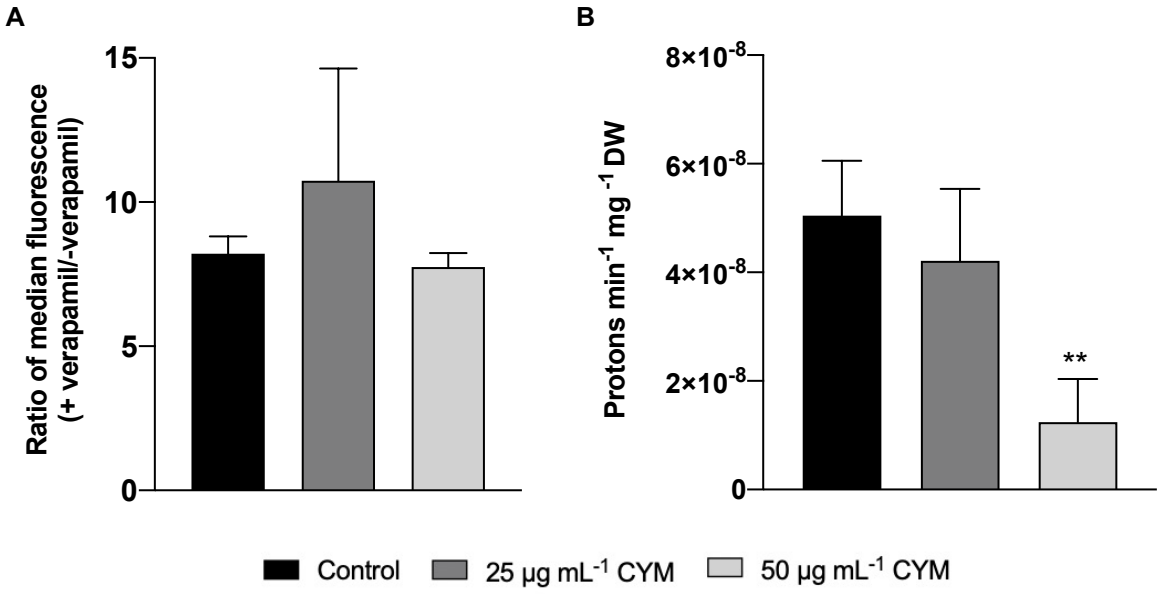

Figure 3.2.6. Effect of CYM on efflux pumps and Pma1p activity. BY4741 cells were treated for 8 h in the presence of 25 or 50 µg mL^{-1} CYM and/or the equivalent volume of DMSO (control). **(A)** For evaluation of efflux pumps, cells were collected, treated with verapamil and stained with calcein AM. Data are presented as the ratio of median of the green fluorescence intensity between verapamil-treated and untreated cells (+ verapamil/ - verapamil). **(B)** Pma1p proton pumping activity was assessed by measuring H^+ efflux triggered by glucose addition. Cells were collected and the pH adjusted to 5.5. Afterwards, 20 mM of glucose was added to induce proton extrusion by Pma1p. The proton extrusion activity was calculated from the maximum slope of the records and represents the rate of acidification. The data displayed are the mean ± S.D. of three independent experiments. Asterisks (**, $P \leq 0.01$) depict significant differences relative to the control.

We therefore next evaluated if CYM-induced alterations in lipid rafts could affect the activity of the proton pumping H^+-ATPase Pma1p, one of the most abundant integral membrane proteins of the yeast plasma membrane and a resident of lipid rafts (21,22). We indeed found that proton pumping was affected by CYM, as exposure of cells to 50 µg mL^{-1} of CYM for 8 h led to a reduction in proton movement out of cells (**Figure 3.2.6B**).

As Pma1p pumps protons from the cytosol to the exterior of the cell coupled to ATP hydrolysis, Pma1p inhibition could be a result of decreased intracellular ATP levels. However, our data revealed that

exposure to CYM is associated with increased intracellular accumulation of ATP (**Figure 3.2.7A**), instead consistent with less ATP consumption as a result of Pma1p inhibition (**Figure 3.2.6B**).

Pma1p activity, coupled with the activity of other pumps, such as the ATPase in the vacuole (V-ATPase), regulates intracellular pH homeostasis, critical for yeast cell survival. We therefore tested if CYM could affect the yeast vacuolar pH with the pH-sensitive probe CDCFDA. **Figure 3.2.7B** shows that CYM-treated cells exhibit a higher fluorescence signal than untreated cells (control), indicating that CYM also affects V-ATPase activity.

Since Pma1p proton pumping activity is also vital to generate an electrochemical gradient, we explored if CYM could cause alterations in plasma membrane potential using the fluorescent anionic probe $DiBAC_4(3)$. Simultaneously, and to distinguish between membrane depolarization and general membrane permeabilization, cells were stained with PI. We observed that the percentage of PI-negative/$DiBAC_4(3)$-positive cells was higher in CYM-treated cells than in nontreated cells, indicating that CYM leads to plasma membrane depolarization prior to loss of plasma membrane integrity (**Figure 3.2.7C**).

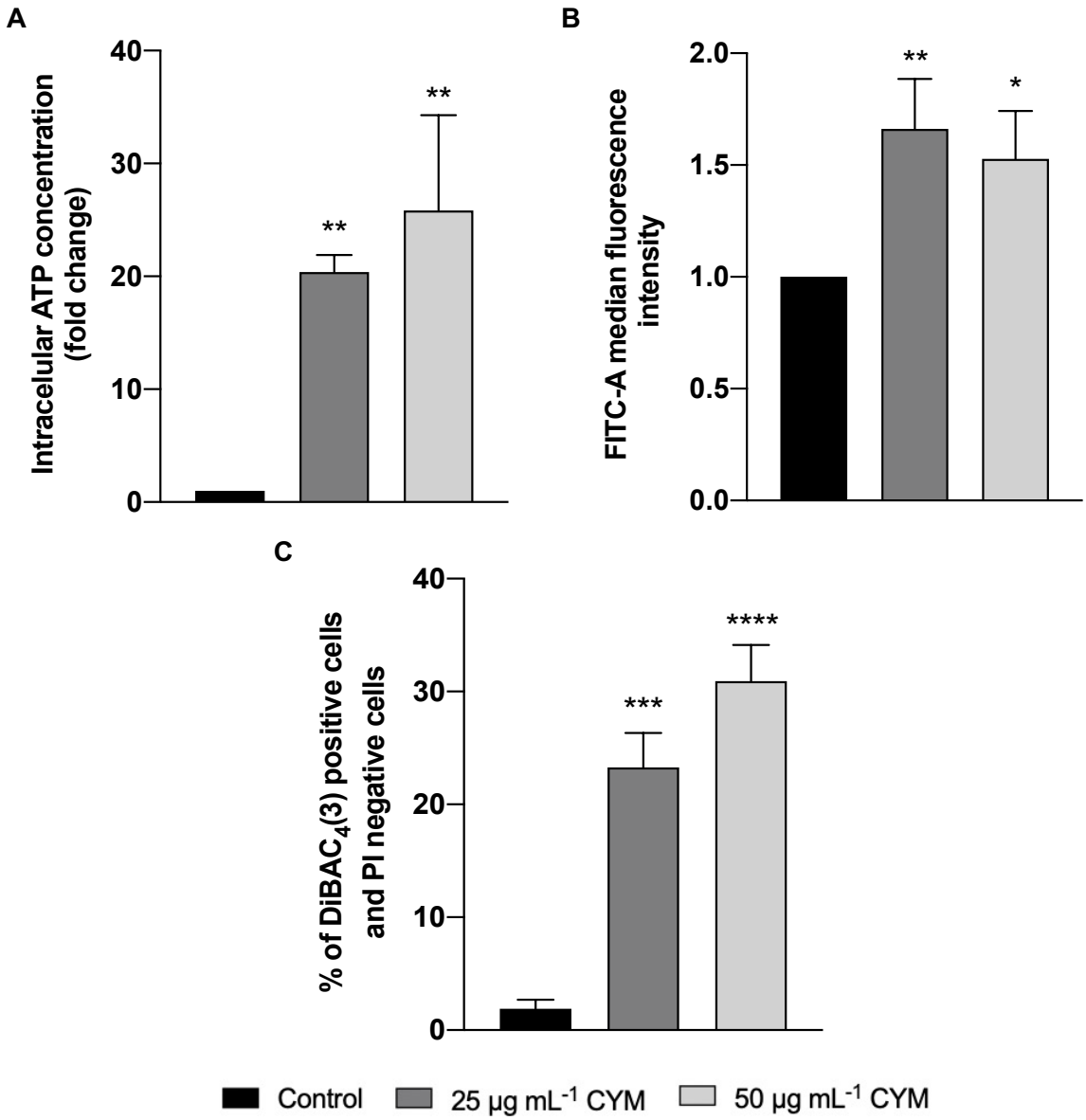

Figure 3.2.7. Effect of CYM on intracellular levels of ATP, vacuolar pH and membrane potential of BY4741 cells. Cells were treated for 8 h in the presence of 25 or 50 µg mL^{-1} of CYM and/or the equivalent volume of DMSO (control). **(A)** Intracellular ATP levels were measured with the BacTiter-Glo™ Microbial Cell Viability kit. Values represent the increase in ATP levels expressed in fold change in comparison with the control. **(B)** Alterations in vacuolar pH were monitored using the CDCFDA probe. Data represent the green median fluorescence intensity normalized to control. **(C)** Plasma membrane potential and integrity were assessed through $DiBAC_4(3)$ and PI staining, respectively. Data represent the percentage of cells with green fluorescence [$DiBAC_4(3)$ positive cells] and without red fluorescence (PI negative cells). The data displayed are the mean ± S.D. of three independent experiments. Asterisks (* ≤ 0.05; **, P ≤ 0.01; ***, P ≤ 0.001; ****, P ≤ 0.0001) depict significant differences relative to the control.

3.2.3. Discussion

CYM is a synthetic fungicide used for foliar applications in a curative and protective manner, mainly against downy mildew diseases and late blight diseases (23,24). As it exhibits a relatively short period of activity when used alone due to its weak persistence (half-life of a few days, depending on the conditions) and mobile nature (K_{oc} 39–238) (25), it has been almost exclusively used with other fungicides, such as mancozeb and copper, to increase overall efficacy (26). Previous studies suggested that CYM can affect several biochemical processes such as growth, respiration, and synthesis of nucleic acids, but most of these alterations were considered secondary effects (27–29). However, despite widespread use, the CYM mode of action remains elusive, complicating efforts to assess how CYM affects different target and non-target organisms and highlighting the importance of careful consideration when using this fungicide. We therefore sought to use the yeast *S. cerevisiae* as model system for an in-depth investigation of the cellular and molecular mechanisms underlying CYM cytotoxicity.

We started by assessing sensitivity of yeast cells to CYM using a fermentable (Glu) or respiratory (Gal) substrate and observed that cells lost viability and plasma membrane integrity earlier in the former conditions. We therefore conclude that the effect of CYM on cell growth and viability is not dependent, at least not solely, on active respiration, and as such it must have additional effects. Therefore, further characterization of the effects of CYM in yeast cells were pursued using glucose as the carbon source.

To gain insight into the possible effects of CYM at the molecular level, we performed two different and complementary screens, transcriptomics and proteome localization. Among other hits, an effect on membrane transporter systems stood out in both screens. On the one hand, there was up-regulation of genes encoding membrane transporters, and multiple membrane proteins appeared in an intracellular localization after CYM treatment. Moreover, several proteins appeared in the vacuole in response to CYM, which could be an indication of autophagy. A starvation phenotype with potential autophagy induction was also suggested by the categories enriched in transcriptomics analysis, such as a decrease in synthesis of most amino acids. Autophagy is considered a pro-survival mechanism that can be triggered by starvation and chemical stress (30), leading to vacuolar degradation of intracellular components (31,32). However, it also plays a critical role in normal development and cell homeostasis with intricate relations with cell metabolism, growth control, balance between cell survival and cell death, as well as ageing (33). We observed only a very tenuous band of free GFP in all conditions tested, which is consistent with basal levels of autophagy and thus disproving that CYM could induce autophagy.

As mentioned above, analysis of the enrichment in GO terms from both screens revealed that CYM affects genes associated with the plasma membrane. Consequently, and due to the importance of plasma membrane composition and organization to proper cellular function (34), we hypothesized that exposure to CYM could lead to plasma membrane alterations. We found that CYM changes plasma membrane organization by inducing intracellular accumulation of ergosterol and perturbing ergosterol-rich lipid rafts, plasma membrane nanodomains enriched in ergosterol and sphingolipids (35). We observed a similar pattern in membrane perturbation of yeast cells treated with the azole fungicide TEB (see chapter 4), known for inhibiting ergosterol biosynthesis. However, the alterations in lipid raft distribution induced by CYM were not accompanied by increased expression of *ERG* genes. Taken together, our results suggests that CYM disturbs ergosterol-rich lipid rafts without affecting ergosterol biosynthesis. Since deletion of *END3*, an essential gene for endocytosis, did not prevent intracellular accumulation of ergosterol, we hypothesize that CYM may impair the sorting of newly synthetized ergosterol to lipid rafts on the plasma membrane. However, it is also possible that CYM leads to increase endocytosis of plasma membrane proteins through a yet uncharacterized mechanism.

Alterations in lipid rafts can affect a myriad of cellular functions, eventually affecting cell fitness and viability, as these domains are associated with several biologically important proteins engaged in the regulation of ion homeostasis (Na^+, K^+), intracellular pH (H^+), nutrient transport, mating processes, drug efflux and stress responses (21). We therefore first assessed if CYM could lead to a decrease in the activity of efflux pumps, which could result in increased intracellular accumulation of CYM and consequent loss of viability. It would also be consistent with a sensitization to other compounds, and would help explain the efficacy of CYM in mixed formulations. However, we did not find any differences on the activity of drug efflux pumps of CYM-treated cells. We next hypothesized that CYM may inhibit the activity of the plasma membrane Pma1p proton pump, one of the most abundant raft proteins. Pma1p generates and maintains an electrochemical gradient across the plasma membrane, which is vital for yeast cell survival since it is used for the uptake of inorganic ions and nutrients and to regulate the intracellular pH. Pma1p generates the electrochemical gradient by pumping protons from the cytosol to the exterior of the cell associated to ATP hydrolysis (36,37). Indeed, we found that CYM reduces the proton pumping activity of Pma1p. One option could be that CYM inhibits this pump, directly or indirectly through lipid raft alterations, and/or increased endocytosis, or that it indirectly leads to intracellular depletion of ATP, in turn inhibiting Pma1p activity. We found that CYM-treated cells have a higher intracellular accumulation of ATP, consistent with the first hypothesis. In addition to intracellular accumulation of ATP, which may not be deleterious *per se*, Pma1p inhibition can also lead to increased

intracellular levels of H^+, affecting plasma membrane potential and intracellular pH homeostasis. We found that CYM led to a decrease in the plasma membrane potential of yeast cells, again suggesting that CYM may function as a Pma1p inhibitor. We also observed that CYM leads to vacuolar alkalinization, suggesting that CYM also affects V-ATPase activity.

As an essential fungal protein, Pma1p has been a proposed target for the development of novel effective antifungal medications. One study previously screened a small molecule library for the ability of compounds to inhibit Pma1p, to identify compounds that could subsequently lead to plasma membrane depolarization and display antifungal activity (38). Other antifungal compounds with different properties have also been described to lead to a similar phenotype, such as lactoferrin and edelfosine, which also display anticancer activity. Both cause alterations in sterol organization at the plasma membrane, loss of Pma1p from lipid rafts and intracellular acidification in *S. cerevisiae* cells (8,39,40), and have been proposed as therapies to aid in the fight against drug-resistant fungal infections. It is conceivable that a similar mode of action for CYM could prove useful in its function as an agrochemical. CYM, which is cytotoxic, could first decrease the levels of target organisms, but plasma membrane alterations would also weaken surviving targets and render them more susceptible to other compounds. This could explain the use of CYM in joint formulations as an effective susceptibility enhancer of the effect of the substance that accompanies it, optimizing its short life.

Our work identifies for the first time the plasma membrane as one of the targets of CYM and proposes a mode of action underlying its antifungal activity: perturbation of lipid raft organization and inhibition of Pma1p and V-ATPase activity, leading to a decrease in plasma membrane potential and intracellular acidification, followed by cell death. These findings therefore contribute to a better understanding of the mechanism of action of CYM and its potential as a fungitoxic agent.

3.3.4. References

1. Deffieu M, Bhatia-Kiššová I, Salin B, Klionsky DJ, Pinson B, Manon S, et al. Increased levels of reduced cytochrome *b* and mitophagy components are required to trigger nonspecific autophagy following induced mitochondrial dysfunction. J Cell Sci. 2013;126:415–26.
2. Gietz RD, Woods RA. Yeast Transformation by the LiAc/SS Carrier DNA/PEG Method. In: Xiao W, editor. Methods in molecular biology. Humana Press Inc., Totowa, NJ; 2006. p. 107–20.
3. Livak KJ, Schmittgen TD. Analysis of relative gene expression data using real-time quantitative PCR and the $2^{-\Delta\Delta_{CT}}$ method. Methods. 2001;25:402–8.
4. Yofe I, Weill U, Chuartzman S, Zalckvar E, Schütze C, Wiedemann N, et al. One library to make them all: streamlining yeast library creation by a SWAp-Tag (SWAT) strategy. Nat Methods. 2016;13:371–8.
5. Weill U, Yofe I, Sass E, Stynen B, Davidi D, Natarajan J, et al. Genome-wide SWAp-Tag yeast libraries for proteome exploration. Nat Methods. 2018;15:617–22.
6. Nair U, Yen W-L, Mari M, Cao Y, Xie Z, Baba M, et al. A role for Atg8-PE deconjugation in autophagosome biogenesis. Autophagy. 2012;8:780–93.
7. Pacheco A, Azevedo F, Rego A, Santos J, Chaves SR, Côrte-Real M, et al. C2-phytoceramide perturbs lipid rafts and cell integrity in *Saccharomyces cerevisiae* in a sterol-dependent manner. PLoS One. 2013;8:1–12.
8. Santos-Pereira C, Andrés MT, Chaves SR, Fierro JF, Gerós H, Manon S, et al. Lactoferrin perturbs lipid rafts and requires integrity of Pma1p-lipid rafts association to exert its antifungal activity against *Saccharomyces cerevisiae*. Int J Biol Macromol . 2021;171:343–57.
9. Maxfield FR, Wüstner D. Analysis of Cholesterol Trafficking with Fluorescent Probes. Methods Cell Biol. 2012;108:367–93.
10. Prudêncio C, Sansonetty F, Sousa MJ, Côrte-Real M, Leão C. Rapid detection of efflux pumps and their relation with drug resistance in yeast cells. Cytometry. 2000;39:26–35.
11. Yu Q, Ding X, Xu N, Cheng X, Qian K, Zhang B, et al. *In vitro* activity of verapamil alone and in combination with fluconazole or tunicamycin against *Candida albicans* biofilms. Int J Antimicrob Agents. 2013;41:179–82.
12. Teng J, Goto R, Iida K, Kojima I, Iida H. Ion-channel blocker sensitivity of voltage-gated calcium-channel homologue Cch1 in *Saccharomyces cerevisiae*. Microbiology. 2008;154:3775–81.
13. Tiligada E, Giannakakou P, Karavokyros I, Delitheos A. Effect of calcium channel blockers on the action of various antitumour agents in the yeast *Saccharomyces cerevisiae*. J Appl Bacteriol.

1996;81:481–5.

14. Zhou S, Cui Z, Urban J. Dead cell counts during serum cultivation are underestimated by the fluorescent live/dead assay. Biotechnol J. 2011;6:513–8.
15. Fritzsche M, Mandenius CF. Fluorescent cell-based sensing approaches for toxicity testing. Anal Bioanal Chem. 2010;398:181–91.
16. Yang KM, Woo JM, Lee SM, Park JB. Improving ethanol tolerance of *Saccharomyces cerevisiae* by overexpressing an ATP-binding cassette efflux pump. Chem Eng Sci. 2013;103:74–8.
17. Leão C, Van Uden N. Effects of ethanol and other alkanols on passive proton influx in the yeast *Saccharomyces cerevisiae*. BBA - Biomembr. 1984;774:43–8.
18. Teixeira MC, Raposo LR, Mira NP, Lourenço AB, Sá-Correia I. Genome-wide identification of *Saccharomyces cerevisiae* genes required for maximal tolerance to ethanol. Appl Environ Microbiol. 2009;75:5761–72.
19. Roberts CJ, Raymond CK, Yamashiro CT, Stevens TH. Methods for studying the yeast vacuole. Methods Enzymol. 1991;194:644–61.
20. Wolff C, Fuks B, Chatelain P. Comparative study of membrane potential-sensitive fluorescent probes and their use in ion channel screening assays. J Biomol Screen. 2003;8:533–43.
21. Mollinedo F. Lipid raft involvement in yeast cell growth and death. Front Oncol. 2012;2:1–15.
22. Kane PM. Proton transport and pH control in fungi. Adv Exp Med Biol. 2016;892:33–68.
23. Fidente P, Di Giovanni C, Seccia S, Morrica P. Determination of cymoxanil in drinking water and soil using high-performance liquid chromatography. Biomed Chromatogr. 2005;19:766–70.
24. Rekanović E, Potočnik I, Milijašević-Marčić S, Stepanović M, Todorović B, Mihajlović M. Toxicity of metalaxyl, azoxystrobin, dimethomorph, cymoxanil, zoxamide and mancozeb to *Phytophthora infestans* isolates from Serbia. J Environ Sci Heal - Part B Pestic Food Contam Agric Wastes. 2012;47:403–9.
25. Kim S, Chen J, Cheng T, Gindulyte A, He J, He S, et al. PubChem 2023 update. Nucleic Acids Res. 2023;51:D1373–80.
26. Toffolatti SL, Venturini G, Campia P, Cirio L, Bellotto D, Vercesi A. Sensitivity to cymoxanil in Italian populations of *Plasmopara viticola* oospores. Pest Manag Sci. 2015;71:1182–8.
27. Ziogas BN, Davidse LC. Studies on the mechanism of action of cymoxanil in *Phytophthora infestans*. Pestic Biochem Physiol. 1987;29:89–96.
28. Ribeiro IC, Veríssimo I, Moniz L, Cardoso H, Sousa MJ, Soares AMVM, et al. Yeasts as a model for assessing the toxicity of the fungicides penconazol, cymoxanil and dichlofluanid.

Chemosphere. 2000;41:1637–42.

29. Tellier F, Carlin-Sinclair A, Fritz R, Cherton JC, Leroux P. Activity and metabolism of cyano-oxime derivatives in various strains of *Botrytis cinerea*. Pestic Biochem Physiol. 2004;78:151–60.
30. Noda T, Ohsumi Y. Tor, a phosphatidylinositol kinase homologue, controls autophagy in yeast. J Biol Chem. 1998;273:3963–6.
31. Reggiori F, Klionsky DJ. Autophagic processes in yeast: Mechanism, machinery and regulation. Genetics. 2013;194:341–61.
32. Farré JC, Subramani S. Mechanistic insights into selective autophagy pathways: Lessons from yeast. Nat Rev Mol Cell Biol. 2016;17:537–52.
33. Ryter SW, Cloonan SM, Choi AMK. Autophagy: A critical regulator of cellular metabolism and homeostasis. Mol Cells. 2013;36:7–16.
34. Stewart GG. The structure and function of the yeast cell wall, plasma membrane and periplasm. In: Stewart GG, editor. Brewing and Distilling Yeasts. Springer, Cham; 2017. p. 55–75.
35. Wachtler V, Balasubramanian MK. Yeast lipid rafts? - An emerging view. Trends Cell Biol. 2006;16:1–4.
36. Serrano R, Kielland-Brandt MC, Fink GR. Yeast plasma membrane ATPase is essential for growth and has homology with (Na^+ + K^+), K^+- and Ca^{2+}-ATPases. Nature. 1986;319:689–93.
37. Serrano R. Structure and function of proton translocating ATPase in plasma membranes of plants and fungi. Biochim Biophys Acta. 1988;947:1–28.
38. Kjellerup L, Gordon S, Cohrt KO, Brown WD, Fuglsang AT WA-M. Identification of Antifungal H+-ATPase Inhibitors with Effect on Plasma. Antimicrob Agents Chemother. 2017;61:1–14.
39. Zaremberg V, Gajate C, Cacharro LM, Mollinedo F, McMaster CR. Cytotoxicity of an anti-cancer lysophospholipid through selective modification of lipid raft composition. J Biol Chem. 2005;280:38047–58.
40. Czyz O, Bitew T, Cuesta-Marbán A, McMaster CR, Mollinedo F, Zaremberg V. Alteration of plasma membrane organization by an anticancer lysophosphatidylcholine analogue induces intracellular acidification and internalization of plasma membrane transporters in yeast. J Biol Chem. 2013;288:8419–32.

3.2.5. Supplementary Material

Table S3.2.i

Table S3.2.ii

Table S3.2.iii

Table S3.2.i. Genes whose expression decreases after exposure to CYM. The differentially expressed genes were ranked based on RNAseq analysis, considering a threshold of log2FoldChange <-2 and adjusted *p* value < 0.05. For each gene, OFR name, SGD description, log2FoldChange and adjusted p value (*p* adj) are indicated.

ORF name	Gene name	SGD Description	log2FoldChange	*p* adj
YGL258W	*VEL1*	Protein of unknown function; highly induced in zinc-depleted conditions and has increased expression in NAP1 deletion mutants; *VEL1* has a paralog, *YOR387C*, that arose from a single-locus duplication	-5.047	3.26E-50
YGL255W	*ZRT1*	High-affinity zinc transporter of the plasma membrane; responsible for the majority of zinc uptake; transcription is induced under low-zinc conditions by the Zap1p transcription factor	-4.656	8.08E-279
YOL154W	*ZPS1*	Putative GPI-anchored protein; transcription is induced under low-zinc conditions, as mediated by the Zap1p transcription factor, and at alkaline pH	-4.276	1.88E-39
YGL256W	*ADH4*	Alcohol dehydrogenase isoenzyme type IV; dimeric enzyme demonstrated to be zinc-dependent despite sequence similarity to iron-activated alcohol dehydrogenases; transcription is induced in response to zinc deficiency	-3.538	9.74E-26
YMR120C	*ADE17*	Enzyme of *de novo* purine biosynthesis; contains both 5-aminoimidazole-4-carboxamide ribonucleotide transformylase and inosine monophosphate cyclohydrolase activities; *ADE17* has a paralog, *ADE16*, that arose from the whole genome duplication; ade16 ade17 mutants require adenine and histidine	-3.299	8.40E-152
YLR237W	*THI7*	Plasma membrane transporter responsible for the uptake of thiamine; contributes to uptake of 5-aminoimidazole-4-carboxamide-1-beta-D-ribofuranoside (acadesine); member of the major facilitator superfamily of transporters; mutation of human ortholog causes thiamine-responsive megaloblastic anemia	-3.148	1.01E-118

YOR387C	*YOR387C*	Putative protein of unknown function; regulated by the metal-responsive Aft1p transcription factor; highly inducible in zinc-depleted conditions; localizes to the soluble fraction; SWAT-GFP and mCherry fusion proteins localize to the endoplasmic reticulum and vacuole respectively; *YOR387C* has a paralog, *VEL1*, that arose from a single-locus duplication	-3.116	5.12E-12
YAL044C	*GCV3*	H subunit of the mitochondrial glycine decarboxylase complex; glycine decarboxylase is required for the catabolism of glycine to 5,10-methylene-THF; also required for all protein lipoylation; expression is regulated by levels of 5,10-methylene-THF	-2.849	1.06E-165
YGR286C	*BIO2*	Biotin synthase; catalyzes the conversion of dethiobiotin to biotin, which is the last step of the biotin biosynthesis pathway	-2.757	1.17E-53
YLR058C	*SHM2*	Cytosolic serine hydroxymethyltransferase; converts serine to glycine plus 5,10 methylenetetrahydrofolate; major isoform involved in generating precursors for purine, pyrimidine, amino acid, and lipid biosynthesis	-2.720	5.03E-115
YMR189W	*GCV2*	P subunit of the mitochondrial glycine decarboxylase complex; glycine decarboxylase is required for the catabolism of glycine to 5,10-methylene-THF; expression is regulated by levels of 5,10-methylene-THF in the cytoplasm	-2.681	1.71E-80
YNL145W	*MFA2*	Mating pheromone a-factor; made by a cells; interacts with alpha cells to induce cell cycle arrest and other responses leading to mating; biogenesis involves C-terminal modification, N-terminal proteolysis, and export; also encoded by *MFA1*	-2.387	3.82E-78
YHR216W	*IMD2*	Inosine monophosphate dehydrogenase; catalyzes the rate-limiting step in GTP biosynthesis, expression is induced by mycophenolic acid resulting in resistance to the drug, expression is repressed by nutrient limitation; *IMD2* has a paralog, *YAR073W/YAR075W*, that arose from a segmental duplication	-2.345	2.97E-39
YOL155C	*HPF1*	Haze-protective mannoprotein; reduces particle size of aggregated proteins in white wines, thereby decreasing turbidity; intragenic repeat expansion controls chronological aging; expansion of intragenic tandem repeats within N-terminus sufficient to cause pronounced life span shortening; repeat expansion shifts cells from sedentary to buoyant, thereby increasing exposure to oxygen, altering methionine, lipid, and purine metabolism	-2.237	5.71E-21

YNR058W	*BIO3*	7,8-diamino-pelargonic acid aminotransferase (DAPA); catalyzes the second step in the biotin biosynthesis pathway; *BIO3* is in a cluster of 3 genes (*BIO3*, *BIO4*, and *BIO5*) that mediate biotin synthesis; *BIO3* and *BIO4* were acquired by horizontal gene transfer from bacteria	-2.160	8.84E-11
YGL032C	*AGA2*	Adhesion subunit of a-agglutinin of a-cells; C-terminal sequence acts as a ligand for alpha-agglutinin (Sag1p) during agglutination, modified with O-linked oligomannosyl chains, linked to anchorage subunit Aga1p via two disulfide bonds	-2.158	2.44E-45
YMR006C	*PLB2*	Phospholipase B (lysophospholipase) involved in lipid metabolism; displays transacylase activity *in vitro*; overproduction confers resistance to lysophosphatidylcholine	-2.132	1.71E-37
YDR345C	*HXT3*	Low affinity glucose transporter of the major facilitator superfamily; expression is induced in low or high glucose conditions; *HXT3* has a paralog, *HXT5*, that arose from the whole genome duplication	-2.128	6.50E-98
YMR319C	*FET4*	Low-affinity Fe(II) transporter of the plasma membrane	-2.068	4.59E-26
YDR019C	*GCV1*	T subunit of the mitochondrial glycine decarboxylase complex; glycine decarboxylase is required for the catabolism of glycine to 5,10-methylene-THF; expression is regulated by levels of levels of 5,10-methylene-THF in the cytoplasm	-2.052	2.11E-63

Table S3.2.ii. Genes whose expression increases after exposure to CYM. The differentially expressed genes were ranked based on RNAseq analysis, considering a threshold of log2FoldChange <2 and *p* adj < 0.05. For each gene, OFR name, SGD description, log2FoldChange and *p* adj are indicated.

ORF name	Gene name	Description	log2FoldChange	*p* adj
YBR294W	*SUL1*	High affinity sulfate permease of the SulP anion transporter family; sulfate uptake is mediated by specific sulfate transporters Sul1p and Sul2p, which control the concentration of endogenous activated sulfate intermediates	6.173	1.22E-149
YHR096C	*HXT5*	Hexose transporter with moderate affinity for glucose; induced in the presence of non-fermentable carbon sources, induced by a decrease in growth rate, contains an extended N-terminal domain relative to other HXTs; *HXT5* has a paralog, *HXT3*, that arose from the whole genome duplication	4.571	1.34E-48
YGR043C	*NQM1*	Transaldolase of unknown function; transcription is repressed by Mot1p and induced by alpha-factor and during diauxic shift; *NQM1* has a paralog, *TAL1*, that arose from the whole genome duplication	4.103	2.43E-98
YFR030W	*MET10*	Subunit alpha of assimilatory sulfite reductase; complex converts sulfite into sulfide	3.840	8.21E-242
YLR092W	*SUL2*	High affinity sulfate permease; sulfate uptake is mediated by specific sulfate transporters Sul1p and Sul2p, which control the concentration of endogenous activated sulfate intermediates	3.816	8.35E-103
YKL001C	*MET14*	Adenylylsulfate kinase; required for sulfate assimilation and involved in methionine metabolism; human homolog *PAPSS2* complements yeast null mutant	3.763	1.02E-199
YJR137C	*MET5*	Sulfite reductase beta subunit; involved in amino acid biosynthesis, transcription repressed by methionine	3.664	6.98E-196
YJR010W	*MET3*	ATP sulfurylase; catalyzes the primary step of intracellular sulfate activation, essential for assimilatory reduction of sulfate to sulfide, involved in methionine metabolism; human homolog *PAPSS2* complements yeast null mutant	3.536	5.10E-146
YJL153C	*INO1*	Inositol-3-phosphate synthase; involved in synthesis of inositol phosphates and inositol-containing phospholipids; transcription is coregulated with other phospholipid biosynthetic genes by Ino2p and Ino4p, which bind the UASINO DNA element	3.381	1.23E-93

YDR253C	*MET32*	Zinc-finger DNA-binding transcription factor; involved in transcriptional regulation of the methionine biosynthetic genes; targets strong transcriptional activator Met4p to promoters of sulfur metabolic genes; feedforward loop exists in the regulation of genes controlled by Met4p and Met32p; lack of such a loop for MET31 may account for the differential actions of Met32p and Met31p; *MET32* has a paralog, *MET31*, that arose from the whole genome duplication	3.339	1.10E-53
YBR116C	*YBR116C*	Dubious open reading frame; unlikely to encode a functional protein, based on available experimental and comparative sequence data; partially overlaps the verified gene *TKL2*	3.303	2.55E-64
YNL277W	*MET2*	L-homoserine-O-acetyltransferase; catalyzes the conversion of homoserine to O-acetyl homoserine which is the first step of the methionine biosynthetic pathway	3.228	3.82E-63
YIR017C	*MET28*	bZIP transcriptional activator in the Cbf1p-Met4p-Met28p complex; participates in the regulation of sulfur metabolism	3.216	1.27E-32
YML123C	*PHO84*	High-affinity inorganic phosphate transporter; also low-affinity manganese transporter; regulated by Pho4p and Spt7p; mutation confers resistance to arsenate; exit from the ER during maturation requires Pho86p; cells overexpressing Pho84p accumulate heavy metals but do not develop symptoms of metal toxicity	3.064	4.93E-28
YLR042C	*NFG1*	Negative regulator of the filamentous growth pathway; inhibits invasive growth by dampening the activity of the filamentous MAPK pathway; localizes to the cell wall and to the vacuole and cell periphery in HTP studies; deletion improves xylose fermentation in industrially engineered strains	3.038	2.74E-25
YGL125W	*MET13*	Major isozyme of methylenetetrahydrofolate reductase; catalyzes the reduction of 5,10-methylenetetrahydrofolate to 5-methyltetrahydrofolate in the methionine biosynthesis pathway	2.936	2.00E-30
YJL116C	*NAC3*	Protein involved in mitochondrion organization; functions with Nca2p to regulate mitochondrial expression of subunits 6 (Atp6p) and 8 (Atp8p) of the Fo-F1 ATP synthase; SWAT-GFP, seamless-GFP and mCherry fusion proteins localize to the vacuole; member of the SUN family; expression induced in cells treated with the mycotoxin patulin; *NCA3* has a paralog, *UTH1*, that arose from the whole genome duplication	2.731	1.53E-35
YCL064C	*CHA1*	Catabolic L-serine (L-threonine) deaminase; catalyzes the degradation of both L-serine and L-threonine; required to use serine or threonine as the sole nitrogen source, transcriptionally induced by serine and threonine	2.695	2.64E-75

YGL205W	*POX1*	Fatty-acyl coenzyme A oxidase; involved in the fatty acid beta-oxidation pathway; localized to the peroxisomal matrix; component of a light sensing pathway, converting light into a hydrogen peroxide signal, modulating nucleo-cytoplasmic shuttling of stress-responsive transcription factor, Msn2p	2.682	2.81E-16
YDL059C	*RAD59*	Protein involved DNA double-strand break repair; repairs breaks in DNA during vegetative growth via recombination and single-strand annealing; anneals complementary single-stranded DNA; forms nuclear foci upon DNA replication stress; required for loading of Rad52p to DSBs; regulates replication fork progression in DNA ligase I-deficient cells; paralog of Rad52p	2.632	5.21E-82
YBR117C	*TKL2*	Transketolase; catalyzes conversion of xylulose-5-phosphate and ribose-5-phosphate to sedoheptulose-7-phosphate and glyceraldehyde-3-phosphate in the pentose phosphate pathway; needed for synthesis of aromatic amino acids; *TKL2* has a paralog, *TKL1*, that arose from the whole genome duplication	2.614	3.27E-09
YLR214W	*FRE1*	Ferric reductase and cupric reductase; reduces siderophore-bound iron and oxidized copper prior to uptake by transporters; expression induced by low copper and iron levels	2.591	9.74E-51
YGR256W	*GND2*	6-phosphogluconate dehydrogenase (decarboxylating); catalyzes an NADPH regenerating reaction in the pentose phosphate pathway; required for growth on D-glucono-delta-lactone; *GND2* has a paralog, *GND1*, that arose from the whole genome duplication	2.581	2.99E-23
YBL048W	*RRT1*	Putative protein of unknown function; conserved across *S. cerevisiae* strains; identified in a screen for mutants with increased levels of rDNA transcription	2.580	4.99E-62
YGR146C	*ECL1*	Protein of unknown function; mitochondrial-dependent role in the extension of chronological lifespan; overexpression increases oxygen consumption and respiratory activity while deletion results in reduced oxygen consumption under conditions of caloric restriction; induced by iron homeostasis transcription factor Aft2p; multicopy suppressor of temperature sensitive hsf1 mutant; induced by treatment with 8-methoxypsoralen and UV-A irradiation	2.520	1.45E-48
YIL160C	*POT1*	3-ketoacyl-CoA thiolase with broad chain length specificity; cleaves 3-ketoacyl-CoA into acyl-CoA and acetyl-CoA during beta-oxidation of fatty acids	2.481	1.21E-14
YER091C	*MET6*	Cobalamin-independent methionine synthase; involved in methionine biosynthesis and regeneration; requires a minimum of two glutamates on the methyltetrahydrofolate substrate	2.441	7.58E-108
YGR087C	*PDC6*	Minor isoform of pyruvate decarboxylase; decarboxylates pyruvate to acetaldehyde, involved in amino acid catabolism; transcription is glucose- and ethanol-dependent, and is strongly induced during sulfur limitation	2.425	9.28E-13

YGR032W	*GSC2*	Catalytic subunit of 1,3-beta-glucan synthase; involved in formation of the inner layer of the spore wall; activity positively regulated by Rho1p and negatively by Smk1p; *GSC2* has a paralog, *FKS1*, that arose from the whole genome duplication	2.401	5.20E-93
YDR380W	*ARO10*	Phenylpyruvate decarboxylase; catalyzes decarboxylation of phenylpyruvate to phenylacetaldehyde, which is the first specific step in the Ehrlich pathway; involved in protein N-terminal methionine and alanine catabolism	2.378	7.34E-25
YLL062C	*MHT1*	S-methylmethionine-homocysteine methyltransferase; functions along with Sam4p in the conversion of S-adenosylmethionine (AdoMet) to methionine to control the methionine/AdoMet ratio	2.349	8.35E-23
YLR054C	*OSW2*	Protein of unknown function reputedly involved in spore wall assembly	2.332	1.36E-18
YDR034W-B	*YDR034W-B*	Predicted tail-anchored plasma membrane protein; contains conserved CYSTM module; related proteins in other organisms may be involved in response to stress; N- and C-terminal fusion proteins localize to the cell periphery; *YDR034W-B* has a paralog, *YBR056W-A*, that arose from the whole genome duplication	2.329	1.14E-22
YOL151W	*GRE2*	3-methylbutanal reductase and NADPH-dependent methylglyoxal reductase; stress induced (osmotic, ionic, oxidative, heat shock and heavy metals); regulated by the HOG pathway; restores resistance to glycolaldehyde by coupling reduction of glycolaldehyde to ethylene glycol and oxidation of NADPH to NADP+; protein abundance increases in response to DNA replication stress; methylglyoxal reductase (NADPH-dependent) is also known as D-lactaldehyde dehydrogenase	2.293	1.92E-59
YAL061W	*BDH2*	Putative medium-chain alcohol dehydrogenase with similarity to *BDH1*; transcription induced by constitutively active *PDR1* and *PDR3*	2.275	1.04E-26
YLR205C	*HMX1*	ER localized heme oxygenase; involved in heme degradation during iron starvation and in the oxidative stress response; expression is regulated by *AFT1* and oxidative stress; relocates to the perinuclear region in the presence of oxidants	2.257	9.39E-51
YKR069W	*MET1*	S-adenosyl-L-methionine uroporphyrinogen III transmethylase; involved in the biosynthesis of siroheme, a prosthetic group used by sulfite reductase; required for sulfate assimilation and methionine biosynthesis	2.228	4.92E-47
YKL107W	*YKL107W*	NADH-dependent aldehyde reductase; involved in the detoxification of acetaldehyde, glycolaldehyde, furfural, formaldehyde and propionaldehyde; localizes to the endoplasmic reticulum; member of the classical short-chain dehydrogenase/reductase family	2.209	1.27E-06

YBR085C-A	*YBR085C-A*	Protein of unknown function; GFP-fusion protein localizes to the cytoplasm and to the nucleus; protein abundance increases in response to DNA replication stress	2.203	3.79E-33
YPR167C	*MET16*	3'-phosphoadenylsulfate reductase; reduces 3'-phosphoadenylyl sulfate to adenosine-3',5'-bisphosphate and free sulfite using reduced thioredoxin as co-substrate, involved in sulfate assimilation and methionine metabolism	2.197	4.07E-66
YLL057C	*JLP1*	Fe(II)-dependent sulfonate/alpha-ketoglutarate dioxygenase; involved in sulfonate catabolism for use as a sulfur source; induced by sulphur starvation	2.156	1.91E-08
YDR536W	*STL1*	Glycerol proton symporter of the plasma membrane; subject to glucose-induced inactivation, strongly but transiently induced when cells are subjected to osmotic shock	2.148	1.26E-06
YOL162W	*YOL162W*	Putative protein of unknown function; proposed to be an inactive evolutionary remnant that along with neighboring gene *YOL163W* may have constituted a second sulfonate transporter and *SOA1* paralog that is intact in *S. uvarum*, *S. eubayanus* and *S.arboricola* and named *SOA2*; member of the Dal5p subfamily of the major facilitator family	2.148	1.73E-13
YGR213C	*RTA1*	Protein involved in 7-aminocholesterol resistance; has seven potential membrane-spanning regions; expression is induced under both low-heme and low-oxygen conditions; member of the fungal lipid-translocating exporter family of protein; *RTA1* has a paralog, *YLR046C*, that arose from the whole genome duplication	2.143	3.09E-09
YLR415C	*YLR415C*	Putative protein of unknown function; *YLR415C* is not an essential gene	2.126	6.99E-29
YMR107W	*SPG4*	Protein required for high temperature survival during stationary phase; not required for growth on nonfermentable carbon sources	2.111	9.63E-18
YNR002C	*ATO2*	Putative transmembrane protein involved in export of ammonia; ammonia is a starvation signal that promotes cell death in aging colonies; phosphorylated in mitochondria; member of the TC 9.B.33 YaaH family; homolog of *Y. lipolytica* Gpr1p; *ATO2* has a paralog, *ADY2*, that arose from the whole genome duplication	2.109	1.48E-14
YDR502C	*SAM2*	S-adenosylmethionine synthetase; catalyzes transfer of the adenosyl group of ATP to the sulfur atom of methionine; comparative analysis suggests that a mitochondrially targeted form may result from translation starting at a non-canonical codon upstream of the annotated start codon	2.099	7.53E-50

YER011W	*TIR1*	Cell wall mannoprotein; expression is downregulated at acidic pH and induced by cold shock and anaerobiosis; abundance is increased in cells cultured without shaking; member of the Srp1p/Tip1p family of serine-alanine-rich proteins	2.091	1.80E-09
YMR169C	*ADL3*	Cytoplasmic aldehyde dehydrogenase; involved in beta-alanine synthesis; uses NAD+ as the preferred coenzyme; very similar to Ald2p; expression is induced by stress and repressed by glucose	2.088	1.18E-42

Table S3.2.iii. List of proteins that changed their localization after treatment with CYM, when compared with nontreated cells. For each protein, ORF name, gene name, SGD description and localization in nontreated cells (control) and after treatment with 25 μg mL^{-1} of CYM, is indicated.

ORF name	Gene name	Protein name	SGD Description	Localization	
				Control	CYM
YBR171W	*SEC66*	Sec66p	Non-essential subunit of Sec63 complex; with Sec61 complex, Kar2p/BiP and Lhs1p forms a channel competent for SRP-dependent and post-translational SRP-independent protein targeting and translocation into the ER; other members are Sec63p, Sec62p, and Sec72p	ER[1]	ER+C[2]
YDL052C	*SLC1*	Slc1p	1-acyl-sn-glycerol-3-phosphate acyltransferase; catalyzes the acylation of lysophosphatidic acid to form phosphatidic acid, a key intermediate in lipid metabolism; enzymatic activity detected in lipid particles and microsomes	ER	ER+C
YDL091C	*UBX3*	Ubx3p	Clathrin-coated vesicle component, regulator of endocytosis; copurifies with the DSC ubiquitin ligase complex; UBX (ubiquitin regulatory X) domain-containing protein that interacts with Cdc48p; required for efficient clathrin-mediated endocytosis; ortholog of fission yeast Ucp10	ER	C
YAL010C	*MDM10*	Mdm10p	Moonlighting protein component of both the ERMES and SAM complex; subunit of the ERMES complex that acts as a molecular tether between the mitochondria and the ER, necessary for both efficient phospholipid exchange between organelles and for mitophagy; SAM/TOB complex subunit that functions in the assembly of outer membrane beta-barrel proteins; involved in mitochondrial inheritance and morphology; ERMES complex often co-localizes with peroxisomes adjacent to mitochondria-ER junctions	M[3]	C

YAR033W	*MST28*	Mst28p	Putative integral membrane protein, involved in vesicle formation; forms complex with Mst27p; member of *DUP240* gene family; binds COPI and COPII vesicles; *MST28* has a paralog, *MST27*, that arose from a segmental duplication	ER	ER+C
YBL011W	*SCT1*	Sct1p	Glycerol 3-phosphate/dihydroxyacetone phosphate sn-1 acyltransferase; dual substrate-specific acyltransferase of the glycerolipid biosynthesis pathway; prefers 16-carbon fatty acids; similar to Gpt2p	ER	ER+C
YBL020W	*RFT1*	Rft1p	Membrane protein required for translocation of Man5GlcNac2-PP-Dol; required for translocation of Man5GlcNac2-PP-Dol from the cytoplasmic side to the lumenal side of the ER membrane but is not the flippase; mutation is suppressed by expression of human p53 protein	ER	C
YBR265W	*TSC10*	Tsc10p	3-ketosphinganine reductase; catalyzes the second step in phytosphingosine synthesis; essential for growth in the absence of exogenous dihydrosphingosine or phytosphingosine; localized to lipid droplets; member of short chain dehydrogenase/reductase protein family	ER	C
YBR273C	*UBX7*	Ubx7p	UBX (ubiquitin regulatory X) domain-containing protein; interacts with Cdc48p; *UBX7* has a paralog, *UBX6*, that arose from the whole genome duplication	ER	ER+C
YBL047C	*EDE1*	Ede1p	Endocytic adaptor; K63-specific Ub-chain binding protein involved in receptor endocytosis; scaffold protein that localizes to nascent endocytic sites after homo-oligomerization and organizes the endocytic machinery; role in autophagy of aberrant clathrin-mediated endocytosis protein condensates; binds membranes in a Ub-dependent manner; interacts with and functions upstream of Cmk2p to suppress stress-induced non-apoptotic cell death; putative cytokinesis regulator	CP[4]+B[5]	CP+B+V[6]
YDR292C	*SRP101*	Srp101p	Signal recognition particle (SRP) receptor alpha subunit; contain GTPase domains; involved in SRP-dependent protein targeting; interacts with the beta subunit, Srp102p	ER	C
YDL161W	*ENT1*	Ent1p	Epsin-like protein involved in endocytosis and actin patch assembly; K63-specific Ub chain binding protein that functions as an endocytic adaptor; binds clathrin via a clathrin-binding domain motif at C-terminus; contains two ubiquitin-interacting motifs; functionally redundant with Ent2p; relocalizes from bud neck to cytoplasm upon DNA replication stress; *ENT1* has a paralog, *ENT2*, that arose from the whole genome duplication	B	C
YDR307W	*PMT7*	Pmt7p	Putative protein mannosyltransferase similar to Pmt1p; has a potential role in protein O-glycosylation	ER	ER
YBR296C	*PHO89*	Pho89p	Plasma membrane Na+/Pi cotransporter; active in early growth phase; similar to phosphate transporters of *Neurospora crassa*; transcription regulated by inorganic phosphate concentrations and Pho4p	ER	C

YBR298C	*MAL31*	Mal31p	Maltose permease; high-affinity maltose transporter (alpha-glucoside transporter); encoded in the *MAL3* complex locus; member of the 12 transmembrane domain superfamily of sugar transporters; functional in genomic reference strain S288C	V	V+CP
YDL204W	*RTN2*	Rtn2p	Reticulon protein; involved in nuclear pore assembly and maintenance of tubular ER morphology; promotes membrane curvature; regulates the ER asymmetry-induced inheritance block during ER stress; role in ER-derived peroxisomal biogenesis; interacts with Sec6p, Yip3p, and Sbh1p; less abundant than *RTN1*; member of RTNLA (reticulon-like A) subfamily; protein increases in abundance and relocalizes to plasma membrane upon DNA replication stress	CP	C
YDR343C	*HXT6*	Hxt6p	High-affinity glucose transporter; member of the major facilitator superfamily, nearly identical to Hxt7p, expressed at high basal levels relative to other HXTs, repression of expression by high glucose requires *SNF3*; *HXT6* has a paralog, *HXT1*, that arose from the whole genome duplication	CP	CP+C
YDR345C	*HXT3*	Hxt3p	Low affinity glucose transporter of the major facilitator superfamily; expression is induced in low or high glucose conditions; *HXT3* has a paralog, *HXT5*, that arose from the whole genome duplication	CP	CP+V
YBL105C	*PKC1*	Pkc1p	Protein serine/threonine kinase; essential for cell wall remodeling during growth; localized to sites of polarized growth and the mother-daughter bud neck	B	C
YBR002C	*RER2*	Rer2p	Forms the dehydrodolichyl diphosphate synthase complex with *NUS1*; major enzyme of polyprenol synthesis in both the ER and in lipid droplets; participates in ER protein sorting	ER	C
YBR004C	*GPI18*	Gpi18p	Functional ortholog of human PIG-V; PIG-V is a mannosyltransferase that transfers the second mannose in glycosylphosphatidylinositol biosynthesis; the authentic, non-tagged protein was localized to mitochondria	ER	ER+C
YCL025C	*AGP1*	Agp1p	Broad-specificity, low-affinity amino acid permease; minor serine permease with major contributions from paralog Gnp1p; involved in uptake of asparagine, glutamine, and other amino acids; expression induced by amino acids and regulated by SPS plasma membrane amino acid sensor system (Ssy1p-Ptr3p-Ssy5p)	ER	ER+C
YBR036C	*CSG2*	Csg2p	Calcium release channel involved in ER calcium homeostasis; integrates ER calcium release with the regulation of sphingolipid metabolism and autophagy; required for mannosylation of inositolphosphorylceramide and for growth at high calcium concentrations; ER membrane protein; contains 10 transmembrane domains and a potential Ca2+ EF-hand motif; protein abundance increases in response to DNA replication stress	ER	ER+C

YDL248W	*COS7*	Cos7p	Endosomal protein involved in turnover of plasma membrane proteins; member of the DUP380 subfamily of conserved, often subtelomeric *COS* genes; required for the multivesicular vesicle body sorting pathway that internalizes plasma membrane proteins for degradation; Cos proteins provide ubiquitin in trans for non-ubiquitinated cargo proteins; the authentic, non-tagged protein is detected in highly purified mitochondria in high-throughput studies	V	V+C
YDR011W	*SNQ2*	Snq2p	Plasma membrane ATP-binding cassette (ABC) transporter; multidrug transporter involved in multidrug resistance and resistance to singlet oxygen species	CP	CP+C
YDR018C	*MLG1*	Mlg1p	Lysolipid acyltransferase; involved in the synthesis of phosphatidic acid from 1-acyl-2-hydroxy-sn-glycero-3-phosphate using oleoyl-CoA as acyl donor and in phospholipid remodeling, incorporating palmitic acid into the sn-1 position of phosphatidylserine and phosphatidylethanolamine; localizes to ER membranes associated with mitochondria; contains three predicted transmembrane domains; similar to *C. elegans* F55A11.5 and maize 1-acyl-glycerol-3-phosphate acyltransferase	ER	C
YDR410C	*STE14*	Ste14p	Farnesyl cysteine-carboxyl methyltransferase; mediates the carboxyl methylation step during C-terminal CAAX motif processing of a-factor and RAS proteins in the ER, localizes to the ER membrane	ER	ER+C
YDR411C	*DFM1*	Dfm1p	ER localized protein; involved in ER-associated protein degradation (ERAD), ER stress, and homeostasis; acts as disaggregase that removes misfolded membrane protein aggregates; interacts with components of ERAD-L and ERAD-C and Cdc48p; derlin-like family member similar to Der1p	ER	ER+C
YBR042C	*CST26*	Cts26p	Acyltransferase; enzyme mainly responsible for the introduction of saturated very long chain fatty acids into neo-synthesized molecules of phosphatidylinositol; required for incorporation of stearic acid into phosphatidylinositol; affects chromosome stability when overexpressed; *CST26* has a paralog, *YDR018C*, that arose from the whole genome duplication	ER	ER+C
YBR054W	*YRO2*	Yro2p	Protein with a putative role in response to acid stress; null mutant is sensitive to acetic acid; transcription is regulated by Haa1p and induced in the presence of acetic acid; protein observed in plasma membrane foci in the presence of acetic acid; the authentic, non-tagged protein is detected in a phosphorylated state in highly purified mitochondria in high-throughput studies	ER	ER+C
YBR058C-A	*TSC3*	Tsc3p	Protein that stimulates the activity of serine palmitoyltransferase; involved in sphingolipid biosynthesis; Lcb1p and Lcb2p are the two components of serine palmitoyltransferase	ER	ER+C
YBR069C	*TAT1*	Tat1p	Amino acid transporter for valine, leucine, isoleucine, and tyrosine; low-affinity tryptophan and histidine transporter; overexpression confers FK506 and FTY720 resistance; protein abundance increases in response to DNA replication stress	ER	ER+C

YDR424C	*DYN2*	Dyn2p	Cytoplasmic light chain dynein, microtubule motor protein; required for intracellular transport and cell division; involved in mitotic spindle positioning; forms complex with dynein intermediate chain Pac11p that promotes Dyn1p homodimerization, potentiates motor processivity; Dyn2p-Pac11p complex important for interaction of dynein motor complex with dynactin complex; acts as molecular glue to dimerize, stabilize Nup82-Nsp1-Nup159 complex module of cytoplasmic pore filaments	ER+P[7]	ER+P+C
YBR179C	*FZO1*	Fzo1p	Mitofusin, protein involved in mitochondrial outer membrane fusion; role in mitochondrial genome maintenance; efficient tethering and degradation of Fzo1p requires an intact N-terminal GTPase domain; targeted for destruction by the ubiquitin ligase SCF-Mdm30p and the cytosolic ubiquitin-proteasome system; activity regulated by ubiquitylation at conserved lysine residues and by deubiquitylases Ubp2p and Ubp12p	M	M+C
YDR456W	*NHX1*	Nhx1p	Na+/H+ and K+/H+ exchanger; required for intracellular sequestration of Na+ and K+; located in the vacuole and late endosome compartments; required for osmotolerance to acute hypertonic shock and for vacuolar fusion	ER	ER+C
YDR459C	*PFA5*	Pfa5p	Palmitoyltransferase with autoacylation activity; likely functions in pathway(s) outside Ras; member of a family of putative palmitoyltransferases containing an Asp-His-His-Cys-cysteine rich domain	CP	CP+C
YGR049W	*SCM4*	Scm4p	Mitochondrial outer membrane protein of unknown function; predicted to have 4 transmembrane segments; import is mediated by Tom70p and Mim1p; interacts genetically with a cdc4 mutation; *SCM4* has a paralog, *ATG33*, that arose from the whole genome duplication	M	M+C
YCR037C	*PHO87*	Pho87p	Low-affinity inorganic phosphate transporter; acts upstream of Pho81p in regulation of PHO pathway; targeted to vacuole via AP-3 pathway; expression is independent of inorganic phosphate concentration and Pho4p activity; contains 12 membrane-spanning segments; *PHO87* has a paralog, *PHO90*, that arose from the whole genome duplication	CP	C
YBR102C	*EXO84*	Exo84p	Exocyst subunit with dual roles in exocytosis and spliceosome assembly; subunit of the the exocyst complex which mediates polarized targeting and tethering of post-Golgi secretory vesicles to active sites of exocytosis at the plasma membrane prior to SNARE-mediated fusion; required for exocyst assembly and targeting of the complex to specific sites on the bud tip plasma membrane; associates the U1 snRNP; role in pre-mRNA splicing and prespliceosome formation; possible *Cdc28* substrate	NP[8]	C

YDR093W	*DNF2*	Dnf2p	Aminophospholipid translocase (flippase); type 4 P-type ATPase; involved in phospholipid translocation, contributing to endocytosis, protein transport, and cellular polarization; localizes primarily to the plasma membrane; localizes to the shmoo tip where it has a redundant role in the cellular response to mating pheromone; *DNF2* has a paralog, *DNF1*, that arose from the whole genome duplication	B	C
YDL012C	*YDL012C*	YDL012Cp	Tail-anchored plasma membrane protein with a conserved CYSTM module; possibly involved in response to stress; may contribute to non-homologous end-joining based on ydl012c htz1 double null phenotype; *YDL012C* has a paralog, *YBR016W*, that arose from the whole genome duplication	B	V
YBR132C	*AGP2*	Agp2p	Plasma membrane regulator of high affinity polyamine and carnitine transport; has similarity to transporters but lacks transport activity; may act as a sensor that transduces environmental signals; has a positive or negative regulatory effect on transcription of many transporter genes; localizes to the plasma membrane, the vacuolar membrane and the ER membrane	ER	C
YDR513W	*GRX2*	Grx2p	Cytoplasmic glutaredoxin; thioltransferase, glutathione-dependent disulfide oxidoreductase involved in maintaining redox state of target proteins, also exhibits glutathione peroxidase activity, expression induced in response to stress; *GRX2* has two in-frame start codons resulting in a shorter isoform that is retained in the cytosol and a longer form translocated to the mitochondrial matrix; *GRX2* has a paralog, *GRX1*, that arose from the whole genome duplication	N	C
YGL041C-B	*YGL041C-B*	YGL041C-Bp	Putative protein of unknown function; identified by fungal homology and qRT-PCR; SWAT-GFP and mCherry fusion proteins localize to the ER	ER	C
YEL025C	*YEL025C*	YEL025Cp	Putative protein of unknown function; GFP-fusion protein localizes to both the cytoplasm and the nucleus	N[9]	N+C
YGL051W	*MST27*	Mst27p	Putative integral membrane protein, involved in vesicle formation; forms complex with Mst28p; member of *DUP240* gene family; binds COPI and COPII vesicles; *MST27* has a paralog, *MST28*, that arose from a segmental duplication	ER	ER+C
YEL063C	*CAN1*	Can1p	Plasma membrane arginine permease; requires phosphatidyl ethanolamine for localization, exclusively associated with lipid rafts; mutation confers canavanine resistance; *CAN1* has a paralog, *ALP1*, that arose from the whole genome duplication	ER	C
YGR147C	*NAT2*	Nat2p	Protein of unknown function; has an apparent role in acetylation of N-terminal methionine residues	M	M+C

YGR149W	*GPC1*	Gpc1p	Glycerophosphocholine acyltransferase; involved in in phosphatidylcholine synthesis; uses acyl-CoA to acylate glycero-3-phosphocholine to yield lyso-hosphatidylcholine; also catalyzes acylation of glycerophosphoethanolamine with acyl-CoA; predicted to be an integral membrane protein	CP	C
YGR152C	*RSR1*	Rsr1p	Ras-type GTPase; required for bud site selection during both axial and bipolar budding, for morphological changes in response to mating pheromone, and for efficient cell fusion; recruits Cdc24p to the incipient bud site, activating its guanyl-nucleotide exchange factor activity and the Rho-like GTPase, Cdc42p; localizes to the plasma membrane, the incipient bud site, polarized growth sites, the cell division site and the vacuole membrane	CP	CP+C
YHR175W	*CTR2*	Ctr2p	Low-affinity copper transporter of the vacuolar membrane; mutation confers resistance to toxic copper concentrations, while overexpression confers resistance to copper starvation; regulated by nonsense-mediated mRNA decay pathway	ER	C
YHR192W	*LNP1*	Lnp1p	Lunapark family member involved in ER network formation; regulates the ER asymmetry-induced inheritance block during ER stress; localizes to ER junctions and this localization is regulated by the yeast atlastin ortholog Sey1p; required for reticulophagy where it is proposed to stabilize the actin-dependent remodeling of the ER; interacts with the reticulon protein Rtn1p; induced in response to the DNA-damaging agent MMS	ER	ER+C
YGL082W	*YGL082W*	YGL082Wp	Putative protein of unknown function; MINDY family deubiquitinase that does not appear to contain catalytic activity; predicted prenylation/proteolysis target of Afc1p and Rce1p; GFP-fusion protein localizes to the cytoplasm and nucleus; Y*GL082W* has a paralog, *YPL191C*, that arose from the whole genome duplication	CP	CP+C
YER014W	*HEM14*	Hem14p	Protoporphyrinogen oxidase; a mitochondrial enzyme that catalyzes the seventh step in the heme biosynthetic pathway, converting protoporphyrinogen IX to protoporphyrin IX; inhibited by diphenyl ether-type herbicides	M	M+C
YGL104C	*VPS73*	Vps73p	Mitochondrial protein; mutation affects vacuolar protein sorting; putative transporter; member of the sugar porter family; *VPS73* has a paralog, *YBR241C*, that arose from the whole genome duplication	VM[10]+P	VM+P+C
YIL023C	*YKE4*	Yek4p	Zinc transporter; localizes to the ER; null mutant is sensitive to calcofluor white, leads to zinc accumulation in cytosol	ER	ER+C
YGR213C	*RTA1*	Rta1p	Protein involved in 7-aminocholesterol resistance; has seven potential membrane-spanning regions; expression is induced under both low-heme and low-oxygen conditions; member of the fungal lipid-translocating exporter family of protein; *RTA1* has a paralog, *YLR046C*, that arose from the whole genome duplication	ER	ER+C

YIL039W	*TED1*	Ted1p	GPI-glycan remodelase; conserved phosphoesterase domain-containing protein; acts together with Emp24p/Erv25p in cargo exit from the ER; deletion confers sensitivity to 4-(N-(S-glutathionylacetyl)amino) phenylarsenoxide	ER	ER+C
YER044C	*ERG28*	Erg28p	Endoplasmic reticulum membrane protein; may facilitate protein-protein interactions between the Erg26p dehydrogenase and the Erg27p 3-ketoreductase and/or tether these enzymes to the ER, also interacts with Erg6p	ER	ER+C
YER056C	*FCY2*	Fcy2p	Purine-cytosine permease; mediates purine (adenine, guanine, and hypoxanthine) and cytosine accumulation; relative distribution to the vacuole increases upon DNA replication stress	CP	CP+V
YER060W	*FCY21*	Fcy21p	Putative purine-cytosine permease; very similar to Fcy2p but cannot substitute for its function	CP	CP+V
YOR165W	*SEY1*	Sey1p	Dynamin-like GTPase that mediates homotypic ER fusion; has a role in ER morphology; interacts physically and genetically with Yop1p and Rtn1p	CP	P
YGR241C	*YAP1802*	YAP1802p	Protein of the AP180 family, involved in clathrin cage assembly; binds Pan1p and clathrin; *YAP1802* has a paralog, *YAP1801*, that arose from the whole genome duplication	B	C
YGR260W	*TNA1*	Tna1p	High affinity nicotinic acid plasma membrane permease; responsible for uptake of low levels of nicotinic acid; expression of the gene increases in the absence of extracellular nicotinic acid or para-aminobenzoate	CP+V	V
YGR263C	*SAY1*	Say1p	Sterol deacetylase; component of the sterol acetylation/deacetylation cycle along with Atf2p; active both in the ER and in lipid droplets; integral membrane protein with active site in the ER lumen; GFP-fusion protein localizes to the ER	CP+P	P
YGL194C-A	*YGL194C-A*	YGL194C-Ap	Putative protein of unknown function; identified based on comparisons of the genome sequences of six *Saccharomyces* species; SWAT-GFP and mCherry fusion proteins localize to the ER	ER	ER+C
YGR281W	*YOR1*	Yor1p	Plasma membrane ATP-binding cassette transporter; multidrug transporter mediates export of many different organic anions including oligomycin	CP	CP+C
YIL105C	*SLM1*	Slm1p	Phosphoinositide PI4,5P(2) binding protein, forms a complex with Slm2p; acts downstream of Mss4p in a pathway regulating actin cytoskeleton organization in response to stress; TORC2 complex substrate and effector; protein abundance increases in response to DNA replication stress; *SLM1* has a paralog, *SLM2*, that arose from the whole genome duplication	PCP[11]	PCP+C

YHL016C	*DUR3*	Dur3p	Plasma membrane transporter for both urea and polyamines; expression is highly sensitive to nitrogen catabolite repression and induced by allophanate, the last intermediate of the allantoin degradative pathway	ER	ER+C
YIL147C	*SLN1*	Sln1p	Transmembrane histidine phosphotransfer kinase and osmosensor; regulates MAP kinase cascade; transmembrane protein with an intracellular kinase domain that signals to Ypd1p and Ssk1p, thereby forming a phosphorelay system similar to bacterial two-component regulators	CP	C
YFL011W	*HXT10*	Hxt10p	Hexose transporter; expressed at low levels and expression is repressed by glucose	V	V+CP
YGR004W	*PEX31*	Pex31p	Peroxisomal integral membrane protein; involved in negative regulation of peroxisome size; partially functionally redundant with Pex30p and Pex32p; probably acts at a step downstream of steps mediated by Pex28p and Pex29p; *PEX31* has a paralog, *PEX30*, that arose from the whole genome duplication	CP	C
YFL042C	*LAM5*	Lam5p	Putative sterol transfer protein; one of six StART-like domain-containing proteins in yeast that may be involved in sterol transfer between intracellular membranes; conserved across eukaryotes; has both GRAM and StART-like (VASt) domains; localizes to membrane contact sites throughout the cell, including nucleus-vacuole junctions and ER-mitochondrial contact sites	ER+P	P+C
YFL054C	*AQY3*	Aqy3p	Putative channel-like protein; similar to Fps1p; mediates passive diffusion of glycerol in the presence of ethanol	CP	CP+C
YGR065C	*VHT1*	Vht1p	High-affinity plasma membrane H+-biotin (vitamin H) symporter; mutation results in fatty acid auxotrophy; 12 transmembrane domain containing major facilitator subfamily member; mRNA levels negatively regulated by iron deprivation and biotin	CP	C
YHR092C	*HXT4*	Hxt4p	High-affinity glucose transporter; member of the major facilitator superfamily, expression is induced by low levels of glucose and repressed by high levels of glucose; HXT4 has a paralog, *HXT7*, that arose from the whole genome duplication	CP	CP+V
YGR131W	*FHN1*	Fhn1p	Protein of unknown function; induced by ketoconazole; promoter region contains sterol regulatory element motif, which has been identified as a Upc2p-binding site; overexpression complements function of Nce102p in NCE102 deletion strain; FHN1 has a paralog, *NCE102*, that arose from the whole genome duplication	CP	CP+C

YGR138C	*TPO2*	Tpo2p	Polyamine transporter of the major facilitator superfamily; member of the 12-spanner drug:H(+) antiporter DHA1 family; specific for spermine; localizes to the plasma membrane; transcription of TPO2 is regulated by Haa1p; *TPO2* has a paralog, *TPO3*, that arose from the whole genome duplication	CP+V	C
YGL012W	*ERG4*	Erg4p	C-24(28) sterol reductase; catalyzes the final step in ergosterol biosynthesis; mutants are viable, but lack ergosterol	ER	C
YJL112W	*MDV1*	Mdv1p	Peripheral protein of cytosolic face of mitochondrial outer membrane; required for mitochondrial fission; interacts with Fis1p and with the self-assembled oligomeric form of the dynamin-related GTPase Dnm1p; *MDV1* has a paralog, *CAF4*, that arose from the whole genome duplication	M	P
YKL187C	*FAT3*	Fat3p	Protein required for fatty acid uptake; protein abundance increases in cortical patches in response to oleate exposure; the authentic, non-tagged protein is detected in a phosphorylated state in highly purified mitochondria in high-throughput studies; *FAT3* has a paralog, *YLR413W*, that arose from the whole genome duplication	CP	CP+V
YLR114C	*AVL9*	Avl9p	Conserved protein involved in exocytic transport from the Golgi; mutation is synthetically lethal with apl2 vps1 double mutation; member of a protein superfamily with orthologs in diverse organisms; relocalizes from bud neck to cytoplasm upon DNA replication stress	B	B+C
YJL196C	*ELO1*	Elo1p	Elongase I, medium-chain acyl elongase; catalyzes carboxy-terminal elongation of unsaturated C12-C16 fatty acyl-CoAs to C16-C18 fatty acids; *ELO1* has a paralog, *ELO2*, that arose from the whole genome duplication	ER	ER+C
YJL212C	*OPT1*	Opt1p	Proton-coupled oligopeptide transporter of the plasma membrane; also transports glutathione and phytochelatin; member of the OPT family	CP	CP+C
YJL214W	*HXT8*	Hxt8p	Protein of unknown function with similarity to hexose transporters; expression is induced by low levels of glucose and repressed by high levels of glucose	CP	CP+V
YML116W	*ATR1*	Atr1p	Multidrug efflux pump of the major facilitator superfamily; required for resistance to aminotriazole and 4-nitroquinoline-N-oxide; *ATR1* has a paralog, *YMR279C*, that arose from the whole genome duplication; protein abundance increases in response to DNA replication stress	CP	CP+C
YJL219W	*HXT9*	Hxt9p	Putative hexose transporter that is nearly identical to Hxt11p; has similarity to major facilitator superfamily (MFS) transporters, expression of *HXT9* is regulated by transcription factors Pdr1p and Pdr3p	CP	CP+V

YOL026C	*MIM1*	Mim1p	Mitochondrial protein required for outer membrane protein import; cooperates with Tom70p to import the subset of proteins with multiple alpha-helical transmembrane segments, including Ugo1p, Tom20p, and others; forms a complex with Mim2p in the outer membrane that functions as cation-selective channel for translocation of positively charged precursor segments; also has a role in assembly of Tom20p into the TOM complex	M	M+C
YKR009C	*FOX2*	Fox2p	3-hydroxyacyl-CoA dehydrogenase and enoyl-CoA hydratase; multifunctional enzyme of the peroxisomal fatty acid beta-oxidation pathway	P	P+C
YKR014C	*YPT52*	Ypt52p	Endosomal Rab family GTPase; required for vacuolar protein sorting, endocytosis and multivesicular body biogenesis and sorting; required for localization of the CORVET complex to endosomes; involved in autophagy and ionic stress tolerance; similar to Vps21p and Ypt53p; mammalian Rab5 homolog; protein abundance increases in response to DNA replication stress	VM+P	VM+P+C
YKR036C	*CAF4*	Caf4p	WD40 repeat-containing protein associated with the CCR4-NOT complex; interacts in a Ccr4p-dependent manner with Ssn2p; also interacts with Fis1p, Mdv1p and Dnm1p and plays a role in mitochondrial fission; *CAF4* has a paralog, *MDV1*, that arose from the whole genome duplication	M	M+C
YMR022W	*UBC7*	Ucb7p	Ubiquitin conjugating enzyme; involved in the ER-associated protein degradation (ERAD) pathway and in the inner nuclear membrane-associated degradation (INMAD) pathway; requires Cue1p for recruitment to the ER membrane; proposed to be involved in chromatin assembly	ER	ER+C
YLR099W-A	*MIM2*	Mim2p	Mitochondrial protein required for outer membrane protein import; involved in import of the subset of proteins with multiple alpha-helical transmembrane segments, including Ugo1p, Tom20p, and Fzo1p; component of a large protein complex in the outer membrane that includes Mim1p and functions as cation-selective channel for translocation of positively charged precursor segments	M	M+C
YMR031C	*EIS1*	Eis1p	Component of the eisosome required for proper eisosome assembly; similar to Uso1p; authentic, non-tagged protein is detected in a phosphorylated state in highly purified mitochondria in high-throughput studies; protein increases in abundance and relocalizes from plasma membrane to cytoplasm upon DNA replication stress; *EIS1* has a paralog, *YKL050C*, that arose from the whole genome duplication	PCP	P
YLR292C	*SEC72*	Sec72p	Non-essential subunit of Sec63 complex; with Sec61 complex, Kar2p/BiP and Lhs1p forms a channel competent for SRP-dependent and post-translational SRP-independent protein targeting and translocation into the ER; other members are Sec63p, Sec62p, and Sec66p	ER	ER+C

YLR342W	*FKS1*	Fks1p	Catalytic subunit of 1,3-beta-D-glucan synthase; transfers glucose from UDP-glucose to growing chains of glucan via β-1,3-glycosidic linkages, translocating polymerized β-1,3-glucan to the extracellular space; role in cell wall synthesis and maintenance; functionally redundant with alternate catalytic subunit Gsc2p; activity regulated by Rho1p, a subunit of the synthase complex; localizes to sites of cell wall remodeling; contains a cellulose-synthase-like fold; antifungal drug target	B+V	V
YMR086W	*SEG1*	Seg1p	Component of eisosome required for proper eisosome assembly; precedes Pil1p/Lsp1p during eisosome formation, controls eisosome length and shape; diffusely distributed, forms heterogeneous patches at plasma membrane in small buds, also found in medium and large buds; expression repressed by cAMP; *SEG1* has a paralog, *SEG2*, that arose from the whole genome duplication	PCP	PCP+P (Cytosol)
YLR356W	*ATG33*	Atg33p	Mitochondrial mitophagy-specific protein; required primarily for mitophagy induced at post-log phase; not required for other types of selective autophagy or macroautophagy; conserved within fungi, but not in higher eukaryotes; *ATG33* has a paralog, *SCM4*, that arose from the whole genome duplication	M	M+C
YLL028W	*TPO1*	Tpo1p	Polyamine transporter of the major facilitator superfamily; member of the 12-spanner drug:H(+) antiporter DHA1 family; recognizes spermine, putrescine, and spermidine; catalyzes uptake of polyamines at alkaline pH and excretion at acidic pH; during oxidative stress exports spermine, spermidine from the cell, which controls timing of expression of stress-responsive genes; phosphorylation enhances activity and sorting to the plasma membrane	CP	C
YLR378C	*SEC61*	Sec61p	Conserved ER protein translocation channel; essential subunit of Sec61 complex (Sec61p, Sbh1p, and Sss1p); forms channel for SRP-dependent protein import; with Sec63 complex is required for SRP-independent protein translocation into the ER; involved in posttranslational soluble protein import into the ER, ERAD of soluble substrates, and misfolded soluble protein export from the ER	ER	ER+C
YKL105C	*SEG2*	Seg2p	Eisosome component; likely plays only a minor role in eisosome assembly; shown to interact with Seg1p by affinity purification and mass spec; SWAT-GFP and mCherry fusion proteins localize to the cell periphery; similar to *A. gossypii SEG* gene which is important for stabilizing eisosomes; *SEG2* has a paralog, *SEG1*, that arose from the whole genome duplication	PCP	P (Cytosol)
YNL323W	*LEM3*	Lem3p	Membrane protein of the plasma membrane and ER; interacts specifically *in vivo* with the phospholipid translocase Dnf1p; involved in translocation of phospholipids and alkylphosphocholine drugs across the plasma membrane	B	ER
YIL114C	*POR2*	Por2p	Putative mitochondrial porin (voltage-dependent anion channel); not required for mitochondrial membrane permeability or mitochondrial osmotic stability; *POR2* has a paralog, POR1, that arose from the whole genome duplication	M	M+C

YPL112C	*PEX25*	Pex25p	Peripheral peroxisomal membrane peroxin; required for the regulation of peroxisome size and maintenance, recruits GTPase Rho1p to peroxisomes, induced by oleate, interacts with Pex27p; *PEX25* has a paralog, *PEX27*, that arose from the whole genome duplication	P	P+C
YOR171C	*LCB4*	Lcb4p	Sphingoid long-chain base kinase; responsible for synthesis of long-chain base phosphates, which function as signaling molecules, regulates synthesis of ceramide from exogenous long-chain bases, localizes to the Golgi and late endosomes; *LCB4* has a paralog, *LCB5*, that arose from the whole genome duplication	B	CP
YOR192C	*THI72*	Thi72p	Transporter of thiamine or related compound; contributes to uptake of 5-aminoimidazole-4-carboxamide-1-beta-D-ribofuranoside (acadesine); shares sequence similarity with Thi7p	CP	CP+V
YPR028W	*YOP1*	Yop1p	Reticulon-interacting protein; ER integral membrane protein involved in the generation of tubular ER morphology; promotes membrane curvature; regulates the ER asymmetry-induced inheritance block during ER stress; role in ER-derived peroxisomal biogenesis; interacts with Yip1p to mediate membrane traffic and with Sey1p to maintain ER morphology; facilitates lipid exchange between the ER and mitochondria	B	B+CP
YOL156W	*HXT11*	Hxt11p	Hexose transporter; capable of transporting a broad range of substrates including: glucose, fructose, mannose and galactose; polyol transporter that supports the growth on and uptake of xylitol with low affinity when overexpressed in a strain deleted for hexose family members; nearly identical in sequence to Hxt9p; has similarity to major facilitator superfamily transporters; involved in pleiotropic drug resistance	CP	CP+V
YPL004C	*LSP1*	Lsp1p	Eisosome core component; eisosomes are large immobile patch structures at the cell cortex associated with endocytosis; phosphorylated on Thr233 upon Pkc1p hyperactivation in a Slt2p MAPK-dependent fashion; null mutants show activation of Pkc1p/Ypk1p stress resistance pathways; member of the BAR domain family	P	P+C
YPR149W	*NCE102*	Nce102p	Protein involved in regulation of pheromone response and mating; contains transmembrane domains; involved in secretion of proteins that lack classical secretory signal sequences; component of the detergent-insoluble glycolipid-enriched complexes (DIGs); *NCE102* has a paralog, *FHN1*, that arose from the whole genome duplication	P+B	CP
YPR165W	*RHO1*	Rho1p	GTP-binding protein of the rho subfamily of Ras-like small GTPases; involved in establishment of cell polarity; regulates protein kinase C1; positive regulatory subunit of the 1,3-beta-D-glucan synthase complex, activating 1,3-beta-glucan synthase (Fks1p and Gsc2p), an enzyme involved in cell wall biosynthesis	B	CP

YPR183W	*DPM1*	Dpm1p	Dolichol phosphate mannose synthase of ER membrane; catalyzes formation of Dol-P-Man from Dol-P and GDP-Man; required for biosynthesis of glycosyl phosphatidylinositol membrane anchor, as well as O-mannosylation and protein N- and O-linked glycosylation	B	B+CP
YNL173C	*MDG1*	Mdg1p	Plasma membrane protein; involved in G-protein mediated pheromone signaling pathway; overproduction suppresses bem1 mutations; *MDG1* has a paralog, *CRP1*, that arose from the whole genome duplication	PCP	CP
YHR002W	*LEU5*	Leu5p	Mitochondrial carrier protein; involved in the accumulation of CoA in the mitochondrial matrix; homolog of human Graves disease protein SLC25A16, which complements yeast null mutant	M	C
YHR146W	*CRP1*	Crp1p	Protein that binds to cruciform DNA structures; *CRP1* has a paralog, *MDG1*, that arose from the whole genome duplication	P+CP	CP
YPL042C	*SSN3*	Ssn3p	Component of the RNA polymerase II mediator complex; cyclin-dependent protein kinase involved in phosphorylation of the mediator component Pgd1p and suppression of transcription activation by RNA polymerase II; involved in glucose repression	N	N+C
YDR219C	*MFB1*	Mfb1p	Mitochondria-associated F-box protein; tether that anchors higher-functioning mitochondria at the mother cell distal tip throughout the cell cycle and at the bud tip prior to cytokinesis; role in maintenance of normal mitochondrial morphology and quality control; interacts with Skp1p through the F-box motif; asymmetrically localized to the mother cell through the cell cycle with some bud tip localization just before cytokinesis; function regulated by the bud site selection machinery	M	M+C
YHR182W	*RGD3*	Rgd3p	GTPase activating protein for Rho3p, involved in cell polarity GFP-fusion protein localizes to the cell periphery and cytoplasm; relocalizes from bud neck to cytoplasm upon DNA replication stress	B	C
YNL042W	*BOP3*	Bop3p	Protein of unknown function; potential Cdc28p substrate; overproduction confers resistance to methylmercury	N	N+C
YML108W	*YML108W*	YML108Wp	Protein of unknown function; structure defines a new subfamily of the split beta-alpha-beta sandwiches; GFP-fusion protein localizes to the cytoplasm and nucleus; relative distribution to the nucleus increases upon DNA replication stress	N	N+C
YIL006W	*YIA6*	Yia6p	Mitochondrial NAD+ transporter; involved in the transport of NAD+ into the mitochondria; member of the mitochondrial carrier subfamily; disputed role as a pyruvate transporter; *YIA6* has a paralog, *YEA6*, that arose from the whole genome duplication	M	M+C

YJL140W	*RPB4*	Rpb4p	RNA polymerase II subunit B32; forms dissociable heterodimer with Rpb7p; Rpb4/7 dissociates from RNAPII as Ser2 CTD phosphorylation increases; Rpb4/7 regulates cellular lifespan via mRNA decay process; involved in recruitment of 3'-end processing factors to transcribing RNAPII complex, export of mRNA to cytoplasm under stress conditions; also involved in translation initiation	N	N+C
YBL004W	*UTP20*	Upt20p	Component of the small-subunit processome; small-subunit processome is involved in the biogenesis of the 18S rRNA	N	N+C
YNL167C	*SKO1*	Sko1p	Basic leucine zipper transcription factor of the ATF/CREB family; forms a complex with Tup1p and Cyc8p to both activate and repress transcription; cytosolic and nuclear protein involved in osmotic and oxidative stress responses	N	N+C
YIL019W	*FAF1*	Faf1p	Protein required for pre-rRNA processing; also required for 40S ribosomal subunit assembly	N	N+C

1 ER – Endoplasmic Reticulum
2 C – Cytosol
3 M – Mitochondria
4 CP – Cell Periphery
5 B – Bud
6 V – Vacuole
7 P – Punctate
8 NP – Nuclear Periphery
9 N – Nucleus
10 VM – Vacuole Membrane
11 PCP – Punctate Cell Periphery

CHAPTER 4 - Development and Application of a Yeast-Based Biosensor for Environmental Monitoring of Tebuconazole in Water Samples

This chapter is adapted from the following publication:

Filipa Mendes, Eduarda Miranda, Leslie Amaral, Carla Carvalho, Bruno B. Castro, Maria João Sousa, Susana R. Chaves (2024) **Novel yeast-based biosensor for environmental monitoring of tebuconazole.** *Applied Microbiology and Biotechnology*. 108:1-12. doi.org/10.1007/s00253-023-12944-z

4.1. Background

Over the last decades, modern agriculture has been increasingly dependent on pesticides and fertilizers to support the growth of the human population (1). Fungicides are among the most frequently used pesticides, and are essential to control diseases that reduce crop production and threaten food security (2). As a consequence of their common and extensive use, fungicides reach aquatic ecosystems, and have been detected at higher concentrations than herbicides and insecticides in European surface waters (3). Despite current efforts towards a more sustainable use of pesticides, fungicide use is predicted to increase as a result of increased fungal resistance, invasive species, and climate change (2). Therefore, environmental monitoring programs urge for fast, cost-effective and disposable systems, with the ability to monitor the increasing number of relevant analytes (4). High-throughput detection technologies of these substances in water samples constitute a useful add-on for environmental scientists and managers, and fungi-based biosensors are particularly suitable for the job.

Among the most common classes of fungicides are demethylation inhibitors (a group of sterol biosynthesis inhibitors), which include azoles. They are regularly used to eliminate or control diseases caused by fungi and oomycetes in agricultural crops and as therapeutic drugs for medical purposes (5). TEB is one of the most frequently applied (6), and it is thus often detected in aquatic ecosystems, where there are concerns about its potentially negative effects on non-target aquatic biota at environmentally-relevant concentrations (7–9). Like other azoles, TEB has a well-known specific mode of action, inhibiting the activity of lanosterol 14-α demethylase, a cytochrome P450 enzyme encoded by the *ERG11* gene (CYP51). This affects ergosterol biosynthesis, ultimately leading to accumulation of sterol precursors and ergosterol depletion (10,11). Ergosterol is the major component of fungal membranes, regulating membrane integrity, fluidity and permeability; consequently, alterations in ergosterol homeostasis and limitations in its availability can affect and even prevent fungal growth (12,13). Ergosterol biosynthesis is a highly conserved and complex process that is regulated by a cascade of 25 biosynthetic enzymes, coded by *ERG* genes (14). In *S. cerevisiae,* this pathway is mainly regulated by the transcription factor Upc2p, which undergoes a conformational change when ergosterol levels decrease, triggering Upc2p translocation to the nucleus and binding to *ERG* promoters, thus causing transcriptional induction of most *ERG* genes (15,16).

Bearing this in mind, the goal of this chapter was to develop a novel yeast-based biosensor for environmental monitoring of TEB in aqueous samples. For that purpose, we used a modified yeast strain expressing a reporter gene controlled by specific promoters that are expressed after exposure to TEB. Moreover, we aimed to clarify if the biosensor developed was specific to TEB or if it was also

capable of detecting other azole compounds, since most of these fungicides share the mode of action (10,11). For this purpose, we selected myclobutanil (MYC), another triazole fungicide used to control fungal diseases in crop production (17), as well as antifungal pharmaceutical azoles used to treat fungal infections, which share the mode of action and can reach aquatic environments via wastewater (18,19), namely clotrimazole (CLO) and fluconazole (FLU).

4.2. Materials and methods

4.2.1. Yeast strains and plasmids

All *S. cerevisiae* strains and plasmids used in this study are listed in **table 4.1**. *S. cerevisiae* BY4741 was used throughout this study as the wild-type strain. Due to the small size (19 kDa), the absence of post-translational modifications, and its high sensitivity, the yeast codon optimized version of NanoLuciferase [yNLuc (20)], was selected as the reporter gene.

The sequences encoding the promoters of *ERG3*, *ERG6*, *ERG11* and *ERG*25 genes were amplified by PCR using genomic DNA isolated from BY4741 cells. Fusions of these promoters upstream of yNLuc were generated by overlap extension PCR, and then cloned into pRS426 (21) by gap repair. After confirmation by Sanger sequencing, the wild-type strain BY4741 was transformed with plasmids using the LiAc/SS Carrier DNA/PEG method (22).

Table 4.1. List of *S. cerevisiae* strains and plasmids used in this chapter.

Strain	Genotype	Source
BY4741	MAT a his3Δ1; leu2Δ0; met15Δ0; ura3Δ0	Euroscarf
BY4741 p*ERG3*pr-yNluc	BY4741 harboring pRS426-ERG25pr-yNluc	This Study
BY4741 p*ERG6*pr-yNluc	BY4741 harboring pRS426-ERG25pr-yNluc	This Study
BY4741 p*ERG10*pr-yNluc	BY4741 harboring pRS426-ERG25pr-yNluc	This Study
BY4741 p*ERG11*pr-yNluc	BY4741 harboring pRS426-ERG25pr-yNluc	This Study
BY4741 p*ERG25*pr-yNluc	BY4741 harboring pRS426-ERG25pr-yNluc	This Study
Plasmid	**Description**	**Source**
p*ERG3*pr-yNluc	*ERG3* promoter fused with yNLuc	This Study
p*ERG6*pr-yNluc	*ERG6* promoter fused with yNLuc	This Study
p*ERG11*pr-yNluc	*ERG11* promoter fused with yNLuc	This Study
p*ERG25*pr-yNluc	*ERG25* promoter fused with yNLuc	This Study

4.2.2. Growth conditions and treatments

Strains were grown in SC medium [2 % (w/v) glucose; 0.17 % (w/v) yeast nitrogen base without amino acids and without ammonium sulphate; 0.1 % (w/v) L-proline, 0.14 % (w/v) drop-out mixture lacking leucine, histidine, tryptophan, and uracil; 0.04 % (w/v) leucine; 0.008 % (w/v) tryptophan; 0.008 % (w/v) histidine, and 0.008 % (w/v) uracil] at 30 °C in an orbital shaker at 200 rpm, with a ratio of flask volume/medium of 5:1. Strains transformed with the indicated plasmids were grown in the same medium lacking uracil. Solid medium contained 2 % (w/v) agar and 0.5 % (w/v) ammonium sulphate instead of L-proline. L-proline was used as the nitrogen source in liquid assays since previous studies demonstrate that a medium containing L-proline as the only source of nitrogen increases the sensitivity of wild type strain S288c to the antifungal FLU (23).

For all assays, cells were grown overnight, then diluted in fresh medium to $OD_{640\ nm}$ = 0.1 and grown for an additional 3 h. Afterwards, cells were treated with TEB (0-5000 μg L^{-1}) or MYC, CLO or FLU [0-162 nM (molar equivalent of 50 μg L^{-1} of TEB)] from Sigma-Aldrich and/or the equivalent volume of DMSO as a negative control (lower than 0.5 %) for up to 30 h. Samples were taken at different time points for subsequent assays. Samples of the wild-type strain BY4741 were collected for cell growth and survival assays, assessment of plasma membrane integrity, evaluation of lipid raft distribution and qRT-PCR. *S. cerevisiae* BY4741 cells harboring p*ERG3*pryNluc (*ERG3*pr), p*ERG6*pryNluc (*ERG6*pr), p*ERG11*pryNluc (*ERG11*pr) or p*ERG25*pryNluc (*ERG25*pr) were used for bioluminescence assays.

4.2.3. Cell survival assays

Cell survival of BY4741 cells treated in the absence or presence of 500 and 5000 μg L^{-1} of TEB was evaluated by counting c.f.u. Briefly, five 10-fold serial dilutions of the cultures were performed, and 40 μL of 10^{-4} or 10^{-5} dilutions (according to each condition) were plated onto YEPD plates [1 % (w/v) yeast extract; 2 % (w/v) peptone; 2 % (w/v) glucose and 2 % (w/v) agar] and incubated at 30 °C for 48 h. The percentage of cell survival was calculated from the number of c.f.u. of each condition in relation to time zero and the control without any treatment.

4.2.4. Assessment of plasma membrane integrity

To assess loss of plasma membrane integrity, usually associated with a cell death process (24), cells were stained with the cell-impermeant dye PI (Sigma-Aldrich). At each timepoint, cells were harvested by centrifugation (0.5 mL $OD_{640\ nm}$ = 0.1) and resuspended in 1× PBS. PI was added to yeast cell suspensions to a final concentration of 2000 μg L^{-1} followed by incubation at RT for 10 min. Plasma

membrane integrity of BY4741 cells treated in the absence or presence of 500 and 5000 μg L^{-1} of TEB was assessed at 0, 3 and 6 h of treatment. After 6 h of treatment, cells were harvested, washed, transferred to fresh medium without fungicide, and grown for an additional 3 h; then, plasma membrane integrity was re-assessed.

Detection of fluorescence was performed with a CytoFLEX (Beckman Coulter Inc.) flow cytometer. Cells with red fluorescence (PI positive cells) were considered to have lost their plasma membrane integrity. Data was analyzed using CytExpert software.

4.2.5 Evaluation of lipid raft distribution by filipin staining

The localization of lipid rafts, plasma membrane nanodomains containing ergosterol in association with sphingolipids (25), was inferred by fluorescence microscopy (Leica Microsystems DM-5000B epifluorescence microscope) using filipin staining (Filipin III from *Streptomyces filipinensis*, Sigma-Aldrich). Filipin is a naturally fluorescent antibiotic dye that binds to ergosterol but not to esterified sterols, and is thus a broadly accepted method to detect regions with high sterol content in the plasma membrane of fungal species (26). Briefly, BY4741 cells were treated for 6 h in the absence or presence of 500 μg L^{-1} TEB, then collected at an $OD_{640\ nm}$ = 0.5 and concentrated 20× in sterile water. Immediately before visualization, cells were incubated with 0.1 g L^{-1} filipin from a stock solution of 5 g L^{-1} (w/v) in methanol for 1 min in the dark (27,28). Cells were then mounted on slides with the anti-fading agent Vectashield (Vector Laboratories) to overcome the instability of this dye and visualized in an epifluorescence microscope.

4.2.6. qRT-PCR

The effect of TEB on the expression levels of *ERG10, ERG7, ERG11, ERG25, ERG6,* and *ERG3* genes was assessed by qRT-PCR. Total RNA from cells exposed to 0, 5 or 50 μg L^{-1} TEB for 8 h was extracted using TRIzol/chloroform and RNA Clean & Concentrator-5 Kit (Zymo Research). Briefly, the upper aqueous phase from TRIzol/chloroform extraction was transferred to a new tube, and RNA was purified with the RNA Clean & Concentrator-5 Kit according to manufacturer's instructions. Then, cDNA was synthesized by reverse transcription from 500 ng of total RNA according to the manufacturer's instructions (iScript™ cDNA Synthesis Kit, Bio-Rad Laboratories). Real-time PCR reactions were performed in an CFX96™ Real-Time System C100™ Thermal Cycler (Bio-Rad Laboratories) using the KAPA SYBR® FAST qPCR Master Mix (2×) Kit (Sigma-Aldrich) according to manufacturer's instructions. PCR controls with no template were also performed for each primer pair. Three biological replicates

were performed, and each sample was measured in duplicate. Quantification was performed using the $2^{-\Delta\Delta Ct}$ method (29) and expression of *ERG* genes was normalized to *ACT1*.

4.2.7. Evaluation of biosensor performance in environmental water samples

To test the performance of the biosensor in real samples, environmental water samples were collected and tested. To maintain aseptic conditions, environmental water samples and distilled water were filtered (0.22μm) prior to analyses. Briefly, *ERG25*pr cells were grown overnight, then diluted in fresh medium to $OD_{640\ nm}$ = 0.1 and grown for an additional 3 h. Afterwards, cells were collected and resuspended in medium containing 9 parts distilled water (control of the experiment) or environmental water samples and 1 part 10× concentrated SC-Glu medium. Samples spiked with 10 μg L^{-1} of TEB and/or the equivalent volume of DMSO and without supplementation were used for bioluminescence assays.

4.2.8. Bioluminescence measurements

For bioluminescence assays, 1 mL of culture ($OD_{640\ nm}$ = 0.5) was collected and resuspended in SC-Glu medium (pH 8) containing 6.25 mM PEG 3350. Nano-Glo substrate (Promega GmbH, Germany) was diluted 1:100 with the supplied buffer and mixed 1:4000 with whole cells in white opaque 96-well microplates (OptiPlate-96). Bioluminescence emissions were recorded using a Varioskan Flash multimode reader (1000 ms integration time). Light emission was expressed in a.u.

4.2.9. Statistical analysis

A one- or two-way ANOVA was used to test the effect of fungicide (in most cases TEB) concentrations on yeast growth, viability, plasma membrane integrity, gene expression, or bioluminescence signal. A Dunnett test was used to assess differences relatively to the control. A significance level of 0.05 was employed in all analyses.

4.3. Results

4.3.1. TEB induces transcription of *ERG* genes at concentrations that do not affect growth, viability, and ergosterol distribution

To characterize the effect of TEB in *S. cerevisiae*, we first assessed the growth of laboratory strain BY4741 in the presence of increasing concentrations of this fungicide for up to 30 h. We observed that medium to low TEB concentrations (50 and 5 μg L^{-1}) did not affect the growth of BY4741 cells (**Figure 4.1A, 4.1B**), while exposure to high concentrations (500 to 4000 μg L^{-1}) for 6 h or longer inhibited cell growth (**Figure 4.1A**), leading to a decrease in the specific growth rate and in the final biomass (**Figure 4.1B**). Nonetheless, cells still grew, suggesting that those concentrations can limit growth of yeast cells but do not result in high levels of cell death. Indeed, we found that exposure to 500 or 5000 μg L^{-1} of TEB for 3 h did not affect cell survival and after 6 h cell survival decreased only slightly, for both concentrations tested (**Figure 4.1C**). As shown in **figure 4.1D**, exposure to 500 and 5000 μg L^{-1} of TEB led to a significant increase in PI staining after 3 h and 6 h, indicating that plasma membrane integrity is compromised. However, this effect was reversible, since the percentage of cells staining with PI drastically decreased if cells were washed after exposure to TEB and subsequently incubated in fresh medium for 3 h (**Figure 4.1D**). We further assessed the effect of TEB on the plasma membrane by visualizing distribution of lipid rafts in control and TEB-treated cells (**Figure 4.1E**). We observed the characteristic punctuated pattern of filipin staining at the plasma membrane in control cells, but intracellular spots became apparent after 6 h of exposure to 500 μg L^{-1} TEB, indicating that TEB-treated cells exhibit intracellular accumulation of ergosterol. A similar phenotype was observed for the highest concentration (50 000 μg L^{-1}, data not shown).

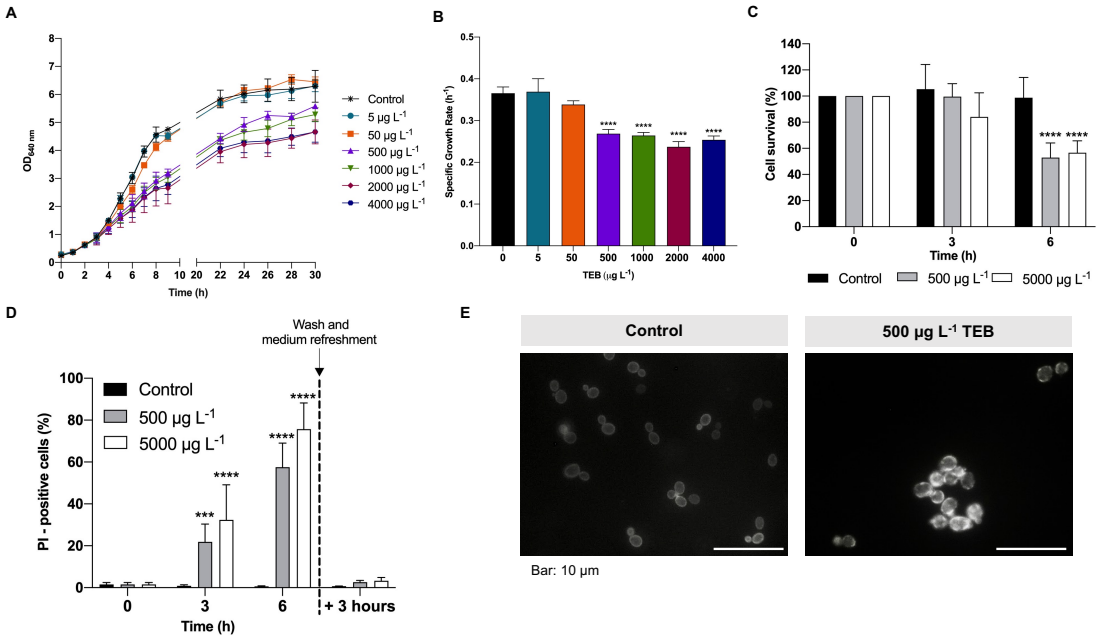

Figure 4.1. Effect of high concentrations of TEB on growth, cell survival, plasma membrane integrity and lipid rafts distribution of *S. cerevisiae* BY4741 cells. Cells were grown overnight and diluted to an $OD_{640\ nm}$ = 0.1, transferred to fresh medium and grown for an additional 3 h then cells were treated with TEB, and/or the equivalent volume of DMSO (control/0), **(A)** In absence or presence of increasing concentrations of TEB (5 – 4000 µg L^{-1}) $OD_{640\ nm}$ were registered over time and the specific growth rates **(B)** were calculated considering the exponential phase in **(A)**. **(C)** Cell survival of BY4741 cells treated with 0, 500 and 5000 µg L^{-1} TEB was determined by standard dilution plate counts and expressed as a percentage of c.f.u. on YEPD plates in relation to time 0. **(D)** Plasma membrane integrity was determined by PI staining of cells treated with 0, 500 and 5000 µg L^{-1} TEB at time point 0, 3, 6 and after 3 h of washing cells and medium refreshment. **(E)** For lipid rafts visualization cells were treated for 6 h in the presence 500 µg L^{-1} of TEB and/or the equivalent volume of DMSO (control), then cells were collected and stained in the dark with 0.1 µg L^{-1} filipin, immediately before visualization under the microscope. Representative fluorescence images of each condition are shown. Due to fast photobleaching of filipin, fluorescence intensity it is not associated with ergosterol levels and only localization can be inferred. The data displayed are the mean ± S.D. of three independent experiments. Asterisks (***, P ≤ 0.001; ****, P ≤ 0.0001) depict significant differences relative to the control.

We further found that even higher concentrations (50 000 µg L^{-1}) and longer treatment periods (up to 72 h) did not increase mutation frequencies of *S. cerevisiae* cells (supplementary material **Table S4.i**). This indicates that TEB is not genotoxic and thus a biosensor would not be prone to TEB-induced mutations.

Next, we characterized the effect of TEB on the expression levels of *ERG* genes involved in different steps of the ergosterol biosynthesis pathway (**Figure 4.2A**). We found that a low concentration (50 µg L^{-1}) leads to upregulation of several genes involved in late steps, although no changes were observed in response to 5 µg L^{-1}. As shown in **figure 4.2B**, 50 µg L^{-1} of TEB increased the relative

expression of *ERG6*, *ERG25* and *ERG3* two, three and four-fold, respectively, when compared to nontreated cells (control). In contrast, the relative expression of *ERG10* and *ERG7* was not significantly altered by either concentration. Although *ERG11* transcription also tended to increase, this change was not statistically significant (**Figure 4.2B**). Based on these results *ERG11*, *ERG25*, *ERG6* and *ERG3* promoters were chosen to construct yeast-based biosensors.

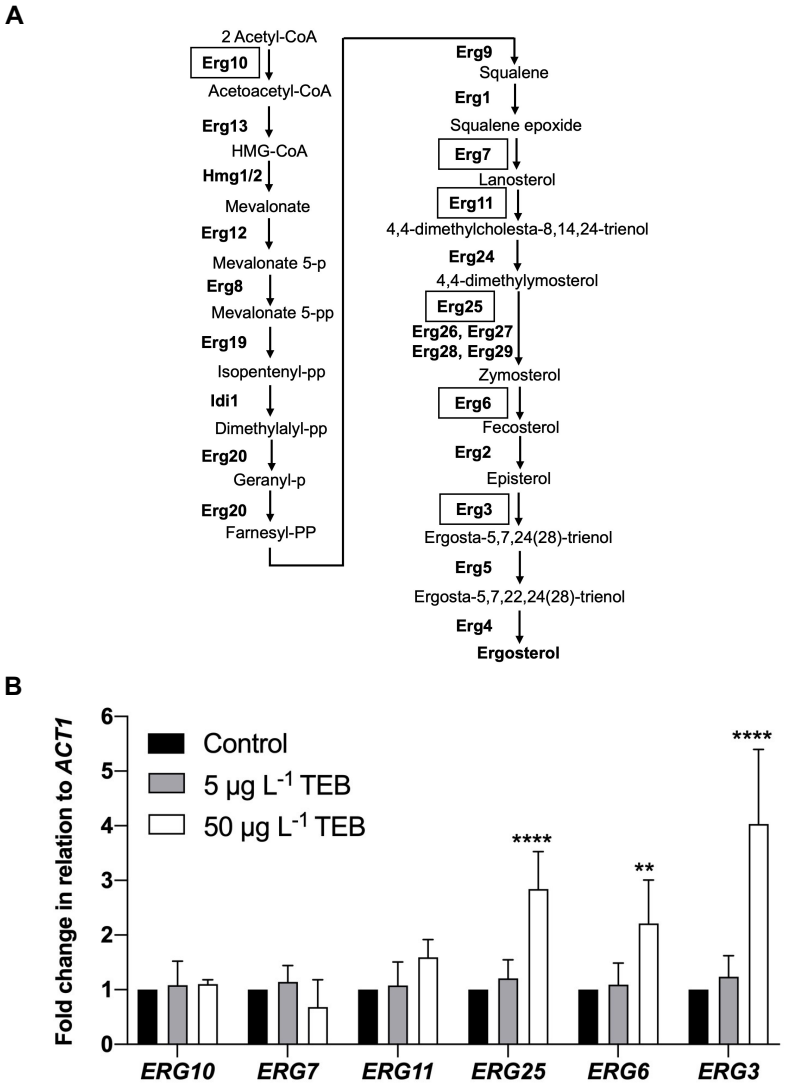

Figure 4.2. Effect of low TEB concentrations on genes involved in ergosterol biosynthetic pathway of *S. cerevisiae.* (A) Ergosterol biosynthetic pathway in *S. cerevisiae.* The levels of boxed genes *ERG10*, *ERG7*, *ERG11*, *ERG25*, *ERG6*, and *ERG3* were assessed by qRT-PCR. **(B)** The *S. cerevisiae* BY4741 wild type cells were treated for 8 h in the presence of 5 and 50 µg L^{-1} of TEB and/or the equivalent volume of DMSO (control); *ACT1* gene was used as normalizer. The expression values are represented as the fold change relative to the nontreated cells (control) and correspond to the mean ± S.D. of three independent experiment. Asterisks (**, P≤ 0.01; ****, P ≤ 0.0001) depict significant differences relative to the control.

4.3.2. A novel biosensor design based on yNLuc expression from *ERG* promoters

We found that biosensors obtained by genetically engineering *S. cerevisiae* cells with a vector expressing yNluc downstream of *ERG11, ERG25, ERG6*, or *ERG3* promoter produced an increased bioluminescence signal in TEB-treated cells, but the signal was only significantly different from control cells in *ERG11*pr, *ERG25*pr and *ERG3*pr biosensors (**Figure 4.3**). Since *ERG*11 is a direct target of TEB (11) and *ERG25*pr and *ERG3*pr biosensors produced a bioluminescence signal in which *p* values were associated with higher significance, we chose only the latter two for further analysis.

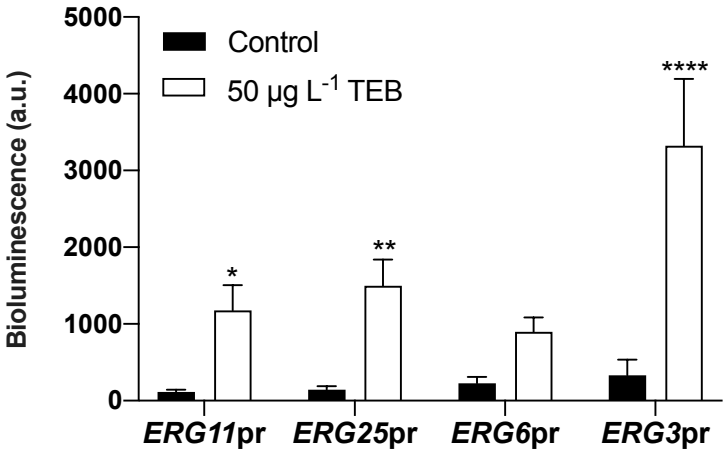

Figure 4.3. Response of biosensor after exposure to TEB. *ERG11*pr, *ERG25*pr, *ERG6*pr and *ERG3*pr cells were incubated, for 8 h, in the presence of TEB (50 µg L^{-1}) and/or the equivalent volume of DMSO (control). Then cells were collected, and bioluminescence was assessed. Values are mean ± S.D. of three independent experiments. Asterisks (*, P ≤ 0.05; **, P ≤ 0.01; ****, P ≤ 0.0001) depict significant differences relative to the control.

Upon further analysis, we observed that the *ERG3*pr biosensor only detected the higher concentration of TEB (50 µg L^{-1}), and lower concentrations resulted in a bioluminescence level comparable to untreated cells (**Figure 4.4A**). On the other hand, the *ERG25*pr biosensor detected two lower concentrations, 5 and 10 µg L^{-1}, after both 6 h and 8 h of exposure (**Figure 4.4B**). We further verified that 4 h of exposure to 50 and even 100 µg L^{-1} was not sufficient for a significant response in this biosensor, whereas extending the time to 24 h only slightly increased the TEB-induced bioluminescence signal, while also increasing in the control (data not shown).

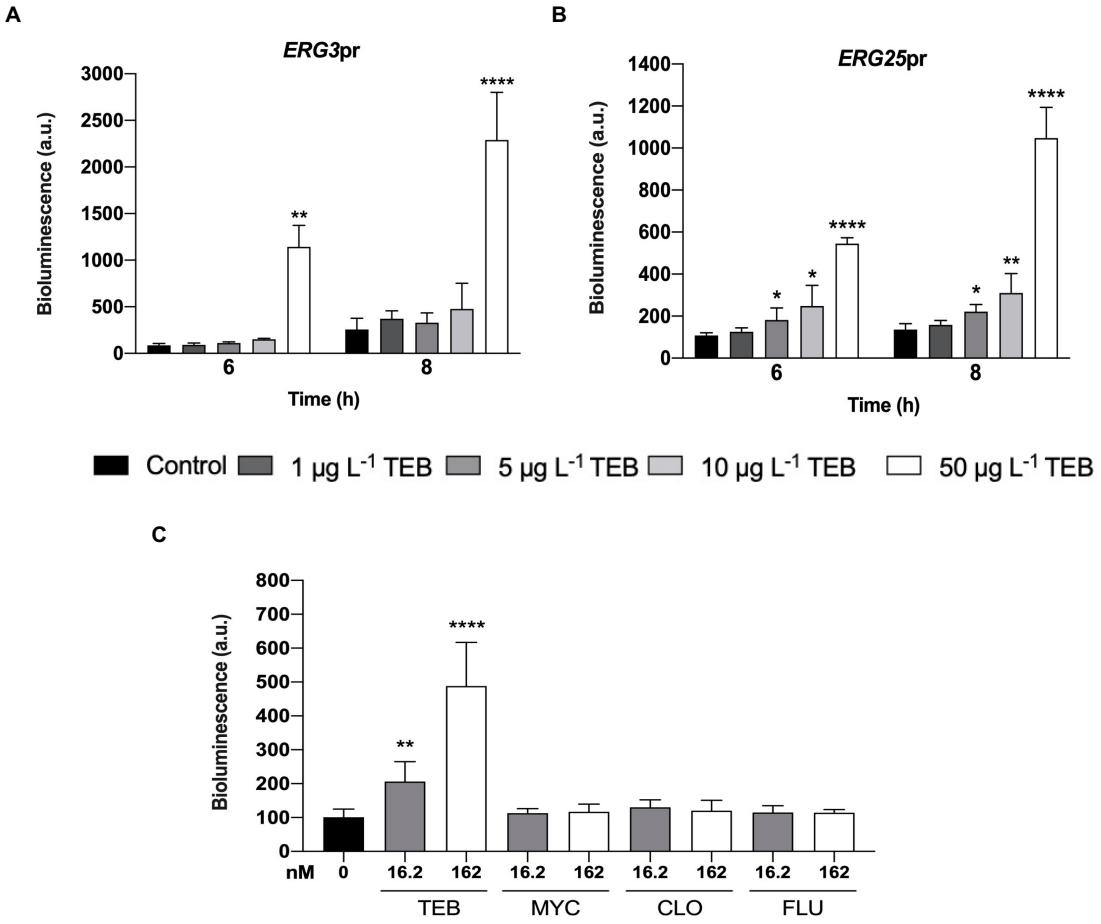

Figure 4.4. Biosensor sensitivity and selectivity to TEB. Sensitivity of biosensors **(A)** *ERG3*pr and **(B)** *ERG25*pr was determined after incubation in the presence of increasing concentrations of TEB (1 - 50 µg L^{-1}) and/or the equivalent volume of DMSO (control). Afterwards, bioluminescence was recorded after 6 and 8 h of treatment. Estimated values of *ERG25*pr LoD (3.3x (σ / S)) and LoQ (10x (σ / S)) based on this experiment were: LoD=0.84/1.24 and LoQ=2.55/3.77 (after 6/8 h), consistent with the statistically significant sensitivity of the biosensor of 5 µg L^{-1}. For determination of *ERG25*pr selectivity **(C)** *ERG25*pr cells were exposed to 0, 16.2 and 162 nM (5 and 50 µg L^{-1}, respectively) of TEB, MYC, CLO and FLU for 6 h, after which bioluminescence was assessed. Values are mean ± SD of three independent experiments. Asterisks (*, P ≤ 0.05; **, P ≤ 0.01; ****, P ≤ 0.0001) depict significant differences relative to the control.

In further analysis of the performance of the *ERG25*pr biosensor, we found there was a significant bioluminescence signal in response to 5 µg L^{-1} and 50 µg L^{-1} of TEB, which was not observed in response to equivalent molar concentrations (16.2 nM and 162 nM) of the azoles MYC, CLO, or FLU (**Figure 4.4C**). Since our final goal is to use the biosensor developed to detect TEB in environmental water samples, we further tested the performance of the biosensor in a wide range of samples collected from eight different sources and hence with different composition (analysis provided in supplementary material **table S4.i**).

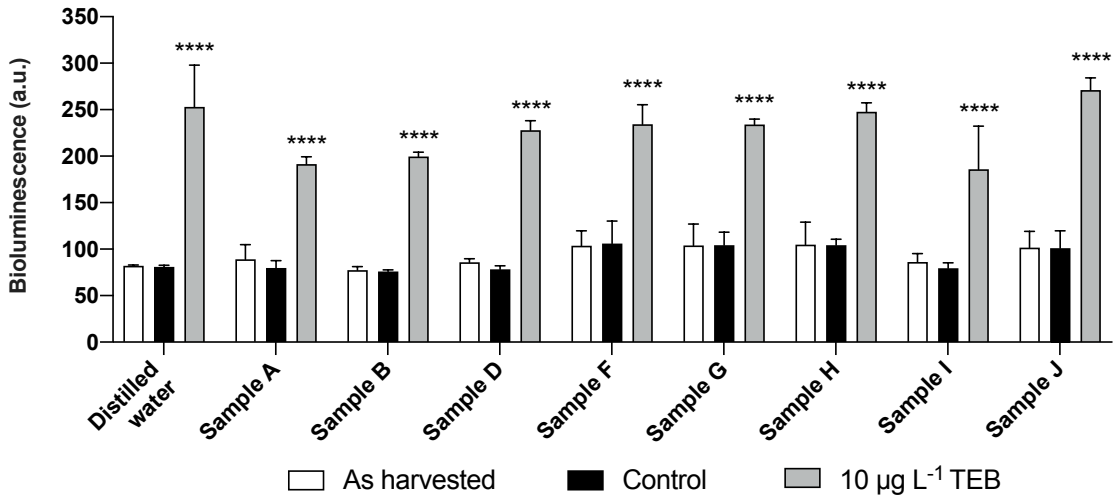

Figure 4.5. Proof-of-concept of biosensor functionality. Eight environmental water samples were analyzed using biosensor *ERG25*pr. Samples (A, B, D, F, G, H, I and J) were collected and filtered. *ERG25*pr cells were incubated in 10× concentrated medium diluted in water samples as harvested, without TEB supplementation (white), in the presence of the equivalent volume of DMSO, control (black), and spiked with 10 µg L^{-1} of TEB (grey), for 6 h. Afterwards, bioluminescence was recorded. Results are obtained in 1 working day. Values are mean ± S.D. of two independent experiments. Asterisks (****, $P \leq 0.0001$) depict significant differences relative to the control and as harvested.

As a proof-of-concept, the environmental water samples collected were analyzed using the *ERG25*pr biosensor, spiked with 10 µg L^{-1} of TEB or the equivalent volume of DMSO, with distilled water used as a control. As seen in **figure 4.5**, the bioluminescence signal obtained was very similar between distilled water and the collected samples and the *ERG25*pr biosensor was able to detect TEB in all spiked samples. We also observed that DMSO (solvent control) did not significantly affect the basal bioluminescence signal (**Figure 4.5**, white bar). Environmental water samples were also analyzed by analytical methods and results showed that TEB was only detected at vestigial concentration in sample A (0.014 µg L^{-1}) and not detected in the remaining samples, meaning its concentration was below the detection limit (LoD = 0.005 µg L^{-1}). Other fungicides such as carbendazim, dimetomorph and metalaxyl were also detected at vestigial concentrations, while copper was detected in all samples (**Table 4.2**). This analysis also revealed the presence of other polluting substances revealing human presence, namely metformin, a drug used to treat type 2 diabetes that was detected in samples I and J at 3 and 2 µg L^{-1}, respectively.

Table 4.2. LoD and concentration of fungicides (carbendazim, copper, dimetomorph, metalaxyl and TEB) detected at environmental water samples analyzed by analytical methods. Samples where fungicide concentration is below the detection limit are identify as ND (not detected).

		Sample							
Fungicide (μg L^{-1})	**LOD**	**A**	**B**	**D**	**F**	**G**	**H**	**I**	**J**
Carbendazim	**0.002**	ND	ND	ND	ND	ND	ND	0.015	0.003
Copper	**0.15**	2.16	1.16	0.92	1.71	1.09	0.91	3.19	6.03
Dimetomorph	**0.002**	0.028	ND	ND	ND	ND	ND	0.005	0.006
Metalaxyl	**0.002**	0.043	0.006	ND	ND	0.005	0.003	0.003	0.006
TEB	**0.005**	0.014	ND	ND	ND	ND	ND	ND	ND

4.4. Discussion

TEB is widely used in agriculture and viticulture to control a plethora of fungal diseases (30). We found no specific information about the regulatory limits of TEB; in Europe, it is not listed as a priority substance and thus no environmental quality standards have been defined. However, the Groundwater Directive from the European Union Commission determines that the concentration of a single pesticide in groundwater should not exceed 0.1 μg L^{-1} [Directive 2006/118/EC (31)]. Locally, TEB has been included in the list of pesticides to monitor to assess the quality of drinking water in Portugal, although specific regulatory limits have not been imposed as of yet [Decree Law ns 306/2017 and 69/2023 (32,33)]. In water courses, TEB is frequently detected at concentrations ranging from 1 to 30 ng L^{-1} (34), but can reach 175-200 μg L^{-1} in extreme runoff events (35,36). At these concentrations, TEB effects can be potentially high, given its effectiveness against many fungi (7–9) and that it can also inhibit human cytochrome P450 sterol 14α-demethylases (37).

Detection of TEB in aqueous samples, such as water, is normally performed by liquid chromatography-tandem mass spectrometry and gas chromatography-mass spectrometry (38). Although these methods are reliable and extremely sensitive, with low detection limits (ng L^{-1}), they are time-consuming, expensive, and do not conform to green chemistry practices, as they require sample preparation with solvents (39,40). Moreover, the necessity of trained technicians and complex procedures prevents implementation in low-tech local laboratories. Further increasing the environmental cost is the carbon footprint associated with shipping of the collection containers and then returning them with the samples. Therefore, it is of utmost importance to strengthen and simplify the environmental monitoring programs available for its detection in aqueous samples. We therefore set out to contribute to monitoring efforts by constructing a yeast biosensor that can detect TEB. For that

purpose, it is necessary that environmentally relevant concentrations (below 200 μg L^{-1}) (35,36) elicit a biological response without negatively affecting cell viability.

As previously shown for other azole compounds (41,42), we found that high concentrations of TEB inhibit growth of *S. cerevisiae* cells and resulted in a small loss of viability. We further found that exposure to TEB for 3 or 6 h resulted in loss of plasma membrane integrity, a common feature of cell death (24). Due to TEB effects on ergosterol biosynthesis (43) and since cell viability was only slightly affected and only after 6 h, we hypothesized that this could be the result of a reversible increase in the permeability to the dye and not to plasma membrane disruption. Indeed, washing the cells after exposure to TEB resulted in a substantial decrease in the percentage of cells stained with PI. This indicates that TEB-treated cells did not reach the point of no return in the cell death process, but instead displayed reversible increased permeability to small molecules. A similar phenotype, with alterations in plasma membrane rigidity, has been described for *S. cerevisiae* mutants defective in the last five steps of the ergosterol biosynthesis pathway, particularly *erg2*Δ and *erg6*Δ. In those mutants, accumulation of ergosterol precursors does not allow a tight packing of the lipid bilayer and thus the occurrence of voids in the plasma membrane increases, increasing the sensitivity of these mutants to small molecules (44–46). In accordance with alterations in plasma membrane integrity, TEB also disturbed lipid rafts, plasma membrane nanodomains enriched in ergosterol and sphingolipids (25), mainly through intracellular accumulation of ergosterol. This pattern in membrane perturbation has been described for methyl-β-cyclodextrin, a sterol chelator that totally extracts ergosterol from plasma membranes, leading to its intracellular accumulation (28,47). Nevertheless, TEB-treated cells still preserved ergosterol staining at the plasma membrane, suggesting that TEB does not lead to full depletion of ergosterol from plasma membranes but does disturb ergosterol-rich lipid rafts. Consistent with these results, we found that TEB induced expression of several *ERG* genes involved in the late steps of ergosterol biosynthesis. Azole-dependent upregulation of genes involved in the late steps of ergosterol biosynthesis has been demonstrated in *Candida* species (48,49) and in *S. cerevisiae* (50–52), mainly using high concentrations. Here, we demonstrate that a low concentration also up-regulates *ERG* genes. Taken together, our results indicate that high concentrations (500 – 5000 μg L^{-1}) of TEB affect growth, viability, and ergosterol distribution of yeast cells, while a lower concentration (50 μg L^{-1}) can stimulate a biological response without affecting yeast growth. We concluded that *S. cerevisiae* is both robust and sensitive to develop a novel yeast-based biosensor for TEB detection in environmental water samples.

To construct the biosensor, we genetically engineered *S. cerevisiae* cells with a plasmid expressing yNluc downstream of *ERG11*, *ERG25*, *ERG6*, or *ERG3* promoters. Among these, the

*ERG25*pr biosensor was the most sensitive, detecting the presence of TEB in a statistically significant manner at concentrations above 5 μg L^{-1}. This *ERG25*pr biosensor also seems to specifically respond to TEB, as it was unable to detect other azoles at low realistic environmental concentrations. We further demonstrate that the biosensor developed can be used in a simple assay, avoiding preparation of environmental water samples, since biosensor performance was not affected by the presence of potential interfering factors such as electrical conductivity (EC), total dissolved solids (TDS), pH and other substances.

Taking its detection limit under consideration, we propose the use of this biosensor to analyze samples from aquatic environments prone to TEB contamination such as superficial waters and wastewaters. Additionally, this novel approach could be used to monitor TEB in drinking water, particularly water from environments close to agricultural fields. In these cases, the presence of TEB will lead to the upregulation of *ERG25,* consequently increasing the expression of the reporter gene yNluc and subsequent production of luciferase protein. This increase will be reflected in bioluminescence emission upon addition of the luciferase substrate. Absence of a bioluminescence signal indicates that no TEB is present or that TEB present in the sample in concentrations under 5 μg L^{-1}, while a significative bioluminescence signal is indicative of TEB presence (**Figure 4.6**). The results gathered in this study indicate that this new method can be an important complementary tool, namely in high throughput scenarios requiring screening of numerous samples, which can be performed by minimally skilled personnel in standard laboratories before chemical analysis by specialized services. In this manner, samples eliciting a positive signal can be further analyzed through conventional methods. Ultimately, this type of screening allows a fast and inexpensive monitoring of TEB contamination in aquatic ecosystems, decreasing its economic cost and consequently enabling the implementation of semi-continuous environmental monitoring of TEB.

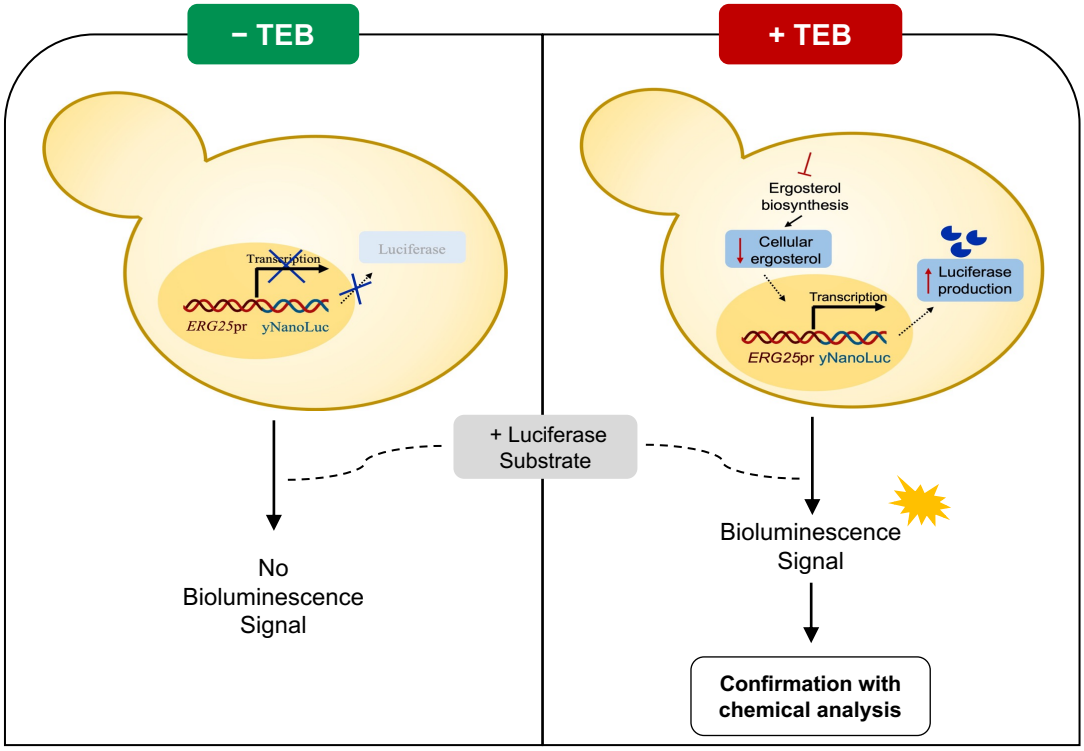

Figure 4.6. Schematic representation of the novel reporter strain for TEB detection in environmental water samples. Samples from aquatic environments prone to TEB contamination (agricultural fields, rivers or wastewater management effluents) can trigger a cellular response such as inhibition of ergosterol biosynthesis that will lead to the decrease of the cellular levels of ergosterol. Consequently, upregulation of *ERG* genes, particularly *ERG25*, will result in the expression of the reporter gene yNluc. As consequence, luciferase production will increase and upon addition of the luciferase substrate, bioluminescence emissions are obtained. Samples without a significative bioluminescence signal indicate that TEB is not present in concentrations above 5 μg L^{-1} (left), while samples with a significative bioluminescence signal indicate presence of TEB (right) and should be further analyzed by conventional methods.

4.5. References

1. Bommarco R, Kleijn D, Potts SG. Ecological intensification: Harnessing ecosystem services for food security. Trends Ecol Evol. 2013;28:230–8.
2. Zubrod JP, Bundschuh M, Arts G, Brühl CA, Imfeld G, Knäbel A, et al. Fungicides: An Overlooked Pesticide Class? Environ Sci Technol. 2019;53:3347–65.
3. Stehle S, Schulz R. Agricultural insecticides threaten surface waters at the global scale. Proc Natl Acad Sci U S A. 2015;112:5750–5.
4. Rodriguez-Mozaz S, Lopez De Alda MJ, Barceló D. Biosensors as useful tools for environmental analysis and monitoring. Anal Bioanal Chem. 2006;386:1025–41.
5. Price CL, Parker JE, Warrilow AG, Kelly DE, Kelly SL. Azole fungicides - understanding resistance mechanisms in agricultural fungal pathogens. Pest Manag Sci. 2015;71:1054–8.
6. Azevedo M-M, Faria-Ramos I, Cruz LC, Pina-Vaz C, Gonçalves Rodrigues A. Genesis of Azole Antifungal Resistance from Agriculture to Clinical Settings. J Agric Food Chem. 2015;63:7463–8.
7. Zubrod JP, Englert D, Feckler A, Koksharova N, Konschak M, Bundschuh R, et al. Does the current fungicide risk assessment provide sufficient protection for key drivers in aquatic ecosystem functioning? Environ Sci Technol. 2015;49:1173–81.
8. Pimentão AR, Pascoal C, Castro BB, Cássio F. Fungistatic effect of agrochemical and pharmaceutical fungicides on non-target aquatic decomposers does not translate into decreased fungi- or invertebrate-mediated decomposition. Sci Total Environ. 2020;712:1–10.
9. Cuco AP, Wolinska J, Santos JI, Abrantes N, Gonçalves FJM, Castro BB. Can parasites adapt to pollutants? A multigenerational experiment with a *Daphnia* × *Metschnikowia* model system exposed to the fungicide tebuconazole. Aquat Toxicol. 2020;226:1–8.
10. Joseph-Horne T, Hollomon D, Loeffler RST, Kelly SL. Altered P450 activity associated with direct selection for fungal azole resistance. FEBS Lett. 1995;374:174–8.
11. Lamb D, Kelly D, Kelly S. Molecular aspects of azole antifungal action and resistance. Drug Resist Updat. 1999;2:390–402.
12. Kathiravan MK, Salake AB, Chothe AS, Dudhe PB, Watode RP, Mukta MS, et al. The biology and chemistry of antifungal agents: A review. Bioorganic Med Chem. 2012;20:5678–98.
13. Kodedová M, Sychrová H. Changes in the sterol composition of the plasma membrane affect membrane potential, salt tolerance and the activity of multidrug resistance pumps in *Saccharomyces cerevisiae*. PLoS One. 2015;10:1–19.
14. Jordá T, Puig S. Regulation of ergosterol biosynthesis in S*accharomyces cerevisiae*. Genes.

2020;11:1–18.

15. Marie C, Leyde S, White TC. Cytoplasmic localization of sterol transcription factors Upc2p and Ecm22p in *S. cerevisiae*. Fungal Genet Biol. 2008;45:1430–8.
16. Yang H, Tong J, Lee CW, Ha S, Eom SH, Im YJ. Structural mechanism of ergosterol regulation by fungal sterol transcription factor Upc2. Nat Commun. 2015;6:1–13.
17. Fonseca FS, Carrão DB, de Albuquerque NCP, Nardini V, Dias LG, da Silva RM, et al. Myclobutanil enantioselective risk assessment in humans through *in vitro* CYP450 reactions: Metabolism and inhibition studies. Food Chem Toxicol. 2019;128:202–11.
18. Crowley PD, Gallagher HC. Clotrimazole as a pharmaceutical: past, present and future. J Appl Microbiol. 2014;117:611–7.
19. Berkow EL, Lockhart SR. Fluconazole resistance in *Candida* species: A current perspective. Infect Drug Resist. 2017;10:237–45.
20. Masser AE, Kandasamy G, Kaimal JM, Andréasson C. Luciferase NanoLuc as a reposter for gene expression and protein levels in *Saccharomyces cerevisiae*. Yeast. 2016;33:191–200.
21. Sikorski RS, Hieter P. A system of shuttle vectors and yeast host strain designed for efficient manipulation of DNA in *Saccharomyces cerevisiae*. Genetics. 1989;122:19–27.
22. Gietz RD, Woods RA. Yeast Transformation by the LiAc/SS Carrier DNA/PEG Method. In: Xiao W, editor. Methods in molecular biology. Humana Press Inc., Totowa, NJ; 2006. p. 107–20.
23. Stella CA, Costanzo R, Burgos HI, Saenz DA, Venerus RD. L-Proline as a Nitrogen Source Increases the Susceptibility of *Saccharomyces cerevisiae* S288c to Fluconazole. Folia Microbiol (Praha). 1998;43:403–5.
24. Kroemer G, Galluzzi L, Vandenabeele P, Abrams J, Alnemri ES, Baehrecke EH, et al. Classification of cell death: Recommendations of the Nomenclature Committee on Cell Death 2009. Cell Death Differ. 2009;16:3–11.
25. Wachtler V, Balasubramanian MK. Yeast lipid rafts? - An emerging view. Trends Cell Biol. 2006;16:1–4.
26. Maxfield FR, Wüstner D. Analysis of Cholesterol Trafficking with Fluorescent Probes. Methods Cell Biol. 2012;108:367–93.
27. Pacheco A, Azevedo F, Rego A, Santos J, Chaves SR, Côrte-Real M, et al. C2-phytoceramide perturbs lipid rafts and cell integrity in *Saccharomyces cerevisiae* in a sterol-dependent manner. PLoS One. 2013;8:1–12.
28. Santos-Pereira C, Andrés MT, Chaves SR, Fierro JF, Gerós H, Manon S, et al. Lactoferrin perturbs

lipid rafts and requires integrity of Pma1p-lipid rafts association to exert its antifungal activity against *Saccharomyces cerevisiae*. Int J Biol Macromol. 2021;171:343–57.

29. Livak KJ, Schmittgen TD. Analysis of relative gene expression data using real-time quantitative PCR and the $2^{-\Delta\Delta_{CT}}$ method. Methods. 2001;25:402–8.
30. Baćmaga M, Wyszkowska J, Borowik A, Kucharski J. Effects of Tebuconazole Application on Soil Microbiota and Enzymes. Molecules. 2022;27:1–15.
31. Directive 2006/118/EC of the European Parliament and of the Council of 12 December 2006 on the protection of groundwater against pollution and deterioration. Off J Eur Union L. 2006;372:19–31.
32. Decree-Law no 306/2017 (2017) Republic Diary No 164/2007, Series 1, pp 5747–5765. https://diariodarepublica.pt/dr/detalhe/decreto-lei/306-2007-640931
33. Decree-Law no 69/2023 (2023) Republic Diary No 161/2023, Series 1, pp 70–73. https://diariodarepublica.pt/dr/detalhe/decreto-lei/69-2023-220113533
34. Kahle M, Buerge IJ, Hauser A, Müller MD, Poiger T. Azole fungicides: Occurrence and fate in wastewater and surface waters. Environ Sci Technol. 2008;42:7193–200.
35. Zubrod JP, Bundschuh M, Schulz R. Effects of subchronic fungicide exposure on the energy processing of *Gammarus fossarum* (Crustacea; Amphipoda). Ecotoxicol Environ Saf. 2010;73:1674–80.
36. Elsaesser D, Schulz R. Mitigation of fungicide pollution in vegetated agricultural surface waters: GIS modelling and monitoring in the field. In: Proceedings of the SETAC Europe 18th Annual Meeting, SETAC Warsaw. 2008. p. 406–7.
37. Warrilow AG, Parker JE, Kelly DE, Kelly SL. Azole Affinity of Sterol 14-Demethylase (CYP51) Enzymes from C*andida albicans* and *Homo sapiens*. Antimicrob Agents Chemother. 2013;57:1352–60.
38. Huang Q, Yu Y, Tang C, Peng X. Determination of commonly used azole antifungals in various waters and sewage sludge using ultra-high performance liquid chromatography-tandem mass spectrometry. J Chromatogr A. 2010;1217:3481–8.
39. Daverey A, Dutta K, Sarkar A. An overview of analytical methodologies for environmental monitoring. In: Brar KS, Hedged K, Pachapur VL, editors. Tools, Techniques and Protocols for Monitoring Environmental Contaminants. Elsevier Inc.; 2019. p. 3–17.
40. Bhadekar R, Pote S, Tale V, Nirichan B. Developments in analytical methods for detection of pesticides in environmental samples. Am J Anal Chem. 2011;2:1–15.

41. Pfaller MA, Messer S, Jones RN. Activity of a new triazole, Sch 56592, compared with those of four other antifungal agents tested against clinical isolates of *Candida* spp. and *Saccharomyces cerevisiae*. Antimicrob Agents Chemother. 1997;41:233–5.

42. Parker JE, Merkamm M, Manning NJ, Pompon D, Kelly SL, Kelly DE. Differential azole antifungal efficacies contrasted using a *Saccharomyces cerevisiae* strain humanized for sterol 14α-demethylase at the homologous locus. Antimicrob Agents Chemother. 2008;52(10):3597–603.

43. FRAC (2022) FRAC Code List. https://www.frac.info/docs/default- source/publications/frac-code-list/fraccode-list-2022%2D%2Dfinal.pdf?sfvrsn=b6024e9a_2. (Accessed on 16 Oct 2023)

44. Welihinda AA, Beavis AD, Trumbly RJ. Mutations in *LIS1* (*ERG6*) gene confer increased sodium and lithium uptake in S*accharomyces cerevisiae*. Biochim Biophys Acta - Biomembr. 1994;1193:107–17.

45. Emter R, Heese-Peck A, Kralli A. *ERG6* and *PDR5* regulate small lipophilic drug accumulation in yeast cells via distinct mechanisms. FEBS Lett. 2002;521:57–61.

46. Abe F, Hiraki T. Mechanistic role of ergosterol in membrane rigidity and cycloheximide resistance in *Saccharomyces cerevisiae*. Biochim Biophys Acta - Biomembr. 2009;1788:743–52.

47. Baumann NA, Sullivan DP, Ohvo-Rekilä H, Simonot C, Pottekat A, Klaassen Z, et al. Transport of newly synthesized sterol to the sterol-enriched plasma membrane occurs via nonvesicular equilibration. Biochemistry. 2005;44:5816–26.

48. Henry KW, Nickels JT, Edlind T homa. D. Upregulation of *ERG* genes in *Candida* species by azoles and other sterol biosynthesis inhibitors. Antimicrob Agents Chemother. 2000;44:2693–700.

49. Song JL, Lyons CN, Holleman S, Oliver BG, White TC. Antifungal activity of fluconazole in combination with lovastatin and their effects on gene expression in the ergosterol and prenylation pathways in *Candida* albicans. Med Mycol. 2003;41:417–25.

50. Bammert GF, Fostel JM. Genome-wide expression patterns in *Saccharomyces cerevisiae*: Comparison of drug treatments and genetic alterations affecting biosynthesis of ergosterol. Antimicrob Agents Chemother. 2000;44:1255–65.

51. Henry KW, Nickels JT, Edlind TD. *ROX1* and *ERG* regulation in *Saccharomyces cerevisiae*: Implications for antifungal susceptibility. Eukaryot Cell. 2002;1:1041–4.

52. Kagan IA, Michel A, Prause A, Scheffler BE, Pace P, Duke SO. Gene transcription profiles of S*accharomyces cerevisiae* after treatment with plant protection fungicides that inhibit ergosterol biosynthesis. Pestic Biochem Physiol. 2005;82:133–53.

4.6. Supplementary Material

Table S4.ii. Mutator phenotype of *mlh1*Δ cells exposed to TEB.

Time (h) / Treatments	*hom3-10* ($\times 10^{-5}$)[a]		
	24	**48**	**72**
Control	3.06 ± 2.3	1.56 ± 0.9	1.56 ± 1.5
500 µg L^{-1}	1.21 ± 0.5	0.962 ± 0.6	1.16 ± 1.0
50 000 µg L^{-1}	1.03 ± 0.2	1.21 ± 0.9	1.37 ± 1.4

[a] Median frequency of seven cultures. Values not statistically significant (Mann–Whitney test).

To determine whether TEB is genotoxic and can induce genomic instability, fluctuation analysis (1) was used. The reporter strain RDKY3615 Δ*mlh1* carries a specific mutation that facilitates quantification of mutation rates, *hom3-10*. The *HOM3* gene encodes aspartate kinase (L-aspartate 4-P-transferase), a cytoplasmic enzyme necessary for threonine biosynthesis (2). Thus, if yeast *hom3-10* mutants are grown on a medium lacking threonine, cells will die unless they revert the mutation. The strain also carrying a mutation in the *MLH1* gene, which plays a role in DNA repair, was used to facilitate measurements as it displays increased basal mutation frequencies (3). Individual RDKY3615 *mlh1*Δ colonies were grown overnight in SC-Glucose medium with L-proline, diluted in fresh medium to $OD_{640\ nm}$ = 0.1 and grown for an additional 3 h. Afterwards, cells were exposed to 0, 500 or 50 000 µg L^{-1} TEB. After 24, 48 and/or 72 h of treatment, cells were collected, washed, diluted in water, and appropriate dilutions plated on SC-Glucose medium (complete and lacking threonine). After 2 days at 30 °C, colonies were counted, and mutation frequencies calculated as described (4).

Table S4.iii. Environmental water sample locations and characteristics. For each sample collected, characteristics such as temperature, dissolved oxygen (% saturation), total phosphorus, EC, TDS and pH were determined.

Sample	Name	Type	River Basin	Latitude	Longitude	Temperature (˚C)	Dissolved Oxygen (% sat.)	Total Phosphorus (mg P/L)	EC (µS/cm)	TDS (mg/L)	pH
A	Ribeira do Tojal	River	Cávado	41,684667	-8,415025	18.4	90	0.018	138	87	6.48
B	Rio Vez	River	Lima	41,880877	-8,426432	20.0	105	0.067	209	138	6.86
D	Refoios do Lima	River	Lima	41,781506	-8,539807	23.1	112	0.063	163	105	7.06
F	Caniçada	Reservoir	Cávado	41,676042	-8,180388	23.2	108	0.025	42	27	7.00
G	Oliveira	River	Ave	41,58626	-8,22512	17.7	102	0.012	137	86	6.82
H	Andorinhas	Reservoir	Ave	41,571226	-8,179073	20.4	93	0.015	109	70	6.64
I	Este (INL)	River	Ave	41,554336	-8,398938	19.2	86	0.122	240	156	6.97
J	Ucha	River	Cávado	41,569742	-8,526438	18.8	90	0.070	178	115	6.84

4.6.1. Supplementary References

1. Lea DE, Coulson CA. The distribution of the numbers of mutants in bacterial populations. J Genet. 1949;49:264–85.
2. Farfán M-J, Aparicio L, Calderón IL. Threonine overproduction in yeast strains carrying the HOM3-R2 mutant allele under the control of different inducible promoters. Appl Environ Microbiol. 1999;65:110–6.
3. Argueso JL, Kijas AW, Sarin S, Heck J, Waase M, Alani E. Systematic Mutagenesis of the *Saccharomyces cerevisiae MLH1* Gene Reveals Distinct Roles for Mlh1p in Meiotic Crossing Over and in Vegetative and Meiotic Mismatch Repair. Mol Cell Biol. 2003;23:873–86.
4. Shell SS, Putnam CD, Kolodner RD. The N Terminus of *Saccharomyces cerevisiae Msh6* Is an Unstructured Tether to PCNA. Mol Cell. 2007;26:565–78.

CHAPTER 5 - Final Considerations and Future perspectives

5.1. Final considerations and future perspectives

The world's population has changed dramatically over the last few centuries. To sustain the ever-growing population, agrochemicals, such as chemical fertilizers and pesticides, have been increasingly used. In fact, the use of pesticides has been the main strategy to minimize crop losses and maximize yields in agriculture (1). However, such a strong reliance on pesticides is far from environmentally sustainable, and thus concerns about their detrimental effects on ecosystems and human health have increased (2,3). In this work, we identified two major challenges: (i) the limited information on the impact of pesticides on non-target microorganisms; and (ii) the costly and logistically-demanding pesticide detection methods that make monitoring programs often impractical. Taking this into consideration, we used the yeast *S. cerevisiae* as a model organism to study two widely used fungicides, CYM and TEB. We chose CYM to address the first issue, since its mechanism of action was not known, and its elucidation may help predict the impact of CYM in different organisms. In parallel, we chose TEB to address the second challenge because its well characterized mode of action allowed for a rational design of a biosensor. Hence, the main goals of the present thesis were to improve the knowledge on the mechanisms underlying cytotoxicity of CYM, and to develop a yeast-based biosensor for detection of TEB. A diverse collection of cell-based molecular, genetic, biochemical and computational approaches were employed to achieve our goals, presented in the two core chapters of this thesis. Chapter 3 is dedicated to clarify the mechanisms underlying CYM cytotoxicity in *S. cerevisiae* cells and is divided in two section: 3.1 is dedicated to unveiling the impact of CYM in respiration of yeast cells, and 3.2 focuses on unveiling the molecular bases of the antifungal activity of CYM. Chapter 4 is focused on the development and application of a yeast-based biosensor for environmental monitoring of TEB in water samples.

While the mode of action of TEB has been well characterized for a long time, little was known regarding the CYM mode of action. In the yeast *S. cerevisiae,* it had been previously shown that CYM can inhibit cell growth, biomass production, and respiration (4), which we confirmed in our study using distinct backgrounds. We directly compared how CYM affects the growth and viability of cells in medium containing glucose or galactose as the carbon source, where respiration is repressed or not, respectively. Our findings indicate that yeast cells lost viability and plasma membrane integrity earlier in medium containing glucose, but that CYM was cytotoxic in both media. We therefore pursued two different approaches for further characterization of the CYM mode of action. First, we investigated the effect of CYM on yeast respiration, under non-repressed conditions, and second, we explored the molecular mechanisms underlying CYM cytotoxicity in cells under repressed respiration conditions.

To assess the effect of CYM on respiration of yeast cells, we used lactate medium, a carbon source that promotes respiration. Our data demonstrated that CYM inhibits oxygen consumption in whole cells, which was not immediate but only occurred after 3 h, then persisting over time. Moreover, our data suggested that CYM acts on the mitochondrial electron transport chain, independently of ATP synthase. Indeed, we showed that CYM inhibits respiration of isolated mitochondria, by specifically targeting C*c*O activity during oxidative phosphorylation. As such, we sought to predict a possible inhibition mechanism using computational tools. Our results suggest a mechanism where CYM and its potential metabolites can block the interaction of cyt *c* with C*c*O, hampering electron transfer and inhibiting C*c*O catalytic activity, similarly to the non-competitive C*c*O inhibitor, ADDA-5 (5). Docking results indicate that protein-protein interaction of C*c*O with cyt *c* can be effectively blocked in yeast by these compounds, due to the interaction of CYM and its potential metabolites with five key residues: Tyr125, Glu142, Glu144, Tyr146 and Asp164 of C*c*O subunit II. Mitochondrial complexes and the respiration process are largely conserved between yeasts and common oomycete pathogens (6), suggesting that the anti-oomycete activity of CYM as an agrochemical fungicide may occur through inhibition of mitochondrial respiration by blocking the C*c*O/cyt *c* interaction, as proposed in this study for yeast cells.

Molecular docking studies performed in this work suggested that CYM has a higher affinity for C*c*O than its metabolites. However, we cannot confirm this possibility without further studies. Thus, it would be interesting to directly test the effects of N-acetylcyanoglycine, the only metabolite commercially available, on C*c*O activity. Additionally, it would be interesting to perform site-directed mutagenesis in some of the residues identified in this work. Computational tools can be used to identify mutations in the C*c*O residues that specifically impair CYM binding without affecting cyt *c* interaction. Then, respiration of yeast cells containing these C*c*O mutations can be measured. If the CYM inhibitory effect is indeed due to the blocking of C*c*O/cyt *c* binding site, then these mutations should significantly reduce or eliminate its ability to inhibit respiration.

Although this study points to mitochondrial respiration, namely the C*c*O/cyt *c* interaction, as one of the targets of CYM, we cannot rule out the possibility of other targets. This is supported by our observation that yeast cells grown in glucose medium display increased sensitivity to CYM. Therefore, we used two unbiased approaches to uncover the global cellular effects of CYM on yeast cells when respiration is repressed: RNA sequencing to determine how this fungicide affects the RNA levels of yeast genes, and a high-throughput microscopic screen to assess CYM effects on protein localization. Among other hits, an effect on membrane transporter systems stood out in both screens. Thus, we

hypothesized that exposure to CYM could lead to alterations in the plasma membrane, whose composition and organization is crucial for proper cellular function (7). Our findings indicate that CYM affects plasma membrane organization by inducing intracellular accumulation of ergosterol, disturbing ergosterol-rich lipid rafts. The results suggest that CYM does not inhibit ergosterol biosynthesis but may impair the sorting of newly synthetized ergosterol to lipid rafts on the plasma membrane, since the deletion of *END3* did not prevent intracellular accumulation of ergosterol. It is also possible that CYM leads to increased endocytosis. Additionally, we did not find any differences on the activity of drug efflux pumps, but found that CYM reduces the proton pumping activity of Pma1p, a plasma membrane protein resident in yeast lipid rafts responsible for generating and maintaining the electrochemical gradient across the plasma membrane (8,9). We found that CYM led to intracellular accumulation of ATP and to a decrease in the plasma membrane potential of yeast cells. Besides Pma1p, we also identified V-ATPase as a potential target of CYM in yeast cells. Altogether, our results suggested that the disturbance of lipid rafts and the inhibition of both Pma1p and V-ATPase activities, followed by a decrease in plasma membrane potential and intracellular acidification, may mediate the antifungal activity of CYM observed in yeast cells.

In addition to transcriptomics and proteome localization screens, further information could be gained from chemogenomic screens. We conducted a preliminary chemogenomic study using two distinct and complementary collections: an overexpression collection, containing 5 330 strains, each expressing an N-terminal SWAT cassette harboring the *TEF2* stronger promotor and m-Cherry upstream of each gene start codon (*TEF2*pr-mCherry library) (10) and a Decreased Abundance by mRNA Perturbation (DAmP) collection, which contains compromised alleles of essential genes (11). We evaluated the fitness of each strain individually, using SD-agar plates supplemented with CYM. However, the results were inconclusive and were not further explored (see supplementary material **Figure S5.i** and **Table S5.i to Table S5.iv**). We observed significant heterogeneity between independent replicas. Indeed, most strains grew on solid agar containing CYM, and as such phenotypic scores relied on colony size, which can vary depending on the position on the plate and is also not a reliable method if small differences are observed. Additionally, the data available for these collections is limited. Therefore, it would be interesting to perform a new chemogenomic study using the overexpression and DAmP collections, along with the knockout deletion collection, using again a non-competitive assay but liquid medium for CYM exposure. By measuring the OD over time in the presence and absence of CYM, it will be possible to extract kinetic growth parameters for each strain and obtain quantitative data to assign a phenotypic score more effectively. This will enable the generation of a chemical-genetic interaction

profile for CYM, which can be compared with other profiles, using the Yeast Phenome, a data library of systematic phenotypic screens of the yeast knock-out collection, that allows the identification of other compounds with similar profiles. Ultimately, this new approach can also identify other targets or even additional mechanisms that were not observed in the screens conducted in this thesis.

Regarding the transcriptomic and proteome localization screens, several questions remain. We observed that several genes whose products are involved in sulfate assimilation and methionine metabolism were up-regulated by treatment with CYM (supplementary material **Table S3.2.ii**). These genes included *SUL1* and *SUL2* (sulfate transmembrane transporter by H^+-symporter), *MET32* and *MET38* (regulators of sulfur metabolism), *MET3*, *MET14*, *MET16*, *MET5* and *MET10* (involved in the first steps of sulfate metabolism), and *MET2* (catalyzes the first step of methionine biosynthetic pathway) (12). We speculate that the up-regulation of these genes is not related with the auxotrophy of the BY4741 strain for methionine, since the growth medium was supplied with this amino acid to complement the auxotrophy of this strain. However, this can also indicate a problem with methionine transport. Thus, a confirmation of the expression levels of some of those genes and comparison with the BY4742 strain, which is not auxotrophic for methionine, is required. The up-regulation of genes involved in sulfate assimilation can also be related to an induction of sulfur starvation caused by CYM. Indeed, both *SUL1* and *SUL2* are strongly induced upon sulfur starvation (13). Therefore, comparing the expression of these genes in cells grown in sulfur-limited conditions, as described elsewhere (13), with cells grown in the presence of CYM can help elucidate this phenotype. Since our results suggest that CYM does not induce autophagy in yeast cells, it is possible that the proposed mechanism for CYM-induced sulfur starvation may not be sufficient to stimulate this phenotype, contrary to what has been previously described for a complete starvation of nitrogen and amino acids in yeast cells (14). However, it would be important to confirm that autophagy is not induced under these sulfur starvation conditions. Additionally, sulfur starvation in yeast cells has been described as an effect of the environmental pollutant chromate, which enters the yeast cells through sulfate transporters and competitively inhibits sulfate uptake (15). Taking in consideration the increased expression of genes related with sulfate assimilation and the hypothesis that CYM induces sulfur starvation, it is possible that CYM, like chromate, inhibits sulfate uptake by competing with sulfate transporters. To confirm this hypothesis, the sensitivity to CYM of a wild-type strain and a mutant strain lacking both *SUL1* and *SUL2* sulfate transporters should be tested.

The proteome localization screen revealed that multiple membrane proteins appeared in an intracellular localization, specifically in the vacuole, after CYM treatment. We ruled out the induction of

autophagy induced by CYM since we did not observe an increase in GFP-Atg8 delivery to the vacuole and consequent cleavage to free GFP. Nevertheless, this mis-localization of membrane proteins may also indicate an increase of endocytosis. Endocytosis of plasma membrane transporters acts as a key regulatory mechanism, allowing yeast cells to adapt to environmental shifts, like fluctuating nutrients or other stresses (16). In this work, we noticed that some plasma membrane transporters known to be regulated by endocytosis in yeast, namely, Hxt3 (17), Hxt4 (18), and Hxt6 (19), were internalized upon treatment with CYM (supplementary material **Table S3.2.iii**), suggesting that CYM could increase endocytosis. To confirm this hypothesis, we can tag these plasma membrane transporters with GFP and assess their internalization in a wild-type strain and a mutant strain deleted in the *END3* gene, following treatment with CYM.

Our results indicate that CYM affects both Pma1p and V-ATPase activity. However, the mechanisms underlying the interaction between CYM and these proton pumps are still unclear. In this context, a computational approach, similar to the one used in this thesis to uncover the effect of CYM on C*c*O activity, will help further understand if CYM may directly interact with proton pumps. If so, it will allow the identification of key residues required for the interaction between CYM and proton pumps, which ultimately can unveil the molecular basis underlying the CYM cytotoxicity in target and non-target organisms. Finally, it would be interesting to confirm the mechanisms underlying CYM cytotoxicity described in this work in the target organisms, namely oomycetes pathogens. It is known that several features distinguish oomycetes from fungi, namely the cell wall composition (20,21). Unlike fungi, oomycetes pathogens (namely *Pythium* and *Phytophthora* species) do not synthesize ergosterol, which make them insensitive to azole compounds (22). Therefore, it is not expected that CYM will affect lipid rafts of oomycetes pathogens since there is no information regarding the existence of such plasma membrane nanodomains in these organisms. Nevertheless, a proteome approach identified proteins present in the cell wall and plasma membrane of *P. infestans*, such as a plasma membrane protein (H^+ ATPase) and a vacuolar protein (H^+ pyrophosphatase) (23). Therefore, it would be interesting to investigate if the Pma1p and V-ATPase of yeast cells and oomycetes pathogens have conserved functions.

Regarding the effects of TEB on yeast cells, we found that high concentrations inhibit yeast growth and decrease cell viability, reversibly compromising plasma membrane integrity. In accordance with alterations in plasma membrane integrity, TEB also disturbed lipid rafts, mainly through intracellular accumulation of ergosterol. We further found that low concentrations of TEB are sufficient to induce expression of several genes involved in ergosterol biosynthesis, namely *ERG11*, *ERG25*, *ERG6*,

and *ERG3*. Considering that lower concentrations of TEB stimulate a biological response without affecting yeast growth, this indicated that *S. cerevisiae* is robust and sensitive to develop a novel yeast-based biosensor for TEB detection in environmental water samples. Therefore, to construct the biosensor, we genetically engineered *S. cerevisiae* cells with a plasmid expressing a reporter, yNluc, downstream of *ERG11*, *ERG25*, *ERG6*, or *ERG3* pr. Among these, the *ERG25*pr biosensor was the most sensitive, detecting the presence of TEB in a statistically significant manner at concentrations above 5 $\mu g\ L^{-1}$. This *ERG25*pr biosensor also seems to specifically respond to TEB, as it was unable to detect other azoles at low, realistic environmental concentrations. We further demonstrated that the biosensor developed can be used in a simple assay, avoiding preparation of environmental water samples, since biosensor performance was not affected by the presence of potential interfering factors such as EC, TDS, pH and other substances. Taking its detection limit into consideration, we propose the use of this biosensor to analyze samples from aquatic environments prone to TEB contamination such as superficial waters, wastewaters and drinking water, particularly water from environments close to agricultural fields. We aimed to increase sensitivity of the yeast-based biosensor developed in this work, since analytical methods have lower detection limits ($ng\ L^{-1}$). To achieve this, we utilized an AD1-9 strain, deleted in seven ATP-binding cassette (ABC) transporters and two transcription factors, which has been described as more sensitive to several compounds (24), harboring p*ERG25*pr-yNluc. However, the bioluminescence signal obtained in response to TEB exposure was very similar between strains (supplementary material **Figure S5.i**). Additionally, we attempted genome integration to promote higher stability and consistency of the biosensor, but this was not successful (25). Similar to TEB, other azole compounds have been shown to up-regulate the expression of *ERG* genes in yeast cells (26,27). Therefore, it would be interesting to identify a common transcriptomic response, such as the up-regulation of certain genes, across several azole compounds. Then, a similar strategy to the one used to develop the biosensor presented in this work could be applied for developing a broader-spectrum yeast-based biosensor for azole detection. This would enable the simultaneous detection of multiple azole compounds, significantly expanding the range of detectable substances using a yeast-based biosensor platform.

5.2. In short

In summary, we used *S. cerevisiae* as model organism to uncover the target and off-target effects of fungicides. Our findings revealed a mechanism of respiratory impairment induced by CYM via inhibition of C*c*O and cyt *c* interaction. Additionally, the plasma membrane was identified for the first time as one of the targets of CYM. The effects on plasma membrane were associated with an inhibition of the proton pumping activity, a decrease in the plasma membrane potential and an intracellular acidification. Overall, these findings suggest new mechanisms that have not been previously described for the antifungal activity of CYM. This contributes to a better understanding of the mechanism of action of CYM, which may be applied to the target organisms of commercial CYM formulations. Using *S. cerevisiae* cells, we also developed a novel approach for environmental monitoring of TEB. This new method can be an important complementary tool, namely in high throughput scenarios requiring screening of numerous samples, since it can be performed by minimally skilled personnel in standard laboratories before chemical analysis by specialized services. Altogether, the results gathered in this study indicate *S. cerevisiae* as a valuable model organism for identifying the effects of fungicides and a useful tool for novel approaches to improve fungicide monitoring programs.

Considering the increasing amount of synthetic chemicals being created, distributed, and released into ecosystems, and the lack of sufficient information to fully understand and predict their impact, an efficient risk assessment is mandatory. This can only be obtained through the collective efforts from interdisciplinary collaborations. In this work, we focused on generating new information and novel tools to improve the risk assessment framework for commonly used fungicides, by studying the impact of CYM and TEB in an eukaryotic model. Using *S. cerevisiae* cells, we unveiled previously unknown mechanisms of action. Our work also recognized that these compounds may pose a potential threat to non-target fungi, the ecological services they provide, and even human health. Additionally, the newly developed detection tool for TEB in water samples offers a valuable approach for environmental monitoring. Overall, this work contributes to knowledge-based environmental protection by assessing the previously overlooked impacts of fungicides. This promotes the sustainable use of fungicides, minimizes their environmental impact, and supports healthy ecosystems. Furthermore, the novel bio-tool for water quality monitoring can be instrumental for improving water quality in high-risk aquatic environments, aligning with global efforts to protect aquatic ecosystems from agrochemical pollution, specifically fungicides.

5.3. References

1. Bommarco R, Kleijn D, Potts SG. Ecological intensification: Harnessing ecosystem services for food security. Trends Ecol Evol. 2013;28:230–8.
2. Malaj E, Von Der Ohe PC, Grote M, Kühne R, Mondy CP, Usseglio-Polatera P, et al. Organic chemicals jeopardize the health of freshwater ecosystems on the continental scale. Proc Natl Acad Sci U S A. 2014;111:9549–54.
3. Brühl CA, Zaller JG. Biodiversity Decline as a Consequence of an Inappropriate Environmental Risk Assessment of Pesticides. Front Environ Sci. 2019;7:1–4.
4. Ribeiro IC, Veríssimo I, Moniz L, Cardoso H, Sousa MJ, Soares AMVM, et al. Yeasts as a model for assessing the toxicity of the fungicides penconazol, cymoxanil and dichlofluanid. Chemosphere. 2000;41:1637–42.
5. Oliva CR, Markert T, Ross LJ, White EL, Rasmussen L, Zhang W, et al. Identification of small molecule inhibitors of human cytochrome *c* oxidase that target chemoresistant glioma cells. J Biol Chem. 2016;291:24188–99.
6. Sierotzki H. Respiration Inhibitors: Complex III. In: Ishii H, Hollomon DW, editors. Fungicide Resistance in Plant Pathogens. Springer, Tokyo; 2015. p. 119–43.
7. Stewart GG. The structure and function of the yeast cell wall, plasma membrane and periplasm. In: Stewart GG, editor. Brewing and Distilling Yeasts. Springer, Cham; 2017. p. 55–75.
8. Serrano R, Kielland-Brandt MC, Fink GR. Yeast plasma membrane ATPase is essential for growth and has homology with (Na^+ + K^+), K^+- and Ca^{2+}-ATPases. Nature. 1986;319:689–93.
9. Serrano R. Structure and function of proton translocating ATPase in plasma membranes of plants and fungi. Biochim Biophys Acta. 1988;947:1–28.
10. Weill U, Yofe I, Sass E, Stynen B, Davidi D, Natarajan J, et al. Genome-wide SWAp-Tag yeast libraries for proteome exploration. Nat Methods. 2018;15:617–22.
11. Breslow DK, Cameron DM, Collins SR, Schuldiner M, Stewart-Ornstein J, Newman HW, et al. A comprehensive strategy enabling high-resolution functional analysis of the yeast genome. Nat Methods. 2008;5:711–8.
12. Thomas D, Surdin-Kerjan Y. Metabolism of sulfur amino acids in *Saccharomyces cerevisiae*. Microbiol Mol Biol Rev. 1997;61:503–32.
13. Boer VM, De Winde JH, Pronk JT, Piper MDW. The genome-wide transcriptional responses of *Saccharomyces cerevisiae* grown on glucose in aerobic chemostat cultures limited for carbon, nitrogen, phosphorus, or sulfur. J Biol Chem. 2003;278:3265–74.

14. Takeshige K, Baba M, Tsuboi S, Noda T, Ohsumi Y. Autophagy in yeast demonstrated with proteinase-deficient mutants and conditions for its induction. J Cell Biol. 1992;119:301–11.
15. Pereira Y, Lagniel G, Godat E, Baudouin-Cornu P, Junot C, Labarre J. Chromate causes sulfur starvation in yeast. Toxicol Sci. 2008;106:400–12.
16. Barata-Antunes C, Alves R, Talaia G, Casal M, Gerós H, Mans R, et al. Endocytosis of nutrient transporters in fungi: The ART of connecting signaling and trafficking. Comput Struct Biotechnol J. 2021;19:1713–37.
17. Snowdon C, van der Merwe G. Regulation of *Hxt3* and *Hxt7* turnover converges on the Vid30 Complex and requires inactivation of the Ras/cAMP/PKA Pathway in *Saccharomyces cerevisiae*. PLoS One. 2012;7:1–10.
18. Hovsepian J, Defenouillère Q, Albanèse V, Váchová L, Garcia C, Palková Z, et al. Multilevel regulation of an α-arrestin by glucose depletion controls hexose transporter endocytosis. J Cell Biol. 2017;216:1811–31.
19. Llopis-Torregrosa V, Ferri-Blázquez A, Adam-Artigues A, Deffontaines E, Van Paul H Heusden G, Yenush L. Regulation of the yeast Hxt6 Hexose Transporter by the Rod1 α-Arrestin, the Snf1 Protein Kinase, and the Bmh2 14-3-3 Protein. J Biol Chem. 2016;291:14973–85.
20. Richards TA, Dacks JB, Jenkinson JM, Thornton CR, Talbot NJ. Evolution of filamentous plant pathogens: gene exchange across Eukaryotic Kingdoms. Curr Biol. 2006;16:1857–64.
21. Latijnhouwers M, De Wit PJGM, Govers F. Oomycetes and fungi: Similar weaponry to attack plants. Trends Microbiol. 2003;11:462–9.
22. Warner SA, Eierman DF, Sovocool GW, Domnas AJ. Cycloartenol-derived sterol biosynthesis in the Peronosporales. Proc Natl Acad Sci. 1982;79:3769–72.
23. Grenville-Briggs LJ, Avrova AO, Hay RJ, Bruce CR, Whisson SC, van West P. Identification of appressorial and mycelial cell wall proteins and a survey of the membrane proteome of *Phytophthora infestans*. Fungal Biol. 2010;114:702–23.
24. Rogers B, Decottignies A, Kolaczkowski M, Carvajal E, Balzi E, Goffeau A. The pleitropic drug ABC transporters from *Saccharomyces cerevisiae*. J Mol Microbiol Biotechnol. 2001;3:207–14.
25. Miranda E. Novel yeast-based biosensor for environmental monitoring. Universidade do Minho; 2021. (Master Thesis)
26. Henry KW, Nickels JT, Edlind TD. *ROX1* and *ERG* regulation in *Saccharomyces cerevisiae*: Implications for antifungal susceptibility. Eukaryot Cell. 2002;1:1041–4.
27. Kagan IA, Michel A, Prause A, Scheffler BE, Pace P, Duke SO. Gene transcription profiles of

Saccharomyces cerevisiae after treatment with plant protection fungicides that inhibit ergosterol biosynthesis. Pestic Biochem Physiol. 2005;82:133–53.

5.4. Supplementary Material

Figure S5.i

Table S5.i

Table S5.ii

Table S5.iii

Table S5.iv

Figure S5.ii

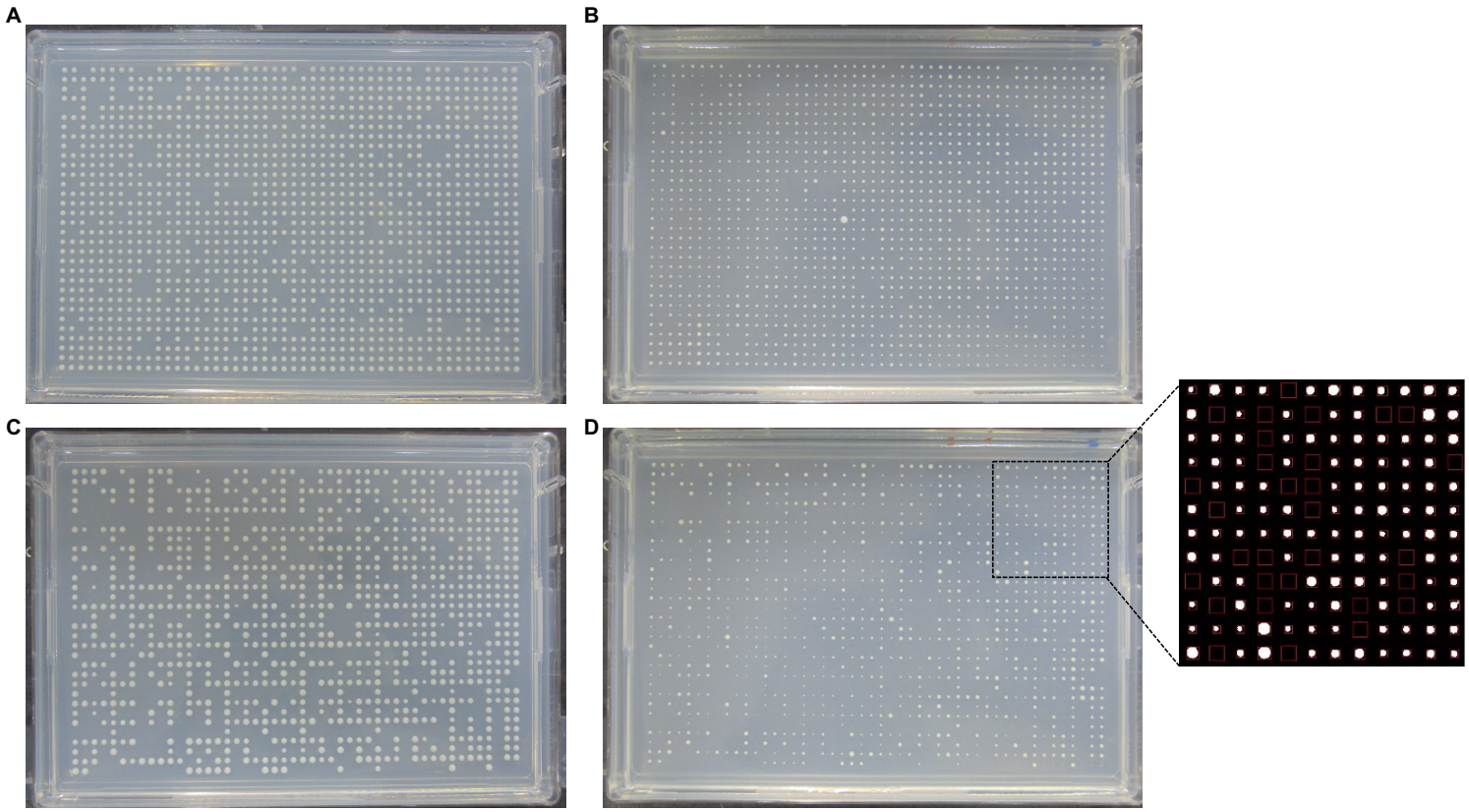

Figure S5.i. Representative images of the chemogenomic study using two distinct and complementary collections. The *TEF2*pr-mCherry overexpression (**A** and **B**) and DAmP (**D** and **C**) collection strains were grown on SD agar medium in 1536-well plates. Subsequently, using the ROTOR HDA (Singer Instruments), cells were transferred to 1536-well SD agar plates (**A** and **C**) or SD agar plates containing 50 μg mL^{-1} of CYM (**B** and **D**), and incubated for 24 h at 30 °C. Plates were imaged after 24 h, and individual colony size assessed using the SGAtools website (http://sgatools.ccbr.utoronto.ca/imageanalysis). The average size obtained for control strains in plates containing CYM, taking in consideration the S.D. of these averages, was used as a reference. Mutant strains whose colony size was 10 % higher than the maximum average size of the control strain or 10 % lower than the minimum average size of the control strain, were considered as resistant or sensitive to CYM, respectively (Table S5.i to Table S5.iv).

Table S5.i. List of genes whose overexpression confers resistance to CYM.

Gene name									
FLR1	*SMY2*	*ATG21*	*NAT1*	*BOP3*	*MSL1*	*CDC5*	*RAD5*	*CMI8*	*SIC1*
ARE2	*SSM4*	*YDR338C*	*YIR042C*	*OSW2*	*BDP1*	*POP2*	*YDL129W*	*FIP1*	*YAP1*
TRS120	*PHO91*	*YNR048W*	*EST1*	*ADH6*	*CBT1*	*YOL038C-A*	*ARP9*	*YKU80*	*COM2*
PPN1	*IVY1*	*HXT1*	*GSY1*	*RLP7*	*DSD1*	*FMP48*	*MRX16*	*UBP14*	*YOR105W*
TRS33	*VPS38*	*CLC1*	*HIS6*	*NOP10*	*YPL247C*	*RRP40*	*AXL1*	*YBL028C*	*UMP1*
ATG3	*RVS167*	*IRC8*	*IME2*	*MAK3*	*BNI1*	*HED1*	*HRB1*	*DHH1*	*STM1*
ALY1	*CSG2*	*TBS1*	*STB2*	*ERG13*	*HAL5*	*SOK1*	*SLX9*	*RRS1*	*SNF1*
DER1	*GEA1*	*APQ12*	*HAP5*	*HOP1*	*PSO2*	*GFD2*	*HHF2*	*GDS1*	*SSK1*
MAM3	*ADR1*	*TOR1*	*RSC30*	*MMS21*	*AAD4*	*OPI10*	*HSL1*	*CDC27*	*NNR1*
PRE7	*VAM6*	*KHA1*	*RPP0*	*ARO7*	*NUP145*	*FIG4*	*SPP41*	*DCP1*	*UTR1*
VMA7	*YLR342W-A*	*RIF2*	*MSG5*	*APT2*	*PTH2*	*CYK3*	*IDS2*	*CAB4*	*SIR1*
ATG12	*POR2*	*LOT5*	*CPA2*	*SIP1*	*HSP104*	*HSC82*	*MGA1*	*YIL055C*	*UTH1*
SEC4	*ACC1*	*ASF2*	*TIF11*	*QCR10*	*SAM1*	*PRE6*	*FRA1*	*DAS1*	*PUP1*
PRE2	*AVL9*	*ZPR1*	*NAT3*	*FAP1*	*DOG2*	*RUP1*	*PIG1*	*WHI5*	*PUP3*
YHR213W-A	*UBP15*	*MED2*	*COA4*	*CLG1*	*ABP1*	*PAU2*	*NUP157*	*IPL1*	*FIN1*
PRE4	*UIP4*	*PBA1*	*COX20*	*UPA1*	*EDC1*	*STT4*	*CPR1*	*MRC1*	*NUP42*
EPT1	*RIM9*	*ESS1*	*YDL057W*	*DGR2*	*NAT4*	*RPL8B*	*SIR3*	*GIS1*	*ESL1*
SIP3	*ATG2*	*HPC2*	*TAF12*	*SLD5*	*ARP7*	*POL4*	*ECM16*	*RPN10*	*AZF1*
SCS2	*ERV14*	*KEL2*	*PRE10*	*RGT1*	*BTT1*	*SGF73*	*HDA3*	*CRN1*	*OTU2*
HOL1	*SSA1*	*YJL107C*	*LOG1*						

Table S5. ii. List of genes whose overexpression confers sensitivity to CYM.

Gene name									
ARL1	*SRP101*	*YCK2*	*TAT1*	*ENT5*	*YNL011C*	*RPP2A*	*YOL019W-A*	*RPB5*	*FPY1*
CUE1	*APL5*	*YLL006W-A*	*TDA7*	*LAM1*	*CPR6*	*NCS6*	*PET8*	*SMD3*	*RPL12A*
RSN1	*YML131W*	*VPS74*	*SMF1*	*STL1*	*IES5*	*SDS3*	*CUZ1*	*SER1*	*POB3*
PEX6	*BMS1*	*FRQ1*	*DAL3*	*SEC5*	*UBA3*	*YBL081W*	*PCL8*	*STE5*	*LCP5*
STE3	*HUR1*	*COS7*	*ENA5*	*PEX18*	*UPC2*	*YNL018C*	*KSP1*	*TEN1*	*OPY1*
LCB1	*YNL095C*	*SAM50*	*MGA2*	*SEC7*	*NOT3*	*SMD1*	*BUD6*	*ASC1*	*JLP2*
NVJ1	*YOR1*	*COS8*	*LYS1*	*SUP35*	*MES1*	*YLR460C*	*YBL071C-B*	*LSM12*	*CYS3*
GRH1	*YDL199C*	*IMH1*	*HEH2*	*PMP2*	*POL2*	*PLP2*	*MET6*	*NUP49*	*ISW1*
CDC6	*COS6*	*RAX1*	*SCD5*	*ATG13*	*MIF2*	*STE20*	*NGR1*	*LYS14*	*MHP1*
PMT1	*YPT6*	*APL4*	*SRP54*	*NDC1*	*URK1*	*MNC1*	*VPS75*	*PPX1*	*SWM1*
YHR214C-D	*DGA1*	*PEX30*	*AMF1*	*SRC1*	*GSH2*	*GUD1*	*ATE1*	*TRM112*	*NPL6*
SNG1	*UBC7*	*EFT1*	*MUP1*	*SSU1*	*SSY5*	*RPL36B*	*SCP1*	*PRS3*	*TFG2*
PCD1	*HUT1*	*CSR2*	*MIN10*	*OPT2*	*YJR023C*	*ALF1*	*RAM2*	*RPL13A*	*EDC2*
TDA9	*SEC22*	*YLR326W*	*YOL163W*	*RPL9A*	*RPS1B*	*ESC2*	*HMI1*	*FMP49*	*APC9*
MDM1	*GYP5*	*VRP1*	*YOL164W-A*	*GCR1*	*KAR9*	*YOR161W-B*	*MCO14*	*SWC5*	*TKL2*
FMP49	*FSF1*	*VBA1*	*APS3*	*PTA1*	*ARG81*	*SDS23*	*ARO1*	*TIM11*	*YPR127W*
YGL140C	*SAK1*	*PEX34*	*VTC5*	*YNL140C*	*ECM22*	*NAT5*	*BUR6*	*BUD2*	*MET10*
SCT1	*VMA9*	*FYV5*	*CTR1*	*YCR102C*	*RPS16A*	*YNR068C*	*STP1*	*PUS5*	*ANK1*
VPS51	*UBP3*	*FAT1*	*VMA11*	*YKR075C*	*APC2*	*LTE1*	*RPG1*	*TFC4*	*YEL023C*
HXT17	*YNL144C*	*VAC17*	*RCI50*	*MAF1*	*CAF120*	*HMO1*	*YMC1*	*MIG1*	*CDC26*
PHO81	*YOL075C*	*NAG1*	*YPT11*	*MOD5*	*MAL33*	*DSN1*	*RPS11B*	*CTL1*	*ENP2*

ALT2	*AAH1*	*GDH3*	*VHR1*	*UBP6*	*YPL222C-A*	*RPS29B*	*IQG1*	*YPR015C*	*KEX1*
CBC2	*DRS1*	*RPL37A*	*PAC11*	*SPS1*	*HOS1*	*RPE1*	*IRR1*	*ARR2*	*MCX1*
NFI1	*PPH3*	*AFI1*	*RCF1*	*YJL077W-A*	*YAF9*	*RPS19B*	*RSF1*	*ASA1*	*SPS22*
PRP11	*LAS17*	*ARC15*	*DNA2*	*ICY1*	*ACK1*	*OAR1*	*HRP1*	*HEK2*	*AEP3*
TFS1	*MTR2*	*OGG1*	*TRM10*	*YKR070W*	*STF2*	*MRX21*	*CTK3*	*YNL339W-A*	*PGM1*
YJR146W	*IPP1*	*NAS2*	*SHB17*	*MAN2*	*HSH155*	*HAP1*	*GLT1*	*RPD3*	*RPS4B*
BLM10	*NAM8*	*YPL277C*	*SRB8*	*YBL029W*	*SSF1*	*HER1*	*TPS2*	*YNL067W-B*	*REH1*
RTC4	*SER3*	*SAS2*	*YBR109W-A*	*WHI4*	*YDR061W*	*HER1*	*ZEO1*	*PFK27*	*SMC6*
SSA3	*RPF1*	*DAL81*	*PAL1*	*THI2*	*MCM3*	*ZAP1*	*RPN7*	*GPX2*	*SPT7*
PUF3	*DOG1*	*MLC2*	*SLK19*	*ECM11*	*SYP1*	*BIR1*	*DPA10*	*FMP41*	*SAE3*
CNS1	*SNT2*	*LEO1*	*WTM2*	*GIR2*	*YNL050C*	*PTC3*	*IRC21*	*EBP2*	*YPR074W-A*
APJ1	*CWC25*	*SWD1*	*ULP2*	*BRE1*	*HUA1*	*YOR389W*	*RPS25A*	*PRX1*	*MRPS5*
SQT1	*AIM6*	*PDC5*	*MDJ2*	*NHP6A*	*SHQ1*	*GCR2*	*RCF2*	*MRP21*	*SAG1*
SAD1	*ARA2*	*ADF1*	*VIP1*	*OAZ1*	*RPS21B*	*AAC3*	*RPB11*	*FLC2*	*SLM3*
HRT3	*AFT1*	*YFR057W*	*DDP1*	*PYK2*	*TOP1*	*ZRG8*	*PHO2*	*ATP1*	*MTF2*
TRP1	*GID10*	*CTF4*	*CDC53*	*PTK1*	*DDC1*	*SPT3*	*RTS1*	*MF(ALPHA)2*	*SLM5*
SAE2	*AMD1*	*MAK11*	*YPL135C-A*	*FIR1*	*IRC24*	*NMA1*	*GLG2*	*PHO11*	*IMG1*
REF2	*LSM2*	*PHO80*	*RPS11A*	*RPS23A*	*RPS14B*	*NEL1*	*YBL113C*	*SCO1*	*MET5*
RNQ1	*EDS1*	*RPS1A*	*VAB2*	*PIC2*	*ACE2*	*TIP41*	*RPS23B*	*FLC3*	*IMG2*
SEN54	*RPL34A*	*TBF1*	*MRS1*	*STD1*	*PTP3*	*YRB2*	*YPL039W*	*PGS1*	*NDE2*
RRP17	*MSN1*	*VIK1*	*SLD2*	*UBC11*	*DMA1*	*DCS1*	*RAD30*	*MBA1*	*DLD1*
DLD2	*FCP1*	*MSS116*	*PDI1*	*YBP2*	*MID1*	*BGL2*	*ENP1*	*MET1*	*ESA1*
SPO1	*RPL1A*	*COQ4*	*ATP22*	*HCM1*	*PRY2*	*DPC29*	*SKG3*	*AGA1*	*AOS1*

TUL1	*YAR1*	*RSM10*	*RSC58*	*NMA2*	*FMP10*	*YHL017W*	*TOS4*	*MSH1*	*ESC8*
MRX19	*NAB2*	*FMP16*	*GCG1*	*MZM1*	*YNL320W*	*YCL049C*	*CEF1*	*MRPL6*	*YGR153W*
YNL019C	*TCD2*	*MRX14*	*SLX8*	*ATP17*	*UIP5*	*PAU13*	*MSN2*	*FYV4*	*DPB4*
PTM1	*LYS2*	*ATP5*	*GPM3*	*HSP150*	*COQ8*	*NOP7*	*RPL13B*	*INP51*	*PXR1*
GCV1	*YOL024W*	*OMS1*	*URA2*	*SDH6*	*GPP2*	*PUS9*	*CFT2*	*INA22*	*RPL33A*
TIP1	*RPL12B*	*MRPS28*	*IMD4*	*ALD5*	*GZF3*	*SOD2*	*MIR1*	*EMP70*	*KNH1*
SHE1	*YFH1*	*PHO3*	*RPR2*	*ICP55*	*DIB1*	*TAD3*	*YLR412C-A*	*PLB3*	*RPP1B*
ATP20	*COX26*	*YCL012C*	*SGD1*	*AIM9*	*LCL1*	*MYO1*	*YCR095W-A*	*RPA135*	*RSM7*
AFT2	*MTO1*	*CRH1*	*YEL008C-A*	*FRE2*	*PDL32*	*TDA1*	*GLG1*	*UBI4*	*MCO12*
PNT1	*RSM24*	*MRX10*	*HSK3*	*JAC1*	*SCW4*	*YKR015C*	*BIO2*	*CTR86*	*ANS1*
AIM24	*OCT1*	*DSK2*	*MLO1*	*JIP5*	*CRS1*	*RRF1*	*HTD2*	*SBE22*	*MRP13*
MAE1	*CCP1*	*NAM2*	*YTA12*	*YOX1*	*CBP3*	*CLD1*	*ARP4*	*MGP12*	*GUP2*
SDH1	*MRPL20*	*SOV1*	*FMP40*	*PHR1*	*SDH5*	*TCM62*	*HMLALPHA2*	*CCA1*	*SDH4*
RSM22	*SIL1*	*MRPL39*	*RPS7A*	*YNL208W*	*GPN2*	*ATM1*	*DAK1*	*GPD2*	*YAH1*
MAS1	*SDH2*	*PGU1*	*MMT2*	*ATP11*	*PAD1*	*CYM1*	*AAT1*	*LIP5*	*MRX6*
COQ9	*PET309*	*SWI5*	*MSF1*	*PPZ1*	*AIM32*	*MRPL24*			

Table S5.iii. List of essential genes whose decreased abundance by mRNA perturbation confers resistance to CYM.

Gene name										
MAK16	*RLP7*	*SAS10*	*SUA5*	*ASK1*	*TOM40*	*RPC25*	*HSF1*	*PRP5*	*PLP2*	*DRE2*
ESF1	*PWP1*	*ULP2*	*TAF12*	*RFC5*	*TAF7*	*RPT1*	*MPS2*	*YJL032W*	*NAT2*	*SEC7*
RSC4	*LST8*	*TFA1*	*GPI17*	*GLE1*	*CCA1*	*GPM1*	*GCD11*	*PDS1*	*NUD1*	*TRZ1*
KEI1	*BDP1*	*CDC9*	*RSC3*	*NHP2*	*TAM41*	*CNS1*	*DAM1*	*NTR2*	*COG3*	*RPF2*
BRN1	*TUB4*	*TTI1*	*MCM6*	*NUP159*	*RBA50*	*DBF4*	*HRP1*	*CDC34*	*TAF3*	*ORC3*
FRQ1	*POL1*	*UFE1*	*TUB1*	*CDC13*	*TFC4*	*DED1*	*YGR114C*	*FAS1*	*PIK1*	*PDI1*
ARH1	*PRE7*	*RTS2*	*SPP41*	*SPP2*	*CAB1*	*RFC1*	*UTP21*	*DPM1*	*SEC2*	*PBN1*
SFI1	*IPA1*	*TIF6*	*TAF4*	*COG4*	*WBP1*	*YOR218C*	*SSU72*	*CDC31*	*ORC1*	*TRL1*
DRS1	*SEC17*	*RKI1*	*RPC19*	*PUP1*	*SIS1*	*DPB2*	*NAR1*	*PZF1*	*POP3*	*SPB1*
NAB2	*SCM3*	*NUP1*	*NAF1*	*RPN7*	*ERG25*	*DFR1*	*NBP1*	*ISD11*	*RFC3*	*DPB11*
SRB6	*YBL073W*	*HTS1*	*GCD7*	*RPC40*	*RPC31*	*BET2*	*SPT5*	*HEM4*	*RPM2*	*MYO2*
NCB2	*PRP40*	*GLN1*	*STT4*	*PIS1*	*PGA1*	*APC5*	*CDC28*	*NOP58*	*UTP14*	*FIP1*
RPB7	*AAR2*	*TAH18*	*CDC3*	*MED4*	*CBK1*	*SEC23*	*MTR2*	*SAH1*	*KRI1*	*RPB3*
MAS1	*GPI16*	*TFC7*	*PGA2*	*HEM15*	*KAP95*	*SMX3*	*RIM2*	*COG2*	*ZIM17*	*MCM4*
SEC27	*URB1*	*RPO31*	*CHS2*	*YPR142C*	*PBR1*	*YPT1*	*NOP9*	*LSM4*	*ERG13*	*GPA1*
RRP17	*RIX1*	*TFB4*	*UGP1*	*NUG1*	*IPI3*	*NIC96*	*LCB2*	*ENP2*	*RPC37*	*PRP2*
ACS2	*RPN5*	*RPT5*	*PRP6*	*GUS1*	*YLR379W*	*SRP1*	*RPS13*	*RSP5*	*TAD2*	*SEC59*
ATM1	*NOP14*	*RDS3*	*SNP1*	*MCM1*	*YPD1*	*POP1*	*CYR1*	*ERG1*	*TRS20*	*TIM23*
PSE1	*RPC53*	*RPO21*	*ORC2*	*RPN3*	*PSF1*	*UTP22*	*PGI1*	*NSA2*	*SEC5*	*TAP42*
PRE5	*MAK11*	*YSH1*	*YRB2*	*RNA14*	*FAL1*	*OLE1*	*RNR2*	*GCD1*	*POP4*	*DBP6*
NMT1	*PKC1*	*YHC1*	*RPG1*	*SRB4*	*IRA1*	*ARC35*	*RPL17A*	*SPT6*	*BET3*	*SEN15*
TSC10	*IQG1*	*ILV3*	*SEC62*	*SRP72*	*MRS6*	*RRB1*	*BOS1*	*MCM2*	*DIS3*	*ESF2*
APC2	*HTB1*	*GRC3*	*ERG11*	*CDC33*	*RET3*	*RIB2*	*LSM8*	*ORC6*	*FOL3*	*RCL1*
USB1	*MCD1*	*PGK1*	*CDC14*	*CUS1*	*BUR6*	*NUF2*	*CFT1*	*PET9*	*SMC5*	*GPI14*
CDC11	*SED5*	*SLY1*	*SGV1*	*NOP8*	*SDA1*	*ROT1*	*CDC60*	*POL12*	*RPT2*	*PRE6*

SCL1	*RPT6*	*RRP43*	*RSC8*	*UTP23*	*SEC4*	*WRS1*	*MTR4*	*IMP3*	*SEN54*	*ECM16*
PTA1	*RSA4*	*TIM17*	*BCD1*	*HSH155*	*SMC1*	*CEF1*	*NET1*	*HRT1*	*NOG1*	*RRN5*
RMP1	*RLP24*	*SSL1*	*PRP45*	*SLD7*	*YGR265W*	*APC11*	*SEN34*	*RRP5*	*SPC24*	*MPE1*
RPN12	*ARP3*	*TAH11*	*CCT3*	*LCB1*	*SPT14*	*RSC58*	*CDC15*	*MED7*	*ARP2*	*IPI1*
POP5	*PRP9*	*UTP4*	*CIA1*	*SRB7*	*FRS2*	*TSC13*	*HEM2*	*TAF9*	*RRN3*	*SPC42*
NMD3	*PRP28*	*UTP20*	*ALA1*	*CWC22*	*PRT1*	*RPA43*				

Table S5.iv. List of essential genes whose decreased abundance by mRNA perturbation confers sensitivity to CYM.

Gene name										
YRA1	*CSE4*	*ESA1*	*STN1*	*DUT1*	*CAB4*	*NUP82*	*NUP116*	*SAD1*	*CDC19*	*STT3*
UTP5	*FBA1*	*GCD10*	*MIA40*	*SSY1*	*TIM10*	*LAS1*	*ERB1*	*ECO1*	*RRP3*	*ALG13*
USO1	*DHR2*	*KAR1*	*RRN7*	*TIM54*	*NOB1*	*TAF10*	*TRM112*	*STH1*	*SWP1*	*POP8*
NOP56	*SHQ1*	*RPN11*	*TOR2*	*SEC1*	*PRP43*	*CDC37*	*PDS5*	*CCT2*	*BRX1*	*BIG1*
YLR198C	*YKL083W*	*PCM1*	*ARC40*	*RIB5*	*SGT1*	*NFS1*	*SEC14*	*PTR3*	*AVO1*	*DUO1*
IMP4	*GLN4*	*GCD2*	*ECM9*	*AFG2*	*PNO1*	*SMC3*	*GWT1*	*PRP4*	*RTP1*	*RFT1*
UTP9	*SPN1*	*SEC3*	*APC4*	*CSL4*	*CBF2*	*ARP4*	*UTP10*	*BRL1*	*TPT1*	*MNP1*
CDC27	*PRP3*	*NRD1*	*RPN8*	*SEN1*	*PRP38*	*YCL041C*	*RVB1*	*TFC3*	*DML1*	*YGL074C*
RAM2	*SNM1*	*RNA15*	*GPN2*	*SEC39*	*TYS1*	*UBC1*	*CAB5*	*DSN1*	*NOP1*	*NBP35*
RPL32	*SEC20*	*PRP31*	*HXT12*	*SUI1*	*GLC7*	*SOF1*	*COF1*	*NCP1*	*SEC26*	*PSF3*
FAF1	*LCD1*	*MVD1*	*KRS1*	*DSL1*	*TFG1*	*CDC1*	*RSC6*	*RPP1*	*SUI2*	*PRP24*
YDL152W	*SMT3*	*NOG2*	*SUP45*	*NSE5*	*YGR190C*	*KRE5*	*GCD14*	*MPS3*	*SPC3*	*RAT1*
ASA1	*POP6*	*ARB1*	*RIB7*	*NDC1*	*TEM1*	*SWI1*	*SPC19*	*TCP1*	*SRP101*	*TFB1*
TIF35	*RRN9*	*YLR339C*	*SEC11*	*MED8*	*POB3*	*ZPR1*	*CTR86*	*KRE9*	*PRP11*	*CDC8*
GPI19	*YLR317W*	*RPL42A*	*RPC11*	*RPC17*	*MRPS18*	*NOP4*	*MSS4*	*CDC6*	*FAD1*	*SNU23*
RSE1	*CWC24*	*ILV5*	*RPB5*	*ACP1*	*PGA3*	*GPI2*	*ERG20*	*ULP1*	*TBF1*	*YDR341C*
GUK1	*SGD1*	*ADE13*	*HEM12*	*YJL015C*	*PFS2*	*SPC29*	*CDC5*	*TIM50*	*RPL33A*	*SPC110*

VRG4	*MMF1*	*SEC61*	*NOC2*	*PDC2*	*KAR2*	*FOL2*	*SEC12*	*IDI1*	*NOP53*	*YPL238C*
TAF8	*ALG14*	*YRB1*	*RPB8*	*MCM7*	*DOP1*	*NSL1*	*EPL1*	*ARP7*	*JAC1*	*SRP68*
NAM9	*SEC31*									

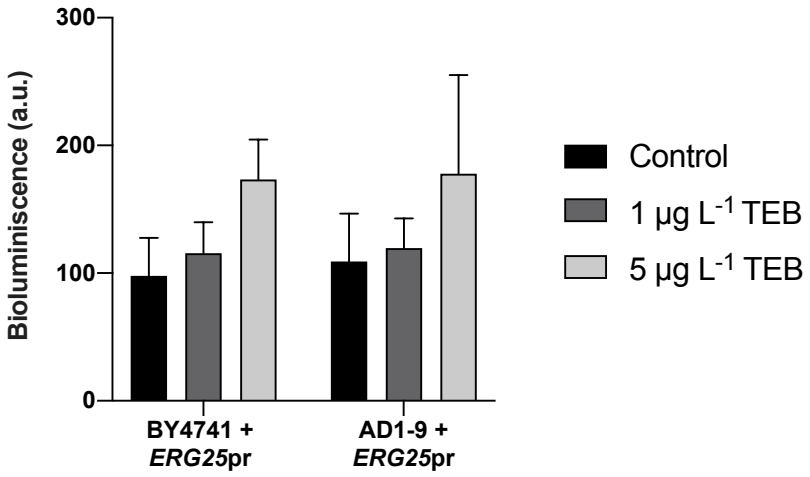

Figure S5.ii. Response of BY471 + *ERG25*pr and AD1-9 + *ERG25*pr strains to TEB. BY4741 + *ERG25*pr and AD1-9 + *ERG25*pr cells were incubated in the absence (control) or presence of TEB (1 and 5 µg L^{-1}) for 6 h; cells were collected, and bioluminescence was assessed. Values are mean ± S.D. of three independent experiments.